High Strain Rate, High Temperature Deformation of Stainless Steel.

Rafael Colás Ortiz

A thesis submitted for the degree of Doctor of Philosophy.

University of Sheffield.
Department of Metallurgy.

December 1983.

A quien la lea.

Summary

In order to clarify the dependence of strain localisation on different parameters, a literature survey is presented covering the theory and observations of instability formation during deformation, dynamic recovery processes, mechanical testing, adiabatic heating and shear band formation.

Several series of experiments were carried out, on titanium bearing steel and on an austenitic stainless steel, to determine the reasons of the inversion of the dependence of the strain to the peak in flow stress on strain rate observed at high strain rates. The materials were deformed under conditions of plane strain and axisymmetric compression, and torsion. Special techniques were developed in order to measure the distribution of strain and temperature within deforming plane strain specimens.

In the strain distribution analysis, it was observed that the range of local strains is dependent on nominal strain rates, but the average value of the local strain either in the whole deforming region or the slip line bands depends only on the value of nominal strain. When the plane strain specimens were deformed with inserted thermocouples, it was found that both the overall temperature increase and the difference in temperature between different local regions of the specimen, increased with the nominal strain rate.

It was shown that, at high strain rates, the stress-strain curve of any material will develop a peak in stress as a result of the increase of temperature due to deformational heating, without the occurrence of any strain instability.

The results emphasise the complexity of deformation under plane strain compression, particularly at high strain rate, but it was possible to compare stress-strain curves obtained under plane strain and axisymmetric compression conditions when the effects of strain and stress distribution and of temperature localisation were taken into account

Contents.

Chapter 1.

Introduction.

In industrial processing, materials are deformed in accordance with complicated schedules in which a certain degree of redundant work is introduced. This redundant work is, in the case of hot rolling, due to sticking friction in the metal-roll interface, in the case of extrusion, it is due partly to the geometry of the process. An extra factor is taken into account in productivity. The different processes have to be performed at high rates of deformation and obtain high outputs.

This combination of high strain rate and redundant work might increase the probability of producing regions in the deforming materials in which the deformation is highly localised. This heterogeneity is important because the mechanical properties of the worked material are a result of the microstructure and distribution of imperfections.

Various theories had been proposed to explain the influence of deformation parameters such as strain rate, temperature and microstucture on the plastic resistence to deformation in metals and alloys. Most of them deal with the existence of a perfectly homogeneous material. Unfortunately, experimental evidence suggests that the range over which a certain material will deform homogeneously is smaller than the range in which a heterogeneous behaviour is expected.

In order to obtain reliable parameters to test the different theories, scaled down mechanical tests are carried out in a controlled environment. Limitations exist in each test due to mechanical instabilities. The onset of

these instabilities is characterized by a maximum in stress in a stress-strain curve. Macroscopic features like necking in tension or buckling in compression are examples of strain localisation, and as such are treated in the literature survey which tries to present the different criteria and general solutions developed for the mathematical problem.

The increase of temperature, due to deformational heating, is important in the development of microstructural instabilities. Any strain sensitive material will present a tendency to deform prefentially in soft regions increasing at the same time the actual temperature. At high temperatures, in which dynamic restoration mechanisms are operative, additional softening is achieved, and at high strain rates localisation of both strain and temperature might be enhanced.

In the text, the onset and the effect of plastic instabilities are treated. The macroscopic case is developed in surveys dealing with mechanical testing at high temperature. The microscopic case is presented in surveys relating the effect of dynamic restoration processes and formation of shear bands observed in high strain rate deformations.

Tests carried out at high strain rates and high temperatures in different materials have presented anomalies with regards to the strain at which the onset of dynamic recrystallisation is achieved, characteristised by a peak in stress in a stress-strain curve (McQueen et al, 1976; Farag and Hamdy, 1977; Fritzemeier et al, 1979; Colás 1980; Leduc, 1980).

The aim of this work is to determine the possible causes of mechanical instabilities at high temperature and high strain rates. Work was carried out in an austenitic AISI type 316 stainless steel tested under axisymmetric and plane strain compression and torsion conditions. Preliminary tests were carried out using the titanium bearing steel studied previously (Colás, 1980; Leduc, 1980).

Chapter 2

Heterogeneous Deformation.

2.1. Introduction.

Heterogeneous or non-uniform deformation exerts a strong influence in each of the main areas concerned with mechanical behaviour of materials: testing, structural strength and forming. The testing of mechanical properties is usually carried-out on so called representative specimens or samples. Unless the deformation is uniform, the test data will not represent the material properties. In structural applications, a safety margin is desirable if the yield stress is exceeded. In this case, widespread plasticity is better than local, unstable behaviour. In forming, there are usually a number of possible forming schedules or paths with respect to the straining conditions. Even if localised deformation does not lead to failure, it may cause disturbing surface defects.

2.2. Stability Criteria.

In order to determine the domain of a homogeneous mode of deformation over a heterogeneous one, some stability criteria have been postulated. Depending on their basis, the criteria can be divided into phenomenological, if they are based on constructions from the stress-strain curves, or physical, if they deal with particular deformation mechanisms.

2.2.1. Phenomenological criteria.

The first instability criterion was given by Considère (1885), who analysed the case of the neck formation in tensile specimens. His geometrical construction is given by the relationship

$$F = \sigma A \tag{2.1}$$

where F, σ and A are the force, stress and cross-sectional area respectively, and by the total differential

$$dF = \sigma dA + A d\sigma \tag{2.2}$$

Under tensile conditions, the force-displacement curve presents a local maximum at the begining of the neck formation, $dF = 0$, then equation (2.2) yields

$$\frac{d\sigma}{\sigma} = \frac{dA}{A} = d\varepsilon \tag{2.3}$$

where ε is the true strain. Under these conditions, the onset of instability will be given by the relationship

$$\gamma - 1 = 0 \tag{2.4}$$

where $\gamma = d\ln\sigma/d\varepsilon$ is an apparent work hardening coefficient, not to be confused with the more common $n = d\ln\sigma/d\ln\varepsilon$.

Hart (1967) assumed that at any stage of deformation the stress is dependent on the previous strain history, and that small changes in strain or strain rate, $\dot{\varepsilon}$, will correspond linearly with small changes in stress,

$$d\sigma = k d\varepsilon + \ell d\dot{\varepsilon} \tag{2.5}$$

where k and ℓ are material parameters that depend on the specimen history. In order to determine the stability he computed the variation in the cross-sectional area increment rate, $d\dot{A}$, as a function of the variation in the cross-sectional area, dA. With these assumptions, in a tensile test, at the point of zero increment of load, $dF = 0$, equations (2.2), (2.3) and (2.5) can be combined

to obtain

$$\frac{d\ln\dot{A}}{d\ln A} = -\frac{1-\gamma-m}{m} \tag{2.6}$$

where $m = d\ln\sigma/d\ln\dot{\varepsilon}$ is the strain rate sensitivity. The criterion is given by

$$\frac{d\ln\dot{A}}{d\ln A} < 0 \tag{2.7}$$

or, with the help of γ and m, the onset of instability is achieved when

$$\gamma = 1 - m \tag{2.8}$$

This criterion is in agreement with the previous one, for strain hardening material with negligible rate dependence, figure 8 a.).

Campbell (1967) presented an analysis assuming that the strain rate of the material is a function of the values of stress and strain. He introduces the strain gradient, $\lambda = \partial\varepsilon/\partial x$, where x is the distance along the axis of the specimen. This strain gradient is defined, for a certain position and time, as

$$\lambda = \frac{1}{1+\varepsilon}\ \frac{d\varepsilon}{dx} \tag{2.9}$$

so that

$$\frac{\partial\lambda}{\partial t} = \frac{1}{1+\varepsilon}\frac{\partial\dot{\varepsilon}}{\partial x} - \frac{\dot{\varepsilon}}{(1+\varepsilon)^2}\frac{\partial\varepsilon}{\partial x} \tag{2.10}$$

The rate dependence of the material is assumed to be governed by the equation

$$\dot{\varepsilon} = g(\sigma, \varepsilon) \tag{2.11}$$

This equation is expected from dislocation theory, since the strain rate is determined by the density and mean velocity of moving dislocations. Assuming

volume constancy, equation (2.11) can be rewritten as

$$\dot{\varepsilon} = g\left[\frac{F}{A_o}(1+\varepsilon),\varepsilon\right] \tag{2.12}$$

where F is the force and A_o the initial cross-sectional area. By substitution of equation (2.12) in (2.10), we obtain

$$\frac{\partial \lambda}{\partial t} + P\lambda = Q \tag{2.13}$$

Where

$$P = \frac{\dot{\varepsilon}}{1+\varepsilon} - \frac{\partial g}{\partial \varepsilon} - \frac{\sigma}{1+\varepsilon}\frac{\partial g}{\varepsilon} \tag{2.14}$$

and

$$Q = -\frac{\sigma}{1+\varepsilon}\frac{\partial g}{\partial \sigma}\frac{1}{A_o}\frac{\partial A_o}{\partial x} \tag{2.15}$$

It follows from (2.13) that in the stable region, where $P < 0$, the strain gradient λ is at any instant tending asymptotically towards a value which depends on the initial non-uniformity of the specimen. A strongly rate-dependent material will show a less rapid movement towards a limiting value.

Jonas et al (1976) extended Hart's criterion, equation (2.7), to allow compressive deformations. Generally, the former constructions cannot be applied to this type of deformation, because the rate of work hardening is usually positive, and hence its effects on the load carrying ability of the sample supplements the rate of increase in cross-section. Instability will be achieved if the rate of flow softening exceeds the rate of area increase. In order to verify those criteria, a sign convention was established, F, σ, ε and $\dot{\varepsilon}$ are negative, m, A and $\dot{A}$ are positive, and, in flow softening materials, $\partial\sigma/\partial\varepsilon$ is first positive and then negative, whereas $\dot{F}$ and γ are first negative and then positive. Their work is summarised in figure 1. For the case of tension, Hart's criterion is achieved after the one proposed by Considère, due to the effect of

the strain rate sensitivity. In figure 1 b.), the case of compression is exemplified. In this case, Considère's criterion is achieved before the one proposed by Hart. It is interesting to notice (Jonas and Baudelet, 1977) that both criteria are not in conflict, but describe different stages in strain concentration.

Other authors (Demeri and Conrad, 1978) considered two elements of slightly unequal length, a and b, where b is longer than a. The non-uniformity in length, $\delta\ell$, for the two elements is given by

$$\delta\ell = \ell_b - \ell_a > 0 \tag{2.16}$$

During plastic flow, the extension rates for the two elements are

$$\dot{\ell}_a = d\ell_a/dt \quad \text{and} \quad \dot{\ell}_b = d\ell_b/dt \tag{2.17}$$

It is considered that non-uniformity will grow if $\dot{\ell}_b - \dot{\ell}_a > 0$. In that case, local plastic flow will be called unstable when

$$\delta\dot{\ell}/\delta\ell < 0 \tag{2.18}$$

Taking into account equations (2.3) and (2.5), the criterion can be written as

$$\gamma + m\alpha = 1 \tag{2.19}$$

which is similar to (2.8) with the parameter $\alpha = \delta \ln\dot{\varepsilon}/\delta\varepsilon$, that represents the elongation stability.

The case of flow instability in torsion is analysed by Semiatin and Lahoti (1981a). They consider that the applied torque, M, is a function of the amount of twist, θ, twisting rate, $\dot{\theta}$, and temperature, T.

$$dM = \frac{\partial M}{\partial \theta} d\theta + \frac{\partial M}{\partial \dot{\theta}} d\dot{\theta} + \frac{\partial M}{\partial \theta} dT \tag{2.20}$$

At a fixed θ, the normalised torque hardening rate, β, is given by

$$\beta = \frac{1}{M}\frac{dM}{d\theta} = \left(\frac{\partial M}{\partial \theta}\, d\theta + \frac{\partial M}{\partial T}\, dT\right)\frac{1}{M d\theta} \tag{2.21}$$

with this relation (2.20) can be rewritten as

$$dM = \beta M d\theta + \frac{M}{\dot{\theta}}\frac{\partial \ln M}{\partial \ln \dot{\theta}}\, d\dot{\theta} \tag{2.22}$$

With the aid of equivalent stress and strain, the strain rate sensitivity can be expressed as

$$m = \frac{\partial \ln \sigma}{\partial \ln \dot{\varepsilon}} \simeq \frac{\partial \ln M}{\partial \ln \dot{\theta}} \tag{2.23}$$

The onset of instability under torsion conditions, equation (2.5) can be rewritten as

$$dM = 0 = \beta M\, d\theta + (M/\dot{\theta})m\, d\dot{\theta} \tag{2.24}$$

So the criterion can be written as

$$\beta M + (M/\dot{\theta})m = 1 \tag{2.25}$$

A further analysis along the lines established by Hart (1967), was formulated by Ferron and Mliha-Touati (1982). This analysis departs from the differential equation (2.5) written as

$$d\ln\sigma = \gamma\, d\varepsilon + m d\ln\dot{\varepsilon} \tag{2.26}$$

where $m = f(\sigma,\dot{\varepsilon})$ and $\gamma = g(\sigma,\dot{\varepsilon})$ are the strain rate sensitivity and the work hardening coefficient. They established as a condition that the values of stress and strain rate when $\gamma = 1$ follow a relationship of the form

$$\sigma = \alpha \dot{\varepsilon}^{\mu} \tag{2.27}$$

where α and μ are constants. They describe a further parameter, β, relating the structural changes for a particular deformation history. If the strain rate sensitivity is constant, the equation for the line of constant structure is given by

$$\sigma = \alpha\beta^{\mu-m} \dot{\varepsilon}^{m} \tag{2.28}$$

Taking into account that $\partial \ln\beta/\partial \ln\dot{\varepsilon} = 0$ for any particular deformation history, equation (2.28) yields to

$$\gamma = (\mu-m)\frac{d\ln\beta}{d\varepsilon} \tag{2.29}$$

Under constant strain rate and with $\mu = 1$, this last equation is transformed into equation (2.8).

Other authors (Huntchinson and Neale, 1977; Ghosch, 1978) assume that an imperfection is defined by the cross-sectional decrement in figure 2. It is assumed that the cross-sectional area at the imperfection is less than that outside by a fraction, f, such that for axial load equilibrium

$$\sigma_i(1-f)A_o\exp(-\varepsilon_i) = \sigma_h A_o \exp(-\varepsilon_h) \tag{2.30}$$

where σ_h, σ_i and ε_h, ε_i are the stresses and strains, respectively inside and outside the imperfection. They use two constitutive laws in order to evaluate a numerical solution of (2.30):

$$\sigma = k\varepsilon^{n}\dot{\varepsilon}^{m} \tag{2.31}$$

and

$$\sigma = k[\varepsilon^{n} + m\ln(\dot{\varepsilon}/\dot{\varepsilon}_o)] \tag{2.32}$$

where k refers to a strength coefficient, n is the strain hardening exponent, m the strain rate sensitivity and $\dot{\varepsilon}_o$ is a reference strain rate at which strain

rate hardening is negligible. They used equation (2.31) for a long wavelength approach, ignoring interaction between the deformation elements and simply consider two regions, an imperfection and the otherwise homogeneous specimen, and equation (2.32) for small wavelength analysis, considering many slices, and their iteration leading to a gradual departure from uniaxiality.

2.2.2. Physical criteria.

Violan (1972, 1973) considers that the plastic deformation of a metal is carried out by the heterogeneous creation and displacement of dislocations. He considers that at any given instant and at a point x of the longitudinal axis there exists a gradient, χ, of a density of dislocations, ρ

$$\chi = \partial\rho/\partial x \tag{2.33}$$

He considers that the density of dislocations depends only on the strain and the relation:

$$\sigma = \sigma_i + \sigma^* \tag{2.34}$$

where σ_i is the internal stress depending on the density of dislocations and σ^* is the active stress, and that

$$\dot{\varepsilon} = \alpha\rho_m b v \tag{2.35}$$

where ρ_m is the density of mobile dislocations, b the Burgers vector, v the dislocations velocity and α a constant. His criterion is given by the expression

$$0 > \frac{1}{\chi}\frac{\partial\chi}{\partial t} \tag{2.36}$$

Assuming that in tension, at any instant and position, the force is the same along the specimen, we get

$$0 = \frac{1}{F}\frac{\partial F}{\partial x} = \frac{1}{\sigma}\frac{\partial \sigma}{\partial x} + \frac{1}{A}\frac{\partial A}{\partial x} \tag{2.37}$$

taking into account the constancy of volume, at any instant

$$\frac{\partial \varepsilon}{\partial x} = \frac{\partial \ln \sigma}{\partial x} \tag{2.38}$$

Assuming that the dislocation density depends only on the strain,

$$\chi = \frac{\partial \rho}{\partial \varepsilon}\frac{\partial \varepsilon}{\partial x} \tag{2.39}$$

and

$$\frac{\partial \chi}{\partial t} = \frac{\partial^2 \rho}{\partial t \partial x} = \frac{\partial \varepsilon}{\partial x}\frac{\partial^2 \rho}{\partial t \partial \varepsilon} + \frac{\partial \rho}{\partial \varepsilon}\frac{\partial^2 \varepsilon}{\partial t \partial x} \tag{2.40}$$

With the above equations, and after algebraical manipulations, the stability criterion is written as

$$\sigma < \frac{\partial \sigma_i}{\partial \rho}\frac{\partial \rho}{\partial \varepsilon} - \frac{\frac{\partial}{\partial \varepsilon}\left(\ln \rho_m \frac{\partial \rho}{\partial \varepsilon}\right)}{\frac{\partial}{\partial \sigma^*}\ln \rho_m v} \tag{2.41}$$

At high strains, assuming ρ_m constant and that ρ increases in the form

$$\rho = \rho_o[1 - k\exp(\varepsilon)] \tag{2.42}$$

where ρ_o and k are constants, and the active stress is given by (Gilman, 1968)

$$v = v_o \left(\frac{\sigma^*}{\sigma_o}\right)^{\eta} \tag{2.43}$$

where v_o, σ_o and η are constants, the stability criterion can be written as

$$\sigma < \frac{\partial \sigma_i}{\partial \rho} \frac{\partial \rho}{\partial \varepsilon} + \frac{\partial \sigma^*}{\partial \ln v} \tag{2.44}$$

With the help of (2.33) this can be written as

$$\frac{\partial \ln \sigma}{\partial \varepsilon} + \frac{\partial \ln \sigma}{\partial \ln v} > 1 \tag{2.45}$$

That is similar to equation (2.8) with a dislocation rate sensitivity.

Other authors (Malaprade et al, 1978; Rouby et al, 1979) present a thermodynamic interpretation of the criterion expressed by Hart (1967). Here, in the presence of a thermally activated jump of obstacles by dislocations, the strain rate is given by

$$\dot{\varepsilon} = \rho_m \Omega \exp(-\Delta G/kT) \tag{2.46}$$

where Ω is a constant, k the Boltzmann constant, ΔG is the free Gibbs activation energy for the jumping process, that in the case of rectangular barriers is given by the formula

$$\Delta G = \Delta G_o - \sigma v \tag{2.47}$$

where v is the activation volume, and ρ_m is the density of mobile dislocations, expressed by the relationship (Gilman, 1968)

$$\rho_m = (\rho_o + c\varepsilon)\exp(-\emptyset\varepsilon) \tag{2.48}$$

where ρ_o is the original dislocation density, c the dislocation multiplication factor and $\emptyset$ is the attrition coefficient of the mobile fraction of dislocations. With the aid of the former equations, equation (2.5) relating the general variation of the stress with strain and strain rate is written as

$$d\sigma = \frac{kT}{v\varepsilon} d\varepsilon - \frac{kT}{v} \left(\frac{c}{\rho_o + c\varepsilon} - \emptyset \right) d\varepsilon \tag{2.49}$$

In this way, equation (2.8) can be written as

$$\frac{kT}{v\sigma}\left(1 - \frac{c}{\beta\varepsilon} + \emptyset\right) > 1 \qquad (2.50)$$

where $\beta = \rho_o c$. From this equation, one can see that a decrease of the test temperature will tend to make the deformation more quickly unstable. Figure 3 shows previous results for ARMCO iron, with respect to the unstable-stable domain found for different grain sizes (Violan, 1973).

2.3. Equations Related to a General Solution.

Argon (1973) considered in detail the conditions of stability and strain localisation for pressure and strain rate sensitivity materials under adiabatic conditions for deformation. Phenomenologically, the strain rate, is given by an expression of the type

$$\varepsilon = \varepsilon_o \exp[-\Delta H(\sigma,\tau,p)/RT] \qquad (2.51)$$

where the pre-exponential ε_o is a product of the volume concentration of dislocation density, the volume of the local rearranging region and a frequency factor incorporating all components of the activation entropy of the process, σ, τ, and p are respectively the applied stress, the plastic resistance of the material, defined as the flow stress in shear at absolute zero and in the absence of any pressure, and the pressure, R the gas constant, T the temperature and ΔH is the activation enthalpy characteristic of the local rearrengement process. Changes in the applied stress, the pressure, the plastic resistance and temperature produce changes in the strain rate given by

$$d\varepsilon = \varepsilon_o \exp\left(-\frac{\Delta H}{RT}\right)\left[-\frac{1}{RT}\frac{\partial \Delta H}{\partial \sigma}d\sigma - \frac{1}{RT}\frac{\partial \Delta H}{\partial \tau}d\tau - \frac{1}{RT}\frac{\partial \Delta H}{\partial p}dp + \frac{\Delta H}{RT^2}dT\right] \tag{2.52}$$

when a local region undergoes plastic deformation only a small portion of the deformation work is stored and produces strain hardening, the major fraction, β, of it is converted into heat.

If the entire part deformed homogeneously, and no heat were lost to surroundings, the rate of temperature rise would be given by

$$\frac{dT}{dt} = \frac{\beta \sigma \dot{\varepsilon}}{\rho c} \tag{2.53}$$

where ρ is the material density and c its specific heat. In the case of heterogeneous deformation, in bands of thickness h, and heat conduction out of such bands, the rate of temperature rise is depressed by a high thermal diffusivity, $\alpha = k/\rho c$, where k is the thermal conductivity, and accentuated by the square of the band thickness and the reciprocal of the time for deformation, $\dot{\varepsilon}/\varepsilon$, considering

$$\frac{dT}{dt} \simeq \frac{\beta \sigma \dot{\varepsilon}}{\rho c}\,\frac{\rho c}{k}\,\frac{h^2 \dot{\varepsilon}}{\varepsilon} = \frac{\beta \sigma \dot{\varepsilon} h^2}{k\varepsilon}\dot{\varepsilon} \tag{2.54}$$

is an adequate representation of the local adiabatic heating effect. With the incorporation of equation (2.52), the fundamental equation of the process can be written as

$$\frac{d\dot{\varepsilon}}{d\varepsilon} = -\frac{1}{RT}\frac{\partial \Delta H}{\partial \sigma}\dot{\sigma} - \frac{1}{RT}\frac{\partial \Delta H}{\partial p}\dot{p} + \left(-\frac{1}{RT}\frac{\partial \Delta H}{\partial \tau}\frac{\partial \tau}{\partial \varepsilon} + \frac{\Delta H}{RT}\frac{\sigma \dot{\varepsilon} \beta h^2}{k\varepsilon T}\right)\dot{\varepsilon} \tag{2.55}$$

Differentiation of equation (2.51) yields

$$\frac{\partial \Delta H}{\partial \sigma} = \frac{1}{\sigma}\frac{\partial \Delta H}{\partial \ln \sigma} = -\frac{RT}{m\sigma} \tag{2.56}$$

where m is the strain rate sensitivity as defined by Hart (1967). Assuming that the activation enthalpy is a function of the ratio of the shear stress to the plastic resistance and that the pressure affects the rearrangement only through its effect on the plastic resistance, equation (2.55) can be written as

$$\frac{d\dot{\varepsilon}}{d\varepsilon} = \frac{1}{m}\frac{\dot{\sigma}}{\sigma} - \frac{1}{m}\frac{\partial \ln \tau}{\partial \ln p}\frac{\dot{p}}{p} + \left(-\frac{1}{m\tau}\frac{\partial \tau}{\partial \varepsilon} + \theta\right)\dot{\varepsilon} \tag{2.57}$$

where θ is the adiabatic heating term $(\Delta H/RT)(\beta\sigma\varepsilon h^2/k\varepsilon T)$. In experiments performed at constant strain rate, the criterion for a maximum in load is given by

$$\frac{1}{m} - \left(1 - \frac{\partial \ln \tau}{\partial \ln p} - \frac{1}{\tau}\frac{\partial \tau}{\partial \varepsilon}\right) + 1 + \theta = 0 \tag{2.58}$$

In the special case where the pressure dependence of the plastic resistance is negligible and the adiabatic heating effect can be ignored the result is

$$1 - \frac{\partial \ln \tau}{\partial \varepsilon} + m = 0 \tag{2.59}$$

which looks like equation (2.8) with the difference that the condition involves the plastic resistance and not the applied stress.

Lin et al (1981) used a very similar approach to that described by Ferron and Mliha-Touati (1982), section 2.2.1, for the case of tensile tests. Here, the plastic strain, the cross-sectional area, and their time rates of change are given by

$$d\varepsilon - d\varepsilon_o = d\ln A_o - d\ln A \tag{2.60}$$

and

$$\dot{\varepsilon} = -\dot{A}/A \tag{2.61}$$

where ε_o and A_o are the initial values for strain and cross-sectional area. Combining equations (2.5), (2.60) and (2.61) it is found that

$$m \frac{d\ln\varepsilon}{d\varepsilon} = \frac{d\ln\sigma}{d\sigma} - \gamma = \frac{d\ln F}{d\varepsilon} + 1 - \gamma \tag{2.62}$$

where F is the load. From those relations, and with the relationship (Kocks et al, 1979)

$$\frac{\partial^2 \ln A}{\partial\varepsilon\,\partial x} = \frac{\partial \ln\dot{\varepsilon}}{\partial x} \tag{2.63}$$

where x is the distance along the axis in the tensile specimen, the differential equation is deduced

$$\begin{aligned}\frac{\partial^2 \ln A}{\partial\varepsilon\,\partial x} &= -\frac{\partial\ln\varepsilon}{\partial\varepsilon}\frac{\partial\varepsilon}{\partial x} + \frac{\partial\ln\varepsilon}{\partial\ln\sigma}\frac{\partial\ln\sigma}{\partial x} \\ &= \frac{\gamma}{m}\frac{\partial\varepsilon}{\partial x} - \frac{1}{m}\frac{\partial\ln\sigma}{\partial x} \\ &= \frac{1}{m}\left[(1-\gamma)\frac{\partial\ln A}{\partial x} + \gamma\left(\frac{\partial\ln A_o}{\partial x} + \frac{\partial\varepsilon_o}{\partial x}\right) - \frac{\partial\ln F}{\partial x}\right]\end{aligned} \tag{2.64}$$

If the load F is uniform and m and γ are constants (Hart, 1967), the solution of the equation is

$$\frac{\partial \ln A}{\partial x} = \frac{\gamma(d\ln A_o/dx + d\varepsilon_o/dx)}{1-\gamma} \exp \frac{1-\gamma}{m} (\varepsilon - \varepsilon_o) - \frac{\gamma}{1-\gamma}\left(\frac{\partial \ln A_o}{\partial x} + \frac{d\varepsilon_o}{dx}\right) \tag{2.65}$$

This equation shows that the gradient ($\partial \ln A/\partial x$) increases infinitely with strain if $\gamma < 1$, but that the specimen remains approximately uniform as straining continues if $\gamma > 1$.

Other authors (Kocks et al 1978, 1979; Kocks, 1981) refute the former analysis (Lin et al, 1981) because m and γ are not material properties depending only on the current state, but they also depend on the history of each cross-section. This is avoided if the time gradients for stress, strain and strain rate in one material element are taken into account. In this case, equation (2.5) is written as

$$m \frac{\partial \ln \varepsilon}{\partial t} = \frac{\partial \ln \sigma}{\partial t} - \gamma \dot{\varepsilon} \tag{2.66}$$

where m and γ are now material properties depending only on the current state, not on the deformation path. A description of gradients in stress, strain and strain rate along the specimen can now be obtained by differentiation of equation (2.66) with the position x. One obtains (Kocks et al, 1979; Kocks, 1981) the equation

$$m \frac{\partial^2 \gamma}{\partial \varepsilon^2} + (\gamma - 1 + \beta) \frac{\partial \gamma}{\partial \varepsilon} - \eta \gamma = 0 \tag{2.67}$$

where $\gamma = -\partial \ln A/\partial x$ describes the relative gradient in cross-sectional area along the specimen; its derivative with respect to strain is equivalent to the strain rate gradient along the specimen

$$\frac{\partial Y}{\partial \varepsilon} = \frac{\partial \ln \dot{\varepsilon}}{\partial x} \tag{2.68}$$

$\beta = \partial Y/\partial \ln \dot{\varepsilon}$ and $\eta = -\partial Y/\partial \ln \sigma$ represent the dependence of the strain hardening coefficient on strain rate and stress. From equation (2.69), a general differential equation for the development of non-uniform deformation becomes (Kocks, 1981)

$$\frac{\partial^2 \ln \dot{\varepsilon}}{\partial \varepsilon \partial x} + (\delta + b) \frac{\partial \ln \dot{\varepsilon}}{\partial x} = -\frac{1}{m} \frac{\partial \ln A}{\partial \varepsilon} - c \frac{\partial \ln A}{\partial x} \tag{2.69}$$

where $\delta = -\partial \ln \dot{\varepsilon}/\partial \varepsilon$ is the deceleration in a creep test, $b = \partial \delta/\partial \ln \dot{\varepsilon}$ and $c = \partial \delta/\partial \ln \sigma$ represent the dependence of this deceleration on strain rate and stress.

The importance of the parameter δ, is shown in figure 4, in the which the developement of the strain gradient ε' with strain for a deformation defect, characterized by a constant initial strain gradient ε'_o. the growth occurs only for $\delta < 0$ but decay is slow for small positive values of this parameter. Figure 5 shows a schematic solution for equation (2.67). One branch corresponds to the evolution of the area gradient due to geometrical defects and the other corresponds to deformation defects.

2.4. Evolution of Plastic Flow.

Jonas and Baudelet (1977) considered an approach similar to that of Campbell (1967), deriving an equation for plastic stability valid in the presence of both mechanical and geometrical defects. Extending the model to include the generation by deformation of spherical cavities and planar cracks.

They found that the effect of machining defects is higher than the effect caused by mechanical defects, considering that the former ones will grow from the initiation of plastic deformation. Generation of spherical cavities or voids and planar cracks during straining increase the tendency towards tensile instability by reducing the effective values of the work hardening coefficient and the rate sensitivity. Void generation also diminishes the reduction in area at fracture.

In other works (Jalinier et al, 1978; Canova et al, 1980), it was considered that the flow can be divided in four different stages, figure 6. In the first stage, the flow is stable, is an interval of defect healing, the strain rate gradients decrease, until a certain strain, ε_k, is reached in the low defect gradient parts of the specimen (Jonas et al, 1976), and this condition is propagated toward the region of steepest strength or area gradients. The second stage corresponds to a very slow localisation. After the last part of the specimen exceeds ε_k and continues until the narrowest part reaches the Considère strain, ε_c. Stage three corresponds to unstable flow concentration, here, Considère's criterion is first reached in the neck and is propagated to the bulk. If the strain rate sensitivity is low or the strength gradient is high, failure can occur before the macroscopic strain reaches the Considère value. Complete flow localisation is reached in the fourth stage, this is achieved when the forming limit is reached in the bulk.

Semiatin and Lahoti (1982, 1983) considered the case of flow localisation of one and two phases titanium alloys under isothermal and nonisothermal sidepressing of cylindrical specimens. In a treatment similar to that of Jonas et al (1976), they reached an expression for the rate of flow localisation, α (Semiatin and Lahoti, 1981)

$$\frac{1}{\varepsilon}\frac{d\varepsilon}{d\sigma} = -\frac{\gamma}{m} = \alpha \qquad (2.70)$$

In agreement with Jonas et al (1976), they predict that materials with α greater than or equal to five are susceptible to persistent flow localisation.

2.5. Conclusions.

As was pointed before (Jonas et al, 1976), the different criteria for instability depend on the actual parameter used to measure the instability, in the testing conditions, and, in general, represent different stages of strain localisation. Figure 7 from Demeri and Conrad (1978), shows the variation for three different criteria. In a material insensitive to the strain rate, the criteria are the same. Furthermore, the criteria are based on different testing conditions, Hart (1967) based his analysis in results from tensile tests, Jonas et al (1976) analysis is based in materials tested under compressive conditions, that present negative strain hardening, and the one by Demeri and Conrad (1978) is based in the gradient concentration along the length of a sheet tested under plane stress conditions.

The influence of the testing conditions arises mainly from the macroscopic features related to the plastic instability. In the case of tensile samples (Considère, 1885; Campbell, 1967; Hart, 1967) or in sheet stretching (Conrad, 1978; Demeri and Conrad, 1978; Needleman, 1978), the instability is associated with the onset of the necking. In the case of axysimmetric compression (Jonas et al, 1976; Kocks, 1980; Semiatin and Lahoti, 1981), the result of the instability is the bulging or barreling in the specimen. In torsion (Kocks, 1980; Semiatin and Lahoti, 1981a), in which the dimensions of the specimen remain constant, the instability is associated with the formation of rings along the gauge length of the specimen. In the more complex case of sidepressing (Semiatin and Lahoti,

1982, 1983), where the material deforms under plane strain conditions, the strain localisation follows the line of maximum shear given as a solution of the slip line field.

The instability is associated with the appearance of a local maximum in a stress strain curve. Under these conditions, metallurgical phenomena like Lüders band formation (Violan, 1972, 1973; Kocks, 1980) or jerky flow (Kocks, 1980) have been analysed successfully. It is interesting to notice that under those former assumptions, dynamic restoration processes, multiple phase deformation and adiabatic heating can be treated from the point of view of instability formation.

Chapter 3.

Instability in Testing Techniques.

3.1. Introduction.

In the former chapter, the criteria established to determine the onset of instability were discussed. Those criteria are based on the existence of a maximum in load in the load-displacement curves obtained in laboratory testing.

The laboratory methods of assessing properties during hot forming are essentially tension, axisymmetric or plane strain compression or torsion. The general merits and limitations of each method have been reviewed previously (McQueen and Jonas, 1971; Sellars and Tegart, 1972; Ahlblom and Sandström, 1982; Nester and Pohland, 1982), and this review will be concerned mainly with phenomena induced by strain localisation during hot working.

3.2. Tension.

In the hot tensile test, necking is the main drawback. It is recognized that if the temperature gradient within the specimen is moderate, it is possible to deform the specimen up to strains of around 0.3 (McQueen and Jonas, 1971). Recently some authors (Plaut and Sellars, 1983) have shown that strains of the order of 1.5 can be deduced if it is considered that the material being strained obeys an equation of state.

It was established (Avery and Backofen, 1965; Hart, 1967) that a large amount of neck-free elongation is related to a high strain rate sensitivity, m. Woodford (1968) measured the total elongation in different metals and alloys under tensile and creep conditions and then related it to the strain rate sensitivity. He assumed that the total elongation values will describe the effect of the strain rate on the deformation mechanisms and does not include an effect on structure. In figure 8 appears a plot of the strain rate sensitivity versus elongation at rupture for a number of different materials. As can be seen, a correlation can be obtained, not withstanding the uncertainties of the sensitivity and the elongation. Due to the high uncertainty in measuring the elongation at the fracture, the reduction of area is taken as a measure of ductility in hot tensile testing (Ahlblom and Sandström, 1982).

Figure 9 shows the effect of strain rate on ductility for a 18Cr-8Ni steel (Gittins et al, 1973). The curve for the specimens tested at 1100 C present a maximum reduction in area around strain rates of 1 sec^{-1}. The low ductility presented at low strain rates is assumed to be due to increase of grain boundary sliding. Around strain rates of 1 sec^{-1}, the material undergoes dynamic recrystallisation before rupture, increasing the ductility (Ahlblom, 1977). At higher strain rates dynamic recrystallisation is probably too slow to be important (Ahlblom, 1977; Ahlblom and Sandström, 1982).

Figure 10 a.) compares stress-strain curves for lead, at room temperature and low strain rates, tested under tension and torsion (Sellars et al, 1976). It can be seen that the values of strain and stress to the peak are comparable. However, inspection of the curves after the first peak shows difference in the rate of fall of the flow stress; this being steeper for tension that for torsion. This can be attributed to the instability of deformation when the work softening associated with dynamic recrystallisation takes place (Jonas and

Luton, 1978; Sellars, 1981). In tension, necks form in the first recrystallising sections and propagate along the specimen (Cottingham, 1968).

3.3. Compression.

This mode of deformation is more suitable for hot working studies since the stress system is closer to those found in deformation processing (McQueen and Jonas, 1971). For the achievement of constant strain rates, computer controlled servohydraulic systems are used for axisymmetric compression (Ahlblom, 1977; Roberts et al, 1979; Fitzsimons et al, 1981) and plane strain compression (Sellars et al, 1976; Pawelski et al, 1978; Beynon, 1979; Foster, 1981).

3.3.1. Axisymmetric compression.

In axial compression of a cylinder without friction at the die contact surfaces, the test specimen undergoes uniform deformation through its volume. No barreling of the cylindrical surfaces occurs and it can be shown that the circunferential and radial strains are tensile and equal to one half of the magnitude of the axial compressive strain. During axial compression with friction at the die contact surfaces, bulging, or barreling, of the free surfaces occurs and the stress and strain distributions are non-uniform (Jonas et al, 1976; Kocks, 1980). Increasing friction or decreasing the height to diameter ratio increases the bulge curvature and degree of non-uniformity (Kuhn, 1978, 1978a; Fitzsimons et al, 1981).

Korbel and Blaz (1980) testing copper found that local oscillations in strain rate occurred in conjunction with stress oscillations, typical of local dynamic recrystallisation. They concluded that mechanical instabilities

reflected in the load, or stress, were connected with nucleation of broad slip bands that seemed to transverse the specimen like Lüders bands. For specimens that did not present load oscillations, no strain rate oscillations were present.

In work with titanium alloys (Semiatin and Lahoti, 1981), it was found that in non-isothermal tests, the strain was localised towards the centre of the specimen, due to the chilling effect over the contact surfaces. Strain concentration was found in a titanium α-β alloy tested under isothermal conditions.

Other authors (Mataya and Krauss, 1981; Mataya et al, 1982) used cylindrical specimens that featured a reduced gauge section where deformation was concentrated. Due to the special geometry, an apparent reduction in the testing volume is developed in the specimen, penetration of the reduced section on the bulk specimen occurs. The ratio of the initial and final reduced gauge volumen is considered to be a measure of the propensity for flow localisation in the material during hot working.

Abdul and Bramley (1973) suggested the testing of annular specimens to calculate stress-strain curves and avoid friction effects, but it is limited by the precision in measuring the rings.

3.3.2. Plane strain compression.

This method has been used less for simulation, although it offers the advantage of having the same mode of deformation as in rolling (Sellars, 1981). An advantage of this test over axisymmetric compression is that the error introduced into the stress and strain calculations is small due to the small change of geometry in contact with the working tools. In axisymmetric compression, the area in contact with the dies increases as the height

decreases, and, in general, the area increase is calculated as a function of the constancy of volume over the whole specimen.

Theoretically, the slip line field for plane strain compression should lie at 45° (Rowe, 1965). Figure 11 represents slip line field solutions for different friction and geometry conditions (Loong, 1976). As can be seen, an increase in the friction coefficient increases the divergence between the main fan axis and the vertical, supporting recent results by Anand and Spitzig (1982).

The complexity of the strain distribution (Beynon, 1979; Beynon and Sellars, 1983; Puchi, 1983) may permit explanation of the difference between the curves in figures 12 and 13, for lead (Sellars et al, 1976), and niobium bearing steel (Foster, 1981) tested with different initial geometries.

Figure 14 shows the strain distribution along the centre line of lead specimens with width over height ratios of a.) 1.6 and b.) 3.0 (Sellars et al, 1976). As can be seen, the strain distribution is a function of the initial geometry. Figure 15 represents the strain distribution within a quarter of a lead specimen tested at room temperature (Sellars et al, 1976).

Figure 10 b.) shows stress-strain curves for lead tested at room temperature at high strain rates. The cases of axisymmetric and plane strain compression and torsion are compared. It can be seen that both compressive tests yield a less steep decrease in stress after the maximum is achieved; the decrease being less steep for plane strain compression. This seems to indicate no instability associated with dynamic recrystallisation for the plane strain tests (Sellars, 1981). Recent results by Barbosa (1983) and Puchi (1983) show that the kinetics of static recrystallisation after deformation in plane strain compression are strongly position dependent.

Other research (Semiatin and Lahoti, 1982, 1983) on titanium alloys suggests that a very strong strain gradient developed in plane strain compression. They found that isothermal and non-isothermal tests presented strain localisation similar to the concentration presented in non-isothermal axisymmetric tests. Work by Chandra et al (1979, 1982) describe the creation of high angle boundaries, in specific regions, after high strains in aluminium deformed under plane strain compression at high temperature.

3.4. Torsion.

This mode of deformation is widely used because of the high strains that can be achieved. The difficulties with the torsion tests arise from the gradient in strain, stress and strain rate from the axis to the surface (Rossard and Blain, 1958; Rossard, 1960; McQueen and Jonas, 1971; Barraclough et al, 1973).

A wide array of specimen geometries has been employed. Barraclough et al (1973) did a systematic study on the effect of variation of the specimen geometry on the stress-strain curves for a wide range of alloys. They concluded that for materials that only exhibit dynamic recovery, the gauge length over radius ratio has little effect on the stress-strain curves. For materials that present dynamic recrystallisation, the strain to the maximum stress increases as the gauge length over radius ratio is reduced below 2:1. At high strain rates, it was concluded that the effect of adiabatic heating was greater as the length over radius ratio was increased.

White and Rossard (1968) show an exponential relationship between the ductility, measured in revolutions to fracture, and the strain rate, reported in revolutions per minute, for a Fe-36Ni alloy. Nikkilä (1972) found that in two

stainless steels, the hot ductility increased with increasing strain rate. Barraclough et al (1973) found that the strain to failure was independent of the gauge length over radius ratio provided a correction was made for deformation penetrating into the fillets between the parallel gauge length and the shoulders.

Results from Lombry et al (1979) on ferritic steels show that at high strains, the deformation was concentrated in specific regions of the material being tested, causing a transformation from low to high angle in some subgrain boundaries.

In figures 10 a.) and b.), the stress-strain curves obtained for lead at low and high strain rates are compared with those of other methods. Comparing the rate of stress decrease after the first maximum in stress, it can be seen that the case of torsion lies between the tension and compression cases. In torsion, banding occurs (Sah et al, 1973; Semiatin and Lahoti, 1981a) along the length of the specimen with "discs" recrystallising at different rates (Sah et al, 1973), and deformation concentrated in different discs.

3.5. Bending.

This method was used by Nicholson et al (1968) in order to determine surface cracking during hot working. More recently, this method has been used at high temperatures by a limited number of researchers (Kuhn, 1978, 1978a; Fitzsimons et al, 1981). The strains in bending are similar to those at the barreled surfaces in axisymmetric compression (Fitzsimons et al, 1981). It is claimed that this test is useful when the work piece to be evaluated is not cylindrical or when the desired tensile stress orientation cannot be obtained by

compression (Kuhn, 1978a).

3.6. Conclusions.

From the works reviewed, it can be concluded that the plastic deformation is not carried out under homogeneous conditions. The degree of heterogeneity depends on the testing method (Barraclough et al, 1973; Mataya and Krauss, 1981; Fitzsimons et al, 1981; Semiatin and Lahoti, 1982, 1983), and on the material being tested (Barraclough et al, 1973; Sellars et al, 1976; Semiatin and Lahoti, 1981, 1981).

In materials in which dynamic recovery is the only operative process, the material deforms homogeneously, and stress-strain curves obtained under different testing conditions can be compared with each other (Barraclough et al, 1973). At high strain, and under severe deformation conditions, heterogeneous deformation, characterized by the formation of high angle boundaries within one grain, occurs in materials that recover dynamically (Chandra et al, 1979, 1982; Lombry et al, 1979). In materials that recrystallise dynamically, the deformation will be localised in the regions in which the critical value for the achievement of the process is obtained (Cottingham, 1968; Korbel and Blaz, 1980; Mataya and Krauss, 1981; Mataya et al, 1982).

Under dynamic recrystallisation conditions, the degree of localisation decreases from tension to torsion to compression (Sellars, 1981). In tension, the localisation is achieved first in the neck and then extends to the rest of the specimen (Cottingham, 1968). In torsion, the instability is created in discs along the gauge section (Sah et al, 1973). In axisymmetric compression, the dynamically recrystallised material lies in broad lines. In the case of plane

strain, recent work by Barbosa (1983) suggests that the localisation is in function of the theoretical slip line field solution.

Chapter 4.

Dynamic Restoration Processes.

4.1. Introduction.

In Chapter 2, it was indicated that instabilities in mechanical testing are associated with the presence of local maxima of stress in a stress-strain curve. At high temperatures, those local maxima in stress are found under dynamic restoration conditions.

Reviews dealing with the generic conditions under which those processes develop have been published by several authors (Jonas et al, 1969; Sellars and Tegart, 1972; Jonas and McQueen, 1975; Tegart and Gittins, 1977; Mecking and Gottstein, 1978; McQueen and Baudelet, 1979; Sellars, 1978). Here, strain localisation, and phenomena related with it, in the course of the dynamic restoration processes will be discussed.

4.2. Dynamic Recovery.

When a recrystallised metal is loaded at constant nominal strain rate, the resultant flow curve can be divided in various parts. In the first one, the work hardening rate decreases, until finally, in the last part or steady state region the net rate of work hardening is zero, figure 16. The steady state regime is characterized by the constancy of stress, at constant temperature and strain rate.

It should be noted that the simple shape of the flow curves illustrated in the previous figure is found when the softening is limited to dynamic recovery processes. In practice, the shape of the curve may be altered as a result of the operation of other mechanisms (Jonas and Luton, 1978; Mecking and Grinberg, 1979; Korbel et al, 1983).

4.2.1. Microstructural developments.

During the stage of positive strain hardening, dislocations become entangled and begin to form a cellular structure. By the time the steady state regime is achieved, the dislocations will have arranged themselves into subgrains whose perfection, dimensions and misorientation depend on the metal, and on the strain rate and temperature of deformation (Jonas et al, 1969). The generation rate is a function of the strain rate and the associated effective stress. The rate of annihilation depends on the dislocation density, and on the easiness of operation of the recovery mechanisms (Jonas and McQueen, 1975).

In steady state deformation, the subgrains appear equiaxed even at large strains, whereas the grains deformed in conformity with the outward change of shape of the object (Farag et al, 1968; Jonas et al, 1968, 1969). This cannot be explained solely by migration of the subboundaries, since not all of them are capable of migrating, and it has been shown that such migration contributes only to 6 to 10% of the strain (Exell and Warrington, 1972). The stable subgrain size depends on the equilibrium dislocation density (Holt, 1970; Roberts and Ahlblom, 1978), which is established by the balance between generation and annihilation rates.

The typical parameters which represent the geometry of the cell structure are the cell size, the misorientation angle across the boundaries and the thickness of the walls themselves (Mecking and Gottstein, 1978). At low

deformation temperatures, the cell walls occupy almost the same volume as the interior of the cells. The misorientation angle is of the order of a few degrees. With increasing deformation temperature, the cells transform into subgrains, the boundaries sharpen and the size increases while the misorientation does not seem to change (McQueen et al, 1967; Mecking and Gottstein, 1978).

4.2.2. High strain instabilities

At high strains and under severe strain conditions, a heterogeneous structure, consisting of grains with a wide spectrum of strain, has been recognized to take place (Lloyd and Kenny, 1978; Mecking and Grinberg, 1979; Korbel et al, 1983).

In recent work, Chandra et al (1979, 1982) in aluminium single-crystals, and Lombry et al (1979) in ferritic steels determined that the misorientations between individual subgrains and their neighbours was transformed from a low angle to a high angle relationship. In the case of aluminium, it was found after deformation under plane strain compression, and in specimens with a strong orientation (Chandra et al, 1979). The size and the interior of those special subgrains were similar to other subgrains with low angle boundaries within the specimen. The high angle boundaries presented a tendency to be distributed in elongated, but fragmented, bands (Chandra et al, 1982).

In the case of the ferritic steels (Lombry et al, 1979), some new grains with size of 20 to 30 μm were created within the original grains of size 150 to 180 μm. The original grain boundaries, with misorientations between 15 to 20° remained, the new grains presenting a misorientation of 5 to 15°.

The development of those high angle boundaries has made other authors (Sheppard and Tutcher, 1980; Belyayev et al, 1981) call this process dynamic recrystallisation, but, formally, it cannot be considered recrystallisation if the high angle boundaries are created by recovery mechanisms of dislocation annihilation without involving a mobile grain boundary.

4.3. Dynamic Recrystallisation.

This phenomenon is characteristic of metals and alloys with low stacking fault energy in which dynamic recovery processes alone are unable to reduce the dislocation density to stable levels during flow. The higher rate of dislocation accumulation in these materials favours the nucleation of new grains during deformation and also provides higher driving forces for recrystallisation (Jonas and McQueen, 1975; Jonas and Luton; 1978).

4.3.1. The flow curve.

The nucleation of the new grains, and therefore the initiation of dynamic recrystallisation, involves a critical strain. In hot deformed single-crystals, this strain is easily identify by the sharp drop in flow stress, figure 17. In polycrystals, at high strain rates or low temperature, the flow stress rises to a maximum at the peak strain, ε_p. After that, as result of dynamic recrystallisation, it diminishes to a value intermediate between the yield stress and the maximum or peak stress. At lower strain rates or higher homologous temperature, the softening produced by dynamic recrystallisation is followed by renewed hardening and a cyclic flow curve of approximately constant period but declining amplitude is traced instead. The effect of decreasing the

strain rate on the shape of flow curves is shown in more detail in figure 18 a). Figure 18 b) showns the effect of increase of temperature.

Luton and Sellars (1969) explained the different behaviours associated with concurrent dynamic recrystallisation in terms of the relative values of the critical strain to the onset of recrystallisation, ε_c, and the strain required to recrystallise a large fraction of the material, ε_x. With respect to the value of the temperature compensated strain rate or Zener-Hollomon parameter, Z, given by the relationship

$$Z = \dot{\varepsilon} \exp(Q/RT) \tag{4.1}$$

where $\dot{\varepsilon}$ is the strain rate, Q the activation energy of the process and R and T are respectively the gas constant and the temperature. At low values of Z, $\varepsilon_x << \varepsilon_c$ and once recrystallisation is initiated, it goes rapidly to completion before those regions which transformed initially can harden sufficiently to effect nucleation a second time, figure 19a). If $\varepsilon_x > \varepsilon_c$, high Z, then several recrystallisation cycles can occur simultaneously and the curve is smoothed out, figure 19b).

4.3.2. Strain to the peak in stress.

The critical strain for the start of recrystallisation is actually slightly less than the peak strain, because, while the first nuclei are softening the material locally, the remaining material continues to become stronger (Jonas and McQueen, 1975; Ahlblom, 1977; Roberts and Ahlblom, 1978; Roberts et al, 1979). According to Rossard (1973), the critical strain and the strain to the peak follow the relationship

$$\varepsilon_c \simeq 5\varepsilon_p/6 \simeq 0.83\varepsilon_p \tag{4.2}$$

From results on nickel (Richardson et al, 1965; Luton and Sellars, 1968), the critical strain is found to pass through a minimum as function of the stress, figure 20. The rising curve at high stresses appears to result from the need for increasing stored energy with increasing strain rate to ensure that boundary migration is sufficiently rapid for growth of the nuclei to occur at all before the dislocation density behind the moving boundary has been increased sufficiently by concurrent deformation to destroy the driving force (Sellars, 1978). Over the same range of stress, the strain that takes place during recrystallisation increases continously, leading to the change form periodic to smooth flow curves. Observations on ferrite (Glover and Sellars, 1973) have shown the existence of an upper stress limit for the occurrence of dynamic recrystallisation, and suggested that this occured when the critical strain is approximately equal to the one required to the achievement of the steady state by dynamic recovery alone.

Other authors (Sandström and Lagneborg, 1975; Ortner and Stüwe, 1976; Roberts and Ahlblom, 1978) have developed recrystallisation criteria based in the effect of the dislocation density gradient within the material. They propose that the driving force of the process is the difference in the densities of dislocations on the two sides of the sweeping mobile boundary.

It was proposed (Sandström and Lagneborg, 1975) that the flow stress is determined by the density of intra-subgrain dislocations in the usual way

$$\sigma = \alpha\mu b\sqrt{\rho_i} \qquad (4.3)$$

where α is a dislocation strengthening parameter, μ the shear modulus, b the Burgers vector and ρ_i is the density of the intra-subgrain dislocations. However, the dislocation density in subboundaries is so much greater than ρ_i that the latter can be neglected from the point of view of driving force for recrystallisation. On this basis, the critical dislocation density for dynamic

recrystallisation, ρ_c, and the stress to the peak, σ_p, can be related by (Roberts and Ahlblom, 1978)

$$\sigma_p = \alpha\mu b\sqrt{\rho_c \ell/\ell_i} \tag{4.4}$$

where ℓ and ℓ_i are respectively the mean free path for the dislocations in the boundaries and within the subgrains respectively.

The model by Roberts and Ahlblom (1978), does not establish any nucleation mechanism. There is strong experimental evidence that in polycrystalline materials, the recrystallisation is initiated by bulging of the pre-existing grain boundaries. Recent results (Hennaut et al, 1982) indicate that at low Z, oscillating flow curves, strain induced grain boundary migration is the mechanism. At high Z, nucleation at grain boundaries is predominant. The size of the nuclei is not determined due to the wide spectrum of bulges size, the smallest corresponding with the mean subgrain size (Ahlblom, 1977). In copper single-crystals, Mecking and Gottstein (1978), found that, at high temperatures, the material presented dynamic recrystallisation. The phenomena being characterized by discontinuous subgrain growth and subsequent twinning at 45° with the specimen axis. Other authors (Gottstein et al, 1979; Wantzen et al, 1979) determined that all the orientations in the recrystallised structure could be identified as one complete twinn chain, notwithstanding different initial orientations.

In single crystals, it is assumed that the gliding dislocations are blocked by obstacles or annihilated after having traveled a mean free path. For continuation of the plastic deformation, new mobile dislocations must be formed, in the way described by (Lücke and Mecking, 1973)

$$d\rho_i = d\varepsilon/\ell b \tag{4.5}$$

Strong experimental evidence suggests that the stress to the peak varies with the Zener-Hollomon parameter in the way of

$$\sigma_p = kZ^n \qquad (4.6)$$

where k and n are material constants. From equation (4.4) and (4.5), it would be expected that the strain to the peak in stress will increase in a similar way as the stress increases with the temperature compensated strain rate parameter.

Figure 21 presents results by Leduc (1980) in titanium bearing and mild steels tested at high strain rates and at different temperatures under plane strain conditions. As can be seen, the strain to the peak increases with the strain rate and then decreases to a value constant for all the test temperatures. Similar results appears to occur with superalloys deformed under axisymmetric compression conditions (Farag and Hamdy, 1976) and austenitic stainless steel tested in torsion (McQueen et al, 1977; Fritzemeier et al, 1979). The normal expected behaviour of strain to the peak increasing with increase of strain rate was found in lead tested under different conditions, figure 22 (Sellars et al, 1976).

4.3.3. *Heterogeneity during dynamic recrystallisation.*

In work with copper single-crystals (Wantzen et al,1979), it was determined that the values of stress and strain to the onset of dynamic recrystallisation varied considerably with the relative orientation of the single-crystals. In work with magnesium alloys (Burrows et al, 1979), it was found that the dynamic recrystallisation was taking place in preferential zones aligned with the planes of maximum resolved shear stress, presenting a very strong alignement of the basal planes with those directions.

Korbel and Blaz (1980) and Mataya et al (1982) found, in copper and in precipitation hardened stainless steel, respectively, strain localisation associated with the presence of dynamic recrystallisation. Sah et al (1973) in nickel found that the recrystallisation kinetics during torsion testing were position dependent.

4.4. Conclusions.

In materials with a high stacking fault energy, the processes of dynamic recovery produce a homogeneous structure, at least at low or medium strains. At high strains, or under severe deformation conditions, the heterogeneity of the recovery processes is manifested by the formation of high angle boundaries. Those boundaries are formed by recovery processes of individual dislocation annihilation, and not by the recrystallisation ones characterized by the massive annihilation of dislocations by a mobile grain boundary.

The heterogeneity of dynamic recrystallisation is manifested since its start is due to the gradient in the dislocation density required to act as driving force for the processes. It is assumed that a grain boundary will migrate due to the difference on the dislocation densities at both sides of the boundary. The small grain size obtained by this means is attributed to be due to the number of nuclei that at any point can grow.

Chapter 5.

Adiabatic Heating and Shear Band Formation.

5.1. Introduction.

If insufficient time is available for dissipation to occur, the heat generated during plastic deformation can be contained within the deforming material. Such a system is often termed adiabatic even though it may not fit the classical definition of a process which occurs without heat being absorbed or lost. In the case of plastic deformation of metals, some dissipation usually occurs, and so, in this context, the definition could be modified to one in which the rate of heat generation is much greater than the rate of heat loss by conduction, radiation or convection.

In general, deformation that has attained these adiabatic conditions is characterised by microstructural changes produced by the increase of temperature and the amount of deformation. White etching shear zones produced in steel are probably the most widely reported evidence of adiabatic deformation (Zener and Hollomon, 1944; Bedford et al, 1974; Stock and Wingrove, 1974). However, evidence of adiabatic deformation has been obtained in a variety of other metals and alloys, including nickel, titanium and aluminium (Stock and Thompson, 1970; Hartmann et al, 1981; Kunze et al, 1981; Semiatin and Lahoti, 1981, 1981a, 1982, 1983).

For large effects, it is necessary for adiabatic heating during deformation to be restricted to a localised region, in which large strain and strain rates occur. Such conditions are encountered in machining (Stevenson, 1974; Jeglic and Packwood, 1978), punching operations (Stock and Thompson, 1970; Stock and

Wingrove, 1971), projectile-target impact (Glenn and Leslie, 1971; Mescall and Papirno, 1974; Olson et al, 1981) and explosive fragmentation (Staker, 1980; Shockey and Erlich, 1981).

5.2. Deformational Heating.

The direct conversion of mechanical work, to produce an average rise in temperature, ΔT, within a material in the absence of any change in internal energy of the material is obtained by (Lindholm, 1974)

$$\Delta T = \frac{1}{\rho c} \int_0^{\varepsilon'} \sigma d\varepsilon - H(T_s, T_o) \qquad (5.1)$$

where ρ is the density, c the specific heat, ε' the maximum strain. $H(T_s,T_o)$ is a function of the internal temperature, T_o, and the superficial one, T_s, and represents the losses of heat. The integral terms represents the increase of temperature due to the deformation.

5.2.1. Temperature measurements during deformation.

In agreement with equation (5.1), it is expected that part of the energy required to deform the material will be converted into heat, producing an increase of temperature that has been measured with the help of heat sensitive films (Coffey and Armstrong, 1980; Sachdev and Hunter, 1982) or with the aid of thermocouples (Sellars et al, 1976; Foster, 1981).

It was found (Sachdev and Hunter, 1982) that even at very low strain rates, 10^{-5} - 10^{-3} sec^{-1}, in which the effect of deformational heating is negligible for practical purposes, the temperature increase is not homogeneous within the specimen, but the specimen is hotter towards the middle, and cooler in the

extremes where deformed regions are in contact with undeformed, cold zones.

Coffey and Armstrong (1980) used a heat sensitive film to obtain evidence of hot spot formation in soft ionic and polymeric crystals subjected to impact or to low level shock loading. The advantage of this method is that it has a good spatial resolution of hot spot detection, but it has the disadventage that the result is only an integrated time story, with no relation between the temperature increase and deformation path. In their experiments with NaCl crystals they realized that even very small energy impacts produced localised temperature increase greater than 100 C, and probably temperatures of the order of 250 C were generated in localised regions around the perimeters of the crystals. They calculated that if the total energy lost in the impact was expended in heating the bulk of the solid, the temperature rise would be only of the order of 50 C, insufficient to exceed the threshold limit of the film.

The advantage of the use of thermocouples can be seen in figures 23 and 24 (Sellars et al, 1976; Foster, 1981), for lead and niobium bearing steel deformed under plane strain conditions with inserted thermocouples at their centre point. The rise of temperature can be correlated with the deformation. The disadventages of this method are the high rate failure of thermocouples (Foster, 1981), the fact that the registered heating might be caused by deformation in the thermocouple, rather than in the material, and the need for contact between the testing material and the thermocouple. The difference between curves A to D in figure 23 may be due to the relative strain necessary to close the hole in which the thermocouple was inserted. Spurious readings might be introduced by elastic deformation effects on the thermo-electric properties of the thermocouple (Harding,1976).

As can be seen in both figures, a higher temperature rise is achieved with bigger specimens or with the increase of strain rate. The temperature rises for adiabatic heating were calculated with the aid of equation (5.1), assuming a homogeneous strain distribution. Materials tested under plane strain conditions present a very strong strain gradient across the specimen (Sellars et al, 1976; Beynon, 1979; Beynon and Sellars, 1983), and that might be the cause of the strain range in which the measured temperature is higher than that calculated for adiabatic heating, equation (5.1), for the specimen tested at the higher strain rate in figure 24.

5.2.2. Determination of the temperature increase due to deformational heating.

Wada et al (1978) proposed a method to determine the distribution and time dependence of temperature, strain rate and strain in plastically deformed materials. It is assumed that the strain rate, $\dot{\varepsilon}$, depends on stress, σ, and temperature, T, as

$$\dot{\varepsilon} = \dot{\varepsilon}_o \sigma^n \exp(-\Delta Q/RT) \qquad (5.2)$$

where $\dot{\varepsilon}_o$ and n are constants, ΔQ is the activation energy for the deformation process and R, the gas constant. This equation can be used specially at high temperatures where deformation is nearly strain independent and the activation energy is constant and nearly equal to that of self diffusion. However, the equation may not describe the plastic behaviour over a wide temperature or stress range with a unique set of constants because of different deformation mechanisms. Figure 25 shows the case in which heat flow is only in the x direction and the regions $x < 0$ and $x > L$, where L is the specimen length, are kept at a constant temperature T_o. In the specimen, the temperature is a function of the position x and the time t. Deformation starts at time zero and

is confined to $0 < x < L$. If the specimen is deformed by pure shear at an average constant strain rate , $\dot{\varepsilon}_o$, we obtain

$$L\dot{\varepsilon}_o = \int_0^L \dot{\varepsilon}\,dx \tag{5.3}$$

substitution of (5.2) in (5.3) yields

$$\sigma = \sigma_o \left(\frac{\dot{\varepsilon}_o L}{\dot{\varepsilon}\,\emptyset}\right)^{1/n} \tag{5.4}$$

where $\emptyset = \int \exp(-Q/RT)dx$ and σ_o is a constant. Using equations (5.2) and (5.4), the strain rate is expressed as

$$\dot{\varepsilon} = \dot{\varepsilon}_o \frac{L\exp(-Q/RT)}{\emptyset} \tag{5.5}$$

Assuming that the ammount of heat generated per unit volume, q, at a point x and time t be expressed as

$$q = \alpha\sigma\dot{\varepsilon} \tag{5.6}$$

where α is the fraction of mechanical work converted into heat, the integral term on the right hand side of equation (5.1), combination of equations (5.4) and (5.6) gives

$$q = \alpha\sigma_o\dot{\varepsilon}_o\left(\frac{\dot{\varepsilon}_o}{\dot{\varepsilon}}\right)^{1/n}(L/\emptyset)^{1+1/m}\exp(-Q/RT) \tag{5.7}$$

The temperature in the specimen during plastic deformation is determined by the rate of heat generation and the rate of heat flow towards both ends of the specimen. Figures 26 a.) and b.) show respectively, temperature and strain rate distribution, at different times, for aluminium under pure shear conditions, with T_o = 500 C and L =30 mm, at three different strain rates. In figures 26

c.), d.) and e.), the temperature, strain rate and strain distribution are represented for aluminium specimens of different sizes tested at T_o = 500 C and $\dot{\varepsilon}_o = 10\ sec^{-1}$.

Foster (1981) developed a two-dimensional finite difference analysis to determine the thermal behaviour in specimens tested under plane strain compression. The case of heat flow during deformation is treated assuming that the deformation heat will flow from the centre of the specimen towards the undeformed sides and to the tools. The method used to determine the temperature rise in the specimen due to deformation was to calculate the work done per unit volume during different strain intervals from the corresponding stress-strain curve. It was assumed that the strain distribution is uniform and that a uniform temperature rise, ΔT, in the time interval, δt, in which a strain increase, $\delta\varepsilon$, occurs, given by

$$\Delta T = \frac{\Delta W}{vc\rho} = \frac{\bar{\sigma}\,\delta\varepsilon}{c\rho} \tag{5.8}$$

where ΔW is the work done over the interval, $\bar{\sigma}$ is the mean stress over the interval of strain, $\delta\varepsilon$, in the elemental volume v, c the specific heat and ρ the density. Figures 27 and 28 show the calculated centre and average temperature versus strain for some of the curves from figures 23 and 24 respectively.

Armstrong et al (1982) calculated the temperature rise in tests carried out by Lindholm (1974) in thin walled torsion specimens. From equation (5.1), they describe the strain dependence of the heating as

$$\frac{dT}{d\varepsilon} = \frac{\sigma}{c^*} \tag{5.9}$$

where $c^* = c\rho$ is the specific heat per unit volume, The plastic instability condition, $d\sigma = 0$, yields

$$\frac{dT}{d\varepsilon} = \frac{n + m}{\varepsilon\beta} \tag{5.10}$$

where $n = d\ln/d\ln$ is the work hardening coefficient, m the strain rate sensitivity and β is the constant in the high temperature-stress relationship

$$\sigma = \sigma_o \exp(-\beta T) \tag{5.11}$$

A temperature increase from 61 to 225 K was calculated using equation (5.10) for the increased shear banding which occurs on going from a strain rate of 0.01 to 98 sec^{-1} in Lindholm's experiments. They considered that the achievement of plastic strains can be assessed on the basis of dislocation displacements, when an adiabatically induced instability is producing localised shear banding. In an experiment involving simple shear deformation, this is described by

$$\int_0^{\gamma'} \tau d\gamma = \int_0^{A'} \tau(b/h)(dA/A) \tag{5.12}$$

where τ and γ are respectively the shear stress and strain, b the Burgers vector, h the specimen gauge length measured perpendicular to the slip planes, dA the elemental area of slip swept out by the dislocations and A the cross-sectional area. The integration of dA covers the total slipped sectional area, A', which is associated with the maximum shear strain γ'. The plastic shearing rate is given by (Orowan, 1940)

$$\dot{\gamma} = \rho b v \tag{5.13}$$

where ρ is the dislocation density and v the average dislocation velocity. Eshelby and Pratt (1956) described the temperature rise at a point on a hypothetical slip plane being transversed by n_1 equally spaced dislocations, occurring on n_2 closely spaced parallel planes, forming a special type of free

running shear band. In this case, the dislocation density, is taken as

$$\rho = (n_s/A_o)n_1n_2 = \rho_s n_1 n_2 \tag{5.14}$$

where ρ_s is the shear band density and n_s the number of shear bands in the longitudinal area of gauge length, A_o. The model of Eshelby and Pratt (1956) gives an increase of temperature

$$\Delta T < \frac{1}{\rho_s}\frac{\tau\dot{\gamma}}{2\pi k} \ln \frac{2k\rho^{3/2}b}{c^*\dot{\gamma}} \tag{5.15}$$

where k is the thermal conductivity. This equation shows that a greater temperature rise is achieved at any strain rate as the density of shear bands is decreased. This conclusion is in agreement with the observations made by Lindholm (1974) that plastic instability occurred at smaller strain values for an increase in the applied strain rate. The only difficulty with the model is that the computed values of ΔT seem far too low to give much of an effect, except for the case of the dislocations being very closely spaced. A model of localised heating, figure 29, is proposed (Armstrong et al, 1982). Two inclusive stages are shown for the developement, figure 29 a.), b.), and catastrophic release, figure 29 c.), of a dislocation pile-up. At t_1, a pile-up of dislocations has begun to form isothermally against a local obstacle in the slip plane. As the shear stress increases, a critical value of concentrated stress, τ_c^*, is reached at t_2, to cause the obstacle to collapse. Upon collapse, the leading dislocations are now driven forward by the concentrated stress at the tip of the pile-up and so the dislocation interaction energy which has been built up isothernally is dissipated adiabatically in a sudden collapse. Under those conditions, for large pile-ups, equation (5.15) is transformed into

$$\Delta T < \frac{n_1^2 n_2}{2} \Delta T_1 \qquad (5.16)$$

where ΔT_1 is he heating effect for the motion of a single dislocation.

5.3. Shear Bands.

The localised shear bands observed in steels and other materials, which have undergone high strain rate deformation, have been given many names. They may be called white bands, layers or streaks, shear bands, untempered martensite lines, fresh martensite streaks or layers, deformation bands or adiabatic shear streaks of bands. However, the basic nature of these bands is still somewhat in doubt.

5.3.1. Early observations.

Early reported observations of these bands were made around the period 1910-20. Probably the earliest systematic study of white bands, made by Trent (1941), was concerned with surface layers produced by rubbing on steel wire ropes, and with layers produced by hammer blows on wires. As a result, the wires tended to split on a 45° plane, and a white etching layer formed on this plane when sufficient deformation had taken place. While these bands were said to consist of martensite which etched white, no acicular structure was apparent. This was assumed to be due to a very fine grain size. It was pointed out that adiabatic conditions could be produced in the wire crushing experiment whereby high local temperatures could be reached and the subsequent cooling would be equivalent to a very severe quench.

Zener and Hollomon (1944) further studied the process of adiabatic shear using punching experiments. They proposed that when the strain rate in a region of localised deformation was high enough, the temperature of the region increased. If the strength loss due to this temperature rise was greater than the increase in strength due to strain hardening, then unstable plastic deformation occurred. They made simple computations which suggested that a temperature rises as high as 1000 C could be attained in a shear band. In their punching experiments, where a hammer was dropped on to a punch, strain rates of 2000 sec^{-1} were obtained and the material in the white etching bands that were produced had suffered strains of nearly 100.

Andrew et al (1950, 1950a) carried out fairly detailed investigations of white etching shear bands in steel specimens. They studied the bands using X-ray diffraction techniques and examined the tempering characteristics of some of the bands they produced. Their diffraction evidence supported the presence of austenite, however, no presence of martensite was obtained althought it was expected that the highest proportion of the white bands would be martensitic, on the grounds of their high hardness. Tempering experiments showed that the apparent decomposition of the austenite, and accompanying precipitation of carbides, usually proceeded from the centre of the white layer. This suggested that the centre of the white layer had attained a higher temperature than the edges, thus allowing more complete solution of the carbon and carbide forming elements.

5.3.2. Impact and penetration studies.

Stock and Thompson (1970) studied the nature of the adiabatic bands produced by projectile and punch penetration in aluminium alloys. They found that parts of the specimen that presented crack bands at the base of the projectile holes showed two regions when examined by transmission electron microscopy, clusters of small knobbley regions surrounded by smooth regions running paralled to the shear direction. Selected area diffraction indicated a grain size of 0.3 to 0.6 μm with misorientation between 5 to 15°. They suggested that material in the band melted and the rapid quenching by the surrounding material produced fine grains.

Stock and Wingrove (1971) investigated high speed shearing of low and high carbon steels. The energy required for punching low carbon steel increased linearly with punch speed, but a maximum was observed in the curve for the higher carbon steel. This was associated with the occurrence of adiabatic deformation where the energy for shearing decreased with the catastrophic flow associated with adiabatic flow. More extensive tests showed that a maximum was also present in the curve for mild steel, but at higher velocities than for the higher carbon steel (Bedford et al, 1974).

Investigations of the fine structure of adiabatic shear bands formed by impact were made by some authors working with quenched and tempered steels (Wingrove, 1971; Glenn and Leslie, 1971; Manganello and Abbott, 1972). In each case, the white bands are considerably harder than the matrix. Thin foils containing the shear bands were examined by transmission electron microscopy, but the structure was difficult to resolve. Diffraction patterns consisted of rings, and a grain size of less than 0.1 μm was indicated (Glenn and Leslie, 1971). The lattice spacing appeared to correspond to martensite (Wingrove, 1971), and small precipitates were sometimes observed. They suggested that at

impact, some regions of the plate are subject to highly concentrated and extremely rapid plastic deformation. The temperature and pressure rise in these regions is sufficient to cause a transformation to austenite, and the cold mass of the plate provides a very rapid quench of austenite to martensite.

Mescall and Papirno (1974) studied the behaviour of spallation induced in steel plates impacted by blunt cylinders with diammeter comparable to the plate thickness. They found that no spallation occurred in hardened and tempered plates up to their failure by adiabatic shear plugging, while softer targets exhibited extensive spallation even before penetration, but did not show evidence of white layering. They concluded that in those experiments, when the deformation process is concluded, there is a rapid quench of the heated zone by the surrounding cooler material.

Moss (1981) used planes of chemical heterogeneity, reference bands, left from casting and rolling of steels to document the shear strains in his experiments with an explosively driven punch. He concluded that those reference bands change shape during plastic deformation according to the orientation of the shear displacement and the amount of plastic shear. In the case of reference bands initially perpendicular to the shear displacement, the slope of those bands was taken as a direct measure of the shear strain. The strains varied through the thickness, having higher values near the surface, $\varepsilon = 572$, while the average shear strain was found to be 5.3. He suggested that changes in carbide and lath morphology, and possibly a magnetic transformation governed the abrupt change in the strain gradient in the shear band, rather than the generally accepted austenite to martensite transformation.

An expression that is found to fit the results for shear stress, τ, versus shear strain, γ, curves under adiabatic deformation experiments is given by (Olsen et al, 1981)

$$\tau = \tau_o(1 + \alpha\gamma)\exp(-\beta\gamma) \qquad (5.17)$$

where τ_o is a constant representing the shear yield stress, α is a hardening parameter and β is a softening one. The shear stress-strain behaviour of equation (5.17) is exemplified in figure 30. The stress is seen to reach a maximum at an instability strain , γ_i, which is simply determined by

$$\gamma_i = \beta^{-1} - \alpha^{-1} \qquad (5.18)$$

With reliable measurements obtained from torsion, they simulated shear band formation under simple shear strain. A simple rectangular body, figure 31 a.), was simulated using the plastic flow relationship (5.17). The bottom surface was held stationary and a constant velocity was applied to the top, corresponding to a constant imposed nominal strain rate. Assuming a velocity of 4000 cm/sec, a computer simulation is described in figures 31 b.), c.) and d.), for different times, in microseconds. Two bands of localised strain grow within the material, the one near the bottom being more diffuse than the one near the top. In figure 31 e.), the plot of the strain values along the axis A-A' appears, the dashed line corresponds to the instability strain γ_i.

5.3.3. Explosive loading.

Thornton and Heiser (1971) observed adiabatic shear zones in explosively loaded thick wall cylinders of low alloy steels, when strain rates as high as 10^8 sec^{-1} within shear bands would be expected. Analysis of these bands was made using microhardness, x-ray diffraction and electron microscopy. The x-ray study suggested a martensitic structure and no retained austenite was detected. From their transmission electron microscopy they suggested a structure of fine grained untempered martensite, with no evidence of carbide precipitation.

Lamborn et al (1974) detonated hollow steel cylinders filled with a high explosive. They used fractographic and metallographic techniques to study the material interactions affecting the fracture and the size of fragments in plain and notched cylinders. They distinguished two modes of fractures, tensile and shear, finding that the last always occurs at the inner surface. In brittle materials, they found an increase of fine fragmentation, associating it with an increased amount of tensile fracture. Other authors (Staker, 1980; Shockey and Erlich, 1981) working with specimens fractured by explosive loads within containing cylinders related the occurrence of white bands, in hard materials, with a fracture mode similar to cleavage. In softer materials, no evidence of white layering appeared and the mode of fracture was by ductile dimpled shear. In specimens taken from directions different from the rolling one (Shockey and Erlich, 1981), it was found that the shear bands lay on planes inclined 45° to the rolling direction, showing very strong texture effects.

5.3.4. Microstructural features.

Work related with microstructure has been carried out in tests at low and high temperatures. In the lower temperature range, the specimens used are deformed at very high strain rate by projectile penetration or explosive loading. In the higher temperature range, the tests are carried out at strain rates equivalent to mechanical processing.

5.3.4.1. Low temperature studies.

Recent work (Murr, 1978; Murr and Kuhlmann-Wilsdorf, 1978) has shown that the operative mechanisms in nickel and copper under shock loading conditions are the same as the ones occurring at lower strain rates.

Jeglic and Packwood (1978) and Zaid (1982) distinguished two different types of bands. One, that etched white, present under very severe testing conditions, in which there was a certain amount of transformation. The second type, found in less severe deformation conditions, in which twinning and slip occurred, was not considered adiabatic due to their normal respond to etchants. Staker (1980) described both sorts of bands in his contained explosion specimens, the former one appeared in hardened and tempered steel, the second one in normalised steels. In both cases, the bands were followed by cracks presenting the same general appearance in the specimen, metallographic inspection being necessary to discriminate between each type of band.

Other authors (Hartmann et al, 1981; Kunze et al, 1981) produced shear zones, in a variety of alloys working under dynamic loading conditions. In quenched and temperaed low alloy steels, the deformation zone was characterized by two parallel white bands, about 10 μm thick, presenting different strain intensities. In a normalized structural steel, the deformation zone was characterized by the highly deformed cementite lamellae without tearing. In a nickel base superalloy, no grain boundaries were detected in the deformed zones. Only carbides and the γ' phase were present. In some regions the austenitic grains in the transition to the undeformed material were severely deformed. In a titanium alloy, no grain boundaries could be recognized in an approximately 40 μm wide deformation zone, however, it appeared that a deformation gradient existed within the zone. In a heat treatable aluminium alloy, the deformation zone was about 200 μm, with different intensities of deformation. The material fractured in the boundary zone, between deformed and undeformed zones. Moss (1981) related the formation of the white bands in hardened steel to a change in the lath morphology, that might be posible if the later mechanism is opperating.

5.3.4.2. High temperature studies.

Other authors working on titanium alloys (Semiatin and Lahoti, 1981, 1982, 1983) and on a tool steel (Ghomashchi, 1983), in isothermal and non-isothermal compression tests, shown the importance of a sharp temperature dependence of the flow stress in producing shear bands while hot forging. In non-isothermal tests, the initial stage of the bands formation involves the development of chill zones in the specimen adjacent to the cooler tools. These zones offer a constraint to uniform flow, their deformation is retarded by the locally high flow stress. As the deformation proceeds, these zones may deform slightly, but it appears that the material elements which undergo localised flow remain the same. In the more complex case of sidepressing, in which the material is deformed under plane strain conditions (Semiatin and Lahoti, 1982, 1983), it was found that the shear localisation was along the lines of the slip line field solution, for both isothermal and non-isothermal conditions. In the cases of isothermal axisymmetric compression and torsion (Semiatin and Lahoti 1981, 1981a) it was found that the shear concentration was structure dependant, appearing to occur in a β, acicular widsmanstatten structure, at all strain rates and temperatures tested. In an $\alpha + \beta$ structure, a combination of low testing temperature and high strain rate was necessary to cause the flow localisation.

Mataya et al (1982) studied the flow localisation and shear band formation in a γ' strengthened austenitic stainless steel, by means of compression of reduced gauge section cylindrical specimens, deformed at different temperatures and strain rates. At high strain rates localised flow in the precipitate structures took the form of macroscopic transgranular shear bands. At low strain rates the localised flow occurred mainly in precipitates free zones along grain boundaries. This localised flow was always associated with the occurrence of dynamic recrystallisation.

Korbel et al (1983) observed in heavily distorted hot rolled aluminium two different regions, one of homogeneously deformed material, and a heterogeneous one forming shear bands. At higher temperatures, some authors have observed the phenomenon of recrystallisation in situ in aluminum (Chandra et al, 1979, 1982) and in ferritic stainless steels (Lombry et al, 1979). In this process the dislocations are accumulated on the subgrain boundaries and at high strains change their low angle relationship to a high angle one, giving the appearance of very small grain size.

5.4. Conclusions.

From several researches (Sellars et al, 1976; Wada et al, 1978; Coffey and Armstrong, 1981; Foster, 1981), it is found that the temperature increase due to deformational heating is not distributed homogeneously, but under certain conditions, the temperature increase is localised in specified zones of the material. The results shown in figures 24 and 28 (Foster, 1981), can be explained if we consider that during certain stages of the deformation, due to the strain distribution in plane strain compression (Sellars et al, 1976; Beynon, 1979; Beynon and Sellars, 1983), the tip of the thermocouple passed through heavily and lightly deformed zones. Registering, in the former case, temperature increases higher than the one expected by adiabatic heating through all the specimen. The reverse would be expected when the thermocouple lay in less than average deformed zones.

Following traditional dislocation analysis, Eshelby and Pratt (1956) reached the conclusion that the temperature rise, produced by dislocations in a shear band will be very small, unless the dislocations were very closely spaced.

Armstrong et al (1982) reformulated this analysing and considering that the dislocations will be forming pile-ups. They considered that very high temperature increase will be produced in a small volume fraction when the dislocations in the pile-ups are liberated and thus explaining the thermal spots observated by Coffey and Armstrong (1981) in ionic and polymeric crystals.

The discussion on shear band formation is still going on. There is no conclusive evidence that the white streaks found in hard steels are formed by a martensitic transformation. Recent studies on different alloys (Hartmann et al, 1981; Kunze et al, 1981) have shown that the heavily distorted bands are encountered in metallic systems that do not present a martensitic transformation, but have supported studies by other authors (Mescall and Papirno, 1974; Jeglic and Packwood, 1978; Staker, 1980; Zaid, 1982) showing the existence of two distinctive types of bands in steels. The first one, associated with hardened and tempered steels, in which the classical white bands are produced, and result in brittle fracture under very severe conditions. The second type, is not considered by some authors (Mescall and Papirno, 1974; Staker, 1980; Zaid, 1982) to be formed under adiabatic conditions, due to the normal response to etchants (Kunze et al, 1981), those bands are encountered in softer steels, generally in the annealed or normalised state, the fracture associated with those bands is more of the dimple ductile type.

There is a common agreement that bands are formed by very small grains or laths, which make difficult any diffraction analysis. It was assumed that during the deformation, the temperature increase was high enough to reach the austenitic transformation temperature, in steels, or the solidus temperature in the aluminium alloys. The strong quench produced by the surrounding material being responsible for the small grain size.

An alternative explanation of the phenomenon can be made by considering that almost all the tests have been carried out at low homologous temperatures, in which the dynamic restoration is only by recovery. In this case the effect of the temperature on the creation of the deformation bands would be similar to the effect encountered in non-isothermal forging (Semiatin and Lahoti, 1981, 1982, 1983; Ghomashchi, 1983), in which very temperature sensitive materials will deform in the hotter regions. Producing shear bands by polygonization mechanisms, rather than by phase transformation. Aditional support comes from the results from Mataya et al (1982) in which they found a correlation between dynamic recrystallisation and strain localisation.

Chapter 6.

Experimental Procedure.

6.1. Introduction.

The preceding literature review has shown that deformation can become unstable and localised in specific regions within materials during testing. Most of the experiments, have been carried out at low temperatures, leaving the hot working domain practically untouched.

The aim of this work was to determine if the inversion in the strain rate dependence of the strain to the peak in stress found by Leduc (1980) in titanium bearing steel at high strain rates was a real phenomenon. Previous research (Colás, 1980) has shown that the peak was due to dynamic recrystallisation. In order to determine if the phenomenon was only characteristic of plane strain, preliminary tests were carried out on titanium steel under axisymmetric compression conditions. The bulk of the research was carried out on an austenitic stainless steel under plane strain compression conditions, but in order to compare the effect of the mode of deformation, axisymmetric compression and torsion tests were also performed.

6.2. Specimen Preparation.

The titanium bearing steel used in preliminary tests was remnant from previous research and the procedure employed to produce these specimens is described elsewhere (Colás, 1980; Leduc, 1980). The stainless steel chosen was

an AISI type 316, provided as bars of rectangular section, 25.4 by 50.8 mm. The chemical analyses for both steels appear in Table I.

6.2.1. Hot rolling of the stainless steel.

In order to produce specimens for plane strain and axisymmetric compression, the bars were cut into small slabs about 100 mm long and hot rolled in a fully instrumented Hille 50 rolling mill in its 2-high reversible configuration. The mill instrumentation has been described previously in detail (Harding, 1976; Leduc, 1980).

Five different rolling schedules were planned to obtain different thermo-mechanical treatments and final thicknesses.

a.) Schedule i.- Heating, three 25% reductions, water quenching.

b.) Schedule ii.- Heating, one 25% reduction, heating, two 25% reductions, water quenching.

c.) Schedule iii.- Heating, two 25% reductions, heating, one 25% reduction, water quenching.

d.) Schedule iv.- Heating, one 25% reduction, heating, three 25% reductions, water quenching.

e.) Schedule v.- Heating, two 25% reductions, heating, three 25% reductions, water quenching.

The heating was carried out at around 1200 C for 30 minutes. Interpass times and time between the last pass and quenching, were 15 seconds in all schedules. The first pass after heating was given 10 seconds after taking the specimen out of the furnace. Schematic diagrams for those schedules are shown in figure 32. The final thicknesses of the strips were of about 10.5 mm for schedules i, ii and iii, 8 mm for schedule iv and 5.5 mm for schedule v, Table II.

Some slabs were rolled with embedded 1.5 mm diameter "Pyrotenax" inconel sheathed, mineral insulated, chromel-alumel thermocouples. The emf was recorded on a "Telsec" millivolt recorder and converted into temperature with the aid of the formula (Sellars et al, 1976)

$$C = -5.781 + 26.28V - 0.1256V^2 + 0.0019V^3 \qquad (6.1)$$

where C is the temperature in degrees Celsius and V the emf in millivolts. This relationship is valid for chromel-alumel thermocouples in the range 200 to 1300 C and has an accuracy of ±0.5 C.

The value of the mean stress, for those specimens rolled with thermocouples, was calculated assuming sticking friction (Sims, 1954)

$$P = \bar{\sigma}\, w \sqrt{R\Delta h}\; Q_p \qquad (6.2)$$

where P is the load, $\bar{\sigma}$ the mean stress, w the strip width, R the roll radius, Δh is the reduction in thickness and Q_p is a geometrical parameter dependent on the initial and final thicknesses, the thickness to the neutral plane and the angles between them.

The recorded load and the initial and final dimensions of the slabs were input in a computer program similar to that of Leduc (1980). The actual dimensions in the intermediate passes were unknown and were calculated by the equation (Beese, 1972)

$$\frac{\ln(w_2/w_1)}{\ln(h_2/h_1)} = k(h_1/w_1)^{1.3} \exp -0.32\, \frac{h_1}{\sqrt{R\Delta h}} \qquad (6.3)$$

where w_1, w_2, h_1 and h_2 are respectively the initial and final widths and thicknesses, k a spread constant that was found equal to 0.33. Due to the increase of breadth of the material during rolling, El-Kalay and Sparling (1968) suggested the following formula to calculate the average width $\bar{w}$

$$\bar{w} = w_r - \frac{1}{3}(w_r - w_b) \qquad (6.4)$$

where w_r and w_b are respectively the width over the crowns and over the bottom and top surfaces.

The relevant data related to those rolling specimens appear in Table II and the temperature versus mean stress plot is shown in figure 33. All the data fall within the same curve, the scatter being greater for the specimens with three or more reductions, but this can be due to additive errors introduced by equation (6.3) when calculating the intermediate widths or to partial recrystallisation.

The specimens used for torsion were machined from 16 mm diameter rods produced in a rod mill from bars 25 mm square and about 150 mm long. The resultant torsion specimens were 15 mm gauge length and 7 mm diameter, giving a gauge length over radius ratio equal to 4.3.

6.2.2. Initial grain sizes.

The different rolling schedules were planned in order to produce a set of grain sizes for the different tests. A series of samples were taken from specimens belonging to different schedules. Those samples were heated-up for 15 minutes at different temperatures and water quenched. Specimens were mechanically polished and etched with the reagents (Ahlblom, 1977; Shpigler and Beraha, 1977)

150 ml H_2O, 50 ml HCl, 2 g $K_2S_2O_5$

or

100 ml H_2O, 100 ml HCl, 10 ml HNO_3

The grain size measurements were obtained by the mean linear intercept technique and the results are shown in figure 34.

Comparing results from figures 33 and 34, it was considered that the difference between the schedules was small. Schedule i was chosen to produce the bulk of the specimens. Schedules iv and v were chosen to provide specimens with different initial geometric conditions, but similar grain sizes.

6.3. The Servo-hydraulic Machine.

This machine was used recently in various research projects (Sellars et al, 1976; Beynon, 1979; Foster, 1980) and only a brief description is given here.

6.3.1. General description.

This machine is controlled by a PDP11/10 computer, the communication between them is through a number of digital to analog and analog to digital converters. The output can be via an X-Y plotter, a teletype or punched tape, figure 35. In the latter case, the data output is from three channels, displacement, load and temperature. In the case of tests without thermocouples, the machine command is registered in order to check the control of the computer. In adition to the testing furnace, the machine is provided with two furnaces that can be set at different temperatures.

By comparing the actual displacement with the machine command, the strain rate is controlled. Different strain rate profiles can be chosen in order to simulate rolling or extrusion or to deform at a constant rate. At high strain rates, problems related to mechanical inertia are avoided by stopping the ram with the wedge, figure 35, at the end of deformation.

Restoration analysis can be carried out in this machine. Up to five deformations can be given to any specimen with different annealing intervals. A quenching rig is installed in the machine in order to retain the microstructure at the end of deformation or after any annealing period.

Before testing, specimens are coated with a convenient lubricant in order to minimize friction effect and, at high temperature, avoid excessive oxidation. For the low temperature testing range, graphite in an oily suspension is used, at high temperatures, glass powder is employed. For this research the water soluble glass DAG2626 supplied by the Aicheson Colloids Co. was employed.

6.3.2. Adaptations for axisymmetric compression testing.

Although the furnaces and tooling are specially designed for plane strain compression, it was possible to carry out tests under axisymmetric compression conditions by placing small cylindrical specimens over the tools, but some limitations had to be taken into account in those tests.

The first limitation in those tests is the size of the specimen. The geometry chosen was based on the tool width and on the handling capabilities of the ancillary equipment attached to the testing machine. The tooling was the same as that in plane strain compression tests, tools 15 mm width and 100 mm long. From figure 35 the position of the tools within the testing furnace can be appreciated. After raising the crosshead, the furnace is set into position by sliding it over the tools. A change in the tools' dimensions would require a change in the furnace dimensions and in the handling equipment. It was considered that specimens with a diameter less than 7 mm will be very difficult to handle and to put into position for the tests. With this geometry, assuming constant volume, the maximum uniaxial strain, neglecting any barrelling, is about 1.5, higher strains will imply that part of the cross-sectional area of

the material is not under the tools. A diagram of a specific holding grip designed to hold the axisymmetric specimens in the conveyor arms and permit the use of the rest of the equipment is shown in figure 36. The holding grip is made from used plane strain specimens, the optimum thickness was found to be about 3 mm. A spring inserted between the conveyor arms in the specimen carriage loads the specimen and keeps it in position. The specimen is spot welded to high temperature resistent wire in order to pull the specimen out in case it sticks to the tools. Unfortunately, the thickness of the holding grip limits the total deformation to less that 1.2. Although the grip was succesfull, in the present research, the specimens were preheated and tested at the same temperature, and, in this case, it was found to be more effective to place the specimens directly over the bottom tool and avoid the difficult centering of the specimen. Barbosa (1983) used this grip more succesfully in non-isothermal tests.

A second limitation exists with regard to the minimum strain rate that can yield acceptable resolution. At low strain rates, the load is small, and the actual value of load is comparable to the digital precision used by the computer to read the data, increasing the scatter.

6.4. Plane Strain Compression Testing.

Different series of tests were designed in order to determine if the inversion in the strain rate dependence of the strain to the peak in stress was achieved in the stainless steel, and under what conditions. Figure 37 shows the relative orientation of different types of specimens. Two different directions are marked for the plane strain specimens, a normal one, corresponding to testing conditions equivalent to that of the rolling schedules, and a transverse

one, corresponding to cross-rolling. Three different orientations appear in the case of the specimens tested in axisymmetric compression, corresponding to directions through the thickness, width and length.

The preparation of an average AISI type 316 stainless steel plane strain compression specimen followed the next steps: a.) Drilling the holes and cutting the specimen from the rolled strip, b.) Shot blasting to remove the high temperature oxide layer, c.) washing the specimen to clean the dust, d.) covering the specimen with the high temperature lubricant.

The preliminary titanium bearing specimens were already machined and chromium plated (Colás, 1980; Leduc, 1980), so only the lubricant coat was added.

The average width of each specimen was calculated with the aid of equation (6.4) and the thickness at the working temperature with equation

$$h_c = h_o[1 + 1.95x10^{-6}(C-20)] \qquad (6.5)$$

where C is the testing temperature in degrees Celsius, and h_o and h_c are the dimensions at room and at the working temperature.

6.4.1. Series of tests.

In order to investigate the inversion of strain to the peak, the following series of tests were carried out.

a.) Grain size effect. Different grain sizes varying from 20 to 160 μm were produced by preheating the specimens at around 900, 1000, 1100 and 1200 C for 15 minutes before testing them at 910 C.

b.) Orientation and geometry effect. Plane strain specimens obtained by means of schedules iv and v were compared with specimens obtained from the normal and transverse orientations produced by schedule i. The tests were carried out at strain rates varying from 0.1 to 100 sec^{-1} at 1008 C after

specimens had been reheated at the same temperature for 15 minutes.

c.) Interrupted tests. Some double deformation tests were carried out at 1008 C at strain rates of 0.5 and 5 sec^{-1}. The deformation was interrupted before the strain to the peak in stress was achieved, specimens were held for different time intervals and reloaded in order to determine restoration index curves. Some interrupted tests were intended to be carried out at strain rates of 50 sec^{-1}, but due to the relative velocities of the ram and the wedge, no second deformation was carried out. In this case, the ram was moving at a faster velocity than the wedge and being stopped by it before the desired strain was achieved.

6.4.2. Determination of stress-strain curves.

In order to obtain true stress-strain curves, the load-displacement data, recorded by the PDP11/10, or the stress-strain data have to be corrected to compensate for external effects.

6.4.2.1. Origin correction.

Beynon (1979) showed that the low slope of the rise in stress at the beginning of the stress-strain curve was due to the squeezing out of excess lubricant from the specimen-tool interface, rather than to deformation of the specimen. Foster (1981) suggested that a correction should be made by adjusting the ram reading by a constant amount until the specimen thickness, derived from the maximum ram displacement reading, was equal to the measured displacement taken as the difference between the initial and final thicknesses at the testing temperature. The origin correction used here is shown in figures 38 and 39 respectively for axisymmetric and plane strain compression tests. In either case, a straight line is fitted to the initial portion of the load-displacement curve, this straight line is cut by a vertical line at a value equal to the

difference between the maximum ram displacement and the measured one. The origin correction is carried out by subtracting the displacement value for each point from the value of displacement at the same load from either one of the straight lines. This correction is an approximation to the hyperbolic behaviour expected in removing the lubricant between the specimen-tool interface. This correction seems reasonable, the curve departs smoothly from the origin and does not present any kink at the point of intersection of the two straight lines.

6.4.2.2. Spread correction.

In the plane strain compression tests, there is always some spread along the tools. When the specimen is large, the spread is a small fraction of the initial breadth, b_o. Thus the spread will not affect the stress in the specimen to any significant level. If b_o is not large, the spread is not negligible and the stress and strain in the specimen are significantly affected by it. In the present work the initial breadth of the specimen is less than 4w, where w is the tool width, and the spread is significant. The final breadth, b, of the specimen was measured after the tests and b/b_o correlated to the amount of deformation by the equation (Sellars et al, 1976)

$$\frac{b}{b_o} = 1 + c - c\left(\frac{h}{h_o}\right)^{1/2} \qquad (6.6)$$

where h_o and h are respectively the initial and final thicknesses, and c is the spread coefficient. The instantaneous thickness, h, can be determined at any time from the corrected ram displacement, section 6.4.2., the corresponding breadth can be calculated by equation (6.6). The spread coefficient, c = 0.28, used in the titanium bearing steel was previously determined (Colás, 1980; Leduc, 1980). Two spread coefficients were found for the stainless steel, figure 40. One corresponding to the normal specimens, c = 0.33, and the second c = 0.66, to the gridded specimens described in section 6.7.

6.4.2.3. Friction effect.

Three types of frictional conditions may exist over the tool-specimen contact area: sliding, partially sticking and fully sticking friction. In the first case, for plane strain compression, the average pressure exerted by the tools , $\bar{p}$, si given by (Foster, 1981)

$$\frac{\bar{p}}{2k} = \frac{h}{\mu w}\left(\exp\ \frac{\mu w}{h} - 1\right) \tag{6.7}$$

where μ is the friction coefficient, h the instantaneous thickness, w the tool width and k the yield stress in pure shear. In the case of axisymmetric compression, the relationship is given by (Sellars et al, 1976)

$$\frac{\bar{p}}{2k} = \frac{2}{m^2}\left[\exp(m^2) - m - 1\right] \tag{6.8}$$

where $m = \mu d/h$ and d is the instantaneous diameter.

As the coefficient of friction increases, the conditions change from sliding to sticking friction. The point at which this change occurs, in plane strain compression, can be determined using (Sellars et al, 1976)

$$Z_o = (h/2\mu)\ \ln(1/2\mu) \tag{6.9}$$

where sliding friction conditions exist over the entire tool face if $Z_o > w/2$. If $Z_o < w/2$ then a band of width $(w - 2Z_o)$ exists down the centre of the tool in which there will be sticking friction, with sliding friction on either side of the band. In this case, the relation is given by (Foster, 1981)

$$\frac{\bar{p}}{2k} = \frac{h}{\mu w}\left(\frac{1}{2\mu} - 1\right) + \frac{(w/2 - Z_o)}{\mu w} + \frac{(w/2 - Z_o)^2}{hw} \tag{6.10}$$

In axisymmetric compression, partially sticking friction exists when (Sellars et

al, 1976)

$$\frac{d}{h} > \frac{1}{\mu} \ln \frac{0.577}{\mu} \tag{6.11}$$

but $\mu < 0.577$. In this case, $\bar{p}/2k$ is given by (Sellars et al, 1976)

$$\frac{\bar{p}}{2k} = \frac{2}{m^2}[(n+1)\exp(m-n)-m-1] + \frac{n^2}{m^2}\left(\frac{0.577}{\mu} + 0.577\,\frac{f}{3h}\right) \tag{6.12}$$

where $n = \mu f/h$ and

$$f = d - \frac{h}{\mu} \ln \frac{0.577}{\mu} \tag{6.13}$$

In plane strain compression, if sticking friction is present over the whole of the tool-specimen contact area, then (Foster, 1981)

$$\frac{\bar{p}}{2k} = 1 + \frac{w}{4h} \tag{6.14}$$

In axisymmetric compression, fully sticking conditions develop when $\mu > 0.577$, in this case (Sellars et al, 1976)

$$\frac{\bar{p}}{2k} = 1 + 0.577\frac{d}{3h} \tag{6.15}$$

6.4.2.4. Temperature and strain rate corrections.

Nominally, the plane strain compression tests are carried out at constant strain rate under isothermal conditions. When testing, the initial velocity of the ram is input, and the computer controls a logarithmic decrease of the ram velocity in order to obtain constant strain rate tests. The control is by means of the comparison between the actual displacement and the one predicted by the machine command. The accuracy of this control depends in the servo-valves, and

produces strain rate oscillations that might influence the shape of the stress-strain curve. The deformation produces an increase of temperature as a function of the deformation work, equation (5.1). By a finite difference program developed by Foster (1981), it is possible to obtain a tabulation of the temperature increase with the strain by means of the integration of the stress-strain curve.

Correction of the stress-strain curve to constant strain rate and constant temperature is carried out assuming that the flow stress dependence on the strain rate and temperature is given by

$$Z = A\,(\sinh \alpha\sigma)^n \tag{6.16}$$

where A, α and n are material constants and Z is the Zener-Hollomon parameter expressed by equation (4.1).

Thus, at a constant strain, the flow stress, σ_i, at temperature, T_i, and strain rate, $\dot{\varepsilon}_i$, can be calculated from the original ones σ_o, T_o and $\dot{\varepsilon}_o$

$$\sigma_i = \sinh^{-1}\left\{\exp\left[\ln(\sinh\alpha\sigma_o) + \frac{Q}{n}\left(\frac{1}{RT_i} - \frac{1}{RT_o}\right) - \frac{\ln\dot{\varepsilon}_o}{\ln\dot{\varepsilon}_i}\right]\right\}/\alpha \tag{6.17}$$

6.4.2.5. Calculation of equivalent stress,strain and strain rate.

The average pressure exerted by the tools on the specimen is given by

$$\bar{p} = \frac{F}{A_i} \tag{6.18}$$

where F is the load and A_i the instantaneous cross-sectional area. In the case of plane strain compression, this area is given by the product of the tool width and the variation of the breadth, equation (6.6), in the case of axisymmetric compression, the variation in area is given by

$$A_i = \frac{A_o h_o}{h_i} \tag{6.19}$$

where h_o and h_i are respectively the initial and instantaneous height. For each of the three types of frictional conditions the value of k, the yield stress in pure shear, can be determined using the appropriate equation, section 6.4.2.3. In order to convert the value of 2k, for plane strain compression, a factor was used (Sellars et al, 1976)

$$f = [1.155(b - w) + w]/b \tag{6.20}$$

where b is the specimen breadth and w the tool width, which takes into account the departure from plane strain conditions observed in practice. Under these conditions, the equivalent uniaxial yield stress, σ, is given by

$$\sigma = \frac{2\ k}{f} \tag{6.21}$$

The strain is given by the relationship

$$\varepsilon = \ln\ (h_o/h_i) \tag{6.22}$$

That for axisymmetric compression does not need any further correction. For plane strain compression this value is multiplied by the factor f, equation (6.22), in order to obtain the equivalent uniaxial strain.

The strain rate is defined as

$$\dot{\varepsilon} = \frac{d\varepsilon}{dt} \tag{6.23}$$

That will be the derivative at each point in a strain-time plot. Due to the oscillations mentioned in previous section, the strain rate was calculated as

$$\dot{\varepsilon}_i = P\ (\ \varepsilon_{i+2} - \varepsilon_{i-2})/5 \tag{6.24}$$

where P is the frequency of readings from the machine, ε_{i+2} and ε_{i-2} are the strain values for two points after and two points before the desired point in the strain-time plot.

6.5. Axisymmetric Compression Testing.

Preliminary work was carried out in titanium bearing steel at 900 and 1000 C in order to determine the viability of this deformation mode in the servo-hydraulic machine. In order to compare the behaviour in stainless steel, and correlate it with the rolling direction, specimens machined from the three different directions, shown in figure 37, were tested at 1000 C.

As was mentioned in section 6.3.2., the specimens were placed in the centre of the tools and deformed at strain rates varying from 0.5 to 50 sec^{-1}. The load-displacement data were corrected for origin and friction as described in sections 6.4.2.1. and 6.4.2.3. The final stress-strain curves were obtained using the corresponding equations, section 6.4.2.5.

6.6. Torsion Tests.

From the preliminary results on the titanium bearing steel, it was felt that a comparison between the two compressive tests and torsion would be interesting. Unfortunately, under torsion, the strain rate that can be achieved is an order of magnitude less than that achieved with the servohydraulic machine, but it covers lower strain rates. The machine used for this tests is fully described elsewhere (Cole, 1979; Al-Jouni, 1983).

The specimens were tested at 905 and 1008 C, and different strain rates, after being reheated for 30 minutes at the same temperatures. The equivalent stress was calculated by the formula (Cole, 1979)

$$\sigma = \frac{3\sqrt{3}\ \Gamma}{2\pi r^3} \qquad (6.23)$$

where Γ is the torque and r the radius of the specimen. The equivalent true strain and strain rate are given by (Cole, 1979)

$$\varepsilon = \frac{a\,\theta}{\sqrt{3}\,\ell} \tag{6.26}$$

$$\dot{\varepsilon} = \frac{a\,\dot{\theta}}{\sqrt{3}\,\ell} \tag{6.27}$$

where $a = 0.742r$ is the effective radius (Barraclough et al, 1973; Barraclough, 1974), ℓ the gauge length, and θ and $\dot{\theta}$ are respectively the angle of twist and the twisting speed.

6.7. Distribution of Strain and Microstructural Features.

Work carried out in aluminium and lead (Beynon, 1979; Beynon and Sellars, 1983) has shown that the strain is not homogeneous within the plane strain specimen. In order to determine the effect of strain rate on the strain distribution, specimens were tested at strain rates of 0.5, 5 and 50 sec^{-1}. Optical metallography was carried out on those specimens and in specimens deformed at 900 C at strain rates of 0.5 and 5 sec^{-1}.

6.7.1. Strain distribution.

The strain distribution was measured in specimens which were cut along the centre-line and had a grid was inscribed on them, figure 41. These specimens were machined in such a way that the testing direction was the same as the rolling one, ie corresponding to the specimens marked as normal in figure 37. In adition to the bolts shown in the figure, the specimens tested at the higher strains were welded at the ends.

The deformation was ended at nominal strains of 0.05, 0.1, 0.2, 0.4, 0.6 and 0.8. All the specimens were quenched after the tests. The final strain obtained by those specimens was always slightly higher than the intended one, epecially at the highest strain rate, due to the mechanical inertia of the moving ram. In order to determine the strain distribution, photographs of the deformed grids were taken. The coordinates of the nodes of the grids were measured by a digitizer connected to a PET desk-top computer available in the Department of Geography. This coordinates were analysed and the strain distribution calculated by means of the programs described in section 6.9.2. and appendix 2.

6.7.2. Measurement of recrystallised fraction.

The non-gridded half of the specimens described in the previous section was used to determine the variation of the dynamically recrystallised fraction, measured by point counting. Other specimens, were tested at strain rates of 0.5 and 5 sec^{-1} at 910 C after being reheated at the same temperature for 15 minutes. The strain given varied from about 0.5 to 1.5 ε_p, where ε_p is the strain to the peak in stress. The specimens were quenched after the deformation.

This average recrystallisation fraction was later compared with the local recrystallised fraction measured along lines of constant strain. This was done by cutting the specimens along planes perpendicular to the grid and tool surfaces. The measurement was then carried out along straight lines of known strain evaluated from the previous strain distribution analysis.

6.8. Temperature Measurement.

Some tests were carried out at 600 C on titanium bearing steel with inserted thermocouples. These specimens were specially machined to 5 mm thickness in order to obtain higher strain rates, the lubricant employed was graphite in an oily suspension (Beynon, 1979; Puchi, 1983). It was intended to obtain strain rates up to 100 sec^{-1}, but the high strength of the material hindered this and only 45 sec^{-1} was obtained.

Three different series of tests were carried out on the stainless steel, two with a single thermocouple embedded in the centre of the samples and another on specimens with two inserted thermocouples.

6.8.1. Specimens with one thermocouple.

In the first series, the thermocouple was inserted to the centre of the specimen, position A in figure 42. The thermocouple was connected to the servo-hydraulic machine and the temperature recorded by the PDP11/10. Specimens 11 mm thick were tested at strain rates around 0.5, 5 and 50 sec^{-1}. Specimens 6 an 8 mm thick, from schedules iv and v, were tested at around 5 sec^{-1} and compared with the thicker specimens. In all cases two deformations were given, the first one up to a strain of 0.05 at 0.5 sec^{-1}, and the second up to around 1.5 at different strain rate. The first deformation was given in order to ensure that the hole in which the thermocouple was inserted was completely closed. A holding period of two minutes was given between the deformations.

In the second series, specimens 11 mm thick were deformed at different strain rates varying from 0.5 to 50 sec^{-1}. The difference from the previous specimens was that the thermocouple was connected to the ultraviolet recorder, mentioned in section 6.2.2., in order to obtain the full temperature evolution

after deformation.

6.8.2. Specimens with two thermocouples.

From the grid analysis, section 6.7.1., it was possible to trace the displacement paths of different regions in the specimen. It was chosen to insert thermocouples in two different regions, marked as B and C in figure 42. Six specimens were employed at strain rates of 0.5, 5 and 50 sec^{-1}, each having two thermocouples, one in the centre, acting as a control, and the second in either region, B or C. The emf was measured as the difference between the couples by connecting each back to back and, in this way, avoid spurious readings due to elastic effects.

A further test was carried out at a strain rate of 5 sec^{-1} in a sample with one thermocouple in the centre connected to a thermocouple in the shoulder of the specimen, position D in figure 42. This was done in order to ensure that the temperature readings were correct.

6.9. Computer Programs.

Two sets of programs were developed in order to analyse mechanical test results and determine the strain distribution within the gridded specimens. Those programs are designed to run interactively in a PRIME 750 computer with virtual memory. Almost all the programs can be run in batch in the same computer. The graphical procedures or subroutines, denominated ghost, belong to the Graphical Output System library, developed by the Culham Laboratories, UKAEA.

6.9.1. Mechanical testing.

All the programs belonging to the first set are written in the implementation by the University of Sheffield of the PASCAL language (Jensen and Wirth, 1978). The non-standard modifications from the current implementation are mentioned in the line by line analysis given in appendix 1. For the sake of simplicity, the whole algorithm was divided into four programs, namely binary-decimal translation, origin correction, stress-strain conversion and graphical output.

6.9.1.1. Binary-decimal translation.

As was mentioned before, the PDP11/10 collects data from the servohydraulic machine by a number of analog to digital converters. The computer dumps the data via punched tape, on which the number of deformations, points per deformation and data from displacement, load and temperature are recorded. In the case of tests in which the temperature is not being measured, the output from the machine command is connected to the temperature input channel, in order to keep a close watch on the computer and the response from the machine. The computer handles the data in the form of two-bytes long integers. The output via the punched tape is in the way of two one-byte long integers, the more significant byte being the second. The parity bit is the 8th bit in the more significant byte. In the case of negative numbers, the complement of the whole two-bytes integer is used in the decimal conversion.

6.9.1.2. Origin correction.

The execution of this program requires a special graphic terminal. It is the only program that cannot be run in batch. The program plots the load-displacemet curve in the screen of the terminal, the first and last point in the interpolation are input, and the computer traces the two straight lines, figures 38 a.) and 39 a.). If the straight lines are the required ones, the data are

corrected, if not, different numbers for the start and end of the interpolation are input until the required lines are obtained. The final corrected curve, figures 38 b.) and 39 b.), is plotted on the screen.

6.9.1.3. Stress-strain conversion.

This program handles the data corrected in the previous program. A subroutine is included in order to process the data from torsion tests. For plane strain compression tests, the friction, spread, temperature and strain rate corrections are carried out. In the case of axisymmetric compression, only the friction correction is included. For all types of tests, the mean stress is calculated for different strain intervals. The calculated data are recorded in tabular and block data form, the latter to be processed by further programs.

6.9.1.4. Graphical output.

This is a multiple purpose plotting program. Stress-strain, strain rate-strain or temperature-strain plots can be obtained. A further option permits to plot any set of data against time.

6.9.2. Strain distribution.

As was mentioned before, a photograph from the deformed grid is taken and digitized in the Department of Geography. In appendix 2 appears a line by line analysis of the computer programs used. The small one, in FORTRAN 77 (Ellis, 1980), is used to convert the decimal numbers obtained from the PET-BASIC into PASCAL standard, i.e. BASIC outputs a decimal number as .01, the same number in PASCAL has to be expressed as 0.01.

The model used is the one described by Beynon (1979), with the difference that in the former case, the strain components are calculated by means of their initial and final coordinates. Here, the strain analysis is carried out for each element, assuming that within it, the deformation is homogeneous. In this case,

the strain components calculated are equivalent to the ones calculated by Beynon for the centre of the element.

In order to correct for any error in the coordinates of the nodes, the points are averaged over a quadrant, assuming that the strain distribution is symmetrical within the four quadrants. A special option is added in the program to consider the case in which the symmetry is only through a mirror plane running along the specimen, like in rolling. For this case, the average is carried out within the two halves.

It is possible to obtain a printout of the values of the strain components and the values of the equivalent and hydrostatic strains. A plot of the coordinates is obtained.

Chapter 7.

Results.

7.1. Preliminary Results.

In order to check previous results on titanium bearing steel (Colás, 1980; Leduc, 1980), preliminary tests were carried out on this steel under axisymmetric compression conditions at 900 C, figure 43, and 1000 C, figure 44. Additional plane strain compression tests were carried out at the higher temperature, figure 44. The curves are corrected for origin, friction and, in the case of plane strain, spread. No temperature correction was attempted. It can be seen that the stress-strain curves obtained are those of a material that recrystallise dynamically. The initial work hardening decreases until a maximum in stress is achieved.

The values for strain to the peak versus strain rate are plotted in figure 45. Additional data from Colás (1980) and Leduc (1980) are included. A number of curves are traced through the data; two of them corresponding to the axisymmetric tests and the rest to plane strain specimens tested at different temperatures. In all cases, a maximum in strain is encountered at a certain strain rate, any further increase in strain rate leads to a decrease in the strain to the peak. The maxima for axisymmetric tests are encountered at about $\dot{\varepsilon} = 15\ sec^{-1}$. For plane strain the maxima are encountered at around $\dot{\varepsilon} = 7\ sec^{-1}$.

At any equivalent strain rate, the value of strain to the peak is higher for the specimens tested under axisymmetric conditions than for plane strain specimens. The difference in value may decrease toward lower strain rates. It is interesting to notice that at the highest strain rate tested, all the values of

strain to the peak for plane strain tests lie within the same scatter band, notwithstanding the difference in testing temperatures.

When plotting the logarithm of the Zenner-Hollomon parameter, Z, against the value of the hyperbolic sine of $\alpha\sigma$, where σ is the peak stress and $\alpha = 7.5 \times 10^{-3}$, a linear relationship is achieved, figure 46. In this case, the value of the activation energy, Q = 300 kJ/mol-K, in Z was taken from Leduc (1980). It is interesting to notice that the value of the peak stress achieved under axisymmetric conditions is higher than the one obtained in the plane strain tests at any equivalent strain rate.

7.2. Mechanical Testing of AISI 316 Stainless Steel.

7.2.1. Initial grain sizes.

The following initial grain sizes were employed during the research:

a.) Plane strain compression. The grain size was obtained from grain growth from specimens obtained from the schedules described in the previous chapter. For specimens prepared from schedule i, four different grain sizes, varying from 19 to 160 μm, were obtained after preheating the specimen for 15 minutes at different temperatures, figure 47. Grain sizes of around 30 μm were obtained from schedules iv and v after preheating the specimens for 15 minutes at around 1000 C, figure 48 a.) and b.).

b.) Axisymmetric compression. All the specimens were machined from slabs obtained form schedule i. Grain size of around 30 μm was obtained after preheating for 15 minutes at about 1000 C, c.f. figure 47 b.).

c.) Torsion. Grain sizes of 30 and 40 μm were obtained from preheating the

specimens for 30 minutes before testing at around 900 and 1000 C respectively, figure 48 c.) and d.).

The specimens were electrolytically etched in concentrated HNO_3 using 4 volts (Cole, 1979).

7.2.2. Stress-strain curves.

The stress-strain curves obtained when testing the stainless steel can be grouped as showing:

a.) Grain size effect. Plane strain specimens were tested with different initial grain size at 910 C, figures 49 to 52.

b.) Geometry and orientation effect. Specimens from different rolling schedules were used to obtain stress-strain curves from plane strain specimens with original thickness of 6, 8 and 11 mm, figures 53 to 55. Additional specimens with initial 11 mm thickness were tested in the transverse direction, figure 56. The ratios for specimen thickness over tool width, h/w, were 0.40, 0.53 and 0.73.

c.) Axisymmetr ic compression. Specimens machined in the trough thickness, width and length directions were tested, figures 57 to 59. Stress-strain curves obtained in specimens with height over diameter equal to 1 are shown in figure 57.

d.) Torsion. Two temperatures were used. The stress-strain curves obtained at 905 C are traced in figure 60, the ones obtained at 1008 C are in figure 61.

In each case, the compressive curves were corrected for origin, friction and, for the plane strain specimens, for spread. As with the titanium bearing steel, no temperature correction was done. It can be seen that all the curves are typical of a material in which the main restoration process is dynamic recrystallisation. The specimens tested at the lowest strain rates, curves A and

B in figure 61, present the periodic oscillations described elsewhere (Rossard and Blain, 1955; Luton and Sellars, 1969).

7.2.3. Strain to the peak.

Figure 62 presents the plot of strain to the peak versus strain rate for the specimens tested at around 900 C. In the plane strain compression tests the effect of the initial grain size is the expected one; the strain to the peak increases as the grain size increases (Ahlblom, 1977; Sellars, 1978; Roberts et al, 1979; Al-jouni, 1983). Maxima in strain to the peak are achieved between strain rates of 2 and 5 sec^{-1}. At the higher range of strain rate, the value of strain to the peak is found to be independent of the original grain size. For comparison, the data from the torsion tests at 905 C are plotted. The strain to the peak increases with the increase of the strain rate through all the tested range. At any equivalent strain rate, the strain to the peak achieved under torsion conditions is higher than the one obtained under plane strain compression with equivalent grain size.

The strain to the peak versus strain rate plot for the specimens tested at around 1000 C appears in figure 63. All the values for the plane strain compression tests lie within the same scatter band, notwithstanding the difference in the initial geometry and testing direction. The maximum in strain to the peak is achieved at around strain rates of 1 sec^{-1}. For the axisymmetric specimens two different behaviours are found, one for the specimens tested in the through the width and through the length directions, and another for those tested in the through the thickness direction, the data for the specimens machined through the thickness with height over diameter ratio equal to one lie between the two curves. In both cases, the maximum in strain to the peak is achieved at around 10 sec^{-1}. The data from the torsion tests agree with the data

from the through the thickness tests, but at low strain rates, the values are higher than the ones that would be expected from plane strain or from torsion at the lower temperature, figure 62. This could be due to the coarser initial grain size in the torsion specimens at the higher temperature, $d_o \simeq 43$ μm, compared with the grain size in the other tests, $d_o \simeq 30$ μm.

Comparing the plane strain data in this figure with those in the former one, it can be observed that the values of strain to the peak at high strain rate are the same for all the specimens tested under plane strain conditions. At lower strain rates, the values of strain to the peak for the specimen tested at 1006 C are lower than those obtained at 910 C with equivalent grain size. The maximum strain to the peak is achieved at a lower strain rate at 1006 C. In all cases the values of strain to the peak are higher for axisymmetric compression and torsion than for plane strain compression.

7.2.4. Stress values.

The dependence of stress on strain rate and temperature for the former curves was evaluated at three distinct levels; low strain, evaluated at 0.15 strain, at the peak and at the steady state.

7.2.4.1. Stress at 0.15 of strain.

The values in stress to this strain level for the specimens tested at the lower temperature are represented in a semilogarithmic plot in figure 64. The stress level is found to be dependent on the initial grain size. For each set of curves, with different initial grain size, the relationship can be approximated to

$$\dot{\varepsilon} = A\exp(\beta\sigma) \qquad (7.1)$$

where A and $\beta = 0.025$ are constants. At high strain rates the values of stress tend to deviate towards higher values of stress. The data obtained from the

torsion tests seem to agree with that for the coarser grain size in plane strain.

In figure 65 the data for the tests carried out at the higher temperature are represented, all the data fall within a scatter band that follows the relationship described by equation (7.2), the value of β is found to be the same that in the former case. The tendency, described previously, to deviate towards higher values of stress at high strain rates is greater in those tests.

In order to check the value of the activation energy employed in the calculation of the Zenner-Hollomon parameter, Q = 460 kJ/mol K (Barbosa, 1983), the data presented in figures 64 and 65 are plotted against Z in figure 66. In this case the relationship is given by

$$Z = A'\exp(\beta\sigma) \qquad (7.2)$$

where A' is a constant. From this plot the value of β = 0.026 agrees with the former one.

7.2.4.2. Peak stress.

The plots of the peak stress values against the strain rate appear in figures 67 and 68 for the tests at 900 and 1000 C respectively. The behaviour encountered in the specimens with different initial grain size, figure 67, is similar to that described at the lower value of strain, but with β = 0.024.

At the higher temperature, the behaviour is different, a series of lines can be fitted with β varying from 0.019 to 0.027 depending on the initial geometry and in the testing conditions. Towards higher values of strain rates, the thinner plane strain specimens achieve a lower value of stress than the thicker ones, and those ones lower than for axisymmetric compression or torsion.

The values of peak stress from the present project are plotted with additional data from the literature versus Z in figure 69. Although the scatter, all the data fit relationship (7.2) with $\beta = 0.025$.

7.2.4.3. Stress at the steady state.

At this stage the stress is plotted against Z only, figure 70. It can be seen the present results agree with the general behaviour observed previously (Barraclough 1974; Ahlblom, 1977; Sellars, 1978; Roberts et al, 1979; Al-jouni, 1983). All the data fall within a scatter band that follows equation (7.2) with $\beta = 0.031$.

7.2.4.4. Grain size effect.

As was mentioned earlier, there was a certain tendency for the material with smaller grain size to achieve higher levels of stress compared with specimens with coarser grain size, figures 64 and 67. It can be seen that in grain sizes coarser than 60 μm the level of stress, both at 0.15 strain and at the peak, depends only in the strain rate, in agreement with previous research (Sah et al, 1974; Roberts et al, 1979).

7.2.5. Static restoration.

Double deformation tests were carried out at strain rates of 0.5 and 5 sec^{-1}. The strain for the first deformation was kept at $0.9\ \varepsilon_p$, the annealing periods were changed from test to test. The calculation of the restoration index, R, is given by the equation

$$R = \frac{\sigma_m - \sigma_2}{\sigma_m - \sigma_1} \qquad (7.3)$$

where σ_m is the flow stress at the end of the first deformation, and σ_1 and σ_2 are the yield stresses in the first and second deformation respectively. The resultant stress-strain curves are shown in figures 73 and 74.

Figure 75 show the restoration curves. The one obtained at 0.5 sec^{-1} presents the high restoration at short times characteristic of materials that present metadynamic recrystallisation (Jonas and McQueen, 1975). Full restoration is achieved after 20 seconds. It is interesting to notice that lower restoration is achieved by the specimens tested at 5 sec^{-1} at short time intervals, but full restoration is achieved within shorter times.

7.3. Strain Distribution Analysis.

In order to determine the distribution of strain, and its effect on the microstructure present in the specimen, series of specimens were deformed at different strain levels and then quenched. Normal specimens were tested at strain rates around 0.5 and 5 sec^{-1} at 910 C, figure 76 a.). The gridded specimens shown in figure 41, were used at the higher temperature at strain rates of 0.5, 5 and 50 sec^{-1}, figure 76 b.). The actual value of the nominal strain was calculated from the load-displacement data in the way described in section 6.4.2.

7.3.1. Results from gridded specimens.

Photographs of the deformed grid were taken from the specimens marked in figure 76 b.). Figure 77 shows the photographs from specimens deformed at nominal strains of 0.05 an 0.1. Figures 78 to 81 show the grids on specimens deformed up to nominal strains of 0.2, 0.4, 0.6 and 0.8 respectively.

The coordinates of the nodes were measured by a digitizer connected to a PET desk-top computer, available in the Department of Geography. With the help of the programs described in appendix 2, the data were analysed and the flow of

material within the specimen was determined, figures 82 to 84.

In the computer analysis, it was assumed that the specimen is divided into the small elements marked by the grid. The value of the different components of strain were calculated assuming perfect plane strain conditions in each element. Only one quadrant of each specimen is represented after the value of strain in each element is averaged with its correspondent element in the other quadrants. Contour maps, figures 85 to 91, were obtained smoothing-out the values of the total strain for each specimen. The strain intervals marked in the figures are

Strain interval.	Strain range.
0	< 0.09
1	0.10 - 0.19
2	0.20 - 0.29
3	0.30 - 0.39
4	0.40 - 0.49
5	0.50 - 0.59
6	0.60 - 0.69
7	0.70 - 0.79
8	0.80 - 0.99
9	1.00 - 1.19
10	> 1.20

The specimens tested at 0.5 sec^{-1} are shown in figures 85 and 86. Figures 87 to 89 are for specimens tested at 5 sec^{-1} and figures 90 and 91 correspond to the specimens tested at 50 sec^{-1}. The parameters related to these specimens are summarised in Table VIII.

From the diagrams, it can be seen that the strain distribution is complex and follows the patterns found previously in lead and aluminium (Sellars et al, 1976; Beynon, 1979; Beynon and Sellars, 1983). This distribution is independent of the strain rate. Two spots are shown in the distribution maps, one with higher than average strain, hard spot, that corresponds to the centre of the "x" in the slip line field solution theory, and a region with less than average strain, soft spot, slightly above the previous one.

Due to mechanical inertia the specimens deformed at the highest strain rate were, in general, overstrained. In order to eliminate any effect due to higher nominal strain the values of strain in each element were normalised by dividing the value of strain in the element by the nominal strain. Histograms of the calculated strain and the normalised strain values appear in figures 92 to 94, the strain intervals used in the first case are the same as in the contour maps, the strain intervals chosen for the normalised values are as follows.

Interval.	Normalised strain range.
0	< 0.29
1	0.30 - 0.59
2	0.60 - 0.89
3	0.90 - 1.19
4	1.20 - 1.49
5	1.50 - 1.79
6	1.80 - 2.09
7	2.10 - 2.39
8	2.40 - 2.69
9	2.70 - 2.99
10	> 3.00

In the case of the strain histograms, at low strains, a maximum exists in each distribution and is more apparent at the lowest strain rate. At high strains, two maxima are developed, one at lower than average and a second one at higher than average strain. These peaks correspond with the previously mentioned hard and soft spots and are more marked towards the higher strain rates. This variation in the behaviour between high and low strains and strain rates is not so apparent for the normalised histograms. Although it was expected that the peak in the normalised strain histograms would be around the interval marked as three, but the overshoot might be due to the assumption of the perfect plane strain conditions when calculating the values of strain.

The values of the average strain were corrected to allow for lateral spreading in the way described in appendix 3. The values of this corrected strain were plotted against the nominal strain, obtained from the corresponding load-displacement curve, figure 76 b.). The data fall in the oscillating form of

relationship previously found in aluminium alloys (Beynon and Sellars, 1983), figure 95. Two cross-overs of the 45° line appear at strains of 0.42 and at 0.77.

In figure 96 the strain in the active slip line field is plotted against the average strain measured on the grid. The small difference in the values indicates that the averaging along the slip line field is closely similar to the overall average value within the area of specimen under the tools. In figure 97 average strains in 10% of the area with the highest strains and in the 10% of the area with the lowest strains are plotted against the nominal strain, and it can be observed the wide spread of these strains is clearly apparent, especially at the highest strain rate.

7.3.2. Metallographic observations.

As was mentioned before, some specimens were deformed up to the strains marked in figure 76 and then quenched in order to observe the microstructural features. The specimens were mechanically polished and electrolytically etched. Micrographs were taken from the centre of the specimen. Figures 98 and 99 show the microstructural evolution in the specimens tested at 910 C. The evolution of microstructure in specimens deformed at the higher temperature appears in figures 100 to 102. In all cases the magnification is 500x.

The structure presented is that of a material that recrystallise dynamically. At the start of the deformation the grains are elongating, and after a certain period small new grains start to grow in the grain boundaries. The structure was always sharper in the material deformed at the higher temperature. At this temperature, it can be seen that the appearance of the newly recrystallised grains change with the strain rate, being more defined and developed as the strain rate increases.

7.3.2.1. Grain size measurements.

The grain size of the specimens was measured by means of the mean linear intercept technique along two orthogonal directions and averaged. Due to the aspect ratio of the unrecrystallised material, a high standard error was introduced.

When plotting the grain size against the strain achieved by the specimen, a tendency for grain refinement, characteristic of dynamic recrystallisation, is observed at both temperatures, figures 103 and 104. Due to the previously mentioned high standard error, only one line is traced in each figure, but there is a consistent decrease in the mean grain size with respect to the Zener-Hollomon parameter as predicted by the theory (Sah et al, 1973; Jonas and McQueen, 1975; Sellars, 1978). Plotting the same grain size against a modified time parameter, calculated as the ratio of the nominal strain over the strain rate, a steeper gradient in the grain refinement is observed with the increase of the Zener-Hollomon parameter, figures 105 and 106.

7.3.2.2. Dynamically recrystallised fraction.

The dynamically recrystallised fraction was calculated by point counting in the same specimens in which the grain size was measured. It was observed that the recrystallised fraction varied within the specimen from place to place, in agreement with the strain distribution patterns obtained previously, figures 85 to 91.

The average recrystallised fraction was then measured over the surface of the specimens, Table IX. These data are plotted against the modified time parameter in figure 107 for the specimens tested at 910 C and in figure 108 for the specimens tested at 1006 C. In all the cases, the recrystallised fraction followed an Avrami type of relationship given by

$$Xv = 1 - \exp[B(\varepsilon/\dot{\varepsilon})^m] \qquad (7.4)$$

where ε and $\dot{\varepsilon}$ are the nominal values of strain and strain rate and B and m are constants. The values of m were of 1.30 and 1.80 for strain rates of 0.547 and 5.163 sec^{-1} respectively, when testing at 910 C, and of 1.68, 3.08 and 3.56 for strain rates of 0.413, 4.824 and 43.06 sec^{-1} respectively for the tests carried out at the higher temperature. The open points marked in figure 108 represent values of local recrystallised fraction measured along lines of constant strain obtained by cutting the specimens along the breadth.

When the values of recrystallised fraction are plotted against average strain (filled points) or local strain (open points) for data measured over the deforming area or constant strain lines, all the data fall within the same scatter band, for the specimens tested at 1006 C, figure 109.

The local values of recrystallised fraction were averaged when the measurements were carried out in different samples, but in regions with equal local strain.

The difference in the values of the exponent m, equation (7.4) may indicate that there is a common feature between the tests carried out at the lower temperature and the tests carried out at the lowest strain rate at the higher temperature. In order to observe if there was a similarity, the recrystallised fraction was plotted against the ratio of the nominal strain over the measured strain to the peak, figure 110. In this curve, it can be seen that all the data fall on two curves, one for the highest strain rate at 1006 C and the second for the other strain rates, notwithstanding the difference in the testing temperature.

7.4. Temperature Measurements.

In order to compare the temperature increase and distribution within the specimens, some tests were carried out with either one of two inserted thermocouples. Some preliminary work was carried out in the titanium bearing steel.

7.4.1. Preliminary work.

Specimens 5 mm thick were used in order to obtain higher strain rates than 50 sec^{-1}. In all cases one thermocouple was inserted in the centre of the sample. A relatively low testing temperature was chosen in order to observe if the temperature increase during deformation would be high enough to cause the local transformation to austenite.

Due to the high strength of this material, figure 111, the highest strain rate achieved was of 48 sec^{-1}. The temperature increase registered by the thermocouples, figure 112, was not high enough under any circumstances to achieve the desired austenitic transformation, but it can be seen that the temperature-strain curves, obtained at high strain rate, present a series of kinks or bumps. The curve marked as the theoretical adiabatic heating was calculated with the help of equation (5.1) from the corresponding stress-strain curve. It can be seen that, except for the curve obtained at the lowest strain rate, all the registered temperature-strain curves lie at higher temperature than the adiabatic one.

7.4.2. Single thermocouple tests.

Tests were carried out on specimens of the standard 11 mm thickness and on one specimen each of 6 and 8 mm thickness. In these tests, double deformation was given and the thermocouple was connected to the computer of the servo-hydraulic machine. The first deformation up to a strain of about 0.05 at a strain rate of about 0.5 sec^{-1} was given in order to ensure the closure of the hole in which the thermocouple was inserted, and obtain a reliable temperature-strain curve. After an annealing period of two minutes, the second deformation was given at strain rates of 0.5, 5 and 50 sec^{-1}, figure 113. The curve marked as E, in which only one deformation was given, was for a specimen deformed with two thermocouples connected back to back. One thermocouple was in the centre and the other in the shoulder of the specimen, in this way, the temperature difference between the two regions was registered.

The actual temperature-strain curves are traced in two figures. In figure 114, the curves for the tests at 0.5 and 50 sec^{-1} are represented. In curves B and C two kinks similar to the ones previously mentioned in figure 112 appear. After the kink, both curves present a temperature increase rate similar to that of the theoretical adiabatic one, B'. The curves obtained at 5 sec^{-1} are plotted in figure 115. In this figure, the specimen with two thermocouples, D, was displaced to make its origin coincide with the origin of the other tests. A is the temperature-strain curve of the specimen 6 mm thick, B of the specimen 8 mm thick. The temperature increases registered fall within the same scatter band, notwithstanding the different testing conditions.

It is interesting to notice the relative position of the theoretical adiabatic curve in relation with the registered one. For low strain rates, the adiabatic curve is higher than the registered one, for high strain rates, the contrary appears, figure 114. At intermediate strain rates, figure 115, the

registered temperature-strain curve lies above the adiabatic one at low strains, but a reverse occurs at high strains.

In order to follow the temperature evolution after deformation, some specimens were deformed with the thermocouples connected to the ultraviolet recorder described elsewhere (Harding, 1976), figure 116. The most notable feature is the high temperature achieved at the highest strain rate, curve F, followed by a very high drop in temperature after the end of deformation. The temperature increases reached by the tests at 5 and 10 sec^{-1} and their respective drops are not as marked. Towards the lower range in strain rate the increase of temperature is moderate and there is not an instantaneous drop in temperature, but rather a smooth decrease.

When plotting the increase of temperature versus strain rate, figure 117, it can be seen that as the strain rate increases both the temperature increase and the dispersion between specimens tested at equivalent strain rates increase. In all cases, the increase of temperature was calculated as the difference between the highest temperature achieved and the initial temperature.

7.4.3. Tests with two thermocouples.

The temperature difference measured between the centre of the specimen and the shoulder, curve D in figure 115, indicates that the readings recorded by the servotest machine when two thermocouples connected back to back are reliable. In this case, the temperature-strain curve obtained by this method is equivalent to any other at the same strain rate after the origin of the different curves coincide. Tests were carried out with two thermocouples in the deformed zone. The temperature-strain curves for the specimens deformed at 0.5 sec^{-1} are shown in figure 118. In the insert the trajectories deduced from the grid analysis, figure 82, are marked. The curves for the specimen deformed at 5 sec^{-1} appear in

figure 119, together with the trajectories deduced from figure 83. In figure 120, the curves for the specimens deformed at the highest temperature are traced. In the insert appears the trace of the thermocouple that was nominally to be in the centre of the specimen, but was displaced. In all cases, the trajectories were deduced from the initial and final positions of the thermocouples. In the inserts only the trajectories up to strains of about 0.8 are drawn. The traces of the specimens correspond to that of the specimens used in the determination of the strain distribution and deformed at strains of 0.4 and 0.8.

It can be seen that as the strain rate increases, the temperature gradient within the specimen increases, helping the explain the dispersion towards high strain rates, figure 117.

Chapter 8.

Discussion.

8.1. Shape of Stress-strain Curves.

The stress-strain curves in figures 43, 44 and 49 to 61 are those of a material that recrystallise dynamically during deformation. In each curve, the peak in stress is due to the interaction between hardening and softening mechanisms.

8.1.1. General Remarks.

In the case of lead, figure 22 (Sellars et al, 1976), no inversion in the strain rate dependence of the strain to the peak in stress is found. The expected relationship (Luton and Sellars, 1969; Sellars, 1978) between the strain to the peak in stress and the strain rate is found. The strain rate at which a maximum in strain to the peak appears is higher for titanium bearing steel, figure 45, than for the stainless steel, figures 62 and 63. The main difference between the three materials is the energy involved in the deformation represented as the area under the stress-strain curve. This energy will produce an increase of temperature given by equation (5.1) that might help to localise the strain within the specimen, and as will be shown later, this increase of temperature by itself modifies the shape of the stress-strain curve.

The strain to the peak achieved under plane strain compression conditions at high strain rates seems to be dependent mainly on the testing method and, only secondarily, on the material. The value of the strain to the peak achieved at the highest strain rate is around 0.20 for the stainless steel and 0.25 for

the titanium bearing steel. In axisymmetric compression this behaviour was not observed, but it might be because not a high enough strain rate was attempted. As can be seen in figure 45, the values of strain to the peak tend to approximate towards a common value at the top end of the experimental strain rate range.

In section 7.2.4., when plotting the stress values at 0.15 strain and to the peak it was observed that the material followed equations (7.1) and (7.2) up to a strain rate of about 10 sec^{-1}. At higher strain rates, the material developed a certain tendency to deviate towards higher values of stress. This tendency was more noticeable when the data were plotted against strain rate. The incorporation of data tested at different temperatures by means of the Zen_er-Hollomon parameter disguised this phenomenon. It is interesting to notice that at the steady state all the values of stress fall within the same scatter band.

The high values of stress obtained in the samples with small grain size, figures 71 and 72, might be due to the thermal history prior to deformation. In order to obtain small grain sizes, the specimens were reheated at low temperatures for short periods of time and this might induce precipitation of the $M_{23}C_6$ carbide. The coarser grain sizes were obtained after preheating the specimens at temperatures higher than that to take $M_{23}C_6$ into solution (Ghomaschi, 1983). Specimens obtained from similar treatments are being studied by Barbosa (1983) to determine if precipitation is responsible for this effect.

8.1.2. Velocity effect.

When plotting the stress values, at low strains and at the peak, against strain rate for the specimens with different initial geometry, figures 65 and 68, it was found that the stress for the specimens varied with the specimen thickness over tool width, h/w, ratio. The higher stress being achieved by

specimens with higher ratios.

By plotting the initial velocity of the ram against the stress levels, figure 121, it was found that the stress values, independent of the initial geometry, followed a relationship of the type

$$V = B\exp(\eta\sigma) \tag{8.1}$$

where V is the ram velocity and B and η are constants. This relationship holds until a velocity of about 100 mm/sec is achieved, $\dot{\varepsilon} \sim 10\ sec^{-1}$ for specimens 11 mm thick. At higher velocities, the values of stress tend to deviate towards higher values. This deviation coincides with the one mentioned previously, and coincides with results previously observed on aluminium at equivalent velocities (Beynon, 1979; Puchi, 1983).

We can consider that the stress-strain curve does not depend on the average strain rate, as defined by equation (6.23), but is a function of the local shear strain rate. The logical suggestion would be to deduce the local shear strain rate from measurements of local strain, but as material which has been strained to different levels is passing through the slip line field all the time, it is not possible to use any straight forward differentiation method, nor is it clear how a finite difference method could be devised because measurements of strain at very close strain intervals are subject to too large errors for them to be reliable for substraction.

The fact that the stress data correlate with the initial ram velocity, figure 121, but not with the average strain rate, might indicate that the local shear strain rate is about twice as high in the thick specimens as in thin specimens for a given nominal strain rate. This might be due to widening of the slip line bands to occupy a longer fraction of the specimen cross section as the specimens become thinner.

8.1.3. Behaviour at high strain rates.

The deviation in flow stress at high strain rates, figure 68, appears in the curves of all the specimens, notwithstanding the different geometry or testing conditions. The fact that the data for axisymmetric compression tests of two initial geometries of specimen lie within one scatter band indicates that the expected exponential relationship, equation (7.2), breaks down at strain rates higher than 10 sec^{-1}. This relationship has been established from torsion tests that in any case had a maximum strain rate around 5 sec^{-1}. In the case of plane strain compression, the phenomenon appears at the same strain rate at both temperatures regardless of initial grain size, figure 67,and if we allow for the relation of velocity to local shear strain rate, discussed above, it will appear at equivalent values of strain rate to that for axisymmetric data.

We cannot consider that this phenomenon is due to the machine because the load levels recorded in axisymmetric and plane strain compression are completely different, as are the velocities for the same strain rate on the two geometries of axisymmetric specimens. However, the cause of the phenomenon is not understood.

8.1.4. Dynamic recrystallisation.

When the recrystallised fraction versus the ratio of the nominal strain over the strain to the peak was plotted, figure 110, it was found that the peak in stress was achieved around 16% recrystallisation, in agreement with observations on stainless steel deformed under axisymmetric compression by Ahlblom (1977).

In figure 122 curves A' B and B' show traces of the experimental curves, reported in figure 63, for plane strain and axisymmetric compression tests. Figure 110 shows that at strain rates up to 5 sec^{-1} the nominal strain to the

peak flow stress, ε_p, occurs at around 16% recrystallisation, whereas at 43 sec^{-1} it occurs at less than 5% recrystallisation. This indicates that some other factor than recrystallisation is causing the curve to flatten off and therefore to reach a peak stress at lower strain than expected.

Considering that, due to recrystallisation alone the peak stress will occur at 16% recrystallisation, leads to a higher value of ε_p by a factor of 1.8. Using this factor leads to the point shown in figure 122, from which curve A' is interpolated. This has eliminated the decrease in the strain to the peak shown in curve A at high strain rate.

It can be considered that the deformation is carried out only in a small portion of the specimen which lies in the active slip line field at any one time. With measurements such as the ones shown in figure 97, it was possible to deduce, from the nominal strain, the value of strain occurring in a small fraction of the material. Measuring from figures 92 to 94 the average strain occurring in 10, 16 and 20% of the total area having the highest local strain leads to ratios of local to nominal strain that have been applied to curve A in figure 122 to obtain curves C, C' and C''. It can be seen that curve C', for 16% of the area, which should correspond with the 16% that recrystallises first, is now in reasonable agreement with the strain levels found in axisymmetric compression, although instability conditions occur at different strain rates in the two types of tests. The existence of two curves for the axisymmetric data might be due to texture effects.

In section 8.1.2. it was mentioned that the local value of shear strain is about twice as high in the thick plane strain specimens as in the thin ones. If the data presented in figure 63 for the plane strain specimens were corrected for this difference, the points obtained from thin specimens should be plotted at half their nominal strain rate relative to the thick specimens. The values of

strain to the peak will coincide at low and high strain rates, but at intermediate strain rates the data would be forming different curves for each geometry, indicating a difference in influence of deformational heating when the slip line field patterns differ.

8.2. Strain Instabilities.

In the literature review it was pointed out that the occurrence of a maximum in stress is a sign of instability or strain localisation. During hot working the instability in lead and austenitic steels can be associated with dynamic recrystallisation (Jonas and Luton, 1978). It has been shown recently that in materials that recover dynamically only, a small peak, attributed to strain localisation, appears in the stress-strain curve (Lombry et al, 1979).

In the stainless steel being studied, the peak appeared under different conditions, but at constant recrystallised fractions, section 8.1.3. In this case, dynamic recrystallisation cannot be considered as the unique cause for the onset of instabilities. Moreover, as can be seen from figure 123, the shape of the stress-strain curves varies with the testing method.

8.2.1. Determination of the onset of instability.

In chapter 2, the principal criteria for the development of instabilities are given. A reasonable criterion is that of Jonas et al (1976) and Semiatin and Lahoti (1981) as expresed by equation (2.70), in which is considered that the flow will be unstable if the parameter alpha is higher than 5.

The slope of the curves shown in figure 123 were measured and the parameter alpha was calculated. The convention of Jonas et al (1976) requires the stress and strain to be negative, in the present treatment, those parameters remained positive and the criterion was changed to alpha less or equal to 5. In figures 124 to 127 appear the traces of this alpha-strain curves for plane strain specimens, 6 and 11 mm thick, axisymmetric compression and torsion respectively. The values of strain at which alpha equals 5 are plotted in figure 128.

From this last figure it can be seen that the instability, leading to a fall in nominal strain to the peak, is developed due to different causes under plane strain, axisymmetric or torsion conditions, although for this last case only one stress-strain curve was analysed.

8.2.2. Causes of instabilities.

In the case of axisymmetric compression, it can be argued that the instability is caused by barreling formation. In figure 129 the load-displacement curves for the axisymmetric specimens are traced, arrows are marked at the change of slope associated by the onset of barreling (Nester and Pohland, 1982). The values of strain associated with those displacements coincide with the strain at which $\alpha = 5$, in agreement with theoretical considerations by Jonas et al (1976) and Kocks (1981). Observing the specimens used in those tests, it can be seen that little barreling has taken place, i.e. little localisation has developed despite the criterion, and in this case, it can be considered that the strain distribution remains homogeneous.

The reduction in the value of strain at which the instability appears at high strain rates for the axisymmetric tests might be due to the effect of the increase of temperature. As can be seen in figure 130, this would produce a peak in stress in hypothetical stress-strain curves. It is assumed that for curve A,

only work hardening and recovery are present and conditions are isothermal. Fully adiabatic conditions were assumed to occur in curve B for a "soft" material and in curve C for a "hard" material, see scales on the left and right hand axes of figure 130 a.), leading to the temperature changes shown in figure 130 b.). Curves B' and C' are obtained when half of the adiabatic temperature increase rate is assumed to affect the material. The result is that the strain at which the peak appears tends to decrease with a harder material or with full adiabatic conditions, as mentioned in section 8.1.1. The decrease in stress was measured by equation (7.2) from the data in figure 66, so it can be considered that the effect of the temperature on the reduction of the strain to the peak in stress will vary from material to material depending in the parameters involved in equation (7.2).

The values for the strain at which $\alpha = 5$ in the plane strain specimens can not be considered as real, because Jonas' criterion is based on nominal values of strain and strain rates, not on the local values that, as can be seen later, are governed primarily by geometry, not microstructure. Furthermore it assumes initial homogeneous deformation, which is never present in plane strain compression.

8.3. Strain Distribution.

The strain values obtained from the grid analysis coincided with previous studies on lead and aluminium (Beynon, 1979; Beynon and Sellars, 1983).

8.3.1. Strain values.

The studies were carried out on specimens with h/w ratio of around 0.7. The contour maps, figures 85 to 91, show a tendency for homogeneity at high strains, in agreement with the work on lead and aluminium that proved that the distribution is more homogeneous in specimens with small h/w ratios, but at the same time, this tendency might be due to limitations in the experimental or computational method.

In figure 95 two cross-overs appear at strains of 0.42 and 0.77. In the case of aluminium only one cross-over was detected at 0.44 strain (Beynon and Sellars, 1983). Under frictionless plane strain compression, a change from 2 to 3 'x's appears when the h/w ratio changes from 2 to 3 (Rowe, 1965). With the present geometric conditions, the h/w ratios of 2 and 3 are calculated to appear at strains of 0.39 and 0.74.

The nominal strain is measured from the stress-strain curve obtained from the load-displacement data. Any redundant work will not be taken into account in this way, but will be introduced in the average value if the strain in each element is calculated. Passing from the stage of two to three 'x's will represent a change of sign in the redundant work. The disparity of the values of strain at which the cross-over is obtained could be due to the effect of friction on the slip line field (Loong, 1976).

In figure 96 the average strain of the elements in an approximate solution of the slip line field is plotted against the average strain in the whole specimen. The small difference might be due to the fact that the slip line field that can be traced at any time represents a solution of the geometric configuration of the specimen and, as can be seen in the contour maps, it might extend out of the area under the tools, or it might be modified by friction (Loong, 1976). The average strain represents the past deformation of the

material under the tools.

When comparing the contour maps or the histograms, figures 92 to 94, at different strain rates, little difference can be detected. However, when plotting the highest and lowest values of strains in 10% of the area, figure 97, the spread of strain at different strain rates can be appreciated. Although the data for the test at 0.5 and 5 sec^{-1} fall within the same scatter band, the values obtained at the lower strain rate are consistently under the strain values obtained at 5 sec^{-1}.

8.3.2. Metallographic observations.

It is interesting to compare figures 108 and 109 in which the measured recrystallised fraction is presented. In the first figure, the nominal fraction, full points, measured over the whole specimen, and the local fraction, empty points, measured in two different regions along lines of constant strain, are plotted as a function of a time parameter calculated as the ratio of the nominal deformation over the strain rate. Here, the data fall within a scatter band and, in certain cases, the average values lie in the middle of the band.

In the second figure, the recrystallised fraction is plotted against the average or local strain, depending on how the fraction was measured. In this case, it can be seen that the recrystallised fraction depends only on the actual value of strain and not on the time elapsed to achieve it, indicating that the dislocation density at higher strain rate provides a higher driving force for dynamic recrystallisation (Sandström and Lagneborg, 1975; Roberts and Ahlblom, 1978).

8.4. Temperature Related Effects.

The effect of temperature on the stress-strain results might be due to the actual increase due to deformational heating, or to its relative distribution within the specimen, or to both.

8.4.1. Deformational heating.

The curves obtained when plotting the strain to the peak in stress versus the strain rate, figures 45, 62 and 63, can be divided into three regions. The first one when the strain to the peak increases with the strain rate, the second when any further increase in strain rate leads to a decrease in the value of strain at which the peak is achieved, and the third one in which the the strain to the peak remains constant. In the case of plane strain compression at 1000 C, figure 63, the first stage finishes around 1 sec^{-1}, the second at around 40 sec^{-1}.

When the temperature evolution during deformation was measured, three different behaviours were found, figures 114 and 115. At low strain rates, the temperature measured by the thermocouple inserted in the centre of the specimen was always lower than the theoretical rise in temperature due to adiabatic heating, equation (5.1). At intermediate strain rates, the measured temperature increase was found to be higher than the calculated one at low strains, but, at high strains, the calculated temperature was higher than the measured one. At high strain rates, the measured temperature was always higher than the adiabatic one, and a bump was appearing towards low strains. Similar behaviour was previously observed in lead, figure 22, and niobium bearing steel, figure 23, but it was attributed to other causes.

The only explanation of the higher than adiabatic temperature increase is that the thermocouple was located in zones with higher than average strain. The extreme case arises at the top strain rates, and as can be seen in the contour maps, figures 90 and 91, and from figure 131, the centre of the specimen is within the slip line band up to strains equivalents to that at which the bump is observed. This same bump might be the result of the cooling down of the material from neighbouring regions when the slip line bands depart from the centre of the specimen.

Considering the temperature difference within the specimen, figures 118 to 120, and the decrease of temperature after deformation, figure 116, a certain effect of temperature distribution can be correlated with those three stages. In the first one, the difference in temperature is small, and when the deformation finishes, the heat is dissipated by convection or radiation to the furnace, curves A to C in figure 116. In the second stage, the difference in temperature is higher, and at the end of deformation, the hotter regions cool down by conduction to the surrounding material, producing the small peak observed in curves D and E. In the third stage, the temperature gradient within the specimen seems to be very high, figure 120, and the cooling produced by the surrounding material may be the very strong drop of temperature shown in curve F, figure 116.

8.4.2. Restoration curves.

In figure 75 the anomalous behaviour of the material during static restoration at strain rates of 5 sec^{-1} was noticed. In the case of the specimen that was annealed for 0.5 sec, we can consider that the temperature at the start of the first deformation was 1006 C. From figure 115, it can be considered that at the end of the deformation, the material is at 1036 C. At this strain rate

equation (7.2) can be employed with the values obtained from figure 69. From this, the stress can be considered to change from 229 to 249 MN/m^2. It can be considered that the annealing period has not taken the material to the initial temperature, but to about 1015 C, figure 116. In this case, the temperature correction of the stress at the start of the second deformation will change the value from 224 to 229 MN/m^2. Using equation (7.3), the restoration index is calculated to be 23.3%.

This rough calculation does not reach the value expected, but indicates that one of the causes for the low restoration index is the increase of temperature during straining, and the subsequent decrease after deformation. An additional factor to the low restoration index obtained at the higher strain rate may be the aspect of the recrystallised fraction, that seems to be different at strain rates of 0.5 and 5 sec^{-1}, figures 100 and 101, although it might be the same fraction if the strain at the end of the first deformation is the same fraction of the strain to the peak at both strain rates, figure 110. Observing the aspect of the stress-strain curves used to calculate those restoration curves, figures 73 and 74, it can be considered that a certain geometry or velocity effect is present. At the start of the second deformation the specimens have an h/w ratio of 0.51, and a change in the width of the slip line bands might be produced and the values of stress then measured will not be equivalent to those measured during the first deformation. This geometry effect will cause a more marked effect at the higher strain rate, figure 68.

8.4.3. Microstructural effects.

In section 7.4.2. it was pointed-out that the microstructure was neater and the dynamically recrystallised grains were more equiaxed as the strain rate maximum increases, figures 98 to 102. In figure 117 the increase of temperature versus strain rate is plotted, and it can be seen that at low strain rate, the deformation is carried out at a lower temperature than at the higher strain rates. The same argument can be used to explain the evolution of the grain size during deformation, figures 104 and 106. The effect might not be so marked at 900 C, figures 103 and 105, because the increase of temperature will not increase the recrystallisation and grain growth kinetics as much as they will be increased from 1000 C.

The apparent change of the Avrami exponent, equation (7.5), in figures 107 and 108 with increase of strain rate is an indication of the increasing effect of deformational heating, which produces an increase in temperature and hence in recrystallisation rate. In figure 109, the effect of this temperature increase is shown to affect in the same proportion the local or nominal values of recrystallisation at each strain rate.

8.4.4. Temperature distribution.

The temperature difference between the centre of the specimen and a special displacement path are plotted in figures 118 to 120. In each curve a number of oscillations appear, and, in order to interprete them, the positions of the thermocouples within the deformation path with respect to the slip line field are illustrated in figure 131.

The coordinates of each point were deduced taking into account the initial and final positions of the thermocouples within the specimens. Up to strains of around 0.8, those coordinates were cross-checked against the deformed grid,

figures 82 to 84. The slip line field was traced to agree with the geometric conditions. The points marked as A, A' and B correspond with those of the curves and inserts in figures 118 to 120 for each strain rate.

It can be seen that the temperature difference increases when the eccentric thermocouple enters the slip line field or when the slip line field does not include the centre of the specimen. The temperature decreases when the contrary occurs. For instance, in figure 119, it can be seen that from the start of deformation up to a strain of 0.1, the temperature difference decreases for curve A and remains constant for curve B. In figure 131 it can be seen that thermocouple A lies outside the slip line fan, but thermocouple B and the one in the centre of the specimen lie within the fan. From 0.1 to 0.2, it seems that thermocouple B is out of the fan and in from 0.2 to 0.5. The thermocouple in the centre is first in and then out of the slip line band. Thermocouple A is out all the time. The result in those cases is that curve B, figure 119, first increases and then decreases. At a strain of about 0.8 this thermocouple goes out of the part of the specimen under the tools, figure 131, resulting in the decrease in temperature registered in figure 119. Thermocouple A goes out of the region under the tools at around a strain of 1.2, but it remains in the region of very high shear, just outside the area under the tools, marked in the contour maps. This results in the very high increase in temperature shown in figure 119.

The excesively high curve marked as B in figure 120 may be a spurious result due to false contact of the couple at the specimen surface, created when the hole in which the thermocouple is insert was closed with a centre punch, and, in this case, the thermocouple will be registering the temperature at the surface and not in the interior of the specimen.

8.4.5. Steady state.

As was mentioned previously, the values of stress at 0.15 strain and peak stress are deviated towards higher values at high strain rate. At the steady state this does not appear, figure 70.

Although all the values lie within a scatter band, the value of β, equation (7.2),is lower than at the smaller strain levels, and the values of stress obtained under torsion are consistently higher than the values obtained in plane strain compression. The values of Z were calculated on the basis of the initial temperature, and, as can be seen in figures 114 and 115, an increase of temperature is achieved during the test. If the values of Z were corrected for the average value of temperature increase as proposed by Foster (1981), it would result in a lower value of β. Also the high deviation towards high stress values would be present at high strain rates. The occurence of this effect at the high strains of steady state eliminates the possibility that it arises from an initial shock loading or transient slip line field effect.

Moreover, if we compare the stress-strain curves of the titanium bearing or the stainless steel, it can be seen that the slope in the stress-strain curve after the peak is achieved in plane strain compression is completely different from that for axisymmetric or torsion. In any case, the value of stress that would be achieved by axisymmetric compression is higher than the value for plane strain at equivalent strain rates.

Both phenomena, the non-deviation of stress at high strain rate and the softening in plane strain might be due to deformational heating, that in the first case may be high enough to counteract the hardening observed at lower stresses. In the second case, the temperature gradient increases and this will reduce the stress value in the way proposed by equation (7.2).

8.5. Comparison of Stress-strain curves

Different mechanical tests were employed to determine the properties of the austenitic steels. It was expected that the relationship between different tests would be straight forward, but the increase of temperature during deformation and the heterogeneity in the plastic deformation made this difficult.

8.5.1. Plane strain and axisymmetric compression.

In figures 95 to 97 the heterogeneity during plane strain deformation is documented. In order to compare the results between both compressive tests, a stress-strain curve obtained under axisymmetric compression was chosen and different corrections were carried out on it.

The first correction was due to strain distribution. The strain in the slip line field was plotted against the nominal strain, figure 132. A third degree polynomial was fitted to the experimental data

$$\varepsilon_s = 0.0095 + 2.16\varepsilon_n - 3.64\varepsilon_n^2 + 2.98\varepsilon_n^3 \qquad (8.2)$$

where ε_s and ε_n are the strain in the slip line field and the nominal one. This relationship was chosen over those in figure 95 and 96 because the material that is to be strained is contained within the slip line field, and, as was indicated in the previous sections, the strain distribution in axisymmetric compression is considered to be homogeneous because the barreling effect in this case can be neglected. By correcting the strain values of the axisymmetric tests by the ratio of the nominal strain (the one present in a homogeneous strain test) over the strain given by the polynomial (the one of the heterogeneous plane strain test) the stress-strain curve is displaced towards the left with the higher initial slope expected in more heterogeneous distributions of strain, curve B in figure 133.

The second correction is due to the stress distribution associated with the strain distribution along slip bands.For this, the histograms in figure 93 were used to calculate the average stress at different strains. The effect of this correction is to decrease the stress values from curve B to curve C in figure 133, i.e. it is trivial.

The most important correction was due to temperature, in this case, it was assumed that at the present strain rate, 5 sec^{-1}, the axisymmetric specimen would be deformed under adiabatic conditions and that the temperature distribution would be homogeneous within the specimen. For plane strain, it was assumed that the material would be deforming in the hottest regions which cross the centre of the specimen at these strains, figures 87 to 89 and 131. From figure 115, the temperature difference, between the temperature measured under adiabatic conditions and that of the average of the temperature-strain curves, was measured at different strains. The values of stress were modified in agreement with equation (7.2) using the values obtained from figure 66. This last correction reduces the difference in stress between the corrected axisymmetric curve, D in figure 133, and the plane strain one, E, to about 2% up to the strain to the peak in stress. At higher strains both curves diverge, but this might be due to different effects of instabilities.

8.5.2. Plane strain compression.

In figure 134 the schematic variation of the local shear strain, developed in the slip line bands, is represented. It is assumed that with v/h constant, where v is the initial velocity of the ram and h the height, constant, a decrease in the value of the local shear strain rate is expected with the increase of the tool width over height ratio up to a value around 3 or 4. When the local shear strain rate is plotted against the nominal strain, a series of

curves are obtained, figure 134 b. The implications of this behaviour are useful to explain the differences in values measured at low and high strains in specimens with different initial geometry, figures 65, 68, 70 and 121.

In figure 135, the stress-strain curves of specimens tested with initial height over tool width ratios of 0.73 and 0.40 are shown as curves A and C. Curve B is obtained when the ratio of initial ram velocities is used as a factor in curve A. This correction is assumed to compensate for the variation in width of the slip line bands, and takes curve B within 2% of curve C. Better correlation, as for figure 133, between curves B and C would probably be obtained if the strain distribution for both geometries were known.

Chapter 9.

Conclusions and Suggestions for Future Work.

From this research, it is possible to draw the following conclusions:

1.) Although in all cases the peak in flow stress encountered in the stress-strain curves, for both titanium bearing and stainless steel, is related to dynamic recrystallisation, at high strain rates the strain to the peak can be markedly reduced by deformational heating, without requiring strain localisation.

2.) In the plane strain compression tests the strain rate range can be divided into three parts:

a.) Low strain rates. Characterized by the expected increase of the strain to the peak in stress with the increase of the strain rate. The temperature increase due to deformational heating is moderate and low temperature gradients are developed. After deformation the temperature decreases in a smooth way.

b.) Intermediate strain rates. In this stage the strain to the peak in stress decreases with the increase of strain rate. There is a marked increase of temperature, the temperature gradients are steeper than for the former stage. After deformation a drop of temperature is characterized by an initial rapid rate in a temperature versus time plot, indicating that significant local temperature gradients have developed within the deformation zone.

c.) High strain rates. The strain to the peak in stress achieves a value that is independent of temperature, geometry or microstructure. The local increases of temperature are very high, as shown by a very strong drop of local temperature immediately after deformation.

3.) The inversion in the dependence of the strain to the peak in flow stress that occurs at intermediate strain rates is due to strain localisation enhanced by local increase of temperature. The fact that this inversion appears at a higher strain rate for axisymmetric tests than for plane strain compression is due to the intrinsic strain heterogeneity in plane strain tests.

4.) In computer simulation of hot working operations, the data obtained at low strain rates are frequently used to predict the behaviour in the hot working domain. The present tests were carried out at equivalent strain rates to those encountered during hot working operations indicate that the stress-strain rate relationships obtained from lower strain rates may break down at strain rates around 10 sec^{-1}, leading to higher flow stresses than predicted.

5.) Grain size has little effect on the inversion in strain to the peak, even though at small grain sizes so $M_{23}C_6$ carbides are present. At low and intermediate strain rates the peak is attained at higher values in samples with coarser grain sizes.

6.) In plane strain compression, it was found that the recrystallised fraction depends on the actual value of strain, either locally or in the average, not on the time required to achieve this strain.

7.) The strain to the peak, at low and intermediate strain rates, is achieved when about 16% recrystallisation is accomplished. At high strain rates the peak appears at lower recrystallised fraction due to temperature increase with strain.

8.) At high strain rates the localisation of temperature rise in the active slip line bands in plane strain compression is detected by implanted thermocouples as they move thorough the active bands. The local temperature rise can be up to twice the value calculated assuming homogeneous adiabatic deformation, indicating the high local shear strain rates that are attained

within the slip bands.

9.) The strain distribution analysis has shown that the average value of strain along active slip bands is independent of the strain rate, but the range of local strain values increases as the strain rate increases.

10.) The difference observed between the initial slope of stress-strain curves obtained under axisymmetric and plane strain compression is due primarily to the complex strain distribution observed in plane strain. A second order effect is given by the stress distribution.

11.) At high strain rates, when the increase of temperature due to deformational heating is significant, the difference in stress level between plane strain and axisymmetric compression tests can be attributed to the temperature gradient developed in plane strain specimens.

12.) It seems that the difference between stress-strain curves obtained from specimens with different initial geometry, h_o/w from 0.7 to 0.4, tested in plane strain compression is due to the change of width of the slip line bands with geometry so that local strain rates are approximately proportional to ram velocity and not to nominal strain rate when the ratio of tool width to specimen height is less than about 3 to 4.

Although it was shown that the value of strain to the peak in stress was affected by the strain and temperature distribution, the following points require further investigation:

1.) It is not clear if the deviation to higher than expected values of stress observed at high strain rates is restricted to testing in compression or is a general phenomenon. It is desirable to look for similar behaviour in tests on different machines, and for actual values of loads registered during rapid working operations.

2.) One of the causes of the high temperature gradients in stainless steel is its relatively thermal conductivity. It would be useful to determine how the phenomena observed in plane strain testing stainless steel are modified in a copper base alloy with much higher conductivity, but the same type of microstructural changes during deformation.

3.) Although it was shown that the strain in the slip line field does not depend directly on the nominal strain rate, it would be interesting to study the strain distribution in specimens with different initial geometry.

Acknowledgements.

First of all, I would like to thank my supervisor Prof. C. M. Sellars, for his continuous encouragement and support during this work, as well as his effort in making me work seriously. I will always recognize the courage of all the people involved in the Department, from A to M floors, in resisting murderous temptations during this long time. I am indebt to the 'Not Working Group' for their help and enthusiasm. Special thanks are due to all the people outside the Department, who in one way or another contributed to this work.

I would like to thank the National Council for Science and Technology, CONACyT, Mexico, the Department of Metallurgy and Davy-McGee for their financial support.

I thank all my friends, without whom, this work would have been submitted earlier.

References.

Abdul N A and Bramley A N, 1973, Proc ICSMA3, Oxford, **1**, 386.

Ahlblom B, 1977, Swed Inst Met Res, Report IM-1208.

Ahlblom B and Sandström R, 1982, Int Met Rev, **1**, 1.

Al-Jouni F E, 1983, Ph D Thesis, Sheffield University.

Anand L and Spitzig W A, 1982, Acta Met, **30**, 553.

Andrew J H, Lee H and Bourne J, 1950, JISI, **165**, 374.

Andrew J H, Lee H and Bourne J, 1950a, ibid, 376.

Argon A, 1973, The Inhomogeneity of Plastic Deformation, ed Reed-Hill, ASM, Ohio, 161.

Armstrong R W, Coffey C S and Elban W L, 1982, Acta Met, **30**, 2111.

Avery H and Backofen W, 1965, ASM Trans Quat, **58**, 551.

Barbosa R, 1983, Ph D Research, Sheffield University.

Barraclough D R, Whittaker H J, Nair K D and Sellars C M, 1973, J Test Eval, 1, 220.

Barraclough D R, 1974, Ph D Thesis, Sheffield University.

Barraclough D R and Sellars C M, 1979, Met Sci, **13**, 257.

Bedford A J, Wingrove A L and Thompson K R L, 1974, J Aust Inst Met, 19, 61.

Beese J G, 1972, JISI, **210**, 433.

Belyayev S P, Likhachev V A, Myslayeyev M M and Sen'Kov O N, 1981, Phys Met Metall, **52**, 143.

Beynon J H, 1979, Ph D Thesis, Sheffield University.

Beynon J H and Sellars C M, 1983, To be published.

Burrows S E, Humpreys F J and White S H, 1979, Proc ICSMA5, Aachen, West Germany, Pergamon, **1**, 607.

Campbell J D, 1967, J Mech Phys Solids, **15**, 359.

Canova G, G'Sell C and Jonas J J, 1980, Can Met Quat, **19**, 259.

Chandra H, Embury J D and Kocks U F, 1979, ibid Burrows et al (1979), 511.

Chandra H, Embury J D and Kocks U F, 1982, Scripta Met, **16**, 493.

Coffey C S and Armstrong R W, 1981, Shock Waves and High Strain Rate Phenomena in Metals: Concepts and Applications, ed Meyers and Murr, Plenum, New York, 313.

Colás R, 1980, M Met Diss, Sheffield University.

Cole A T, 1979, Ph D Thesis, Sheffield University.

Conrad H, 1978, J Mech Work Tech, **2**, 67.

Considère A, 1885, Ann Ponts Chaus, **9**, 574.

Cottingham D M, 1968, Deformation Under Hot Working Conditions, Spec rep 108, Iron and Steel Inst, London, 145.

Demeri M Y and Conrad H, 1978, Scripta Met, **12**, 389.

Eshelby J D and Pratt P L, 1956, Acta Met, **4**, 560.

El-Kalay A K and Sparling L G, 1968, JISI, **206**, 152.

Ellis T M R, 1980, Estructured FORTRAN, Sheffield University.

Exell S F and Warrington D H, 1972, Phil Mag, **26**, 1121.

Farag M M and Hamdy M M, 1976, Met Trans, **7A**, 221.

Farag M M, Sellars C M and Tegart W J McG, 1968, ibid Cottingham (1968), 60.

Ferron G and Mliha-Touati M, 1982, Scripta Met, **16**, 911.

Foster S R, 1981, Ph D Thesis, Sheffield University.

Fitzsimons G, Kuhn H A and Vemkateshwar R, 1981, J Metals, **33**, 11.

Fritzemeier L, Luton M J and McQueen H J, 1979, ibid Burrows et al (1979), 95.

Gilman J J, 1968, Ap Mech Rev, **21**, 767.

Ghomashchi M R, 1983, Ph D Thesis, Sheffield University.

Glover G and Sellars C M, 1973, Met Trans, **4A**, 765.

Gittins A, Hinton L G and Tegart W J McG, 1973, Man Eng Trans, **2**, 199.

Ghosh A K, 1978, Formability: Analysis, Modeling and Experimentation, ed Hecker, Ghosh, Hegel, Met Soc AIME, 14.

Glenn R C and Leslie W C, 1971, Met Trans, **2A**, 2945.

Gottstein G and Kocks U F, 1983, Acta Met, **31**, 175.

Gottstein G, Zabardjadi D and Mecking H, 1979, Met Sci, **13**, 223.

Harding R A, 1976, Ph D Thesis, Sheffield University.

Hart E W, 1967, Acta Met, **15**, 351.

Hartmann K H, Kunze H D and Meyer L W, 1981, ibid Coffey and Armstrong (1981), 325.

Hennaut J, Othmezouri J and Charlier J, 1982, Z Metall, **73**, 744.

Helt D L, 1970, J Appl Phys, **41**, 3197.

Hughes K E, Nair K D and Sellars C M, 1974, Met Tech, **1**, 161.

Hutchinson J W and Neale K W, 1977, Acta Met, **25**, 839.

Immarigeon J P A and Jonas J J, 1974, Acta Met, **22**, 1235.

Jalinier J M, Christoduolo N, Baudelet B and Jonas J J, 1978, ibid Ghosh (1978), 29.

Jeglic F S and Packwood F S, 1978, Metallography, **11**, 43.

Jensen K and Wirth N, 1978, PASCAL: User Manual and Report, Springer-Verlag, New York.

Jonas J J and Baudelet B, 1977, Acta Met, **25**, 43.

Jonas J J, Holt R A and Coleman C E, 1976, Acta Met, **24**, 911.

Jonas J J and Luton M J, 1978, Advances in Deformation Processing, ed Burke, Weiss, Plenum, New York, 215.

Jonas J J and McQueen H J, 1975, Treatise on Materials Science and Technology, Vol 6: Plastic Deformation of Materials, ed Arsenault, Academic, New York, 395.

Jonas J J, McQueen H J and Wong W A, 1968, ibid Cottingham (1968), 21.

Jonas J J, Sellars C M and Tegart W L McG, 1969, **14**,1.

Kocks U F, 1981, Progress in Materials Science: Chalmers Anniversary Volume, ed Christian, Haasen, Massalski, Pergamon Press, Oxford, 185.

Kocks U F, Jonas J J and Mecking H, 1978, ibid Ghosh (1978), 9.

Kocks U F, Jonas J J and Mecking H, 1979, Acta Met, **27**, 419.

Korbel A and Blaz L, 1980, Scripta Met, **14**, 829.

Korbel A, Dobrzanski F and Richert M, 1983, Acta Met, **31**, 293.

Kuhn H A, 1978, ibid Jonas and Luton (1978), 159.

Kuhn H A, 1978a, ibid Ghosh (1978), 259.

Kunze H D, Hartmann K H and Jurgen R, 1981, Pract Met, **18**, 261.

Lamborn I R, Bedford A J and Walsh B E, 1974, Mechanical Properties at High Rates of Strain, Conf Ser 21, Inst Physics, 251.

Leduc L A, 1980, Ph D Thesis, Sheffield University.

Lin H, Hirth J P and Hart E W, 1981, Acta Met, **29**, 819.

Lindhom U S, 1974, ibid Lamborn et al (1974), 3.

Lloyd D J and Kenny D, 1978, Scripta Met, **12**, 903.

Lombry R, Rossard C and Thomas B J, 1979, Report IRSID PA3 2141.

Loong S H, 1976, B Eng Thesis, Sheffield University.

Lücke K and Mecking H, 1973, ibid Argon (1973), 223.

Luton M J and Sellars C M, 1969, Acta Met, 17, 1033.

Malaprade G, Rouby D and Fantozzi G, 1978, Scripta Met, **12**, 1083.

Manganello S J and Abbott K H, 1972, J Mater, **17**, 231.

Mataya M C, Carr M J and Krauss G, 1982, Met Trans, **13A**, 1263.

Mataya M C and Krauss G, 1981, J Appl Metalworking, **2**, 28.

McQueen H J and Baudelet B, 1979, ibid Burrows et al (1979), 329.

McQueen H J and Jonas J J, 1971, Metal Forming: Interrelations Between Theory and Practice, ed Hoffmanner, Plenum, New York, 393.

McQueen H J, Petkovic R, Weiss H and Hinton L G, 1977, The Hot Deformation of Austenite, ed Ballance, Metallurgical Soc AIME, New York,113.

McQueen H J, Wong W A and Jonas J J, 1967, Can J Phys, **45**, 1225.

Mecking H and Gottstein G, 1978, Recrystallisation of Metallic Materials, 2nd Ed, ed Haessner, Dr Rieder Verlag, Stuttgart, 195.

Mecking H and Grinberg A, 1979, ibid Burrows et al (1979), 289.

Mescall J F and Papirno R, 1974, Exp Mech, **14**, 257.

Moss G L, 1981, ibid Coffey and Armstrong (1981), 299.

Murr L E, 1978, Scripta Met, **12**, 201.

Murr L E and Kuhlmann-Wisdorf D, 1978, Acta Met, **26**, 847.

Needleman A, 1978, ibid Ghosh (1978), 54.

Nester W and Pohland K, 1982, Arch Eisenh, **53**, 139.

Nicholson A, Smith D and Shaw P, ibid Cottingham (1968), 161.

Nikkilä K, 1972, Scan J Met, **1**, 9.

Olson G B, Mescall J F and Azrin M, 1981, ibid Coffey and Armstrong (1981), 221.

Orowan E, 1940, Proc Phys Roy Soc Lon, **52**, 8.

Ortner B and Stüwe H P, 1976, Z Metall, **67**, 672.

Pawelski O, Rudiger U and Kaspar R, 1978, Stahl Eisen, **98**, 181.

Plaut R L and Sellars C M, 1983, To be published.

Puchi E S, 1983, Ph D Thesis, Sheffield University.

Richardson G J, Sellars C M and Tegart W J McG, 1966, Acta Met, **14**, 1225.

Roberts W and Ahlblom B, 1978, Acta Met, **26**, 801.

Roberts W, Bodén H and Ahlblom B, 1979, Met Sci, **13**, 195.

Rogers H and Shastry C V, 1981, ibid Coffey and Armstrong (1981), 285.

Rossard C, 1973, ibid Abdul and Bramley (1973), **2**, 175.

Rossard C, 1960, Met Corros Ind, **35**, 102, 140 and 190.

Rossard C and Blain P, 1958, Rev Met, **55**, 573.

Rouby D, Malaprade G and Fantozzi G, 1979, ibid Burrows et al (1979), 565.

Rowe G W, 1965, An Introduction to the Principles of Metal Working, Arnold, London.

Ryan N D, McQueen H J and Jonas J J, 1982, ASM Fall Meeting, St Luis, Mo, USA.

Sachdev A K and Hunter J E, 1982, Met Trans, **13A**, 1063.

Sah J P, Richardson G J and Sellars C M, 1973, Ind J Tech, **11**, 445.

Sandström R and Lagneborg R, 1975, Acta Met, **23**, 387.

Sellars C M, 1978, Phil Trans R Soc Lon, **288A**, 147.

Sellars C M, 1981, Les Traitements Thermomécaniques, 24ème Colloque de Metallurgie, Saclay, 111.

Sellars C M, Sah J P, Beynon J H and Foster S R, 1976, Report SRC B/RG/1481.

Sellars C M and Tegart W J McG, 1972, Int Metall Rev, **17**,1.

Semiatin S L and Lahoti G D, 1981, Met Trans, **12A**, 1705.

Semiatin S L and Lahoti G D, 1981a, ibid, 1719.

Semiatin S L and Lahoti G D, 1982, ibid, **13A**, 275.

Semiatin S L and Lahoti G D, 1983, ibid, **14A**, 105.

Sheppard T and Tutcher M G, 1980, Met Sci, **12**, 579.

Shockey D A and Erlich D C, 1981, ibid Coffey and Armstrong (1981), 249.

Shpigler B and Beraha A, 1977, Color Metallography, ASM, Metals Park.

Sims R, 1954, Proc Inst Mech Engs, **168**, 191.

Staker M R, 1980, Scripta Met, **14**, 677.

Stevenson M G, 1974, ibid Lamborn et al (1974), 393.

Stock T A C and Thompson K R L, 1970, Met Trans, **1A**, 219.

Stock T A C and Wingrove A L, 1971, J Mech Eng Sci, **13**, 110.

Tegart W J McG and Gittins A, 1977, ibid McQueen et al (1977), 1.

Teodosin C, Nicolae V, Soos E and Radu C G, 1979, Rev Roum Sci Tech, **24**, 13.

Thornton P A and Heiser F A, 1971, Met Trans, **2A**, 1416.

Trent E M, 1941, JISI, **143**, 401.

Violan P, 1972, Scripta Met, **6**, 1175.

Violan P, 1973, Scripta Met, **7**, 867.

Wada M, Nakamura T and Kinoshita N, 1978, Phil Mag, **38**, 167.

Wantzen A, Karduck P and Gottstein G, 1979, ibid Burrows el al (1979), 517.

White F E and Rossard C, 1968, ibid Cottingham (1968), 14.

Wingrove A L, 1971, J Aust Inst Met, **16**, 67.

Woodford D A, 1969, Trans ASM, **62**, 291.

Zaid A I O, 1982, Pract Met, **19**, 43.

Zener C and Hollomon J H, 1944, J Appl Phys, **15**,22.

```
1   Program Bintape (input,output,newfile,oldfile);
2
3   const k = 256;
4   type dimens = 1..500; dimen = array [dimens] of real;
5      arra = array [1..5] of integer;
6   var disp,load,temp : dimen; nop : arra;
7      nfile,ofile : alfa;
8      oldfile,newfile : text;
9      ch : char; nt,m,kt : integer; preg : boolean;
10
11     procedure reading;
12      var i,n1,n2,ntp,j,ival : integer;
13
14        function correc (i,j:integer) : integer;
15        begin
16           correc:=k*(j-255)+i-264
17        end;
18
19     begin
20        for i:=1 to nt do
21        begin
22           read(oldfile,n1,n2);kt:=kt+2;
23           nop[i]:=(n2*k+n1) div 2
24        end;
25        ntp:=nop[nt];
26        for j:=1 to 3 do
27        begin
28           for i:=1 to ntp do
29           begin
30              if (kt+2)mod 13 = 0 then
31              begin
32                 readln(oldfile,n1,n2);kt:=kt+2
33              end else
34              if (kt+1)mod 13 = 0 then
35              begin
36                 readln(oldfile,n1);read(oldfile,n2);kt:=kt+2
37              erd else
38              begin
39                 read(oldfile,n1,n2);kt:=kt+2
40              end;
41              if n2 >= 128 then ival:=correc(n1,n2)
42              else ival:=n2*k+n1;
43              case j of
44                 1 : disp[i]:=(ival)/100;
45                 2 : load[i]:=ival;
46                 3 : temp[i]:=ival
47              end
48           end
49        end
50     end;
```

Appendix 1
Programs Used to Determine the Stress-strain Curves.

The next programs are written in the PASCAL version described in chapter 5. In order to obtain the stress-strain curves, the programs have to be processed in the given order.

1.1 Binary to Decimal Translation (Program Bintape).

In this program the original data provided by the PDP11/10 are translated into decimal code. For this, the punched tape is loaded into the ICL1906S computer by means of a standard program and then the data are transfered into the PR1ME750 for which the programs are written.

Line 1.- Program heading, with its name and the name of the files used to communicate with the environment.

Lines 3 to 9.- Declaration of global constant, types and variables used through all the program. The non-standard type alfa, line 9, is defined as packed array [1..8] of char.

Lines 11 to 50.- Procedure used to read the binary numbers provided. Those data are recorded in a file whose lines are thirteen numbers long. Here, all the decimal numbers are formed by the combination of two, eight bit long, bytes. In the form n2*256+n1, line 42. In the case of negative numbers, the sign is taken as a '1' in the first bit of the second byte, in that case, the complement of the two bytes is taken as the actual number, function correc, lines 14 to 17.

The numbers to be read, by this procedure, are the number of points at the end of each deformation, the total number of points being equal to the points at the end of the last deformation. The data are recorded in blocks. First, all the displacement, then all the load, and eventually all the temperature data are read. The displacement readings are converted to the actual ones by dividing them by 100, line 44.

```
1   Program Bintape (input,output,newfile,oldfile);
2
3   const k = 256;
4   type dimens = 1..500; dimen = array [dimens] of real;
5      arra = array [1..5] of integer;
6   var disp,load,temp : dimen; nop : arra;
7      nfile,ofile : alfa;
8      oldfile,newfile : text;
9      ch : char; nt,m,kt : integer; preg : boolean;
10
11     procedure reading;
12      var i,n1,n2,ntp,j,ival : integer;
13
14        function correc (i,j:integer) : integer;
15        begin
16           correc:=k*(j-255)+i-264
17        end;
18
19     begin
20        for i:=1 to nt do
21        begin
22           read(oldfile,n1,n2);kt:=kt+2;
23           nop[i]:=(n2*k+n1) div 2
24        end;
25        ntp:=nop[nt];
26        for j:=1 to 3 do
27        begin
28           for i:=1 to ntp do
29           begin
30              if (kt+2)mod 13 = 0 then
31              begin
32                 readln(oldfile,n1,n2);kt:=kt+2
33              end else
34              if (kt+1)mod 13 = 0 then
35              begin
36                 readln(oldfile,n1);read(oldfile,n2);kt:=kt+2
37              end else
38              begin
39                 read(oldfile,n1,n2);kt:=kt+2
40              end;
41              if n2 >= 128 then ival:=correc(n1,n2)
42              else ival:=n2*k+n1;
43              case j of
44                 1 : disp[i]:=(ival)/100;
45                 2 : load[i]:=ival;
46                 3 : temp[i]:=ival
47              end
48           end
49        end
50     end;
```

Appendix 1
Programs Used to Determine the Stress-strain Curves.

The next programs are written in the PASCAL version described in chapter 5. In order to obtain the stress-strain curves, the programs have to be processed in the given order.

1.1 Binary to Decimal Translation (Program Bintape).

In this program the original data provided by the PDP11/10 are translated into decimal code. For this, the punched tape is loaded into the ICL1906S computer by means of a standard program and then the data are transfered into the PRIME750 for which the programs are written.

Line 1.- Program heading, with its name and the name of the files used to communicate with the environment.

Lines 3 to 9.- Declaration of global constant, types and variables used through all the program. The non-standard type alfa, line 9, is defined as packed *array [1..8] of char*.

Lines 11 to 50.- Procedure used to read the binary numbers provided. Those data are recorded in a file whose lines are thirteen numbers long. Here, all the decimal numbers are formed by the combination of two, eight bit long, bytes. In the form n2*256+n1, line 42. In the case of negative numbers, the sign is taken as a '1' in the first bit of the second byte, in that case, the complement of the two bytes is taken as the actual number, function correc, lines 14 to 17.

The numbers to be read, by this procedure, are the number of points at the end of each deformation, the total number of points being equal to the points at the end of the last deformation. The data are recorded in blocks. First, all the displacement, then all the load, and eventually all the temperature data are read. The displacement readings are converted to the actual ones by dividing them by 100, line 44.

```
51      procedure writing;
52      var i,j : integer;
53      begin
54         write (newfile,nt:4,' ');
55         for i:=1 to nt do
56         write (newfile,nop[i]:4,' '); writeln (newfile);
57         for j:=1 to 3 do
58         begin
59            for i:=1 to nop[nt] do
60            begin
61               if (i)mod(10)<>0 then
62               begin
63                  case j of
64                     1 : write (newfile,load[i]:7:2,' ');
65                     2 : write (newfile,disp[i]:7:3,' ');
66                     3 : write (newfile,temp[i]:7:3,' ')
67                  end
68               end else
69               begin
70                  case j of
71                     1 : writeln (newfile,load[i]:7:2);
72                     2 : writeln (newfile,disp[i]:7:3);
73                     3 : writeln (newfile,temp[i]:7:3)
74                  end
75               end
76            end;
77         if (nop[nt])mod(10)<>0 then writeln (newfile)
78         end
79      end;
80
81   begin
82      repeat
83         write('Data file? '); readln(ofile);kt:=0;
84         reset(oldfile,ofile); read(oldfile,nt);kt:=kt+1;
85         while nt <> 1 do
86         begin
87            read (oldfile,nt);kt:=kt+1
88         end;
89         read(oldfile,nt);nt:=nt-48;kt:=kt+1;
90         reading;
91         nfile[1]:='m';nfile[2]:='_';
92         for m:=1 to 6 do
93         nfile[m+2]:=ofile[m];
94         rewrite(newfile,nfile); writing;
95         write('Finish? ');readln(ch);
96         case ch of
97            'Y','y','1' : preg:=true;
98            'N','n','0' : preg:=false
99         end
100      until preg;
101   end.
```

Lines 51 to 79.- Recording of the decimal numbers into a new file. The first line contains the number of deformations and the number of points at the end of each deformation. The rest of the data are recorded in ten numbers long lines. The recording order is first load, then displacement, and temperature at the end.

Lines 81 to 101.- Main body, the program is repeated for different tests. A negative answer is required to leave the program, lines 95 to 100. The only additional data needed is the name of the file in which the original binary numbers are recorded. In order to avoid confusion with the data, the first number to be taken into account has to be a '1'. The second number, is the number of deformations in the test, this number is not a binary, but the corresponding ASCII value, line 89.

The decimal numbers are recorded in a new file. Assuming that the original name was FILE, the modified data are recorded under the name M_FILE.

```
1   Program Origcor (input,output,origfil,modfil);
2
3   type num = 1..500; arra = array[num] of real; cinq = 1..5;
4      arrb = array[cinq] of boolean; arrc = array[cinq] of integer;
5   var load,disp,temp : arra; preg : arrb; nop: arrc; ch : char;
6      origfil,modfil : text; title,rfile : alfa;
7      nt,i : integer; h0,hf,hi,loads,slope,orden : real;
8
9      function desc(ch:char) : boolean;
10     begin
11        case ch of
12           'Y','y','1' : desc:=true;
13           'N','n','0' : desc:=false
14        end
15     end;
16
17     procedure naming;
18     var i : integer;
19     begin
20        rfile[1]:='m'; rfile[2]:='_';
21        for i:=1 to 6 do rfile[i+2]:=title[i]
22     end;
23
24     function dive (y : real) : real;
25     begin
26        dive:=(y-orden)/slope
27     end;
28
29     procedure correct;
30     var k1,k2,i,j : integer; cg : real;
31
32        procedure maxdisp;
33        var i : integer; mx : real;
34        begin
35           mx:=0; for i:=1 to nop[nt] do
36           if mx < disp[i] then mx:=disp[i];
37           hi:=mx-hi
38        end;
39
40        procedure linearint;
41        var i,m : integer; sx,sx2,sy,syx,delta : real;
42        begin
43           sx:=0; sx2:=0; sy:=0; syx:=0;
44           m:=k2-k1+1; for i:=k1 to k2 do
45           begin
46              sx:=sx+disp[i]; sx2:=sx2+sqr(disp[i]);
47              sy:=sy+load[i]; syx:=syx+load[i]*disp[i]
48           end;
49           delta:=m*sx2-sqr(sx);
50           orden:=(sy*sx2-syx*sx)/delta;
51           slope:=(m*syx-sx*sy)/delta
52        end;
53
54        procedure picnow; ghost;
55        procedure erase; ghost;
```

1.2. Origin Correction (Program Origcor).

This program was written specially for the case of high temperature deformation, in which a thick coat of lubricant is formed. The uncertainty of the origin is created by this coat, and, in the special case of small strains, this error can be very high. In order to avoid errors at the end of the test, a correction similar to the one proposed by Foster (1981) is used in order to correlate the measured and the recorded displacements. An option is provided in case the lubricant thickness is negligible, as in low temperature tests. The data recorded by the PDP10/11 is transformed into actual load values in this program. This program has to be run iteratively in a graphic terminal.

Line 1.- Program heading, similar to the previous one.

Lines 3 to 7.- Declaration of the global types and variables.

Lines 9 to 15.- Function used to determine the result of decisions.

Lines 17 to 22.- Procedure used to correlate the test name and the file in which the data are recorded.

Lines 24 to 27.- Determination of the displacement level as a function of the load in the straight portion of the load-displacement curve.

Lines 29 and 30.- Heading of the procedure used to carry out the origin correction.

Lines 32 to 38.- The maximum value of displacement is determined and compared with the measured one obtained from substracting the final thickness from the initial one.

Lines 40 to 52.- Determination of the straight portion of the load-displacement curve by means of least square method.

Lines 54 and 55.- Plotting procedures from the GHOST library.

```
56          procedure curveplot;
57          type names = packed array[1..20] of char;
58          var titulo : names; j,n : integer;
59             procedure typecs(nom:names;l:integer); ghost;
60             procedure paper(i:integer); ghost;
61             procedure hrdchr(i:integer); ghost;
62             procedure ptplot(xx,yy:arra;l,j,k:integer); ghost;
63             procedure pspace(x1,x2,x3,x4:real); ghost;
64             procedure map(x1,x2,x3,x4:real); ghost;
65             procedure positn(x1,x2:real); ghost;
66             procedure scalsi(x1,x2:real); ghost;
67             procedure border; ghost;
68          begin
69             if loads = 1/20 then cg:=10
70             else cg:=200;
71             if preg[5] then
72             begin
73                paper(1); pspace(0.2,1.2,0.3,1);
74                map(-1,5,-cg/10,cg); hrdchr(1)
75             end;
76             erase; border; scalsi(1,cg/10); positn(2.5,1);
77             typecs('Load vs displacement',20); n:=nop[nt];
78             j:=172; ptplot(disp,load,1,n,j);
79             positn(-1,-1.5); picnow; preg[5]:=false
80          end;
81
82          procedure linearplot;
83          var i : integer; x,y : real;
84             procedure point(x1,x2:real); ghost;
85             procedure join(x1,x2:real); ghost;
86          begin
87             y:=0; x:=dive(y); point(x,y); x:=hi; y:=hi*slope+orden;
88             join(x,y); x:=hi; y:=cg; join(x,y); picnow
89          end;
90
91          procedure finalcor;
92          var i,k,n : integer;
93          begin
94             k:=0; n:=nop[nt];
95             for i:=1 to n do if dive(load[i]) < hi then k:=k+1;
96             if k > nop[1] then k:=nop[1];
97             for i:=1 to k-1 do disp[i]:=disp[i]-dive(load[i]);
98             for i:=k to n do disp[i]:=disp[i]-hi
99          end;
```

Lines 56 to 80.- Drawing of the frame. The plotting scale is chosen depending on the load range at which the test was carried out. The plotting procedures are from the GHOST library.

Lines 82 to 89.- Plotting of the straight line interpolated. This straight line is cut at the displacement resultant of the difference between the measured and the recorded displacements, line 37.

Lines 91 to 99.- Displacement correction. This is done in two ways, if the value of the displacement is less than the difference calculated in line 37, then a value of displacement is substracted from the interpolated straight line. If it is higher, the value of the difference between displacements is substracted from the displacement at that point.

```
100       begin
101          for i:=1 to nop[nt] do disp[i]:=-disp[i]; maxdisp;
102          if hf <= h0 then
103          begin
104             curveplot;
105             repeat
106                write('First and last points to be ');
107                write('interpolated? ');readln(k1,k2);
108                linearint;
109                linearplot;
110                write('Is correct the interpolation? ');readln(ch);
111                preg[i]:=desc(ch)
112             until preg[i];
113             erase; finalcor;
114             curveplot
115          end
116       end;
117
118       procedure reading;
119       var i,j : integer;
120       begin
121          naming; reset(origfil,rfile); read(origfil,nt);
122          for i:=1 to nt do read(origfil,nop[i]); readln(origfil);
123          for j:=1 to 3 do for i:=1 to nop[nt] do
124          if i mod 10 = 0 then
125          case j of
126             1 : readln(origfil,load[i]);
127             2 : readln(origfil,disp[i]);
128             3 : readln(origfil,temp[i])
129          end else
130          case j of
131             1 : read(origfil,load[i]);
132             2 : read(origfil,disp[i]);
133             3 : read(origfil,temp[i])
134          end
135       end;
136
137       procedure writing;
138       var i,j : integer;
139       begin
140          rewrite(modfil,title); write(modfil,nt,' ');
141          for i:=1 to nt do write(modfil,nop[i]); writeln(modfil);
142          for j:=1 to 3 do
143          begin
144             if (nop[nt] mod 10 <> 0) and (j <> 1) then writeln(modfil);
145             for i:=1 to nop[nt] do
146             if i mod 10 = 0 then
147             case j of
148                1 : writeln(modfil,load[i]:7:4,' ');
149                2 : writeln(modfil,disp[i]:7:3,' ');
150                3 : writeln(modfil,temp[i]:7:3,' ')
151             end else
152             case j of
153                1 : write(modfil,load[i]:7:4,' ');
154                2 : write(modfil,disp[i]:7:3,' ');
155                3 : write(modfil,temp[i]:7:3,' ')
```

Lines 100 to 116.- Main body of this procedure. The origin correction is only to be carried out for initial thickness greater than the final one. The load-displacement curve is plotted. The first and last points belonging to the linear interpolation are input, and the straight line is plotted. If the line interpolated is not the required one, the procedure can be repeated, until the required line is encountered.

Lines 118 to 135.- Procedure used to load the data from the 'M_FILE' produced by the former program.

Lines 137 to 158.- Recording of the resultant data under the name 'FILE'.

```
156             end
157          end
158       end;
159
160       procedure grend; ghost;
161
162    begin
163       preg[5]:=true;
164       repeat
165          write('Specimen number? '); readln(title);
166          naming; reading;
167          write('Was recorded the temperature? '); readln(ch);
168          preg[1]:=desc(ch); if not preg[1] then
169          for i:=1 to nop[nt] do temp[i]:=disp[i];
170          write('inicial and final thickness? ');
171          readln(h0,hf); hi:=h0-hf;
172          write('Load range? '); readln(loads); loads:=loads/2000;
173          for i:=1 to nop[nt] do load[i]:=-load[i]*loads;
174          correct; writing;
175          write('Finish? '); readln(ch);
176          preg[2]:=desc(ch)
177       until preg[2];
178       if not preg[5] then grend
179    end.
```

Line 160.- GHOST procedure used to end the graphical output.

Lines 162 to 179.- Main body of the program. As in the former program, the execution is repeated until a negative answer is given, lines 175 to 178. As additional data the initial and final thickness and the load range are input. As has been pointed, the correction is done in the displacement, and the original values of displacement will be stored in the third channel, temperature. If the test was carried out with thermocouples, it has to be indicated. In the case of tests carried out at low temperature, in which the lubricant coat is negligible, the origin correction can be avoided inputing a final thickness greater than the initial one. The load is transformed to its actual value in lines 171 and 172.

```
1   Program Servotest (Input,output,Infile,outfiles);
2
3   const pi = 3.14159; cons1='Do you want to record the data? ';
4      cons2='Printout of tables? '; cons3='Finish? ';
5   type dimens = 1..500 ; cinc = 1..5; deci = 1..10;
6      arra = array [dimens] of real; arrb = array [1..50] of real;
7   var preg : array [deci] of boolean; des,nam : char;
8      nop,max : array [cinc] of integer;
9      discr : (axi,plane,tor); Infile,outfiles : text;
10     test,dfile : alfa; k,jt,nt,ij : integer;
11     load,disp,temp,stress,strain,srate,ener : arra;
12     defo,tempt,vel : arrb; h0,hf : real;
13
14     function descicion (ch : char) : boolean;
15     begin
16        case ch of
17           'Y','y','1' : descicion:=true;
18           'N','n','0' : descicion:=false
19        end
20     end;
21
22     procedure naming;
23     var i : integer;
24     begin
25        dfile[1]:=nam; dfile[2]:='_';;
26        for i:=3 to 8 do
27        dfile[i]:=test[i-2]
28     end;
29
30     procedure maxim;
31     var i,j,l,mx : integer;
32     begin
33        l:=1; mx:=1; for j:=1 to nt do
34        begin
35           for i:=l to nop[j] do
36           if disp[mx] < disp[i] then mx:=i;
37           max[j]:=mx; l:=nop[j]+1
38        end
39     end;
40
41     procedure reading (var dat1,dat2,dat3 : arra);
42     var i,j : integer;
43     begin
44        if nam = 'n' then
45        begin
46           write ('Test number? ');readln (test);
47           for i:=1 to 8 do dfile[i]:=test[i]
48        end else
49        naming;
50        reset(infile,dfile);read(infile,nt);
51        for i:=1 to nt do read (infile,nop[i]);
52        for j:=1 to 3 do
53        begin
54           for i:=1 to nop[nt] do
55           if i mod 10 = 0 then
56           case j of
```

1.3. Stress-strain Analysis (Program Servotest.)

Stress, strain, strain rate and temperature analysis can be processed with this program for different testing conditions like axisymmetric or plane strain compression or torsion. The resultant data are recorded in different files, to be processed by ulterior programs.

Line 1.- Program heading.

Lines 3 to 12.- Global constants, types and variables.

Lines 14 to 20.- Function used to determine decisions.

Lines 22 to 28.- Procedure in which the different files used, in input as well as output, are named.

Lines 30 to 39.- Determination of the points at which the maximum displacement is achieved for each deformation.

Lines 41 to 68.- Reading procedure similar to the ones described previously, the difference is that different files, with different variables, might be accessed during the execution.

```
57              1 : readln(infile,dat1[i]);
58              2 : readln(infile,dat2[i]);
59              3 : readln(infile,dat3[i])
60           end
61           else
62           case j of
63              1 : read(infile,dat1[i]);
64              2 : read(infile,dat2[i]);
65              3 : read(infile,dat3[i])
66           end
67        end;
68     end;
69
70     procedure axisymmetric;
71     var i,l : integer; d0,t,fc,r0 : real;
72
73        procedure radfric;
74        const fk =0.577;
75        var i : integer; d,h,k,c,dc,dd,k1,k2 :real;
76        begin
77           k:=ln(fk/fc)/fc;
78           for i:=1 to nop[nt] do
79           begin
80              h:=h0-disp[i];d:=d0*sqrt(h0/h);
81              if fc >= fk then
82              stress[i]:=stress[i]/(1+fk*d/(3*h))
83              else
84              c:=fc*d/h;
85              if d/h <= k then
86              stress[i]:=stress[i]*sqr(c)/(2*(exp(c)-c-1))
87              else
88              begin
89                 dc:=d-h*k;dd:=fc*dc/h;
90                 k1:=(dd+1)*(exp(c-dd)-c-1)*2/sqr(c);
91                 k2:=sqr(dd/c)*(fk/fc+fk*dc/(3*h));
92                 stress[i]:=stress[i]/(k1+k2)
93              end
94           end
95        end;
96
97     begin
98        discr:= axi;
99        write ('Initial diameter and height, final height? ');
100        readln (d0,h0,hf); r0:=d0/2;l:=1;
101        write('Friction coefficient? ');readln(fc);
102        for i:=1 to nop[nt] do
103        begin
104           t:=h0-disp[i];
105           strain[i]:=ln(h0/t);
106           stress[i]:=load[i]*1000/(pi*exp(strain[i])*sqr(r0))
107        end;
108        if fc>0 then radfric
109     end;
```

```
110     procedure planestrain;
111     const psc = 1.155;
112     var i : integer; b0,tw,fc,sc,b,f,t : real;
113        ch : char;
114
115        procedure friction;
116        const f1=0.05; f2=0.389;
117        var i : integer; t,z,d : real;
118        begin
119           for i:=1 to nop[nt] do
120           begin
121              t:=h0-disp[i];
122              if fc < f1 then
123              stress[i]:=stress[i]/((t/(fc*tw))*(exp(fc*tw/t)-1))
124              else if fc > f2 then
125              stress[i]:=stress[i]/(1+tw/(sqr(2)*t))
126              else
127              begin
128                 z:=t/(2*fc)*ln(fc/2);
129                 d:=(fc/2-1)*t/(fc*tw)+(tw/2-z)/(fc*tw)+sqr(tw/2-z)
130                                                        /(tw*t);
131                 stress[i]:=stress[i]/d
132              end
133           end
134        end;
135
136        procedure tempcor;
137        const r=1.987;kel=273;
138        var def,t,q0,alpha,srat,en,x,y,z : real;
139           i,jc,k : integer;
140
141           procedure datacall;
142           var i,j : integer;
143           begin
144              nam:='t'; naming;
145              reset (infile,dfile); readln (infile,jc);
146              for j:=1 to 2 do
147              begin
148                 for i:=1 to jc do
149                 case j of
150                    1 : read (infile,defo[i]);
151                    2 : read (infile,tempt[i])
152                 end
153              end
154           end;
155
156           function sinh(x : real) : real;
157           begin
158              sinh:=(exp(x)-exp(-x))/2
159           end;
160           function asinh(x : real) : real;
161           begin
162              asinh:=ln(sqr(x)+1)
163           end;
```

Lines 70 to 109.- Procedure used in the analysis of axisymmetric compression tests. Additional data needed are the dimensions of the specimen and the friction coefficient. The stress is calculated assuming constancy of volume, line 106. If the friction coefficient is greater than zero, the procedure in lines 73 to 95 is accessed. In this procedure, the case of sliding, partially and fully sticking friction is analysed according with the friction coefficient and the geometrical conditions.

Lines 110 to 113.- Heading of the procedure used to determine the stress-strain curves under plane strain conditions.

Lines 115 to 134.- The effect of friction in plane strain is calculated. As for axisymmetric compression, the three friction cases are taken into account.

Lines 136 to 139.- Heading of the procedure used to calculate the effect of increase of temperature during deformation on the stress-strain curves.

Lines 141 to 154.- Loading of the values of strain and temperature at the end of the strain interval obtained as result of the program described by Foster (1981).

Lines 156 to 163.- Definition of the hyperbolic sine and the inverse hyperbolic sine.

```
164          begin
165             write ('Act energy, alpha? ');
166             readln(q0,alpha); write('Exponent of the ');
167             write('Z vs stress relationship? ');readln(en);
168             if not preg[5] then
169             begin
170                write('Average strain rate? ');readln(srat)
171             end;
172             datacall; k:=1; def:=0;
173             for i:=1 to nop[nt] do
174             if preg[5] then srat:=srate[i];
175             begin
176                case (strain[i]>=def)and(strain[i]<def+defo[k]) of
177                   true :
178                      begin
179                         t:=tempt[k]+(strain[i]-defo[k])*(tempt[k+1]-
180                            tempt[k])/(defo[k+1]-defo[k]);
181                         y:=alpha*stress[i];z:=sinh(y);
182                         x:=exp(ln(srat*exp(q0/r*(1/(tempt[i]+kel)-
183                            1/(t+kel))))/en);x:=z/x;z:=asinh(x);
184                         stress[i]:=z/alpha
185                      end;
186                   false :
187                      if strain[i]>=def+defo[k] then
188                      def:=def+defo[i];k:=k+1
189                end
190             end
191          end;
192
193       begin
194          discr:=plane;
195          write ('Old data? '); readln (ch);
196          preg[5]:=descicion(ch); preg[6]:=false;
197          if preg[5] then
198          begin
199             nam:='r'; reading(stress,strain,srate);
200             write ('Temperature correction? '); readln (ch);
201             preg[6]:=descicion(ch);
202             write ('Friction coefficient? '); readln (fc);
203             if fc > 0 then friction
204          end else
205          begin
206             write('Thickness, breadth and tool width? ');readln(h0,b0,tw);
207             write('Friction and spread coefficients? ');readln(fc,sc);
208             for i:=1 to nop[nt] do
209             begin
210                t:=h0-disp[i]; b:=b0*(1+sc-sc*sqrt(t/h0));
211                f:=(psc*(b-tw)+tw)/b; strain[i]:=ln(h0/t)*f;
212                stress[i]:=load[i]*1000/(tw*b*f)
213             end;
214             if fc > 0 then friction
215          end;
216          if preg[6] then tempcor
217       end;
```

Lines 164 to 191.- The temperature correction is carried out in this procedure, the Zener-Hollomon equation, lines 165 to 167, is used to correct at the same time the variations in the strain rate. The temperature increase for each point is found interpolating the values taken by the procedure described in lines 141 to 154.

Lines 193 to 217.- Main body of the procedure used to calculate the stress-strain curves under plane strain conditions. A decision is taken in line 195. If the test was previously processed without the temperature or the friction corrections, the data are reloaded from a file called 'R_FILE', and only the required corrections are carried out, lines 199 to 203. If the test has not been processed, the testing geometry, as well as the friction and spread coefficients are input, lines 206 and 207. The stress-strain curve is calculated, lines 210 to 212, and the friction and the temperature corrections are carried out.

```
218       procedure torsion;
219       const l =0.362; ll=0.4343; s3=1.732;
220       var i : integer; gl,gd,radm,tc,vang,vdef,a : real;
221       begin
222          discr:=tor; radm:=pi/180;
223          write('Gauge length and diameter? ');readln(gl,gd);
224          write('Torque calibration? ');readln(tc);a:=sqr(gd)*gd;
225          write('Angular velocity? ');readln (vang);
226          vdef:=ll*ln(l*vang*gd/(s3*gl));
227          for i:=1 to nop[nt] do
228          begin
229             strain[i]:=radm*l*gd*disp[i]/(s3*gl);
230             stress[i]:=12*tc*load[i]*s3/(pi*a);
231             srate[i]:=vdef
232          end
233       end;
234
235       procedure strainrate;
236       var ch : char; i,j,l,p :integer; min : real;
237
238          procedure strrat;
239          const k2=0.4343;
240          var i,j,l : integer; sr : real;
241          begin
242             i:=1; write ('Frecuency? '); readln (p);
243             for j:=1 to nt do
244             begin
245                for i:=i+2 to max[j]-2 do
246                begin
247                   sr:=strain[i+2]-strain[i-2];
248                   if (sr<=0) and ((i<>1) or (i<>2)) then
249                   srate[i]:=srate[i-1]
250                   else if i=1 then srate[i]:=0.001
251                   else srate[i]:=k2*ln(sr*p/5)
252                end;
253                sr:=srate[i+2];srate[i]:=sr;srate[i+1]:=sr;
254                sr:=srate[max[j]-2];
255                for i:=max[j]-1 to nop[j] do srate[i]:=sr;
256                i:=nop[j]+1
257             end
258          end;
259
260          procedure energy;
261          var i,j,k,l,m : integer; int,ene,del,din : real;
262             de : boolean;
```

Lines 218 to 233.- The stress-strain curve is obtained for the torsion tests. The specimen geometry and the testing conditions are input.

Lines 235 and 236.- Heading of the procedure used to determine the strain rate, temperature, energy and average stress an strain rate in the tests.

Lines 238 to 258.- The strain rate for each point is calculated. The values for strain for two points behind and two points ahead are substracted and divided by the time interval of readings, line 251. The beginning two points and the last two points of each deformation are taken as the values of the third and the third to the last points respectively. The values of strain rate in this part are reported as logarithmic.

Lines 260 tO 262.- Heading of the procedure used to determine the area under the curve at each point, as well as the average stress and strain rate for a set interval of strains.

```
263             procedure origen;
264             var ko : integer; te : boolean;
265             begin
266                de:=false; te:=true;
267                for ko:=i to i+4 do
268                if (strain[ko+1]-strain[ko]) < 0 then te:=false;
269                if not te then i:=i+5
270             end;
271
272          begin
273             i:=1; k:=1; m:=0; int:=0; de:=true;
274             defo[1]:=0; tempt[1]:=0; vel[1]:=0;
275             write('integral interval for mean stress? ');readln(din);
276             for j:=1 to nt do
277             begin
278                ene:=0; i:=i;
279                repeat
280                   if (strain[i] > int) and de then origen;
281                   if strain[i]>int then
282                   begin
283                      if strain[i]<=int+din then
284                      begin
285                         ene:=ene+ener[i]; m:=m+1; i:=i+1
286                      end else
287                      begin
288                         k:=k+1;defo[k]:=strain[i];
289                         del:=defo[k]-defo[k-1];
290                         if del<=0 then tempt[k]:=tempt[k-1]
291                         else tempt[k]:=ene/del;ene:=0;
292                         if m=0 then vel[k]:=vel[k-1]
293                         else vel[k]:=p*del/m;m:=0;
294                         if int+din<=strain[max[j]] then
295                         int:=int+din
296                         else
297                         int:=strain[max[j]]
298                      end
299                end;
300             until i < max[j];
301             i:=nop[j]+1
302          end;
303          jt:=k
304       end;
305
306       procedure temcor;
307       const x1=40; c1=0.675; c2=0.125; c3=0.0019; c4=5.781;
308       var i : integer; t : real;
309       begin
310          for i:=1 to nop[nt] do
311          begin
312             t:=temp[i]/x1;
313             temp[i]:=c1*temp[i]-c2*sqr(t)+c3*sqr(t)*t-c4
314          end
315       end;
```

Lines 263 to 270.- The origin correction, carried out in the way indicated in the previous progam, might introduce strain oscillations, as result of elastic effects, around zero. The origin of the energy related parameters, and that of the curve, is taken to be as the first positive value of strain after the oscillations.

Lines 272 to 304.- The energy for each point is calculated by means of a trapezoidal integration. The interval of strains at which the average stress is calculated in input, line 275. This calculation is not started until the strain is greater than zero. The average stress is then calculated as the sum of the energies for all the points in the interval of interest, from zero, up to the nominal strain, and then divided by the nominal strain.

Lines 306 to 315.- The millivolts recorded by the thermocouple connected into the third channel in the PDP10/11 are converted into degrees Celsius by means of the equation in line 313.

```
316       begin
317          if discr<>tor then strrat;
318          ener[1]:=0;
319          for i:=2 to nop[nt] do
320          ener[i]:=(stress[i]+stress[i-1])*(strain[i]-strain[i-1])/2;
321          write ('Energy table? ');readln (ch);
322          preg[7]:=decision(ch); if preg[7] then energy;
323          if discr=plane then
324          begin
325             write ('Temperature conversion? ');readln (ch);
326             preg[8]:=decision(ch);
327             if preg[8] then temcor
328          end
329       end;
330
331       procedure printout ;
332       const def = '     deformation '; x = '  '; y = '      ';
333          tex='        disp      load      temp      stress     strain';
334          tex1='     srate     ener'; z = '*****';
335          tab='       mean stress      strain    mean strain rate';
336       var i,j,l : integer;
337       begin
338          if preg[2] then
339          begin
340             nam:='p'; naming; rewrite(outfiles,dfile);
341             writeln(outfiles,y,z,test,z); writeln (outfiles);
342             writeln(outfiles,tex,tex1);writeln(outfiles);l:=1;
343             for j:=1 to nt do
344             begin
345                writeln(outfiles,def,j:1); for i:=l to nop[j] do
346                writeln(outfiles,y,disp[i]:8:3,x,load[i]:8:1,x,temp[i]:8:3,
347                   x,stress[i]:8:3,x,strain[i]:8:4,x,srate[i]:8:4,x,
348                   ener[i]:8:3);
349                l:=1+nop[j]
350             end
351          end;
352          if preg[7] then
353          begin
354             writeln(outfiles);writeln(outfiles);
355             writeln(outfiles,tab);writeln (outfiles);
356             j:=1;writeln(outfiles,def,j:1);
357             for i:=1 to jt do
358             begin
359                if defo[i]<=strain[nop[j]] then
360                writeln(outfiles,x,y,tempt[i]:9:4,x,y,defo[i]:8:5,
361                   x,y,vel[i]:8:5)
362                else j:=j+1;writeln(outfiles,def,j:1)
363             end
364          end
365       end;
```

Lines 316 to 329.- Main body of this general procedure. The strain rate will be calculated in the way previously described for non-torsional tests, lines 238 to 258. For plane strain tests, the temperature conversion, for specimens tested with thermocouples, is carried out.

Lines 331 to 365.- Printout of the values calculated through the program. The data are going to be printed in columnar form, in a file with the name 'P_FILE'. The values of average stress and strain intervals are obtained at the end of the file.

```
366       procedure recording;
367       var i,j : integer;
368       begin
369          if preg[5] then nam:='f' else nam:='r'; naming;
370          rewrite(outfiles,dfile);
371          write(outfiles,nt:4,' ');
372          for i:=1 to nt do write(outfiles,nop[i]:4,' ');writeln(outfiles);
373          for j:=1 to 4 do
374          begin
375             for i:=1 to nop[nt] do
376             if i mod 10 = 0 then
377             case j of
378                1 : writeln (outfiles,stress[i]:7:2);
379                2 : writeln (outfiles,strain[i]:7:4);
380                3 : writeln (outfiles,srate[i]:7:2);
381                4 : writeln (outfiles,temp[i]:7:4)
382             end else
383             case j of
384                1 : write (outfiles,stress[i]:7:2,' ');
385                2 : write (outfiles,strain[i]:7:4,' ');
386                3 : write (outfiles,srate[i]:7:2,' ');
387                4 : write (outfiles,temp[i]:7:4,' ')
388             end;
389             writeln (outfiles)
390          end;
391          if rop[nt] mod 10 <> 0 then writeln (outfiles)
392       end;
393
394    begin
395       repeat
396          nam:='n'; reading (load,disp,temp); preg[5]:=false;
397          write ('Axisymmetric, plane strain or torsion? ');
398          readln (des); maxim;
399          case des of
400             'A','a','1' : axisymmetric;
401             'P','p','2' : planestrain;
402             'T','t','3' : torsion
403          end;
404          strainrate;
405          for ij:=1 to 3 do
406          begin
407             case ij of
408                1 : write (cons1);
409                2 : write (cons2);
410                3 : write (cons3)
411             end;
412             readln(des);preg[ij]:=decision(des)
413          end;
414          if preg[1] then recording;
415          if preg[2] or preg[7] then printout;
416       until preg[3]
417    end.
```

Lines 366 to 392.- Recording of the calculated values to be processed later. If the answer to the question in line 195 was affirmative, the values of stress, strain, strain rate and temperature obtained will be recorded under the 'F_FILE' name. If not, the data will be recorded under 'R_File'.

Lines 394 to 417.- Main body. The load, displacement and temperature data are loaded from a file called 'FILE'. Depending on the deformation conditions, the different parts of the program will be accessed, lines 397 to 403. As in the former cases, the program will be repeated until a negative answer is provided, line 416.

```
1     Program Grafres (input,output,dummy);
2
3     type arrb = 1..500; ses = 1..6;
4        arra = array[arrb] of real;
5     var preg : array [ses] of boolean; simb : array [1..3] of integer;
6        datos : array [1..4,arrb] of real; nom : array [ses] of alfa;
7        dummy : text; arch,nomb : alfa; np,nd,lk : integer; ch : char;
8        xs,ys,xp,yp : real;
9     value nom=('Stress  ','Strain  ','S rate  ','Temper  ','Displ   ',
10       'Time    '); simb = (43,42,172);
11
12       function desc (ch : char) : boolean;
13       begin
14          case ch of
15             'Y','y','1' : desc:=true;
16             'N','n','0' : desc:=false
17          end
18       end;
19
20       procedure reading;
21       var i,k : integer;
22       begin
23          reset (dummy,arch); read (dummy,i); k:=1;
24          while k <> i do
25          begin
26             read (dummy,np); k:=k+1
27          end;
28          readln (dummy,np);
29          for k:=1 to nd do
30          for i:=1 to np do
31          if i mod 10 = 0 then readln (dummy,datos[k,i])
32          else read (dummy,datos[k,i])
33       end;
34
35       procedure plotter;
36       var dep,indep : arra; discr : (stress,strate,temper);
37          i,j : integer; inicio : boolean; xd,yd : real;
38          procedure typecs (name:alfa;i:integer); ghost;
39          procedure place (i,j:integer); ghost;
40          procedure ghfror (i:integer); ghost;
41          procedure ctrori (x:real); ghost;
42          procedure redpen; ghost;
43          procedure blkpen; ghost;
44          procedure grnpen; ghost;
45
46          procedure transform (k1,k2 : integer);
47          var i : integer;
48          begin
49             for i:=1 to np do dep[i]:=datos[k1,i];
50             if preg[5] then for i:=1 to np do indep[i]:=i
51             else for i:=1 to np do indep[i]:=datos[k2,i]
52          end;
```

1.4. Plotting Output (Program Grafres).

This program is a multiple purpose plotting program. The data can be loaded from different files, and different graphs can be obtained.

Line 1.- Program heading.

Lines 3 to 10.- Declaration of global types and variables. The non-standard value statement is used to initialize global variables.

Lines 12 to 18.- Function used to determine decisions.

Lines 20 to 33.- Procedure used to load the data to be plotted. The data is stored in a two-dimensional array, in which the variables are kept in columnar mode.

Lines 35 to 44.- Heading of the main plotting procedure.

Lines 46 to 52.- Definition of the arrays used to plot the graphs. The values from the two-dimensional matrix are loaded into two one-dimensional arrays or vectors.

```
53          procedure marco;
54          const cos1='Maximum values for strain and stress? ';
55             cos2='Maximum value for strain? ';
56             cos3='Divisions for strain and stress axis? ';
57             cos4='Divisions for strain axis? ';
58             cos5='Minimum and maximum values of temperature? ';
59          var x,y : real; i : integer;
60             procedure filnam (name:alfa;i:integer); ghost;
61             procedure paper (i:integer); ghost;
62             procedure pspace (x1,x2,x3,x4:real); ghost;
63             procedure cspace (x1,x2,x3,x4:real); ghost;
64             procedure map (x1,x2,x3,x4:real); ghost;
65             procedure window (x1,x2,x3,x4:real); ghost;
66             procedure scalsi (x1,x2:real); ghost;
67             procedure qadrnt; ghost;
68             procedure border; ghost;
69             procedure frame; ghost;
70          begin
71             if iricio then
72             begin
73                i:=1; x:=0; y:=1; inicio:=false;
74                paper(i); filnam(nomb,8); ghfror(i);
75                cspace(x,y,x,y); qadrnt; pspace(0.13,0.87,0.38,0.94)
76             end else
77             begin
78                frame; blkpen
79             end;
80             case discr of
81                stress : begin
82                            write(cos1); readln(xs,ys); write(cos3);
83                            readln(xd,yd); yp:=0; xp:=0
84                         end;
85                strate : begin
86                            if not preg[2] then
87                            begin
88                               write(cos2); readln(xs);
89                               write(cos4); readln(xd)
90                            end;
91                            yp:=-2; ys:=3; yd:=1; xp:=0
92                         end;
93                temper : begin
94                            if not preg[2] then
95                            begin
96                               write(cos1); readln(ys,xs);
97                               write(cos3); readln(xd,yd)
98                            end;
99                            write(cos5); readln(yp,ys); xp:=0; yd:=50
100                        end
101            end;
102            map(xp,xs,yp,ys); window(xp,xs,yp,ys); border; redpen;
103            scalsi(xd,yd); xp:=xp-xd; window(xp,xs,yp,ys); xp:=xp+xd
104         end;
```

Lines 53 to 104.- Definition of the plotting space and frame drawing. Two normal plots are considered, stress-strain and temperature-strain. In the strain rate-strain curves, the strain rate is plotted logarithmically. To plot different curves, lines 93 to 100 are used.

```
105         procedure axis (k1,k2 : integer);
106         var i,j : integer; x,y : real;
107         begin
108            i:=55; j:=3; place(i,j); typecs(nomb,6);
109            i:=48; j:=49; place (i,j); typecs(nom[k2],6);
110            i:=6; j:=28; x:=1; place(i,j); ctrori(x);x:=-x;
111            typecs(nom[k1],6); ctrori(x); grnpen
112         end;
113
114         procedure infor;
115         const al1='Stress-strain curve? ';
116            al2='Strain rate-strain curve? ';
117            al3='Temperature-strain curve? ';
118         var i : integer;
119         begin
120            for i:=2 to 4 do
121            begin
122               case i of
123                  2 : write (al1);
124                  3 : write (al2);
125                  4 : write (al3)
126               end;
127               readln(ch); preg[i]:=desc(ch)
128            end
129         end;
130
131         procedure dibuja;
132         var i,j,k : integer; x : real;
133            procedure ptplot(xx,yy:arra;i,j,k:integer); ghost;
134         begin
135            case discr of
136               stress : k:=1;
137               strate : k:=2;
138               temper : k:=3
139            end;
140            i:=simb[k];j:=1;ptplot(indep,dep,j,np,i)
141         end;
142
143         procedure trans(i,j :integer);
144         begin
145            transform(i,j); marco; axis(i,j); dibuja
146         end;
```

Lines 105 to 112.- Procedure used to draw and write the axis in the graphs.

Lines 114 to 129.- Decision of the graph required.

Lines 131 to 141.- Plotting of the desired graph.

Lines 143 to 146.- Procedure used only on the servotest related analysis. The order of operations is given to obtain each plot.

```
147       begin
148          inicio:=true;
149          write ('Is time the independant variable? ');
150          readln (ch); preg[5]:=desc(ch);
151          if preg[5] then
152          begin
153             write ('Number of the set? '); readln(i);
154             transform(i,1); i:=6; j:=5; discr:=temper;
155             marco; axis(j,i);dibuja
156          end else
157          begin
158             write ('Servotest analysis? '); readln(ch);
159             preg[6]:=desc(ch);
160             if preg[6] then
161             begin
162                infor; j:=2; if preg[2] then
163                begin
164                   i:=1; discr:=stress; trans(i,j)
165                end;
166                if preg[3] then
167                begin
168                   i:=3; discr:=strate; trans(i,j)
169                end;
170                if preg[4] then
171                begin
172                   i:=4; discr:=temper; trans(i,j)
173                end
174             end else
175             repeat
176                write('Independent variable (strain)? '); readln(j);
177                write('Dependent variable (stress or temperature)? ');
178                readln(i); discr:=temper; trans(i,j);
179                write('Another curve? '); readln(ch);
180                preg[1]:=desc(ch);
181             until preg[1]
182          end
183       end;
184
185       procedure grend; ghost;
186
187    begin
188       write('File name and number of variables? '); readln(arch,nd);
189       nomb[1]:='g'; for ik:=2 to 8 do nomb[ik]:=arch[ik];
190       reading; plotter; grend
191    end.
```

Lines 147 to 183.- Main body of the plotting procedure. The first option is to plot any of the variables against time, this is done by plotting the variable against its index, lines 149 to 156. The servotest related analysis is the second option. The first graph to be plotted is the stress-strain curve, then the strain rate-strain and the temperature-strain curve at the end, lines 158 to 173. Any other sort of plot can be obtained, lines 175 to 182.

Line 185.- End of the plotting output.

Lines 187 to 191.- Main body, the name of the file and the number of variables recorded in it has to be given. Due to problems with plotting routines, this program is not repeated, it has to be executed for every curve.

```
      PROGRAM BASDAT
      DIMENSION IBASE(21),JBASE(10),KXVAL(21,40),KYVAL(21,40)
      CHARACTER NOMBRE*15,FILES(10)*8
      PRINT *,'Name of file? '
      READ (*,10) NOMBRE
   10 FORMAT (A15)
      PRINT *,'Number of tests? '
      READ (*,*) NT
      OPEN (8,FILE=NOMBRE,FORM='FORMATTED')
      DO 100 KT=1,NT
      PRINT *,'Test number? '
      READ (*,12) FILES(KT)
   12 FORMAT (A8)
      PRINT *,'Number of columns and X rows? '
      READ (*,*) NX,NL
      NY=21
      OPEN (9,FILE=FILES(KT),FORM='FORMATTED')
      DO 110 I=1,NL
      READ (8,*) X,Y
  110 IBASE(I)=INT(10*Y)
      DO 120 I=1,10
      READ (8,*) X,Y
  120 JBASE(I)=INT(10*X)
      DO 130 J=1,NX
      DO 130 I=1,NY
      READ (8,*) X,Y
      KXVAL(I,J)=INT(10*X)
  130 KYVAL(I,J)=INT(10*Y)
      NY=NL
      WRITE (9,20) NX,NY
      WRITE (9,14) (IBASE(I),I=1,NY)
      WRITE (9,14) (JBASE(I),I=1,NL)
      WRITE (9,18) ((KXVAL(I,J),KYVAL(I,J),I=1,NY),J=1,NX)
   14 FORMAT (1516)
   18 FORMAT (1416)
   20 FORMAT (316)
  100 CLOSE (9)
      CLOSE (8)
      CALL EXIT
      END
```

Appendix 2
Strain Distribution Analysis Under Plane Strain Conditions.

The coordinates of the nodes in the gridded specimens are digitised with the aid of a Commodore PET, desk top computer, available in the Department of Geography. The data recorded on a cassette tape are loaded into the PR1ME750 computer.

2.1. Numerical compatibility (PROGRAM BASDAT).

In PASCAL fractional number is defined to start with '0'. In BASIC, All the fractions are written without the '0'. This program was written in FORTRAN77, in order to read the data from the digitasing program and convert them into data accesible by PASCAL.

Lines 1 to 3.- Program heading and dimensioning of variables.

Lines 4 to 9.- Identification of the file that contains the digitised data.

Lines 10 to 28.- Loading of the data. Those numbers are read with free format . Different files are opened in order to record the data from each test, line 17.

Lines 30 to 36.- Recording the data in the new files.

```
1     Program Straindist (input,output,infile,outfile);
2
3     type cuar = 1..40; vin = 1..21; cin = 1..11; dos = 1..2;
4        puntos = array [vin,cuar] of integer;
5        coords = array [vin,cuar,dos] of integer;
6        grids = array [vin,cuar] of real;
7        nomb = packed array [1..19] of char;
8     var def,undef : coords; euno,edos,eundos,edil,etot : grids;
9        preg : array [cin] of boolean; des : char;
10       infile,outfile : text; rfile,title : alfa; titulo : nomb;
11       nx,ny,mt : integer; mean,stand : real;
12       freq : array [cin] of integer;
13
14       function deftot (e1,e2,e12:real) : real;
15       const dter = 0.6667;
16       begin
17          deftot:=dter*sqrt(sqr(e1)-e1*e2+sqr(e2)+3*sqr(e12))
18       end;
19
20       function desc (ch : char) : boolean;
21       begin
22          case ch of
23             'Y','y','1' : desc:=true;
24             'N','n','0' : desc:=false
25          end
26       end;
27
28       procedure reading;
29       var i,j,k,l,m,n : integer;
30
31          procedure readdef;
32          var i,j,l,m,n : integer;
33          begin
34             i:=1; for j:=1 to nx do
35             begin
36                for i:=1 to ny do
37                begin
38                   if i mod 7 =0 then readln(infile,m,n)
39                   else read(infile,m,n); i:=i+1;
40                   def[i,j,1]:=m; def[i,j,2]:=n
41                end
42             end
43          end;
44
45       begin
46          reset(infile,title); readln(infile,nx,ny);
47          for i:=1 to ny do
48          begin
49             if (i mod 15 = 0) or (i = ny) then
50             readln(infile,n) else read(infile,n);
51             for j:=1 to nx do undef[i,j,2]:=n
52          end;
53          for i:=1 to nx do
54          begin
55             if (i mod 15 = 0) or (i = nx) then readln(infile,m)
56             else read(infile,m);
```

2.2. Strain Distribution (Program Straindist).

In this program, the analysis of the grid is carried out assuming the model proposed by Beynon (1979).

Line 1.- Program heading.

Lines 3 to 12.- Declaration of global types and variables.

Lines 14 to 18.- Calculation of the strain in each element assuming plane strain conditions.

Lines 20 to 26.- Function used to determine outcome from decisions.

Lines 28 and 29.- Heading of the procedure used to read the coordinates of the deformed and undeformed specimens.

Lines 31 to 43.- Procedure used to read the coordinates of the nodes in the deformed specimen.

Lines 45 to 60.- Reading or the undeformed coordinates. Those are input as two orthogonal vectors, assuming that the values keep constant within the specimen.

```
57            for j:=1 to ny do undef[j,1,1]:=m
58          end;
59          readdef
60        end;
61
62        procedure deformation;
63        const medpi = 1.5708;
64        var i,j : integer; coa,cob,oba : real;
65          xway : array [cuar] of real; yway : array [vin] of real;
66
67          function norma (k1,l1,k2,l2:integer;arrc:coords) : real;
68          var m : integer; xx : array [dos] of real;
69          begin
70            for m:=1 to 2 do
71            xx[m]:=sqr(arrc[k2,l2,m]-arrc[k1,l1,m]);
72            norma:=sqrt(xx[1]+xx[2])
73          end;
74
75          function escal (i,k:integer) : real;
76          var xx : array [dos,dos] of real; n,m : integer;
77          begin
78            for m:=1 to 2 do
79            for n:=1 to 2 do
80            case m of
81              1 : xx[m,n]:=def[i,k,n]-def[i+1,k,n];
82              2 : xx[m,n]:=def[i,k,n]-def[i,k+1,n];
83            end;
84            escal:=xx[1,1]*xx[1,2]+xx[2,1]*xx[2,2]
85          end;
86
87          procedure cuadrs (i,m : integer);
88          begin
89            cob:=norma(i,m,i+1,m,def);
90            coa:=norma(i,m,i,m+1,def);
91            oba:=escal(i,m)/(cob*coa)
92          end;
93
94        begin
95          for i:=1 to nx-1 do xway[i]:=norma(1,1,1,i+1,undef);
96          for i:=1 to ny-1 do yway[i]:=norma(1,1,i+1,1,undef);
97          for j:=1 to ny-1 do
98          for i:=1 to nx-1 do
99          begin
100           cuadrs(j,i);
101           euno[j,i]:=ln(cob/yway[j]);
102           edos[j,i]:=ln(coa/xway[i]);
103           if abs(oba) > 1 then
104           if oba > 1 then oba:=1 else oba:=-1;
105           eundos[j,i]:=medpi-arccos(oba);
106           ed1[j,i]:=euno[j,i]+edos[j,i];
107           etot[j,i]:=deftot(euno[j,i],edos[j,i],eundos[j,i])
108         end
109       end;
```

Lines 62 to 109.- Procedure employed in the strain calculations. The distance between the nodes in the undeformed, lines 95 and 96, and in the deformed, procedure in lines 87 to 92, are calculated. It is assumed that the deformation is homogeneous and under perfect plane strain conditions. The different components of strain are calculated with the aid of the model proposed by Beynon (1979), lines 101 to 106. It is assumed that the node moves from the original undeformed position to the final one along a straight line. The total strain is calculated with the aid of von Misses criterion, line 107.

```
110       procedure printout;
111       const e = '******'; d = '  '; c = '     ';
112       var i,j,k,kn : integer; xref : real;
113
114          procedure prints (arra : grids);
115          var vas : packed array [vin] of char;
116              i,j,k : integer;
117
118             function values (k:integer;x:real) : char;
119             var m : integer;
120             begin
121                case k of
122                   1 : if x < 0 then values:='_' else values:=' ';
123                   3 : values:='.';
124                   2,4,5 : begin
125                              if k = 4 then x:=10*(x-trunc(x));
126                              if k = 5 then
127                              begin
128                                 x:=10*(x-trunc(x));
129                                 x:=10*(x-trunc(x)); x:=round(x)
130                              end;
131                              m:=abs(trunc(x)); values:=chr(m+176)
132                           end
133                end
134             end;
135
136          begin
137             writeln(outfile,c,titulo);writeln(outfile);
138             if preg[1] then writeln(outfile,e,e,e,e,e,e,'******')
139             else writeln(outfile,e,e,e,e,e,e,e,e,e,e,e,e,e,'***');
140             for j:=1 to nx-1 do
141             begin
142                for k:=1 to 5 do
143                begin
144                   write(outfile,'* ');
145                   for i:=1 to ny-1 do
146                   vas[i]:=values(k,arra[i,j]);
147                   for i:=1 to ny-2 do
148                   write(outfile,vas[i],' * ');
149                   writeln(outfile,vas[ny-1],' *')
150                end;
151                if preg[1] then writeln(outfile,e,e,e,e,e,e,'******')
152                else writeln(outfile,e,e,e,e,e,e,e,e,e,e,e,e,e,'***')
153             end;
154             writeln(outfile)
155          end;
156
157          procedure printstats;
158          const i = '_________'; v = '                |';
159             q = '            ';
160          var i,j,k : integer; x1,x2,x3 : real;
161          begin
162             writeln(outfile,c,'Statistical distribution'); x3:=0.09;
163             writeln(outfile); writeln(outfile,q,'Frequency');
164             writeln(outfile,q,d,i,i,i,i,i,i,i,i,i); writeln(outfile,v);
165             for i:=1 to 11 do
```

Lines 110 to 112.- Heading of the procedure employed to obtain the general printout.

Lines 114 to 134.- Function used to determine the character needed in each printing space. Due to the size of the specimens, the numbers are not printed in horizontal way, but vertical.

Lines 157 to 184.- Printout of the statistical distribution. Eleven strain intervals are selected and a mark is placed in the corresponding interval for each deformed element.

```
166             begin
167                k:=freq[i];
168                if (i=1) or (i=11) then
169                begin
170                   write(outfile,c,d,d);
171                   if i=1 then write(outfile,'<= 0.09 |');
172                   if i=11 then write(outfile,'>= 1.00 |')
173                end else
174                begin
175                   x1:=(i-1)/10; x2:=x1+x3;
176                   write(outfile,c,x1:4:2,' - ',x2:4:2,' |')
177                end;
178                if k <> 0 then for j:=1 to k do write(outfile,'*');
179                writeln(outfile); writeln(outfile,v)
180             end;
181             writeln(outfile,q,d,i,i,i,i,i,i,i,i,i); writeln(outfile);
182             writeln(outfile,c,'Average = ',mean:4:3);
183             writeln(outfile,c,'Standard deviation = ',stand:4:3)
184          end;
185
186       begin
187          rfile[1]:='o'; rewrite(outfile,rfile); writeln(outfile);
188          writeln(outfile,c,e,d,title,e);writeln(outfile);
189          if preg[3] then
190          begin
191             write('All the data? '); readln(des); preg[2]:=desc(des);
192             if preg[2] then kn:=5 else kn:=1;
193             for k:=1 to kn do
194             case k of
195                1 : begin
196                       titulo:='Total strain       '; prints(etot)
197                    end;
198                2 : begin
199                       titulo:='Horizontal strain  '; prints(edos)
200                    end;
201                3 : begin
202                       titulo:='Vertical strain    '; prints(eund)
203                    end;
204                4 : begin
205                       titulo:='Shear strain       '; prints(eundos)
206                    end;
207                5 : begin
208                       titulo:='Dilatational strain'; prints(edil)
209                    end
210             end
211          end;
212          write ('Real final deformation? '); readln (xref);
213          if xref <> 0 then
214          begin
215             for i:=1 to ny-1 do for j:=1 to nx-1 do
216             edil[i,j]:=etot[i,j]/xref; prints(edil)
217          end;
218          if preg[9] then printstats
219       end;
```

Lines 186 to 219.- Main body of the printing procedure. Different tables will be printed, one for the total strain, and one for each component of strain, if desired, lines 191 to 210. If given the strain achieved by the specimen, the ratio of the total elemental strain over the final strain will be calculated for each element, lines 212 to 217. The output of the statistical distribution is optional, line 218.

```
220       procedure stats;
221       var i,j,k,l,it,fl : integer; x1,x2,x3 : real;
222       begin
223          write('First element under the tools? '); readln(it);
224          if not preg[1] then
225          begin
226             write('Last element under the tools? '); readln(fl)
227          end else fl:=nx-1;
228          for i:=1 to 11 do freq[i]:=0;
229          k:=0; x1:=0; x2:=0;
230          for i:=1 to ny-1 do
231          for j:=it to fl do
232          begin
233             x3:=etot[i,j];
234             x1:=x1+x3; x2:=x2+sqr(x3); k:=k+1;
235             l:=trunc(10*x3);
236             if l >= 10 then l:=10;
237             freq[l+1]:=freq[l+1]+1
238          end;
239          mean:=x1/k; stand:=sqrt((x2-sqr(x1)/k)/(k-1))
240       end;
241
242       procedure promedio;
243       var i,j,mx,my,ns : integer;
244
245          procedure average (arra : grids);
246          var i,j,k : integer;
247          begin
248             for i:=1 to nx-1 do
249             for j:=1 to my-1 do
250             arra[j,i]:=(arra[j,i]+arra[ny-j,i])/2;
251             if preg[3] then
252             begin
253                for i:=1 to my-1 do
254                for j:=ns to mx-1 do
255                arra[i,j]:=(arra[i,j]+arra[i,nx-j+ns-1])/2
256             end
257          end;
```

Lines 220 to 240.- The statistical analysis can be carried out with any number of elements, it is only necessary to indicate the first and last elements under the tools, lines 223 to 227. The mean strain and the standard deviation are calculated, line 239.

Lines 242 and 243.- Heading of the procedure used to take the average over a quadrant of the specimen.

Lines 245 to 257.- Average of the strain values assuming specular symmetry with respect to the centre planes.

```
258         procedure avcord;
259         var i,j,k,l : integer;
260
261            function promd (i,j : integer) : integer;
262            begin
263               promd:=(abs(i)+abs(j))div(2)
264            end;
265
266         begin
267            for i:=1 to nx do
268            for j:=1 to my-1 do
269            for k:=1 to 2 do
270            def[j,i,k]:=promd(def[j,i,k],def[ny-j+1,i,k]);
271            if preg[3] then
272            begin
273               for i:=1 to my do
274               for j:=ns to mx-1 do for k:=1 to 2 do
275               def[i,j,k]:=promd(def[i,j,k],def[i,nx-j+ns,k]);
276               for j:=1 to ns-1 do def[my,j,1]:=abs(def[my,j,1]);
277               for j:=ns to mx-1 do
278               def[my,j,1]:=promd(def[my,j,1],def[my,nx-j+ns,1]);
279               k:=2*def[my-1,1,2]-def[my-2,1,2];
280               for i:=1 to mx do def[my,i,2]:=k;
281            end
282         end;
283
284      begin
285         write('Plain strain? '); readln(des);
286         preg[3]:=desc(des); if preg[3] then
287         begin
288            write('Middle column? '); readln(mx); ns:=nx-2*(nx-mx)
289         end else
290         begin
291            mx:=nx; ns:=1
292         end;
293         write('Middle row? '); readln(my);
294         for i:=1 to 4 do
295         case i of
296            1 : average (etot);
297            2 : average (edos);
298            3 : average (euno);
299            4 : average (eundos)
300         end;
301         avcord; nx:=mx; ny:=my;
302         for i:=1 to ny-1 do
303         for j:=1 to nx-1 do
304         begin
305            etot[i,j]:=(deftot(euno[i,j],edos[i,j],eundos[i,j])+
306               etot[i,j])/2;
307            edi[i,j]:=euno[i,j]+edos[i,j]
308         end
309      end;
```

Lines 258 to 282.- Average of the coordinates assuming specular symmetry.

Lines 284 to 309.- Main body of the averaging procedure. The program is designed to take into account the symmetry of rolling, in which the specular plane is along the rolling direction. For the case of plane strain, the option is defined between lines 285 to 289, two specular planes, dividing the grid into four, are taken into account. The strain components are averaged in lines 294 to 300, and the coordinates in line 301. The resultant total average strain, and the corresponding dilatational strain, are calculated in lines 304 to 308.

```
310       procedure plotting;
311       type plt = array [cuar] of real;
312       var xpl,ypl : plt; l,j,k,l : integer; y1,y2,y3,y4 : real;
313          procedure filnam (nom:alfa;l:integer); ghost;
314          procedure pcscen (x1,x2:real;nom:alfa;l:integer); ghost;
315          procedure paper (l:integer); ghost;
316          procedure hrdchr (l:integer); ghost;
317          procedure ghfror (l:integer); ghost;
318          procedure ptplot (xx,yy:plt;l,j,k:integer); ghost;
319          procedure curveo (xx,yy:plt;l,j:integer); ghost;
320          procedure pspace (x1,x2,x3,x4:real); ghost;
321          procedure map (x1,x2,x3,x4:real); ghost;
322          procedure erase; ghost;
323          procedure border; ghost;
324          procedure blkpen; ghost;
325          procedure redpen; ghost;
326          procedure grnpen; ghost;
327          procedure picnow; ghost;
328
329          procedure plotdef;
330          var l,j,k,l,m : integer;
331             procedure plotnl (x1,x2:real;l:integer); ghost;
332          begin
333             redpen;
334             for l:=1 to nx-1 do
335             for j:=1 to ny-1 do
336             begin
337                k:=(def[j+1,l+1,1]+def[j,l,1]) div 2;
338                l:=(def[j+1,l+1,2]+def[j,l,2]) div 2;
339                m:=round(100*etot[j,l]);
340                plotnl(k,l,m)
341             end
342          end;
343
344          procedure cuadrs;
345          const a=0.028; b=0.11; c=0.138;
346          var l : integer; d,e,f : real;
347          begin
348             blkpen; f:=0.82;
349             for l:=1 to 11 do
350             begin
351                e:=f; d:=e-a; f:=d-a;
352                pspace(b,c,d,e); border
353             end
354          end;
355
356       begin
357          if mt = 1 then
358          begin
359             paper(1); rfile[1]:='g'; filnam(rfile,8);
360             write('Definitive? ' ); readln(des);
361             preg[7]:=desc(des); ghfror(1)
362          end;
363          pspace(0.04,0.966,0.33,0.886);
364          if preg[7] then
365          begin
```

Lines 310 to 327.- Heading of the main procedure used to obtain the graphic output. The external graphical procedures are from the GHOST library.

Lines 329 to 342.- The value of the total strain will be drawn in the centre of each element, if desired.

Lines 344 to 354.- Drawing of small squares along the final plot.

```
366             y1:=0.19; y2:=0.653; ghfror(0);
367             case (mt)mod(3) of
368                0 : begin
369                       y3:=0.056; y4:=0.334; cuadrs
370                    end;
371                1 : begin
372                       y3:=0.722; y4:=1
373                    end;
374                2 : begin
375                       y3:=0.39; y4:=0.668
376                    end
377             end;
378             pspace(y1,y2,y3,y4);
379          end;
380          if preg[1] then map(-50,1200,-50,700)
381          else map(-1250,1250,-750,750);
382          if preg[7] then
383          begin
384             if (mt-1)mod(3) = 0 then erase;
385          end else erase;
386          blkpen; border; hrdchr(1); pcscen(50,600,title,8); redpen;
387          for i:=1 to ny do
388          for j:=1 to nx do
389          begin
390             xpl[j]:=def[i,j,1]; ypl[j]:=def[i,j,2]
391          end;
392          ptplot(xpl,ypl,1,nx,42);
393          grnpen; for i:=1 to nx do
394          for j:=1 to ny do
395          begin
396             xpl[j]:=def[j,i,1]; ypl[j]:=def[j,i,2]
397          end;
398          curveo(xpl,ypl,1,ny);
399          for i:=1 to ny do
400          for j:=1 to nx do
401          begin
402             xpl[j]:=def[i,j,1]; ypl[j]:=def[i,j,2]
403          end;
404          curveo(xpl,ypl,1,nx);
405          plcnow;
406          write('Do you want the strain values on the plot? ');
407          readln(des); preg[8]:=desc(des); if preg[8] then plotdef
408       end;
409
410       procedure grend; ghost;
```

Lines 356 to 408.- Main body of the drawing procedure. Different sizes of plots are considered. For the case of the whole specimen, the space is defined in lines 364 and 381. For the small final specimens, the space is defined between lines 366 to 380. The nodal points are plotted, lines 387 to 392, and contouring routines are adjusted through them to determine the border between contiguous elements, lines 393 to 495. The annotation of the strain values is optional, lines 406 and 407.

Line 410.- Procedure used to end the graphical output.

```
411     begin
412        mt:=1;
413        repeat
414           write('Test number? '); readln(title); rfile[2]:='_';
415           for nx:=1 to 6 do rfile[nx+2]:=title[nx]; reading;
416           deformation;
417           write('Quadrant average? '); readln(des);
418           preg[1]:=desc(des);
419           if preg[1] then promedio;
420           plotting;
421           write ('Statistical analysis? '); readln(des);
422           preg[9]:=desc(des);
423           if preg[9] then stats;
424           write('Do you want the strain values? '); readln(des);
425           preg[3]:=desc(des);
426           if preg[3] then printout;
427           write('Finish? '); readln(des);
428           preg[5]:=desc(des); mt:=mt+1;
429        until preg[5];
430        grend
431     end.
```

Lines 411 to 431.- Main body of the program. As in the programs described in the former appendix, the execution is repeated until a negative answer is provided, lines 427 to 429. The file containing the data from the undeformed and from the deformed grids is provided, lines 414 to 415. For each specimen, the deformation values will be calculated, if required averaged, and then the printed and graphical output will be carried out.

Appendix 3

Correction of the Average Strain by Lateral Spreding.

In order to compare the nominal strain, obtained form the stress-strain curve calculated with the programs in appendix 1, and the average strain, obtained from the programs in appendix 2, an allowance has to be made for the non-perfect plane strain compression conditions in the second case.

Expressing the deformation of an element in terms of principal strains, the condition of zero dilatation is given by

$$\varepsilon_1 + \varepsilon_2 + \varepsilon_3 = 0 \qquad \text{(A3.1)}$$

Under perfect plane strain compression $\varepsilon_2 = 0$ and

$$\varepsilon_3 = -\varepsilon_1 \qquad \text{(A3.2)}$$

In the present case, ε_2 is not zero, and is defined as

$$\varepsilon_2 = \ln(b/b_o) \qquad \text{(A3.3)}$$

where b and b_o are the final and initial breadth of the specimen respectively. The other two components are defined as

$$\varepsilon_1 = \ln(h/h_o)$$

and

$$\varepsilon_3 = -(\varepsilon_1 + \varepsilon_2) \qquad \text{(A3.4)}$$

With (A3.3) and (A3.4), the effective strain, ε_{ef}, can be calculated as

$$\varepsilon_{ef} = \frac{2}{3}\left[(\varepsilon_1 - \varepsilon_2)^2 + (\varepsilon_2 - \varepsilon_3)^2 + (\varepsilon_3 - \varepsilon_1)^2\right]^{1/2} \qquad \text{(A3.5)}$$

The calculation of the strain components in the grids were carried out assuming $\varepsilon_2 = 0$, in this case, an apparent strain, ε_{ap} is calculated as

$$\varepsilon_{ap} = \frac{2}{3}\varepsilon_1 \tag{A3.6}$$

The correction of the average strain, $\bar{\varepsilon}$, is obtained by

$$\bar{\varepsilon}_c = -(\varepsilon_{ap} - \varepsilon_{ef}) \tag{A3.7}$$

where $\bar{\varepsilon}_c$ is the corrected final value.

Table I

Chemical composition of the steels employed.

Element	Ti bearing steel	AISI 316 SS	Accuracy	Method
C	0.12	0.024	*	*
Cr	<0.02	16.70	± 0.02	Quantometer
Ni	<0.02	12.20	± 0.02	Quantometer
Mo	<0.02	2.63	± 0.02	Quantometer
Mn	1.30	1.50	± 0.02	Quantometer
Si	0.14	0.29	± 0.02	Quantometer
Ti	0.06	--	± 0.01	Quantometer
Al	0.028	--	± 0.003	Quantometer
N	0.015	--	± 0.001	Chemical

All values are in percent

* in Ti bearing steel, the C was analysed by conductimetric means giving an accuracy of± 0.01%, in the stainless steel, Leco equipment was used giving an accuracy of± 0.001%.

Table II

Rolling data from AISI type 316 stainless steel.

Schedule	Pass	t (mm)	w (mm)	r (%)	RoT (C)	ReT (C)	Load (kN)	$\bar{\sigma}$ (MN/m^2)
	1	19.01	52.62	25.2	1094	1167	220	201
i	2	14.16	53.61	25.5	992	----	285	285
	3	10.56	53.70	25.4	914	----	356	391
	1	18.95	52.75	25.7	1100	1160	235	212
i	2	14.12	53.94	25.5	999	----	276	274
	3	10.49	54.26	25.7	914	----	327	353
	1	18.82	52.35	26.2	1084	1152	222	200
i	2	14.02	53.10	25.5	1012	----	253	253
	3	10.34	53.57	26.2	936	----	407	446
	1	19.03	52.16	25.4	1106	1152	219	212
ii	2	14.22	53.77	25.3	1077	1164	218	212
	3	10.21	54.33	27.7	990	----	269	285
	1	19.10	53.68	25.1	1117	1170	210	193
iii	2	14.30	55.07	25.1	NR	----	265	253
	3	10.21	57.56	28.6	1051	1157	263	249
	1	19.05	53.07	25.0	1143	1198	183	172
iv	2	14.29	53.51	25.0	NR	1201	203	210
	3	10.72	53.83	25.0	NR	----	265	311
	4	8.02	54.13	25.0	NR	----	305	412
	1	18.91	53.62	25.8	1142	1197	193	176
	2	13.90	54.15	26.5	1012	----	247	239
v	3	10.22	54.52	26.5	1090	1204	206	220
	4	7.51	54.78	26.5	973	----	239	280
	5	5.57	55.30	25.8	NR	----	307	397
	1	18.91	53.21	25.8	1130	1190	183	163
	2	13.90	53.74	26.5	1037	----	221	214
v	3	10.22	54.11	26.5	1091	1197	202	216
	4	7.51	54.37	26.5	954	----	246	289
	5	5.57	54.48	25.8	833	----	307	404

t = thickness.
w = width.
r = reduction.
RoT = rolling temperature.
ReT = reheating temperature.
$\bar{\sigma}$ = mean stress.
NR = not recorded.

Table III

Initial grain size for AISI 316 stainless steel.

Rolling Schedule	Preheating Temperature	Testing Temperature	Grain Size
i	904	910	18.9 ± 1.8
i	1010	910	29.6 ± 2.4
i	1095	910	59.3 ± 2.6
i	1194	910	158.4 ± 4.1
iv	1006	1006	30.9 ± 1.7
v	1006	1006	31.7 ± 2.0
torsion	905	905	30.2 ± 1.5
torsion	1008	1008	42.9 ± 1.9

Temperature in degrees Celsius, grain size in μm.

Table IV

Results from stress-strain tests in Ti bearing steel.

Test	Type	T [C]	h_o [mm]	b_o [mm]	b_f [mm]	$\dot{\varepsilon}$ [sec^{-1}]	ε_p	σ_{p_2} [MN/m^2]
RC054	AS	889	9.94	6.98	3.10	0.55	0.311	159
RC055	AS	889	10.06	6.97	3.91	1.09	0.352	184
RC050	AS	889	9.90	7.02	5.75	5.20	0.423	215
RC057	AS	889	10.12	7.00	5.54	7.50	0.439	227
RC051	AS	889	10.12	6.98	5.54	10.80	0.480	233
RC058	AS	889	9.96	6.98	3.13	13.30	0.526	236
RC059	AS	889	9.95	7.06	3.05	16.20	0.526	250
RC053	AS	889	9.96	7.03	5.22	27.20	0.500	256
RC060	AS	889	10.00	7.01	2.81	38.70	0.469	281
RC052	AS	889	9.90	7.07	4.77	50.20	0.439	291
RC069	PS	992	10.09	50.00	2.28	5.13	0.316	153
RC070	PS	992	10.02	50.10	2.16	10.60	0.323	162
RC071	PS	992	9.99	50.10	2.16	15.60	0.281	170
RC072	PS	992	10.11	50.10	2.07	47.10	0.259	211
RC063	AS	992	10.01	7.04	3.59	5.35	0.374	174
RC064	AS	992	9.82	6.95	3.42	10.90	0.418	186
RC065	AS	992	9.99	6.97	3.57	16.10	0.393	191
RC066	AS	992	9.91	7.08	3.39	27.00	0.388	208
RC067	AS	992	9.96	6.99	3.39	38.20	0.383	219
RC068	AS	992	9.95	7.06	3.39	49.00	0.381	235

T = Temperature.

PS = Plane strain.

AS = Axisymmetric.

h_o = Initial thickness in plane strain or height in axisymmetric tests.

b_o = Initial width in plane strain or diameter in axisymmetric tests.

h_f = Final thickness in plane strain or height in axixymmetric tests.

$\dot{\varepsilon}$ = Nominal strain rate.

ε_p = Strain to peak stress.

σ_p = Peak stress.

Table V

Stress strain data from plane strain compression tests in AISI type 316 stainless steel.

Test	b_o [mm]	b_f [mm]	t_o [mm]	t_f [mm]	$\dot{\varepsilon}$ [sec^{-1}]	σ_p [MN/m^2]	σ_s [MN/m^2]	$\sigma_{0.15}$ [MN/m^2]	ε_p
RC095	49.90	61.18	10.92	2.18	0.533	254	193	238	0.318
RC096	50.00	60.58	10.97	2.29	1.075	269	205	253	0.323
RC097	50.10	60.45	11.01	2.32	2.144	282	210	268	0.328
RC098	50.00	59.28	10.91	2.26	5.295	296	214	288	0.338
RC099	49.90	59.13	11.04	2.31	8.043	300	217	293	0.299
RC0102	54.14	63.61	10.66	1.98	10.91	307	228	296	0.328
RC0103	53.88	63.56	10.66	1.95	16.16	313	233	305	0.308
RC0104	54.54	63.95	10.73	3.06	26.61	322	243	320	0.259
RC0105	49.90	53.50	10.94	2.17	47.40	343	252	340	0.219
RC0106	49.90	60.23	10.99	2.22	0.543	238	191	224	0.348
RC0107	50.00	60.09	11.04	2.33	1.078	257	205	240	0.359
RC0108	50.00	59.98	15.01	2.24	2.102	266	210	251	0.353
RC0109	50.00	59.64	10.94	2.25	5.272	279	215	267	0.348
RC0110	54.38	64.10	10.82	2.16	7.944	285	221	272	0.343
RC0111	53.67	63.51	10.77	2.12	10.55	287	224	277	0.328
RC0112	53.97	63.16	10.80	2.14	15.86	291	228	285	0.289
RC0113	54.55	63.32	10.75	2.03	24.19	305	240	300	0.239
RC0114	50.00	58.13	10.90	2.10	47.70	330	253	327	0.189
RC0279	55.17	60.69	10.92	4.80	0.175	191	203	198	0.348
RC0280	54.95	61.72	10.93	4.09	0.482	236	215	221	0.369
RC0119	54.37	64.60	10.79	2.19	1.109	245	210	229	0.368
RC0115	54.96	64.09	10.85	2.19	2.182	258	214	239	0.338
RC0117	53.96	63.27	10.78	2.08	11.15	282	226	266	0.331
RC0118	54.31	63.52	10.74	2.06	16.49	287	254	280	0.313
RC0282	55.09	61.24	10.96	3.71	46.58	320	282	313	0.214
RC0283	64.82	62.09	10.95	3.71	0.091	189	177	165	0.363
RC0284	56.13	62.50	11.00	3.76	0.177	210	200	195	0.393
RC0121	50.00	60.50	10.99	2.40	0.557	232	208	212	0.418
RC0125	53.71	63.96	10.72	2.34	2.047	250	218	235	0.423
RC0126	54.18	63.25	10.68	2.13	5.309	259	221	243	0.428
RC0127	54.73	63.42	10.74	2.24	7.743	274	226	252	0.408
RC0129	54.22	63.35	10.76	2.22	13.98	285	243	268	0.378
RC0122	50.00	58.96	10.97	2.30	24.65	296	246	288	0.264
RC0123	50.10	58.51	11.01	2.27	48.99	313	252	307	0.219

Test	b_o	b_f	t_o	t_f	$\dot{\varepsilon}$	σ_p	σ_s	$\sigma_{0.15}$	ε_p
RC0178	56.61	64.55	6.20	1.92	0.092	138	116	135	0.310
RC0179	56.34	63.74	6.13	1.87	0.177	150	125	143	0.326
RC0180	56.40	64.35	6.14	1.76	0.462	165	143	157	0.330
RC0181	56.24	64.45	6.10	1.72	1.047	175	153	169	0.330
RC0182	56.03	63.53	6.16	1.75	2.039	185	159	178	0.322
RC0183	56.35	64.14	6.10	1.71	5.121	203	173	195	0.310
RC0184	56.00	64.04	6.16	1.79	10.28	213	179	209	0.294
RC0185	55.41	63.43	6.16	2.76	20.94	225	188	222	0.240
RC0186	55.39	63.23	6.17	1.65	50.01	253	203	245	0.226
RC0187	55.39	63.53	6.11	1.69	70.41	269	206	261	0.216
RC0188	55.83	63.53	6.08	1.64	103.4	278	216	273	0.204
RC0175	55.16	63.43	8.15	2.19	0.105	139	110	132	0.320
RC0176	55.16	63.53	8.03	2.02	0.208	153	125	144	0.326
RC0177	55.44	63.33	8.00	2.02	0.529	169	139	160	0.330
RC0158	55.73	62.61	8.08	2.06	1.092	179	147	169	0.332
RC0159	55.64	63.74	8.12	2.07	2.057	192	153	180	0.340
RC0160	55.57	63.53	8.09	2.12	5.127	209	169	200	0.326
RC0161	55.29	62.40	8.05	2.09	10.08	223	176	216	0.298
RC0172	55.08	63.63	7.97	2.03	22.35	235	181	230	0.237
RC0173	55.08	63.84	8.00	1.89	48.09	260	191	257	0.205
RC0174	55.08	63.43	8.14	2.03	65.33	271	204	269	0.197
RC0155	54.27	62.51	10.95	3.08	0.095	146	111	139	0.359
RC0154	55.09	64.35	10.92	2.93	0.206	160	121	152	0.365
RC0138	54.62	65.06	11.03	3.50	0.622	176	134	164	0.365
RC0137	56.08	65.16	10.92	3.37	1.008	187	144	181	0.355
RC0153	56.26	64.75	10.90	2.81	2.097	200	147	194	0.342
RC0150	56.64	64.45	10.92	2.60	5.298	216	158	206	0.333
RC0151	57.14	64.75	10.92	2.61	10.84	229	179	219	0.308
RC0152	55.30	63.84	10.82	2.61	21.25	249	191	242	0.217
RC0145	56.86	63.33	10.97	3.01	53.31	278	213	269	0.189
RC0219	46.37	60.08	10.81	2.94	0.095	148	110	141	0.299
RC0276	48.90	56.71	11.07	3.34	0.178	163	117	155	0.313
RC0277	53.51	60.24	11.08	3.40	0.512	181	145	169	0.358
RC0230	46.99	59.37	10.96	3.15	5.075	222	166	209	0.334
RC0228	50.47	61.73	10.87	3.13	10.18	238	182	226	0.312
RC0229	46.40	58.73	10.89	3.04	45.91	285	208	284	0.195

b_o = Initial breadth.

b_f = Final breath.

t_o = Initial thickness.

t_f = Final thickness.

$\dot{\varepsilon}$ = Strain rate.

σ_p = Peak stress.

σ_s = Steady state stress.

$\sigma_{0.15}$ = Stress at 0.15 strain.

ε_p = Strain to peak stress.

Table VI

Stress strain data from axisymmetric compression tests in AISI 316 stainless steel.

Test	Direction	h_o [mm]	d_o [mm]	h_f [mm]	$\dot{\varepsilon}$ [sec^{-1}]	σ_p [MN/m^2]	$\sigma_{0.15}$ [MN/m^2]	ε_p
RC0254	t	10.27	7.18	4.06	0.523	185	164	0.465
RC0255	t	10.19	7.09	3.97	1.052	198	173	0.505
RC0256	t	10.34	7.18	3.98	2.090	208	184	0.530
RC0257	t	10.21	7.17	3.99	5.266	236	204	0.560
RC0258	t	10.31	7.14	4.11	10.11	257	220	0.615
RC0259	t	10.34	7.10	3.88	20.35	269	239	0.530
RC0260	t	10.21	7.15	3.73	46.65	306	277	0.420
RC0293	t	7.26	7.14	2.97	0.765	196	169	0.495
RC0294	t	7.13	7.10	3.01	2.705	229	192	0.560
RC0292	t	7.23	7.13	2.92	23.26	287	258	0.570
RC0291	t	7.37	7.13	2.65	56.25	314	285	0.440
RC0168	w	10.40	7.08	5.01	0.529	185	160	0.517
RC0167	w	10.33	7.16	4.02	1.048	211	178	0.538
RC0166	w	10.55	7.08	4.22	2.113	216	186	0.541
RC0171	w	10.29	7.15	5.61	5.165	240	209	0.624
RC0164	w	10.51	7.12	3.79	10.84	250	219	0.649
RC0163	w	10.40	7.12	3.64	21.11	275	247	0.605
RC0162	w	10.20	7.17	2.56	50.21	311	274	0.583
RC0253	l	10.32	7.18	4.31	0.520	190	162	0.515
RC0247	l	10.36	7.17	4.18	1.063	199	170	0.535
RC0248	l	10.39	7.14	4.31	2.068	219	187	0.575
RC0249	l	10.37	7.14	4.34	5.098	242	206	0.620
RC0250	l	10.37	7.10	4.12	10.49	255	215	0.640
RC025)	)	10.33	7.17	3.96	20.72	277	239	0.615

h_o = Initial height.

d_o = Initial diammeter.

$\dot{\varepsilon}$ = Strain rate.

σ_p = Peak stress.

$\sigma_{0.15}$ = Stress at 0.15 strain.

ε_p = Strain to peak stress.

h_f = Final height.

Direction = Testing direction.

t = Thickness.

w = Width.

l = Length.

Table VII

Stress strain data from torsion tests in AISI 316 stainless steel.

Test	l [mm]	d [mm]	$\dot{\varepsilon}$ [sec^{-1}]	σ_p [MN/m^2]	$\sigma_{0.15}$ [MN/m^2]	σ_s [MN/m^2]	ε_p
RC09T	14.30	7.11	0.018	146	139	121	0.299
RC08T	14.72	6.93	0.028	168	154	158	0.408
RC07T	14.80	7.04	0.354	224	182	197	0.448
RC05T	14.43	7.01	0.703	238	198	219	0.468
RC06T	14.71	6.98	1.499	266	219	235	0.557
RC011T	14.82	6.97	0.0032	82	70	74	0.299
RC010T	14.60	7.00	0.014	110	104	90	0.348
RC012T	14.74	7.04	0.031	120	110	105	0.368
RC01T	14.92	7.02	0.356	170	147	151	0.423
RC04T	15.08	6.97	0.670	185	154	162	0.458
RC02T	14.73	7.01	1.379	194	161	169	0.493

l = Gauge length.

d = Gauge diammeter.

$\dot{\varepsilon}$ = Strain rate.

σ_p = Peak stress.

σ_s = Steady state stress.

$\sigma_{0.15}$ = Stress at 0.15 strain.

ε_p = Strain to peak stress.

Table VIII

Strain data from the gridded specimens.

Test	ε_{ef}	ε_{ap}	$\bar{\varepsilon}$	$\bar{\varepsilon}_c$	ε_{nom}	ε_{slf}	$\Delta\%$
RC0139	0.137	0.155	0.207	0.189	0.137	0.219	5.5
RC0140	0.191	0.218	0.298	2.71	0.202	0.324	8.0
RC0141	0.373	0.420	0.447	0.400	0.401	0.508	12.0
RC0224	0.551	0.615	0.587	0.523	0.538	0.526	6.2
RC0220	0.697	0.778	0.789	0.701	0.735	0.831	5.1
RC0226	0.072	0.082	0.113	0.103	0.058	0.156	27.6
RC0147	0.180	0.201	0.227	0.206	0.131	0.236	3.8
RC0148	0.273	0.308	0.323	0.288	0.243	0.365	11.5
RC0149	0.568	0.621	0.509	0.456	0.458	0.560	9.1
RC0225	0.586	0.644	0.622	0.564	0.573	0.630	1.3
RC0222	0.712	0.790	0.798	0.720	0.734	0.822	2.9
RC0142	0.196	0.218	0.231	0.209	0.147	0.254	9.1
RC0143	0.256	0.320	0.336	0.304	0.268	0.373	9.9
RC0144	0.499	0.558	0.507	0.448	0.470	0.531	4.5
RC0223	0.656	0.719	0.695	0.632	0.662	0.705	1.4
RC0221	0.738	0.820	0.865	0.783	0.779	0.891	2.9

ε_{ef} = Effective strain.
ε_{ap} = Apparent strain.
$\bar{\varepsilon}$ = Average strain.
$\bar{\varepsilon}_c$ = Corrected average strain.
ε_{nom} = Nominal strain.
ε_{slf} = Strain in the slip line field.
$\Delta\%$ is the variation between and $_{slf}$.

Table IX

Metallographic data from the AISI 316 stainless steel.

Specimen	Temperature [C]	$\dot{\varepsilon}$ [sec^{-1}]	ε	Xv	d [μm]
RC0245	910	0.547	0.162	0.115	15.6 ± 3.5
RC0244	910	0.547	0.240	0.185	14.3 ± 4.8
RC0236	910	0.547	0.334	0.219	13.3 ± 5.0
RC0238	910	0.547	0.451	0.285	13.1 ± 5.5
RC0242	910	0.547	0.547	0.569	11.3 ± 3.7
RC0243	910	5.163	0.134	0.099	13.7 ± 3.9
RC0241	910	5.163	0.232	0.191	11.9 ± 3.6
RC0235	910	5.163	0.319	0.231	11.2 ± 4.9
RC0237	910	5.163	0.419	0.394	10.5 ± 4.5
RC0239	910	5.163	0.561	0.409	8.7 ± 4.1
RC0139	1006	0.413	0.137	0.0	23.5 ± 3.1
RC0140	1006	0.413	0.202	0.077	19.7 ± 4.0
RC0141	1006	0.413	0.401	0.228	14.5 ± 4.7
RC0224	1006	0.413	0.538	0.376	13.9 ± 4.9
RC0220	1006	0.413	0.735	0.518	12.6 ± 1.8
RC0226	1006	4.824	0.058	0.0	26.6 ± 3.6
RC0147	1006	4.824	0.131	0.018	25.8 ± 5.3
RC0148	1006	4.824	0.243	0.064	23.0 ± 6.2
RC0149	1006	4.824	0.458	0.268	17.0 ± 6.0
RC0225	1006	4.824	0.573	0.574	13.6 ± 3.5
RC0222	1006	4.824	0.734	0.811	11.7 ± 1.4
RC0142	1006	43.06	0.147	0.052	21.8 ± 3.9
RC0143	1006	43.06	0.268	0.093	16.6 ± 3.8
RC0144	1006	43.06	0.470	0.394	12.2 ± 2.5
RC0223	1006	43.06	0.662	0.886	12.5 ± 1.9
RC0221	1006	43.06	0.779	0.980	9.8 ± 1.3

$\dot{\varepsilon}$ = Strain rate.

ε = Nominal strain.

Xv = Volume fraction recrystallised.

d = Mean overall grain size.

Figure 1.- Schematic representation of σ, $d\sigma/d\varepsilon$ and γ versus ε; a.) tension, b.) compression. Showing the difference between Considère's criterion (C) and Hart's criterion (H) for both cases (Jonas et al, 1976).

Figure 2.- Schematic diagram of a specimen tested under tensile conditions. The homogeneous and the imperfect areas are shown (Ghosch, 1978).

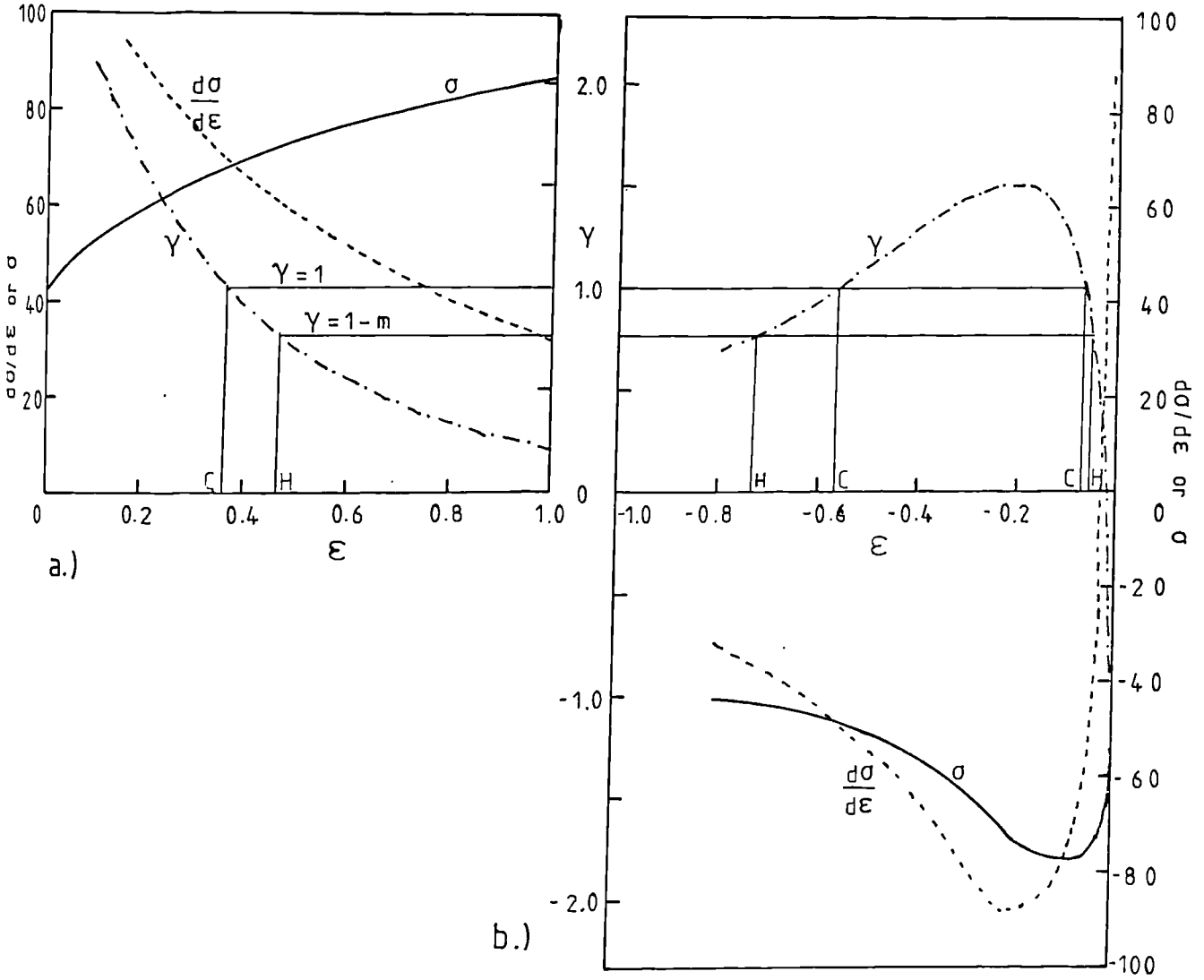
a.)
b.)
σ
dσ/dε
Y
Y = 1
Y = 1 - m
C
H
ε
dσ/dε or σ
dσ/dp or σ
dσ/dp

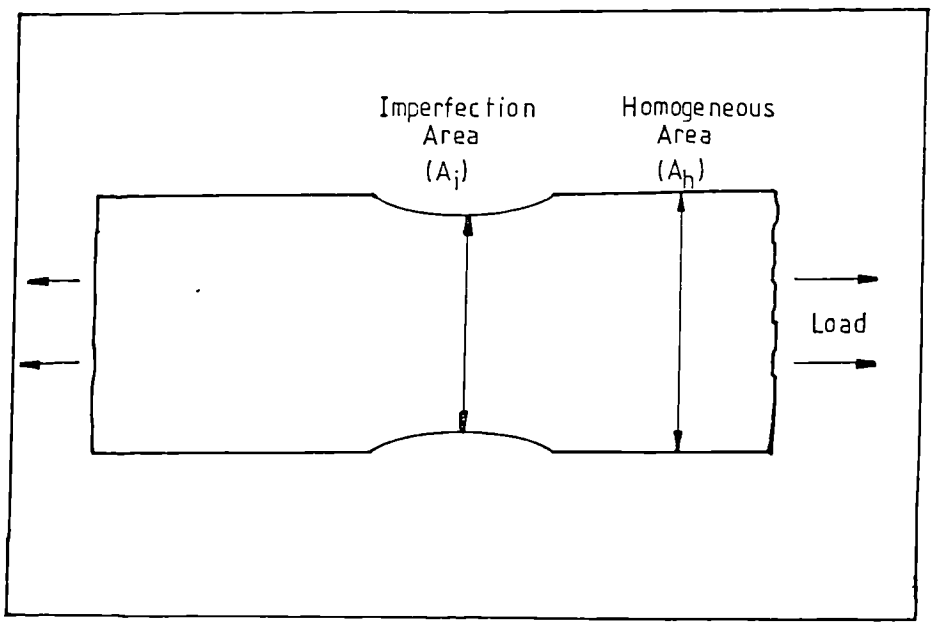
Imperfection Area
(A_i)
Homogeneous Area
(A_h)
Load

Figure 3.- Stable and unstable domains in ARMCO iron. Grain sizes a.) 17 μm, b.) 25 μm, c.) 40 μm (after Violan, 1973).

Figure 4.- Importance of the deceleration parameter δ_p, upon the strain gradient, ε', with strain (Kocks, 1980).

Figure 5.- Schematic representation of the solutions of equation (2.69) One branch correspond to the effect of mechanical defects, the other branch to the deformation defects (Kocks, 1980).

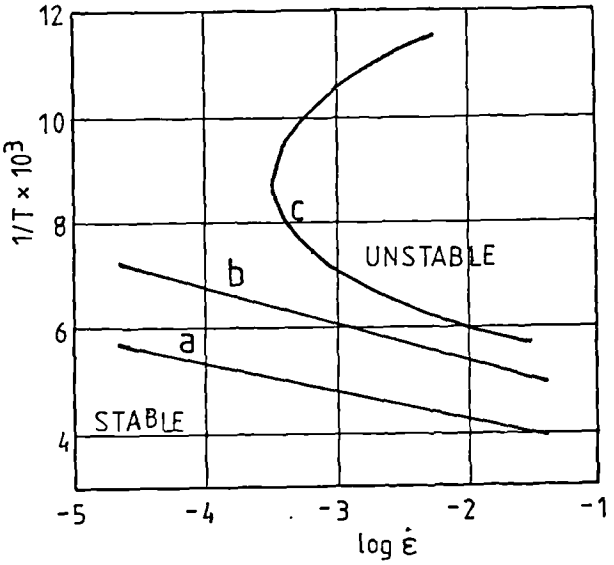
12
10
8
6
4
1/T x 10³
c
b
a
UNSTABLE
STABLE
-5
-4
-3
-2
-1
log ε̇

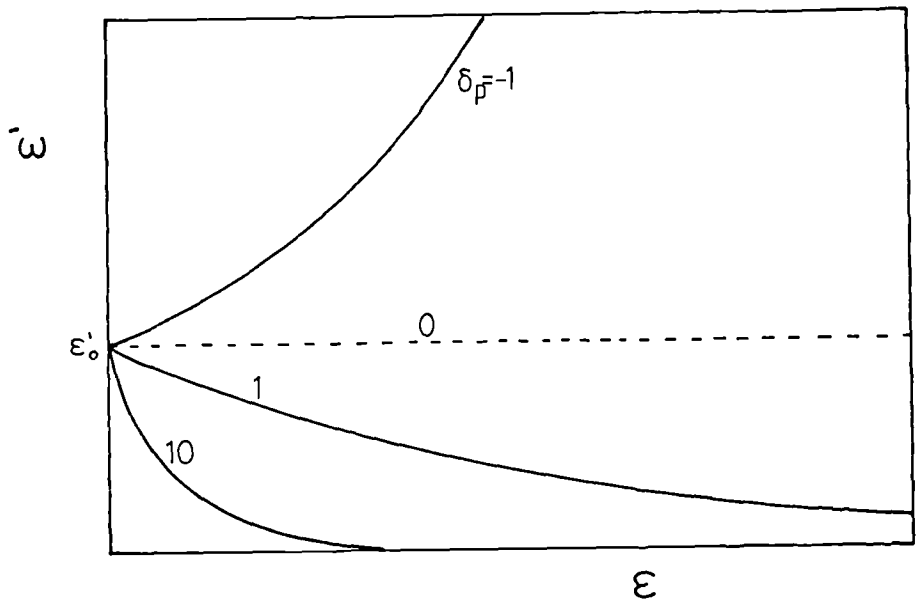
ω̇
δp=-1
0
ε̇₀
1
10
ε

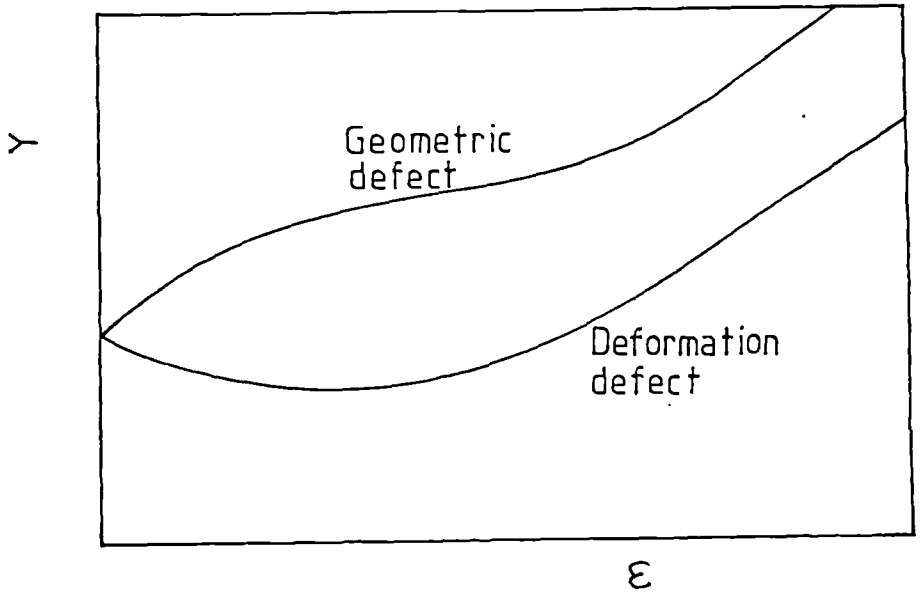
γ
Geometric defect
Deformation defect
ε

Figure 6.- Load strain curve for a material showing the four stages of flow localisation (Jalinier et al, 1978).

Figure 7.- Representation of three different instability criteria (Demeri and Conrad, 1978).

Figure 8.- Correlation of strain rate sensitivity and total elongation for a variety of materials (Woodford, 1969).

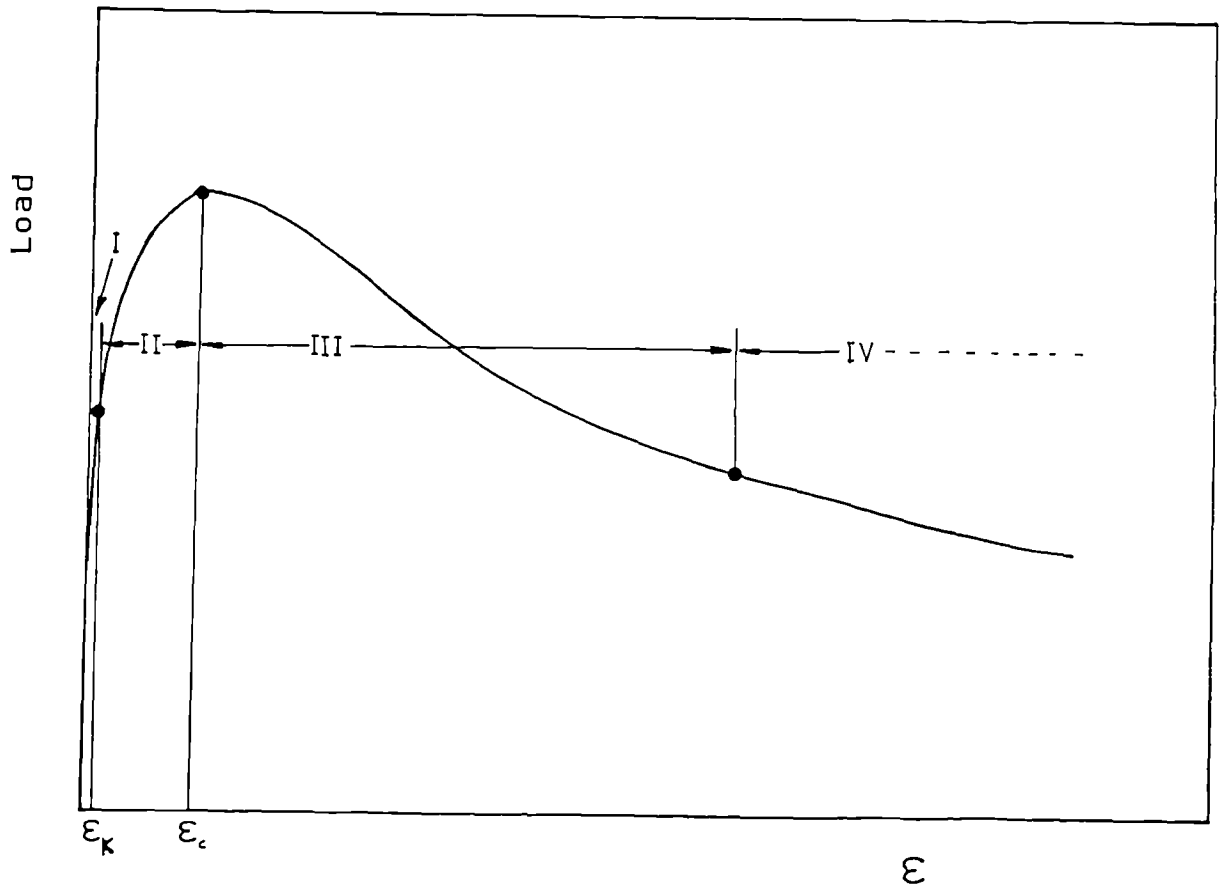
Load
I
II
III
IV
ε_K
ε_c
ε

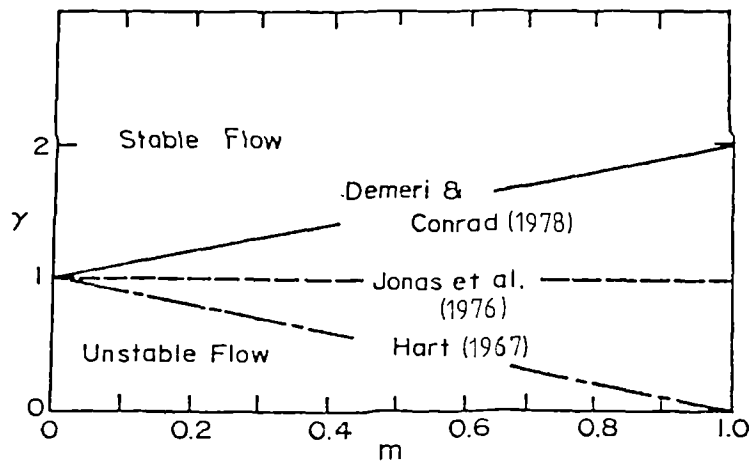
Stable Flow
Demeri & Conrad (1978)
Jonas et al. (1976)
Hart (1967)
Unstable Flow
γ
m
0
1
2
0.2
0.4
0.6
0.8
1.0

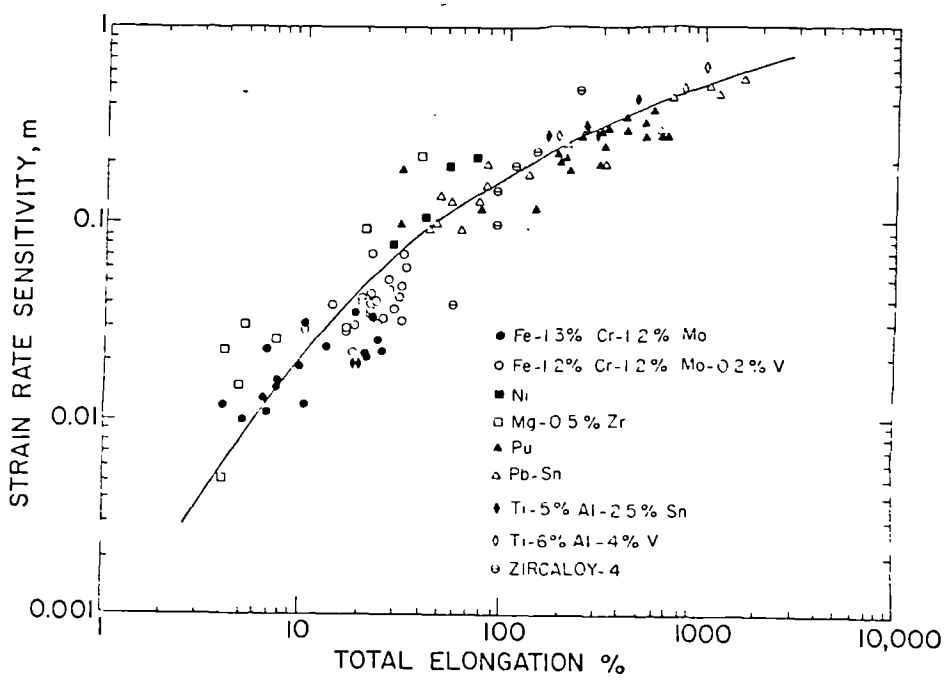
STRAIN RATE SENSITIVITY, m
TOTAL ELONGATION %
0.001
0.01
0.1
1
10
100
1000
10,000
Fe-13% Cr-12% Mo
Fe-12% Cr-12% Mo-02% V
Ni
Mg-05% Zr
Pu
Pb-Sn
Ti-5% Al-25% Sn
Ti-6% Al-4% V
ZIRCALOY-4

Figure 9.- Effect of strain rate on ductility of 18Cr, 8 Ni steel; full lines mean specimen heated directly to test temperature; dashed lines mean specimen annealed for one hour before testing (after Gittins and Tegart, 1973).

Figure 10.- Comparison of stress-strain curves obtained for lead at room temperature using different test methods, a.) at low strain rate, b.) at high strain rate (Sellars, 1981).

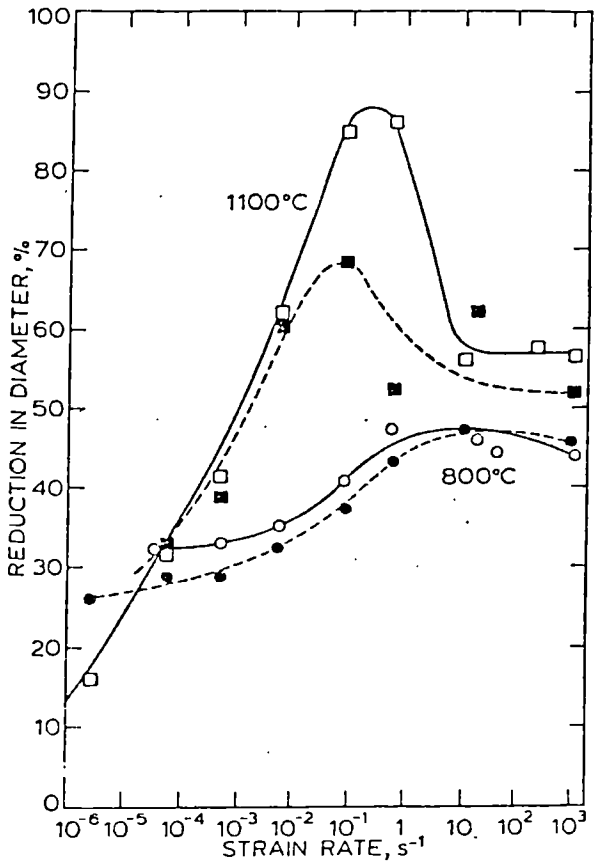
REDUCTION IN DIAMETER, %
STRAIN RATE, s⁻¹
1100°C
800°C

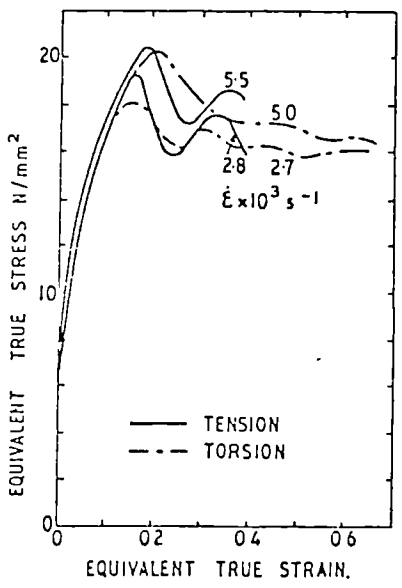
EQUIVALENT TRUE STRESS N/mm²
EQUIVALENT TRUE STRAIN.
5·5
5·0
2·8
2·7
Ė x10³ s⁻¹
TENSION
TORSION

a.)

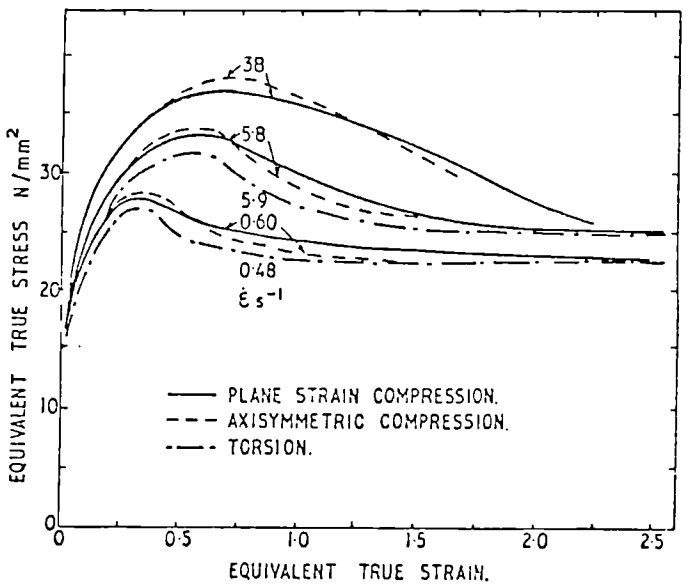
EQUIVALENT TRUE STRESS N/mm²
EQUIVALENT TRUE STRAIN.
3·8
5·8
5·9
0·60
0·48
Ė s⁻¹
PLANE STRAIN COMPRESSION.
AXISYMMETRIC COMPRESSION.
TORSION.

b.)

Figure 11.- Theoretical slip line field solution for plane strain compression tests with different geometry and different friction coefficient (after Loong, 1976).

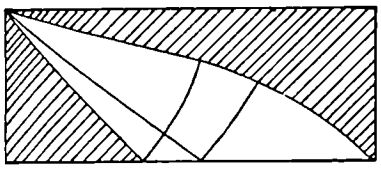

h/w = 0.40
μ = 0.15

Rigid zones

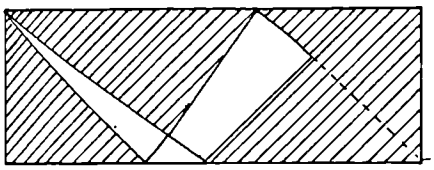

h/w = 0.36
μ = 0.15

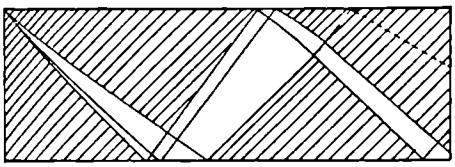

h/w = 0.33
μ = 0.15

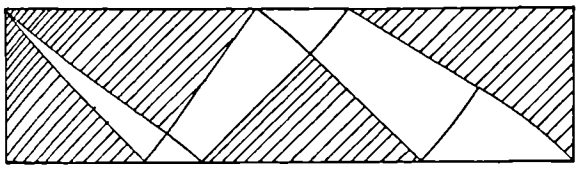

h/w = 0.26
μ = 0.15

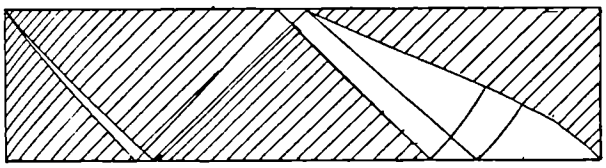

h/w = 0.25
μ = 0.05

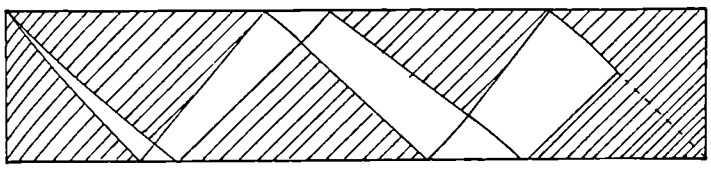

h/w = 0.21
μ = 0.10

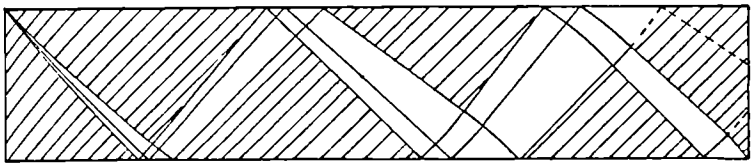

h/w = 0.20
μ = 0.10

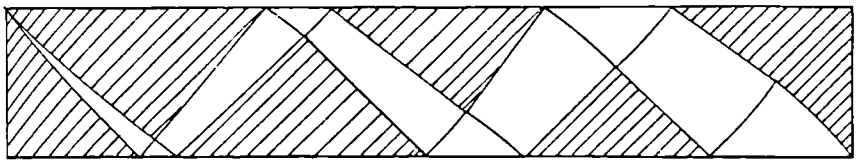

h/w = 0.18
μ = 0.10

Figure 12.- Effect of geometry in lead specimens tested at different strain rates at room temperature under plane strain compression conditions (Sellars et al, 1976).

Figure 13.- Effect of geometry on niobium bearing steel under plane strain compression conditions (Foster, 1981).

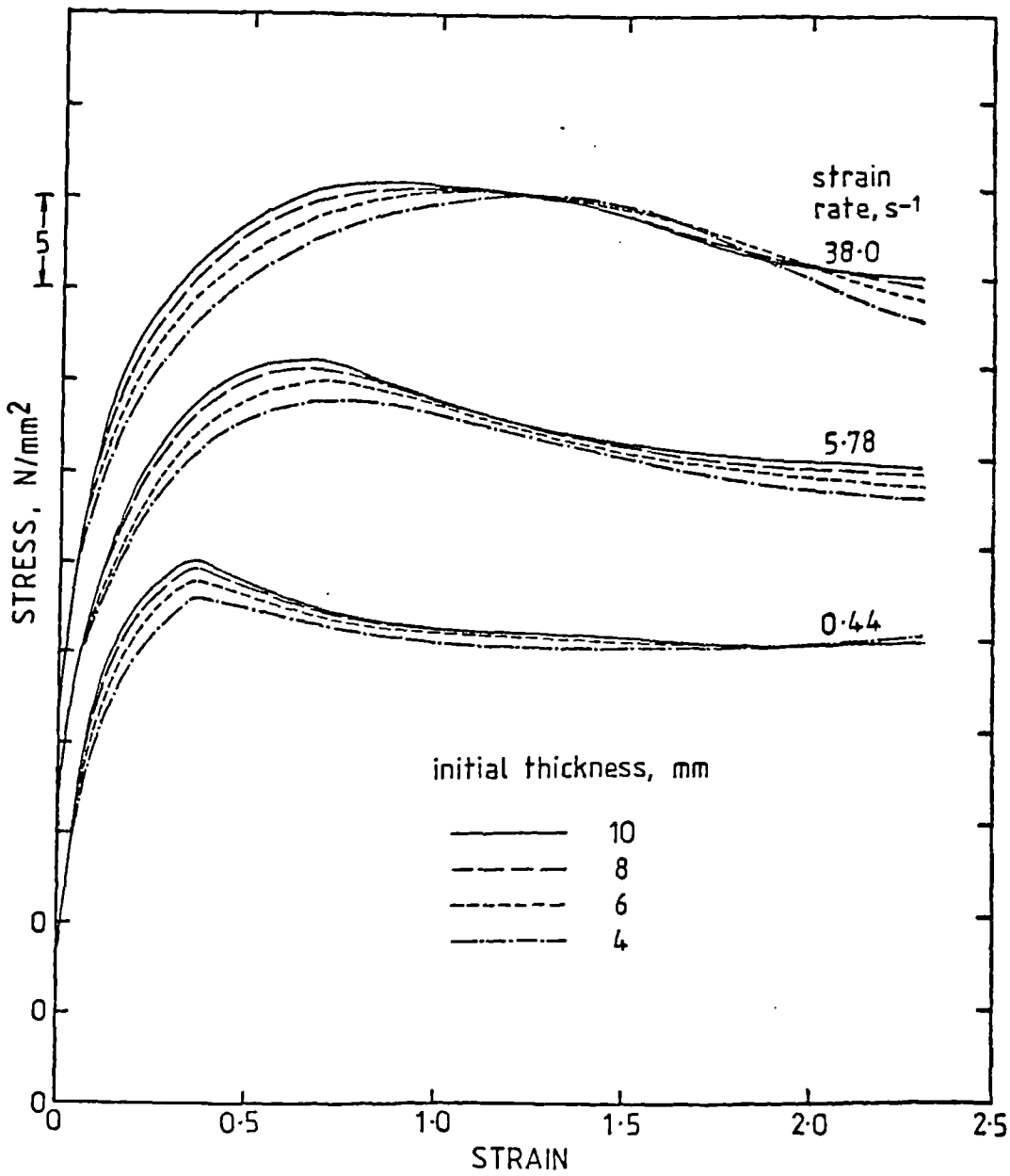
strain rate, s⁻¹
38·0
5·78
0·44
initial thickness, mm
10
8
6
4
STRESS, N/mm²
STRAIN
0
0·5
1·0
1·5
2·0
2·5

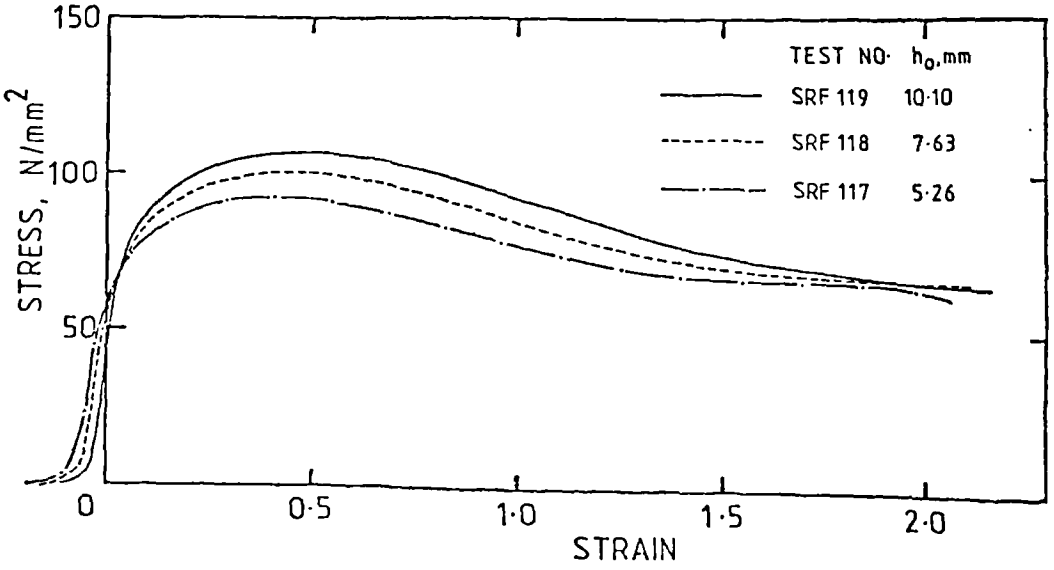
TEST NO· h₀,mm
SRF 119 10·10
SRF 118 7·63
SRF 117 5·26
STRESS, N/mm²
STRAIN
150
100
50
0
0·5
1·0
1·5
2·0

Figure 14.- Strain at centre-line of plane strain compression specimens, a.) width over height (w/a) equal to 1.6, b.) w/a = 2.0 (Sellars et al, 1976).

Figure 15.- Strain distribution field for plane strain compression in lead tested at room temperature. Data should be multiplied by 1.155 to obtain uniaxial values of strain (Sellars et al, 1976).

	h_o, mm	w/h	ε	DEF.
○	9·98	1·61	0·52	1st
●	9·74	1·64	0·53	2nd
△	7·07	1·62	0·19	1st

	h_o, mm	w/h	ε	DEF.
●	9·80	1·96	0·70	3rd
○	9·72	2·00	0·71	1st
▲	7·07	1·99	0·39	2nd

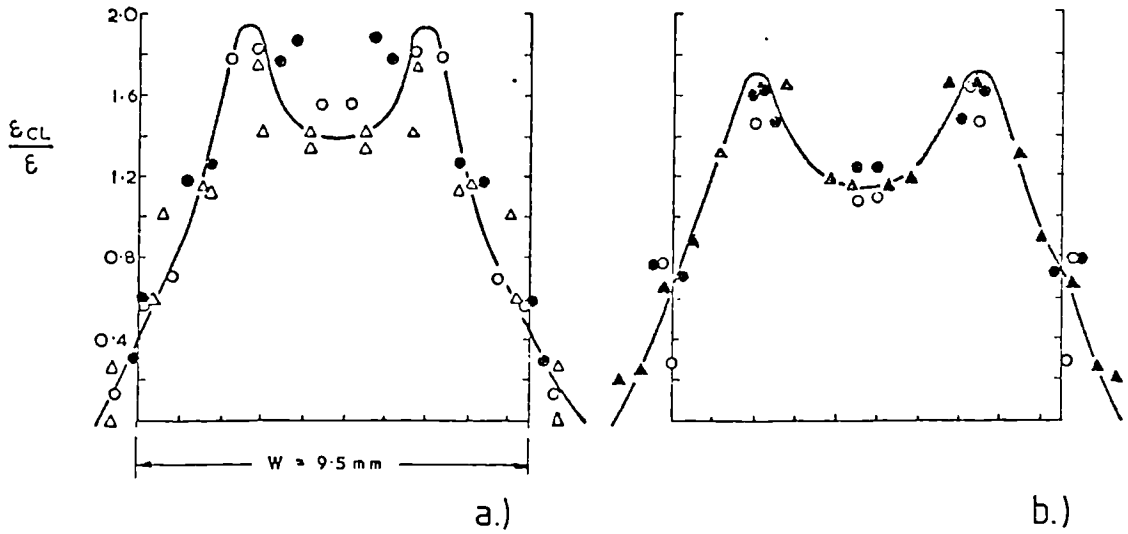

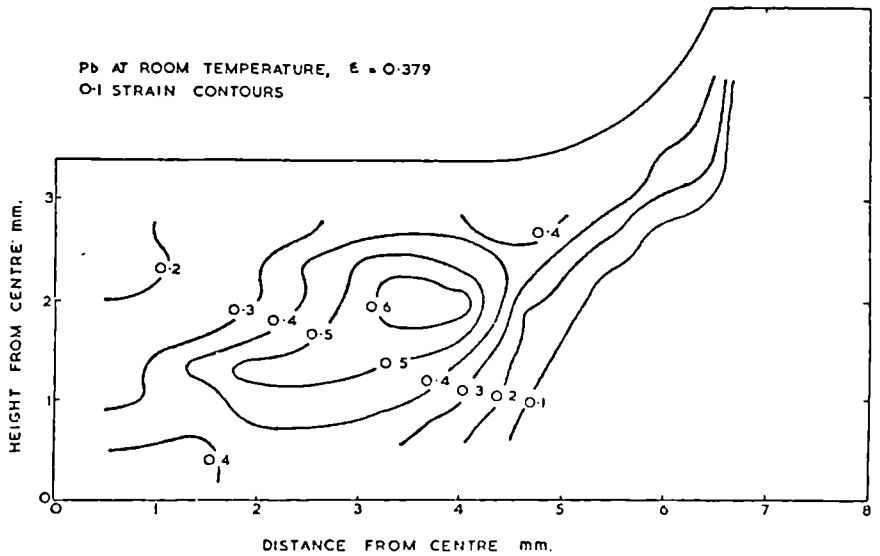

Figure 16.- Stress-strain curves for Armco iron tested at different strain rates at 700 C (Immarigeon and Jonas, 1974).

Figure 17.- True resolved shear stress-true resolved shear strain for <111> single crystals a.) nickel, b.) copper (Gottstein and Kocks, 1983).

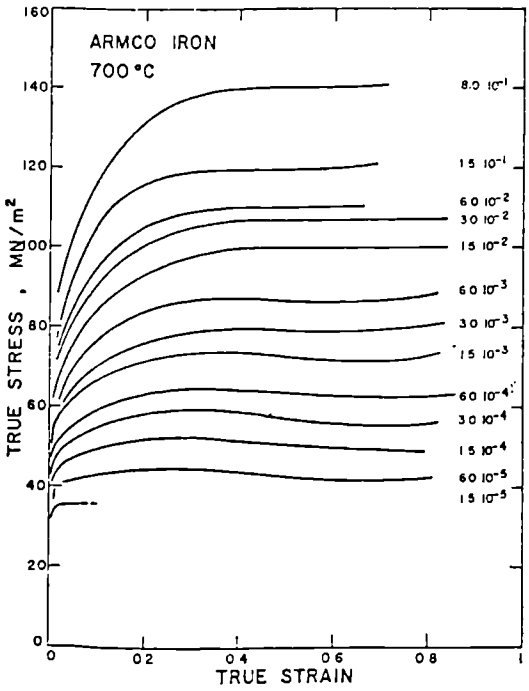
ARMCO IRON
700 °C
TRUE STRESS , MN/m²
TRUE STRAIN
8.0 10⁻¹
1.5 10⁻¹
6.0 10⁻²
3.0 10⁻²
1.5 10⁻²
6.0 10⁻³
3.0 10⁻³
1.5 10⁻³
6.0 10⁻⁴
3.0 10⁻⁴
1.5 10⁻⁴
6.0 10⁻⁵
1.5 10⁻⁵

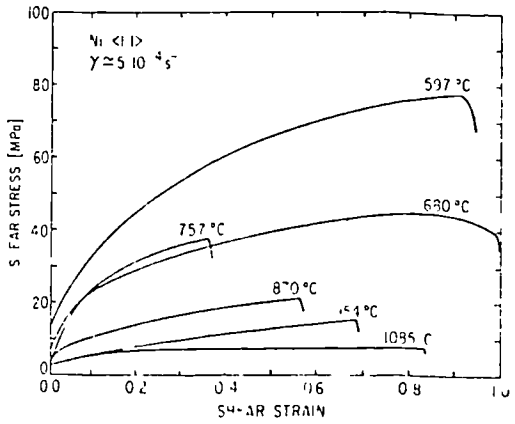
Ni <111>
597 °C
680 °C
757 °C
870 °C
1085 °C
SHEAR STRAIN

a.)

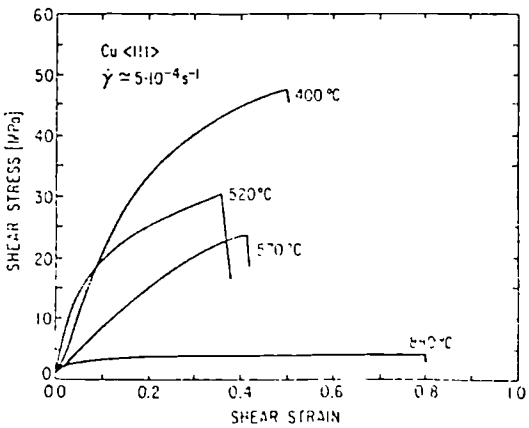
Cu <111>
400 °C
520 °C
570 °C
SHEAR STRESS [MPa]
SHEAR STRAIN

b.)

Figure 18.- Stress-strain curves for materials that recrystallise dynamically. a.) Effect of strain rate on mild steel tested in torsion at 1100 C (after Rossard and Blain, 1955). b.) Effect of testing temperature on nickel tested in torsion at $\dot{\varepsilon} = 0.016\ sec^{-1}$ (after Luton and Sellars, 1969).

Figure 19.- Predicted stress-strain curves for dynamic recrystallisation. a.) A cyclic stress-strain curve when the critical strain to initiate recrystallisation is greater than, the strain occurring in the time for a large fraction of recrystallisation, $\varepsilon_c > \varepsilon_x$. b.) A steady state curve for the condition when $\varepsilon_c < \varepsilon_x$. The strain for completion of the first cycle ε_s equals the sum, $\varepsilon_c + \varepsilon_x$ (Luton and Sellars, 1969).

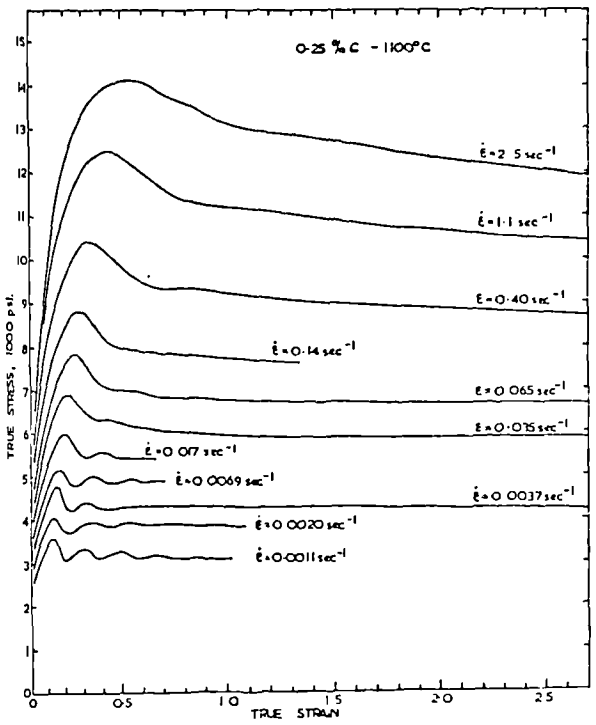
0·25 % C - 1100°C
TRUE STRESS, 1000 p.s.i.
TRUE STRAIN
$\dot{\varepsilon}$ = 2·5 sec^{-1}
$\dot{\varepsilon}$ = 1·1 sec^{-1}
$\dot{\varepsilon}$ = 0·40 sec^{-1}
$\dot{\varepsilon}$ = 0·14 sec^{-1}
$\dot{\varepsilon}$ = 0·065 sec^{-1}
$\dot{\varepsilon}$ = 0·035 sec^{-1}
$\dot{\varepsilon}$ = 0·017 sec^{-1}
$\dot{\varepsilon}$ = 0·0069 sec^{-1}
$\dot{\varepsilon}$ = 0·0037 sec^{-1}
$\dot{\varepsilon}$ = 0·0020 sec^{-1}
$\dot{\varepsilon}$ = 0·0011 sec^{-1}

a.)

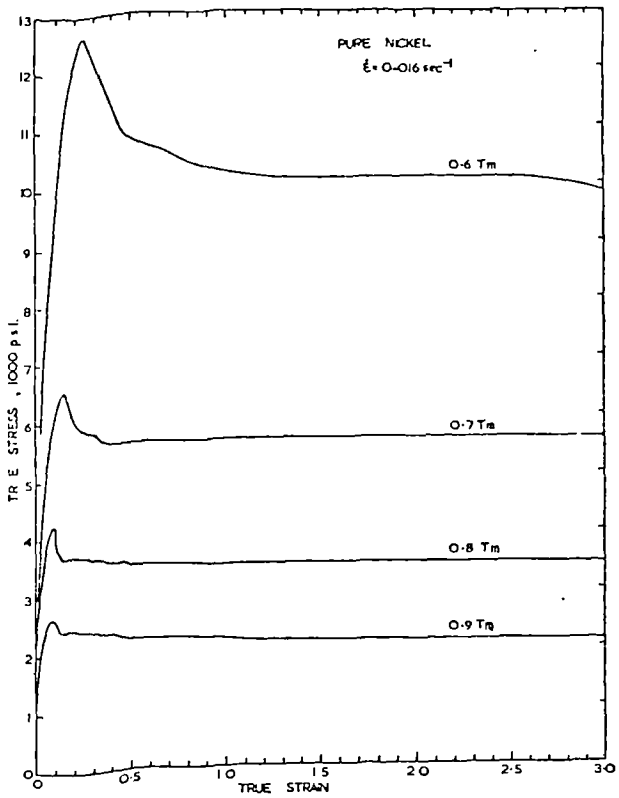
PURE NICKEL
$\dot{\varepsilon}$ = 0·016 sec^{-1}
0·6 Tm
0·7 Tm
0·8 Tm
0·9 Tm
TRUE STRESS, 1000 p.s.i.
TRUE STRAIN

b.)

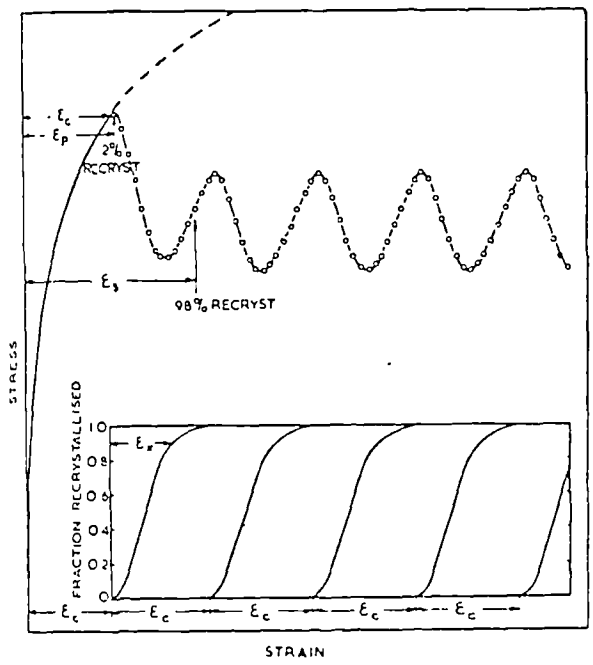
ε_c
ε_p
2% RECRYST
ε_s
98% RECRYST
STRESS
FRACTION RECRYSTALLISED
ε_w
ε_c ε_c ε_c ε_c ε_c
STRAIN

a.)

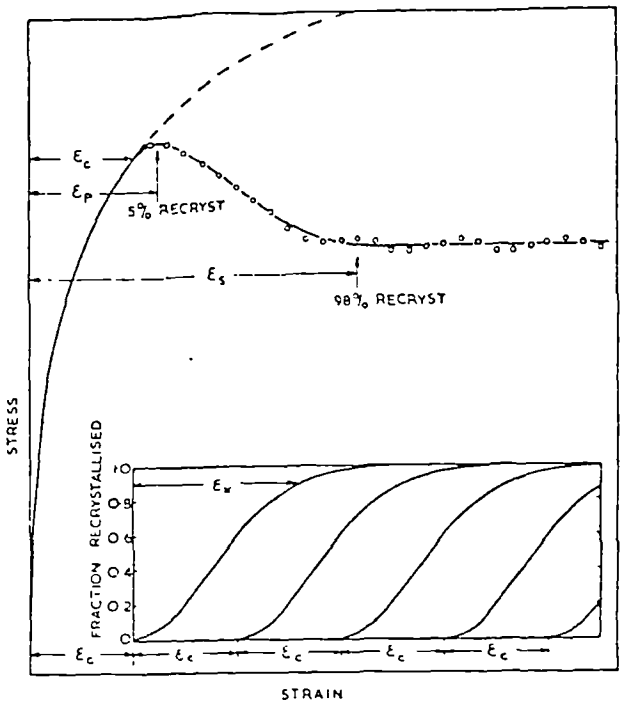
ε_c
ε_p
5% RECRYST
ε_s
98% RECRYST
STRESS
FRACTION RECRYSTALLISED
ε_w
ε_c ε_c ε_c ε_c ε_c
STRAIN

b.)

Figure 20.- Relation between the critical shear strain γ_c for the onset of dynamic recrystallisation to take place and the shear strain γ_R expected for the onset of steady state if softening were by recovery only (Sellars, 1978).

Figure 21.- Dependence of the strain to the peak in stress with strain rate for a mild steel and a titanium bearing steel tested under plane strain conditions (Leduc, 1980).

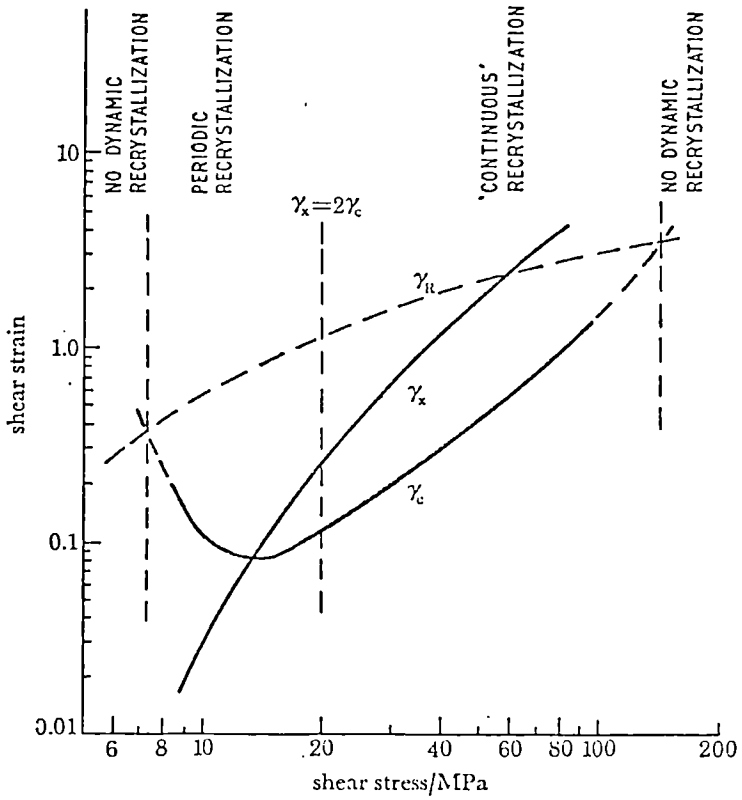
NO DYNAMIC RECRYSTALLIZATION
PERIODIC RECRYSTALLIZATION
'CONTINUOUS' RECRYSTALLIZATION
NO DYNAMIC RECRYSTALLIZATION
$\gamma_x=2\gamma_c$
γ_R
γ_x
γ_c
shear strain
10
1.0
0.1
0.01
6 8 10 20 40 60 80 100 200
shear stress/MPa

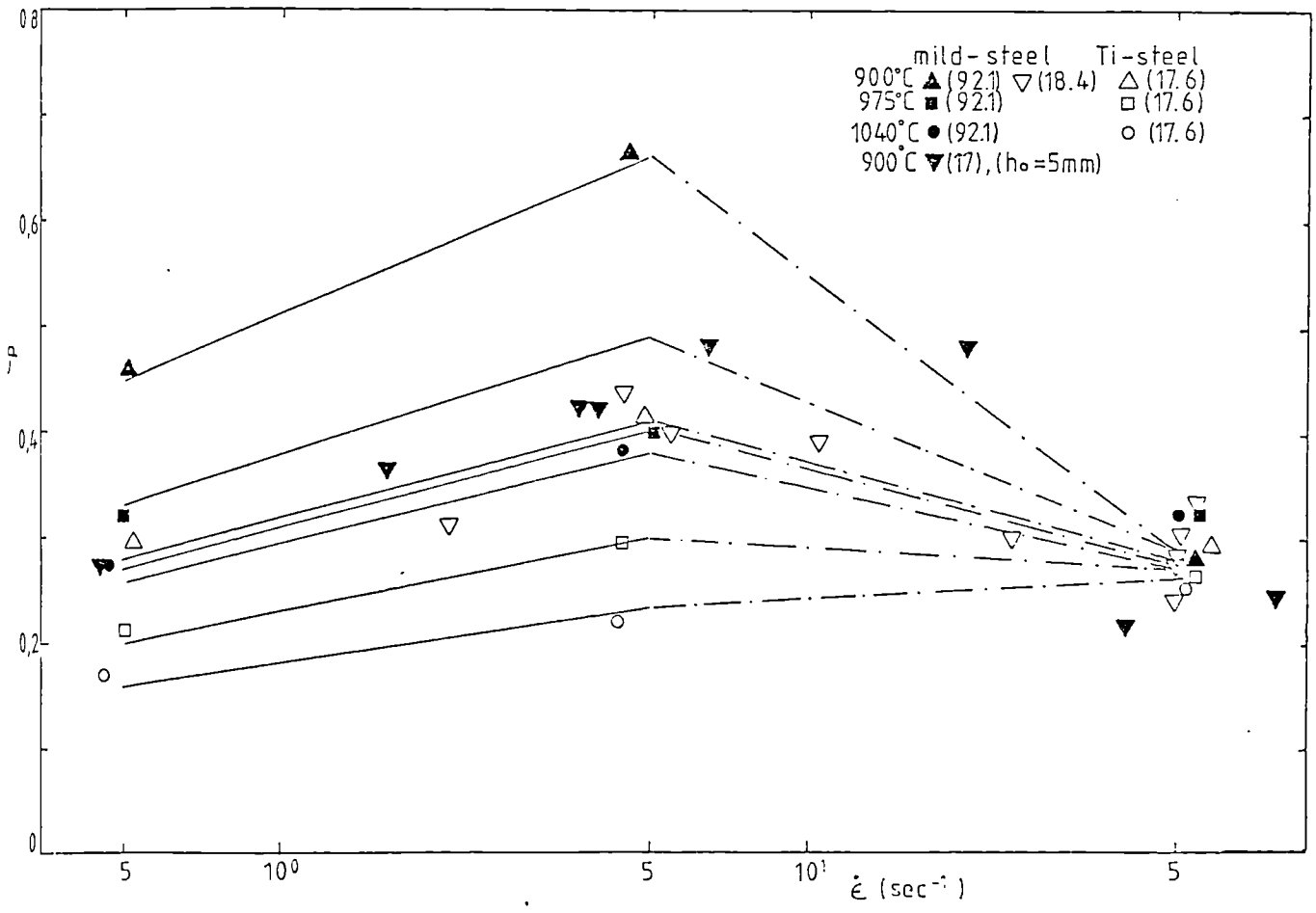
mild-steel Ti-steel
900°C ▲(92.1) ▽(18.4) △(17.6)
975°C ■(92.1) □(17.6)
1040°C ●(92.1) ○(17.6)
900°C ▼(17), (h_o=5mm)
0,8
0,6
0,4
0,2
0
5
10^0
5
10^1
5
$\dot{\epsilon}$ (sec^{-1})

Figure 22.- Dependence of the strain to the peak in stress with strain rate for lead tested under different conditions (after Sellars et al, 1976).

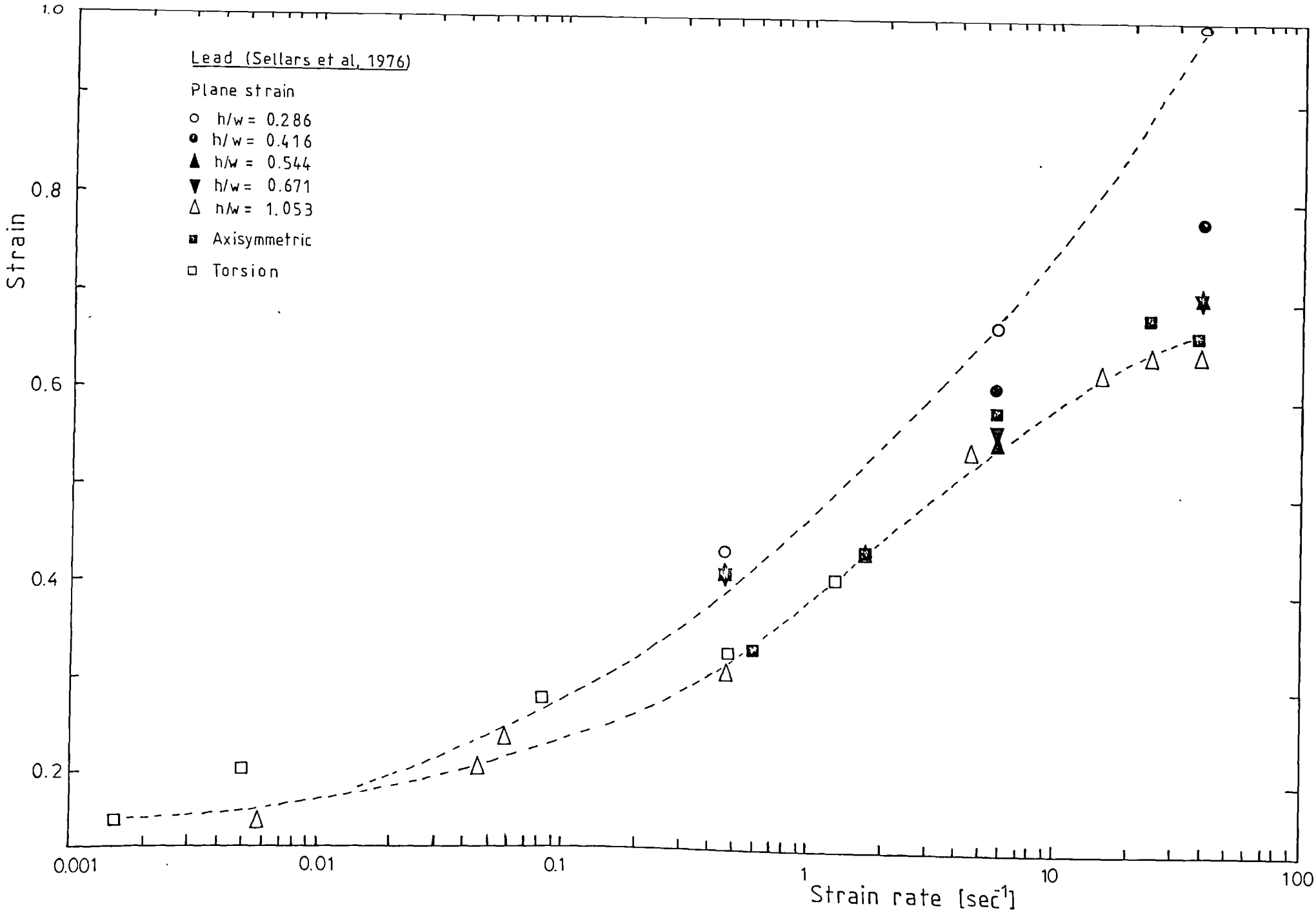
Lead (Sellars et al, 1976)
Plane strain
h/w = 0.286
h/w = 0.416
h/w = 0.544
h/w = 0.671
h/w = 1.053
Axisymmetric
Torsion
Strain
Strain rate [sec⁻¹]
1.0
0.8
0.6
0.4
0.2
0.001
0.01
0.1
1
10
100

Figure 23.- Temperature-strain curves of different initial thickness lead specimens tested at room temperature and different strain rates (Sellars et al, 1976).

Figure 24.- Temperature-strain curves of niobium bearing steel tested at different strain rates (Foster, 1981).

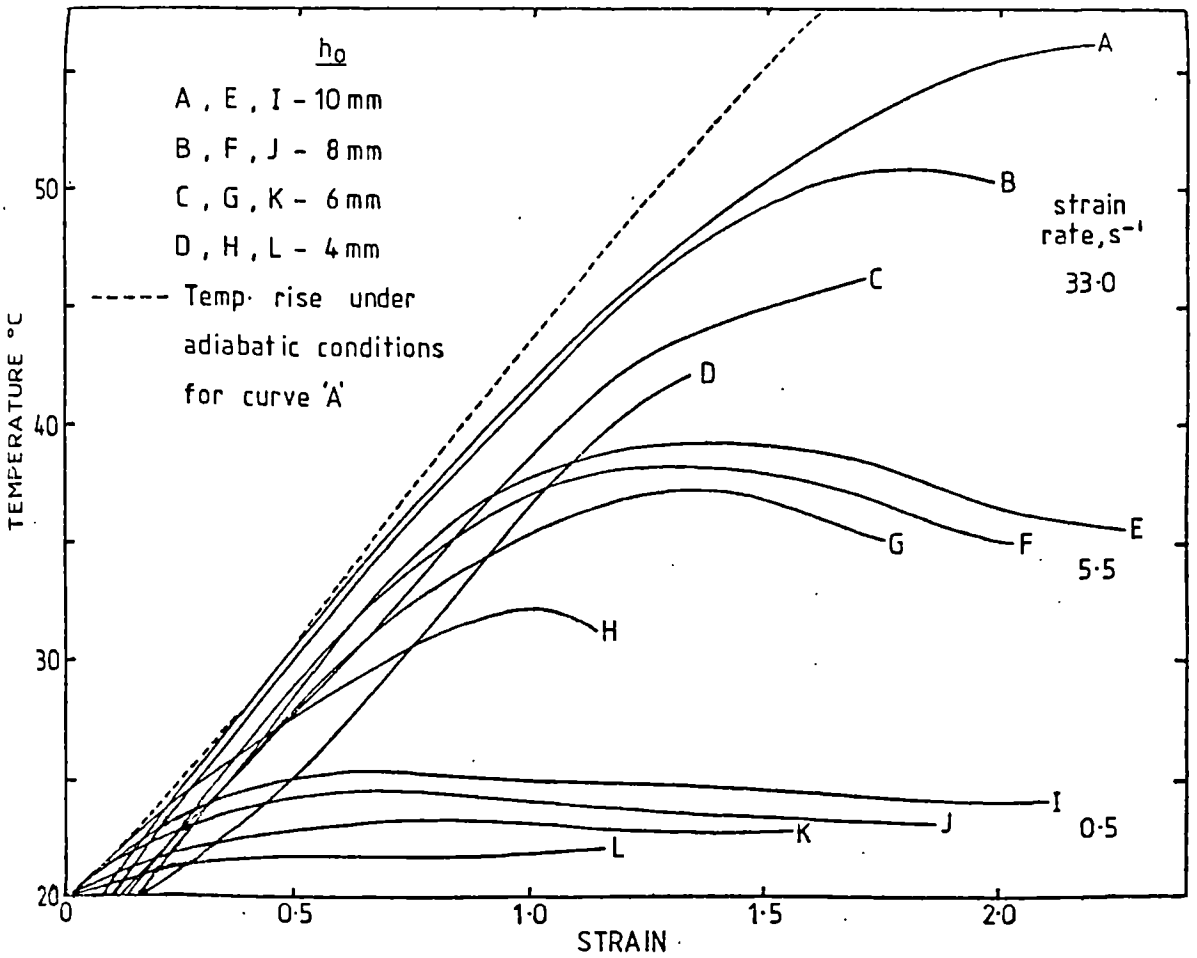
h_0
A , E , I - 10 mm
B , F , J - 8 mm
C , G , K - 6 mm
D , H , L - 4 mm
----- Temp· rise under adiabatic conditions for curve 'A'
strain rate, s^{-1}
33·0
5·5
0·5
A
B
C
D
E
F
G
H
I
J
K
L
TEMPERATURE °C
50
40
30
20
0
0·5
1·0
1·5
2·0
STRAIN

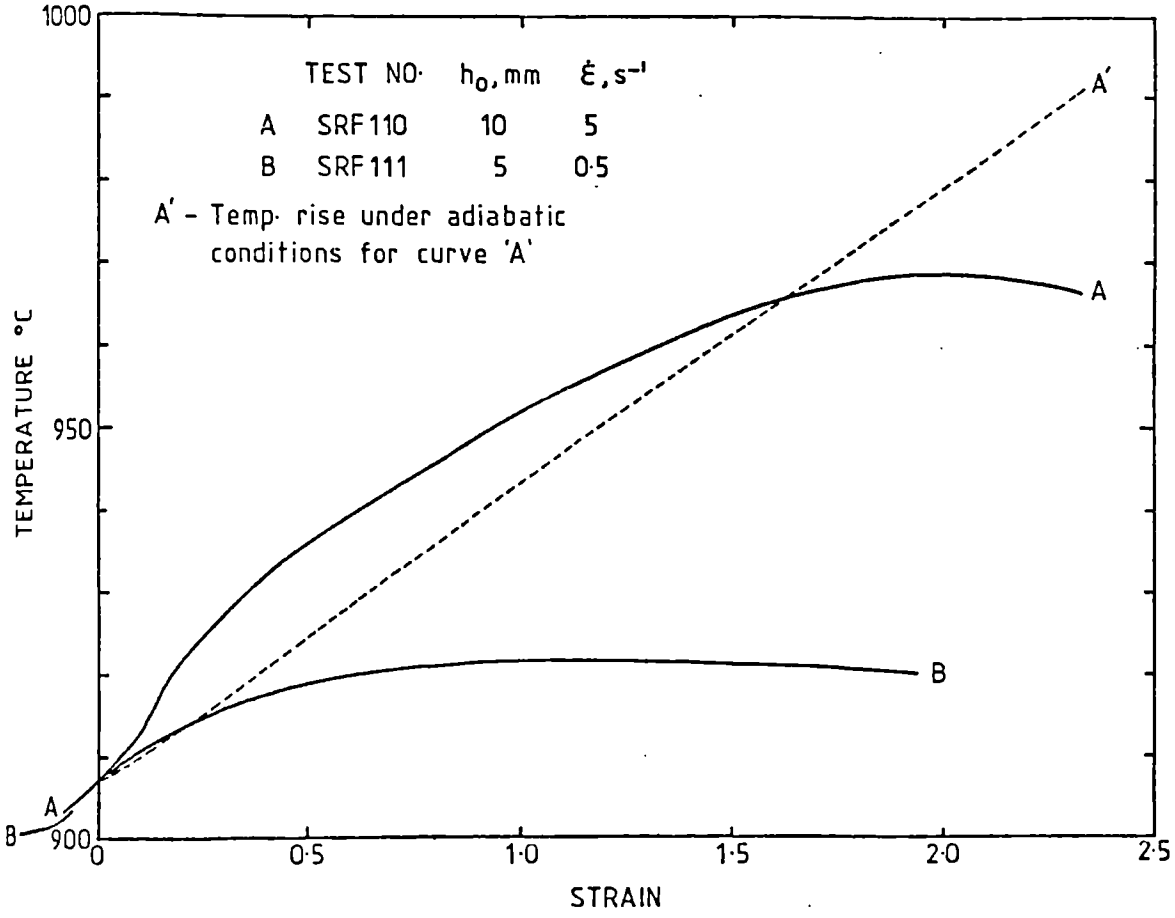
TEST NO· h_0, mm $\dot{\varepsilon}$, s^{-1}
A SRF110 10 5
B SRF111 5 0·5
A' - Temp· rise under adiabatic conditions for curve 'A'
A'
A
B
TEMPERATURE °C
1000
950
900
0
0·5
1·0
1·5
2·0
2·5
STRAIN

Figure 25.- Specimen to be deformed in the interval $0 < x < L$. The temperature during the deformation is a function of the position and the time (Wada et al, 1978).

Figure 26.- Temperature, strain rate or strain distribution at different time intervals for deformed aluminium specimens shown in figure 25 (Wada et al, 1978).

a.) Effect of strain rate in temperature distribution, T_o = 500 C, L = 30 mm.

b.) Effect of strain rate in strain rate distribution, T_o = 500 C, L = 30 mm.

c.) Effect of size in temperature distribution, T_o = 500 C, $\dot{\varepsilon}_o$ = 10 sec^{-1}.

d.) Effect of size in strain rate distribution, T_o = 500 C, $\dot{\varepsilon}_o$ = 10 sec^{-1}.

e.) Effect of size in strain distribution, T_o = 500 C, $\dot{\varepsilon}_o$ = 10 sec^{-1}.

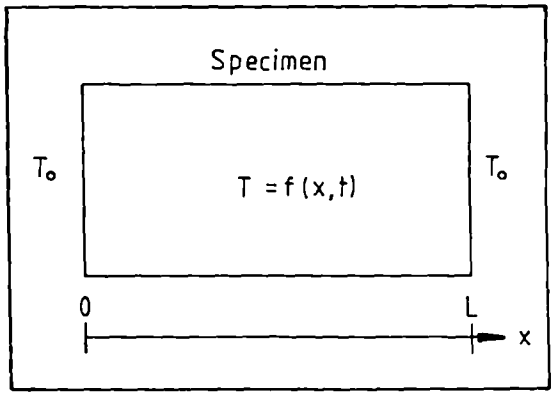
Specimen
T_o
$T = f(x,t)$
T_o
0
L
x

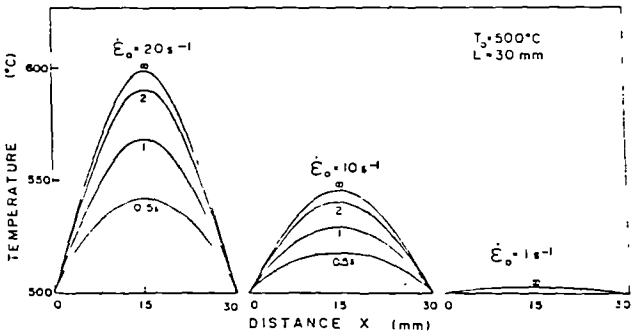
$\dot{\varepsilon}_o = 20\,s^{-1}$
$T_o = 500°C$
$L = 30$ mm
$\dot{\varepsilon}_o = 10\,s^{-1}$
$\dot{\varepsilon}_o = 1\,s^{-1}$
TEMPERATURE (°C)
600
550
500
0
15
30
DISTANCE X (mm)

a.)

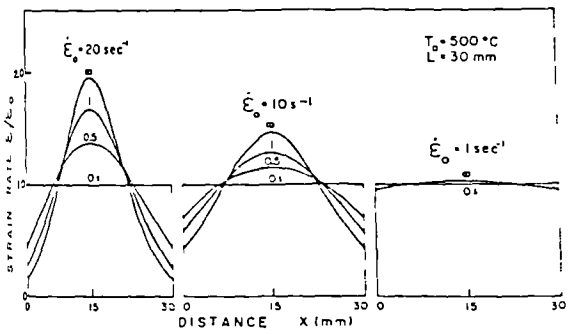
$\dot{\varepsilon}_o = 20\,sec^{-1}$
$T_o = 500°C$
$L = 30$ mm
$\dot{\varepsilon}_o = 10\,s^{-1}$
$\dot{\varepsilon}_o = 1\,sec^{-1}$
STRAIN RATE $\dot{\varepsilon}/\dot{\varepsilon}_o$
0
15
30
DISTANCE X (mm)

b.)

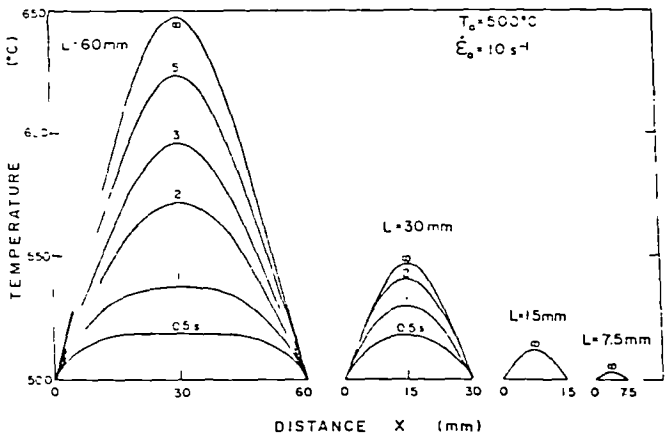
$T_o = 500°C$
$\dot{\varepsilon}_o = 10\,s^{-1}$
L = 60mm
L = 30mm
L = 15mm
L = 7.5mm
TEMPERATURE (°C)
650
600
550
500
0
30
60
15
75
DISTANCE X (mm)

c.)

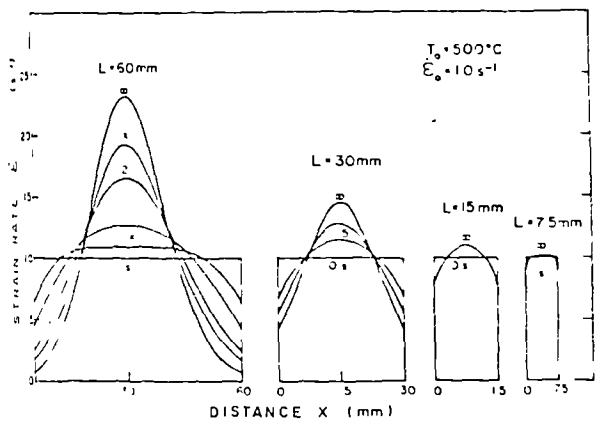
$T_o = 500°C$
$\dot{\varepsilon}_o = 10\,s^{-1}$
L = 60mm
L = 30mm
L = 15mm
L = 7.5mm
STRAIN RATE $\dot{\varepsilon}/\dot{\varepsilon}_o$
0
5
30
15
75
DISTANCE X (mm)

d.)

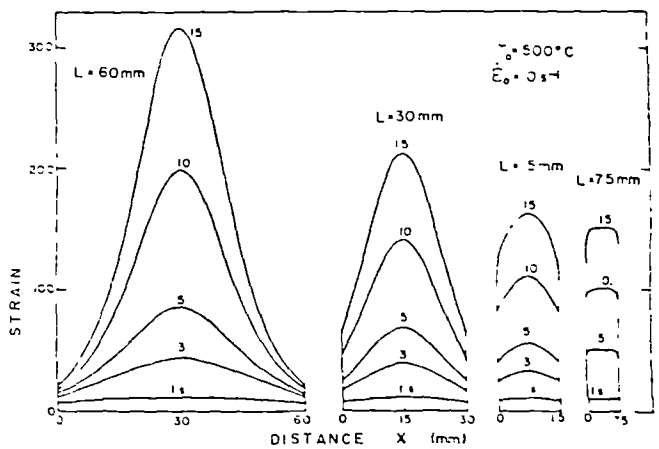
$T_o = 500°C$
$\dot{\varepsilon}_o = 0\,s^{-1}$
L = 60mm
L = 30mm
L = 5mm
L = 7.5mm
STRAIN
0
30
60
15
5
75
DISTANCE X (mm)

e.)

Figure 27.- Comparison of the computed centre and average temperatures and the measured one for some of the tests in figure 23 (Foster, 1981).

Figure 28.- Comparison of the computed and measured centre temperatures for the tests in figure 24 (Foster, 1981).

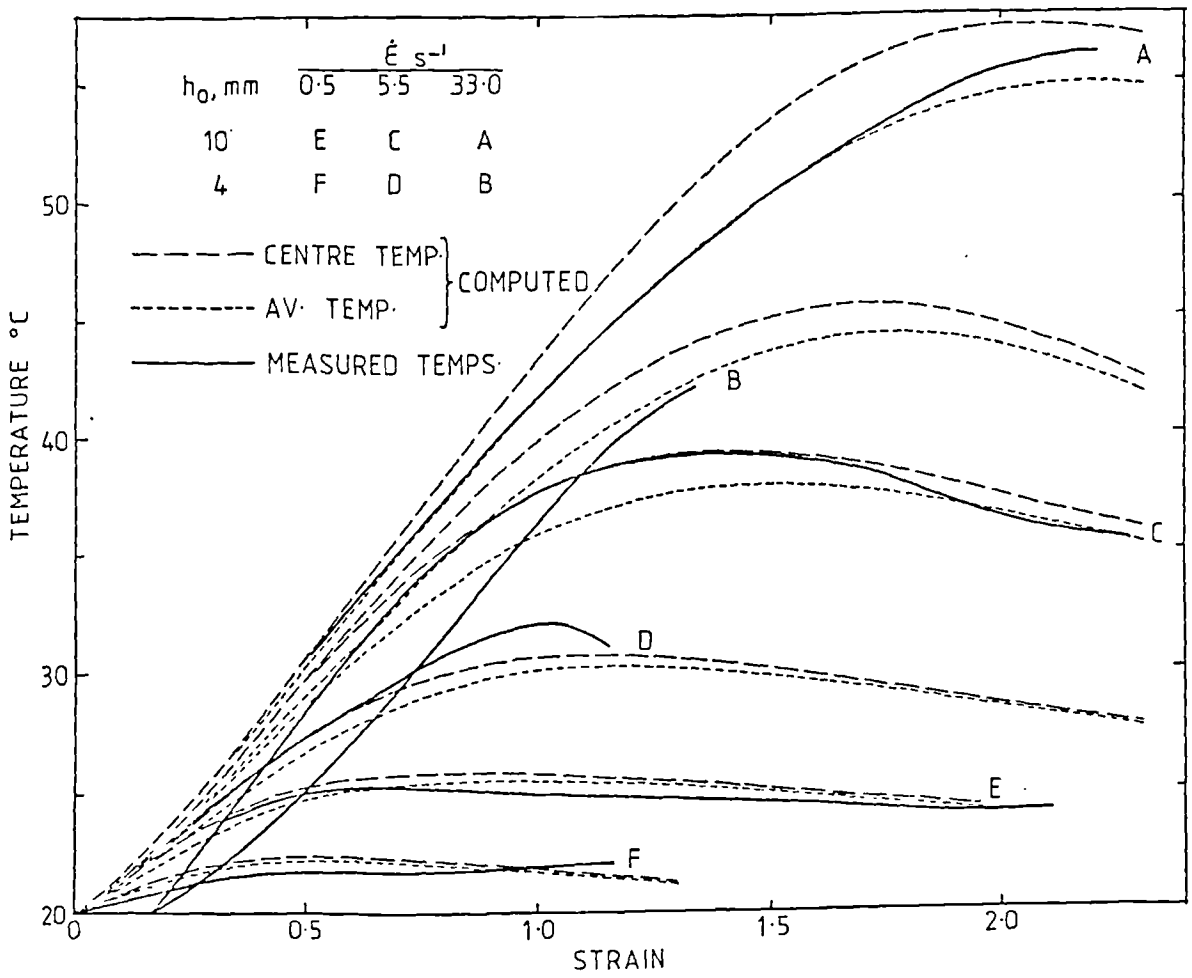
$\dot{\varepsilon}$ s^{-1}
h_0, mm 0·5 5·5 33·0
10 E C A
4 F D B
CENTRE TEMP.
AV. TEMP.
COMPUTED
MEASURED TEMPS.
A
B
C
D
E
F
TEMPERATURE °C
STRAIN
20
30
40
50
0
0·5
1·0
1·5
2·0

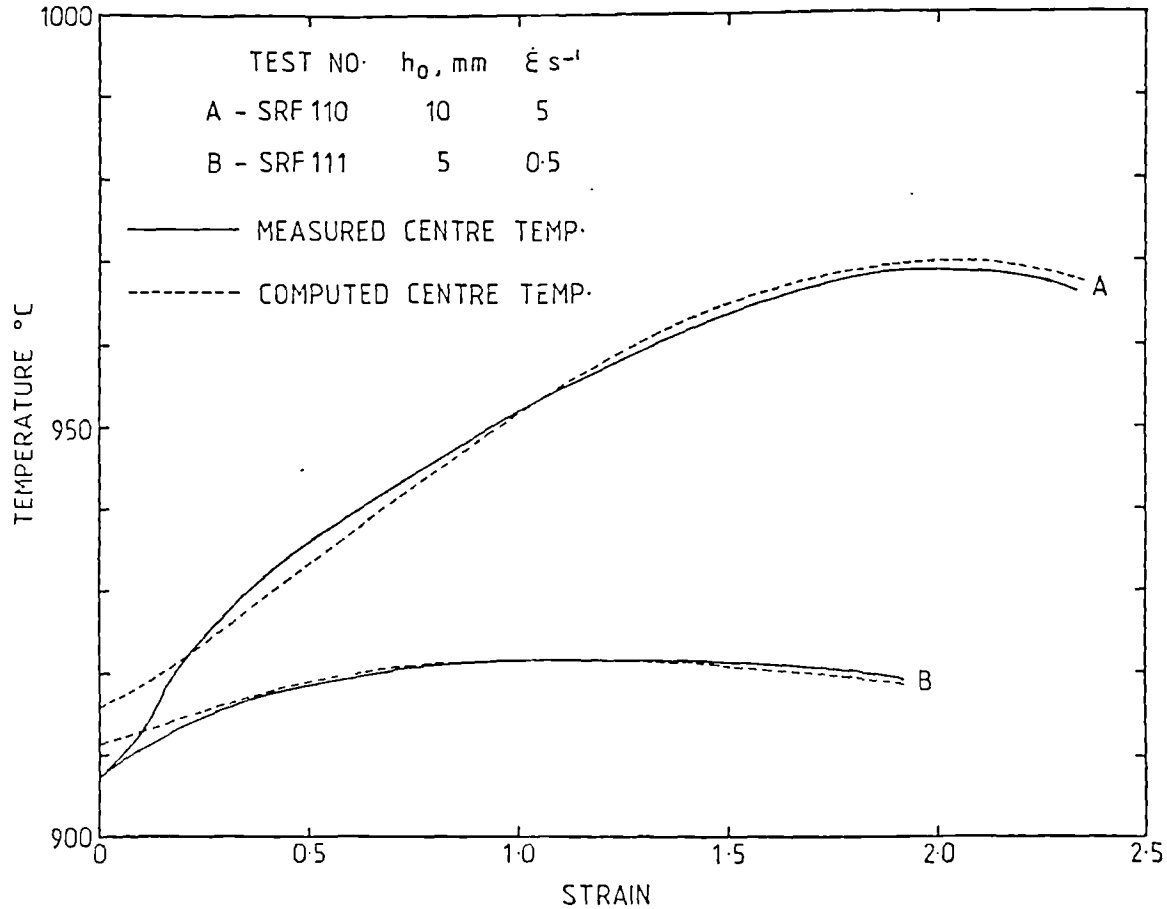
TEST NO. h_0, mm $\dot{\varepsilon}$ s^{-1}
A - SRF 110 10 5
B - SRF 111 5 0·5
MEASURED CENTRE TEMP.
COMPUTED CENTRE TEMP.
A
B
TEMPERATURE °C
STRAIN
900
950
1000
0
0·5
1·0
1·5
2·0
2·5

Figure 29.- The isothermal built-up and essentially adiabatic collapse of a dislocation pile-up avalanche (Armstrong et al, 1982).

Figure 30.- Schematic representation of equation (5.17) for adiabatic deformation in shear stress-shear strain curves (Olsen et al, 1981).

Figure 31.- Strain distribution analysis for a material deformed according to equation (5.17). a.) Initial grid, b.) grid after 50 μsec, c.) after 70 μsec, d.) after 100 μsec, e.) shear strain values along A-A' for different times.

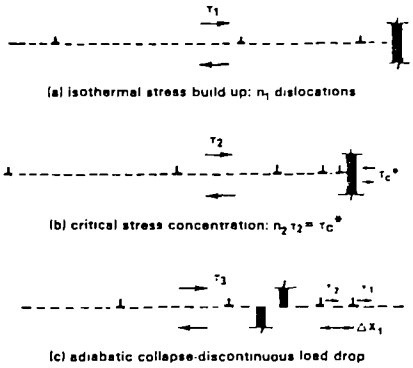
(a) isothermal stress build up: n_1 dislocations
(b) critical stress concentration: $n_2 \tau_2 = \tau_c^*$
(c) adiabatic collapse-discontinuous load drop

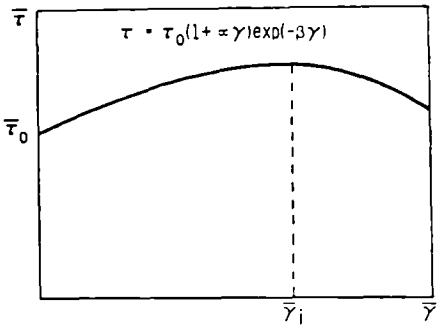
$\bar{\tau} = \tau_0(1+\alpha\bar{\gamma})\exp(-\beta\bar{\gamma})$
$\bar{\tau}$
$\bar{\tau}_0$
$\bar{\gamma}_i$
$\bar{\gamma}$

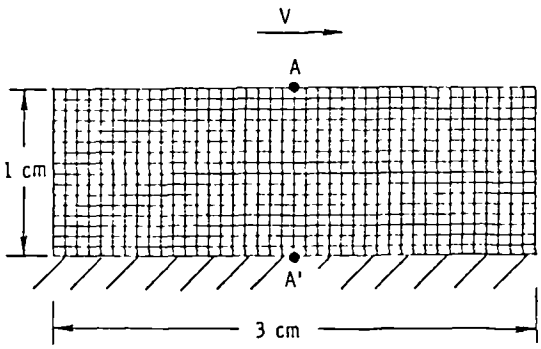
V
A
1 cm
A'
3 cm

a.)

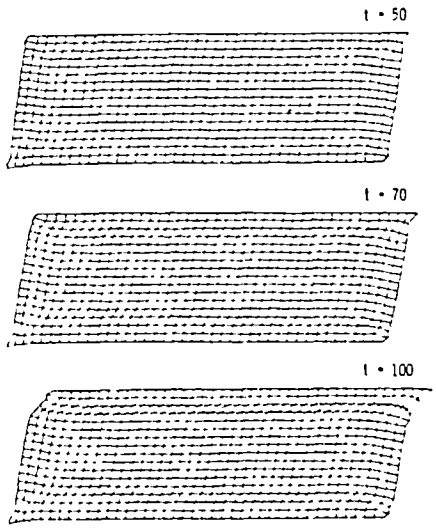
t = 50
t = 70
t = 100

b.)

c.)

d.)

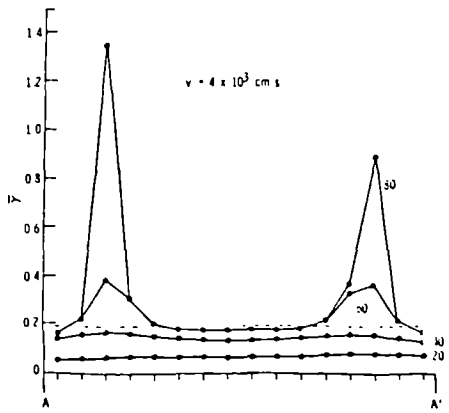
v = 4 x 10³ cm s
50
20
10
20
A
A'

e.)

Figure 32.- Schematic representation of the five rolling schedules.

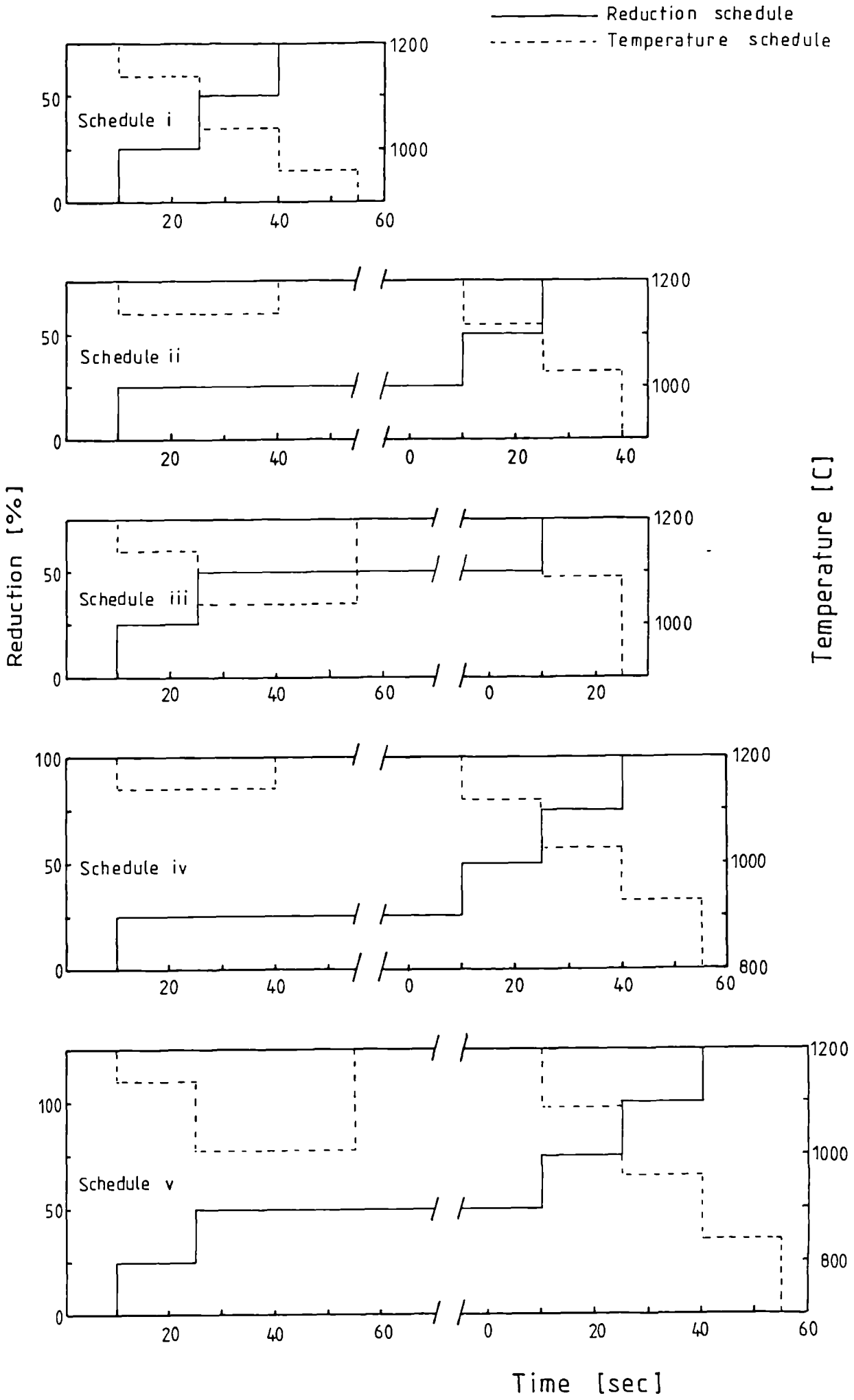
Reduction schedule
Temperature schedule
Schedule i
Schedule ii
Schedule iii
Schedule iv
Schedule v
Reduction [%]
Temperature [C]
Time [sec]
1200
1000
800
50
100
0
20
40
60

Figure 33.- Mean stress-temperature plot for the rolled slabs, table II.

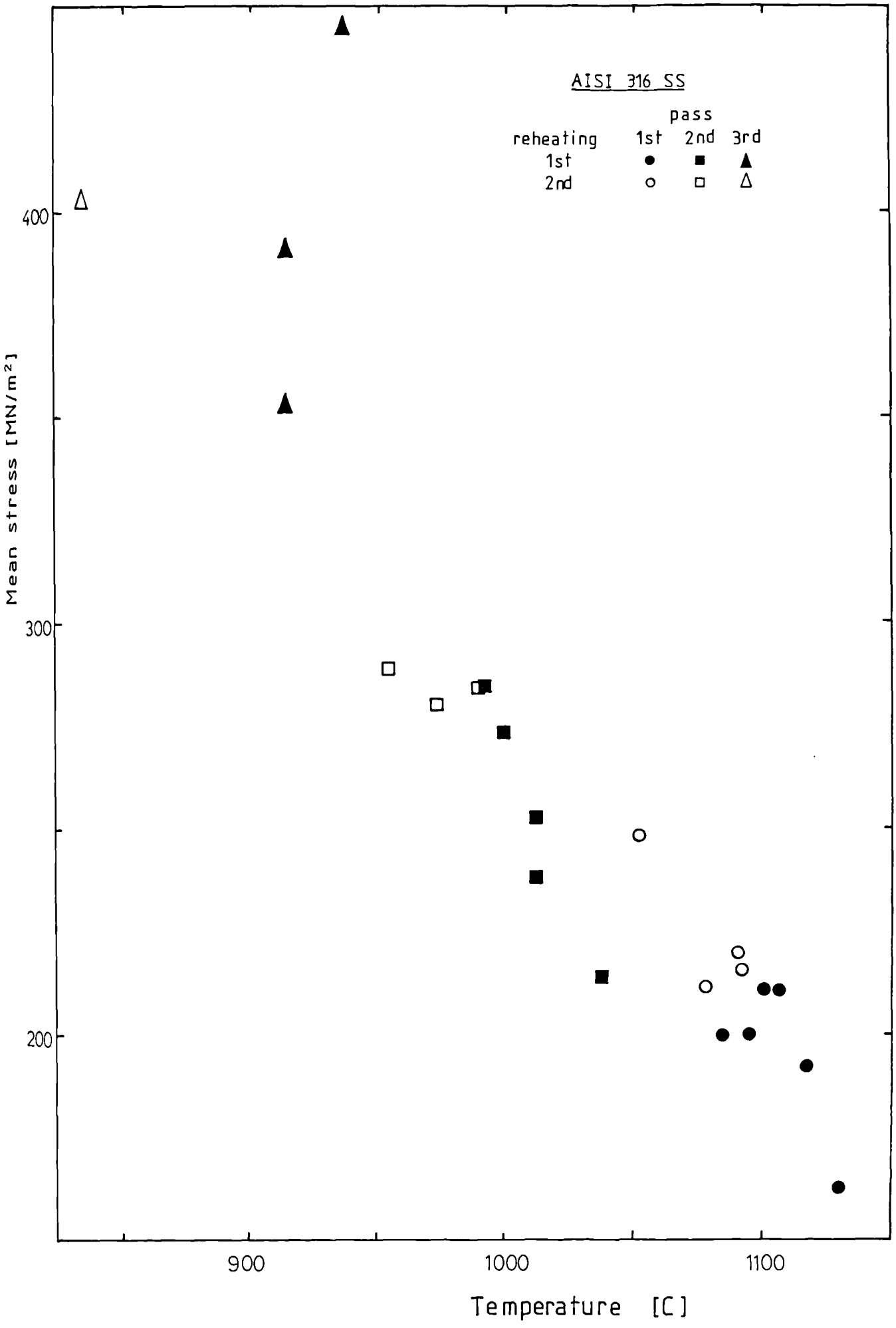
AISI 316 SS
pass
reheating 1st 2nd 3rd
1st
2nd
400
300
200
Mean stress [MN/m²]
900
1000
1100
Temperature [C]

Figure 34.- Effect of reheating temperature for the AISI type 316 stainless steel. Holding periods of 15 minutes.

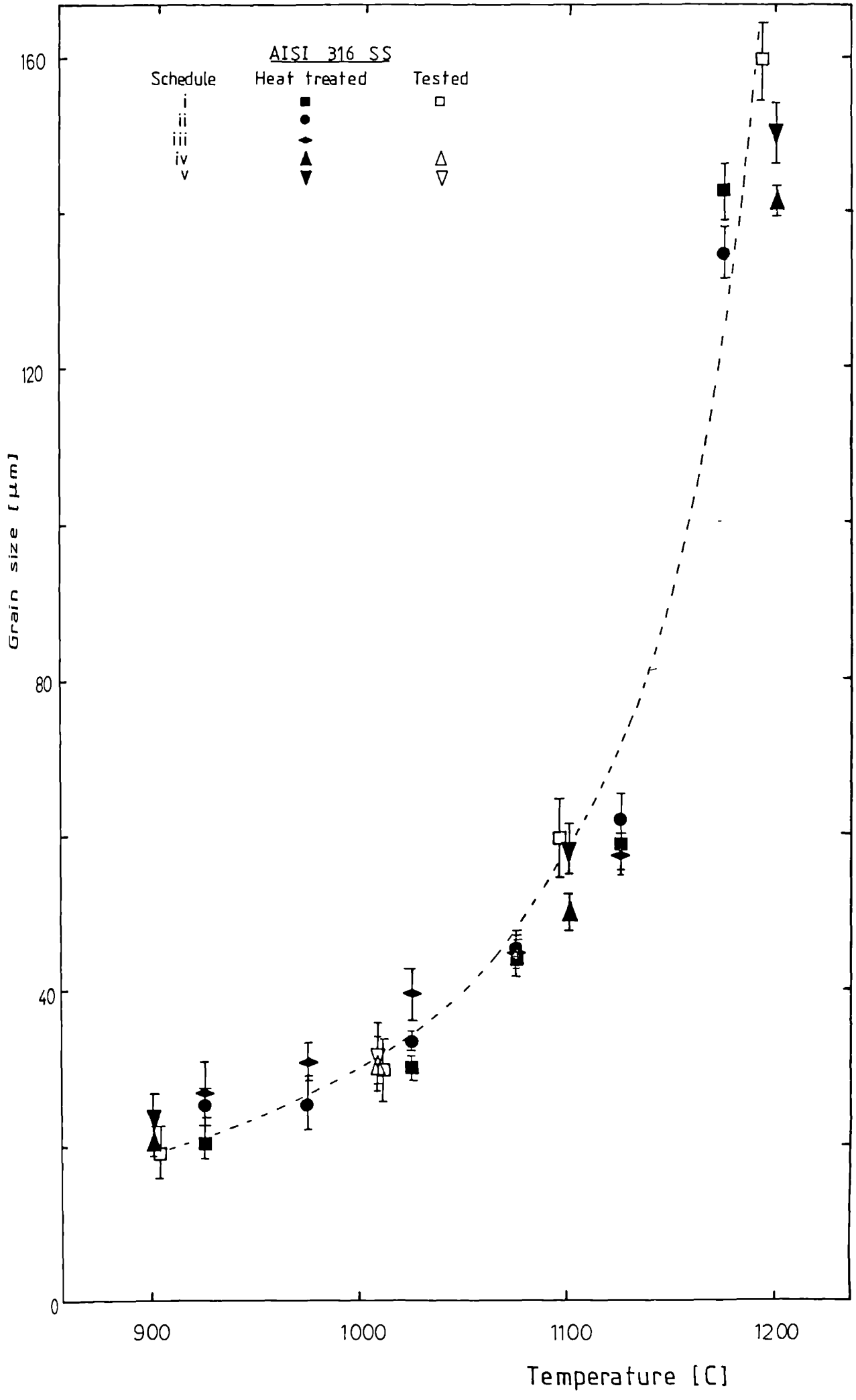
AISI 316 SS
Schedule
Heat treated
Tested
i
ii
iii
iv
v
160
120
80
40
0
Grain size [μm]
900
1000
1100
1200
Temperature [C]

Figure 35.- Schematic diagram of the servohydraulic compression machine showing the principal parts. The input and output senses are towards the servo-amplifier.

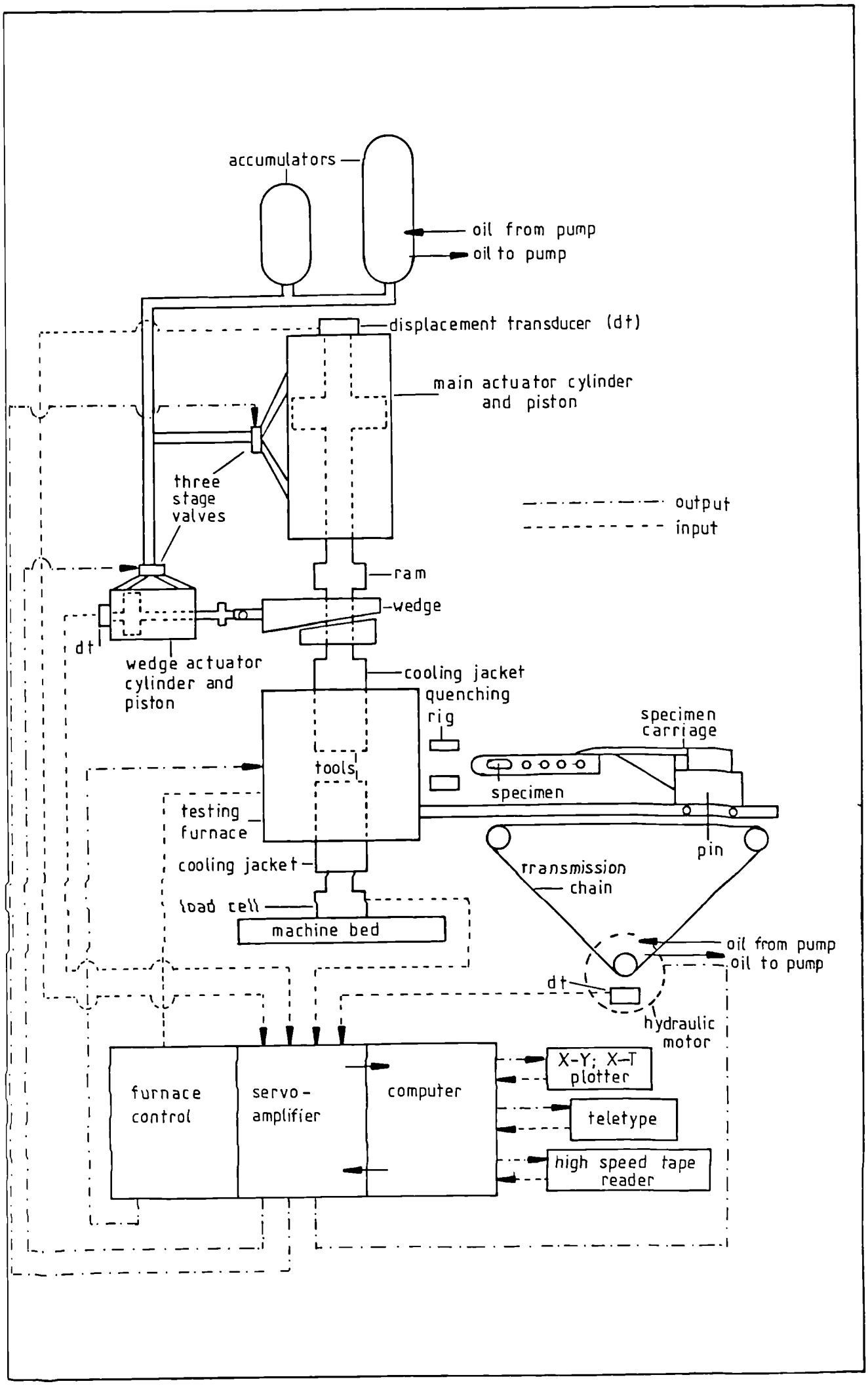
accumulators
oil from pump
oil to pump
displacement transducer (dt)
main actuator cylinder and piston
three stage valves
output
input
ram
wedge
dt
wedge actuator cylinder and piston
cooling jacket
quenching rig
specimen carriage
tools
specimen
testing furnace
pin
cooling jacket
transmission chain
load cell
machine bed
oil from pump
oil to pump
dt
hydraulic motor
furnace control
servo-amplifier
computer
X-Y; X-T plotter
teletype
high speed tape reader

Figure 36.- Schematic diagram of the device used to transfer the axisymmetric compression specimens around the different furnaces.

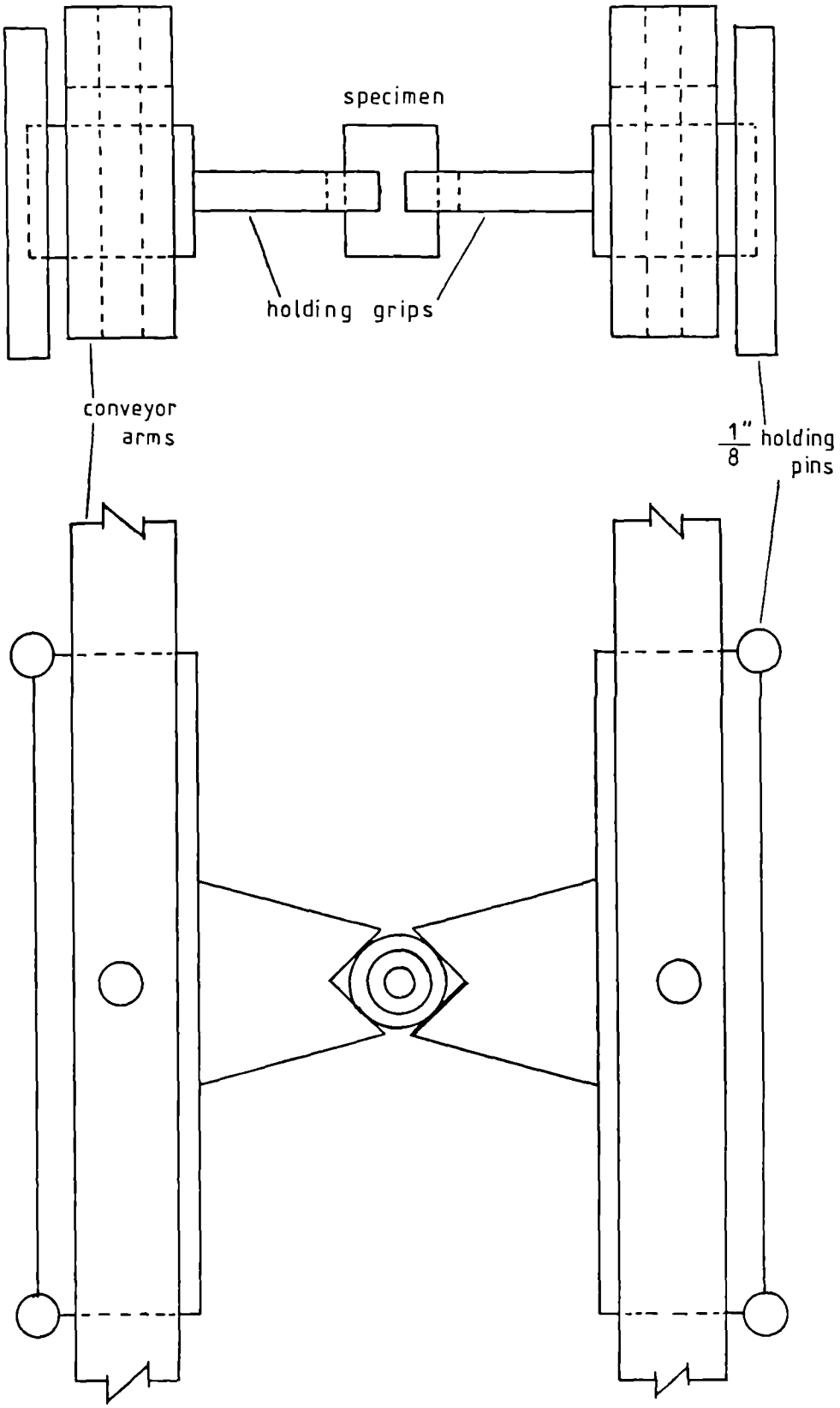

Scale 2:1

Figure 37.- Schematic diagram showing the relative testing directions with respect to the rolling one.

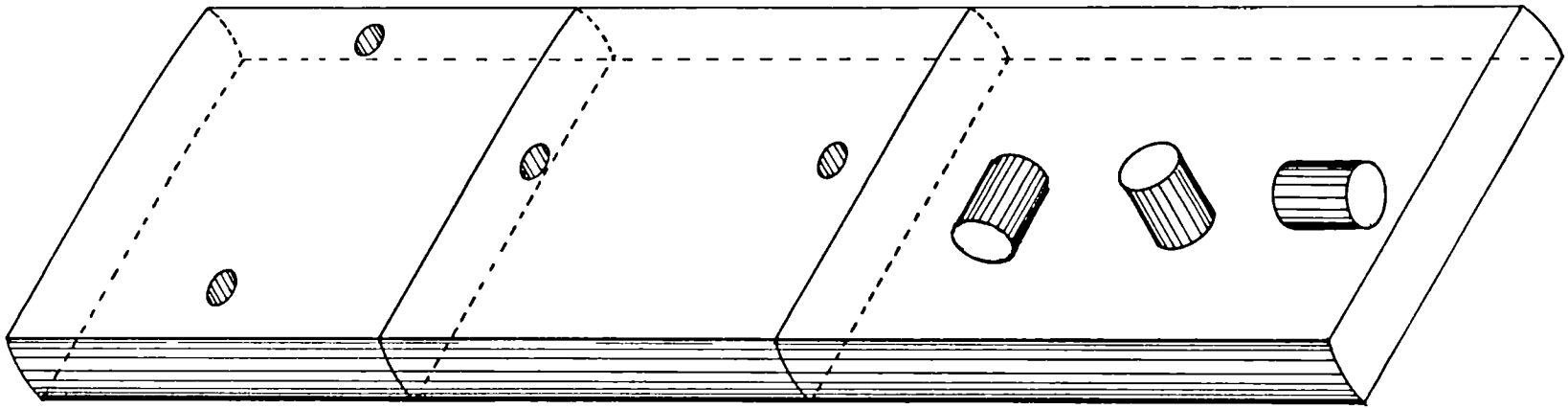

Rolling direction

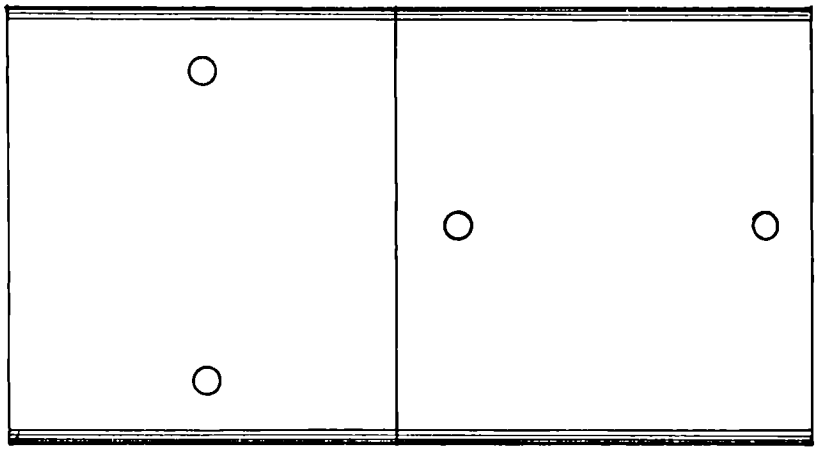

transverse

normal

Plane strain specimens

Axisymmetric specimens

width thickness length

Scale 1:1

Figure 38.- Load-displacement curves for AISI 316 stainless steel tested under axisymmetric compression. a.) Before origin correction. b.) After origin correction.

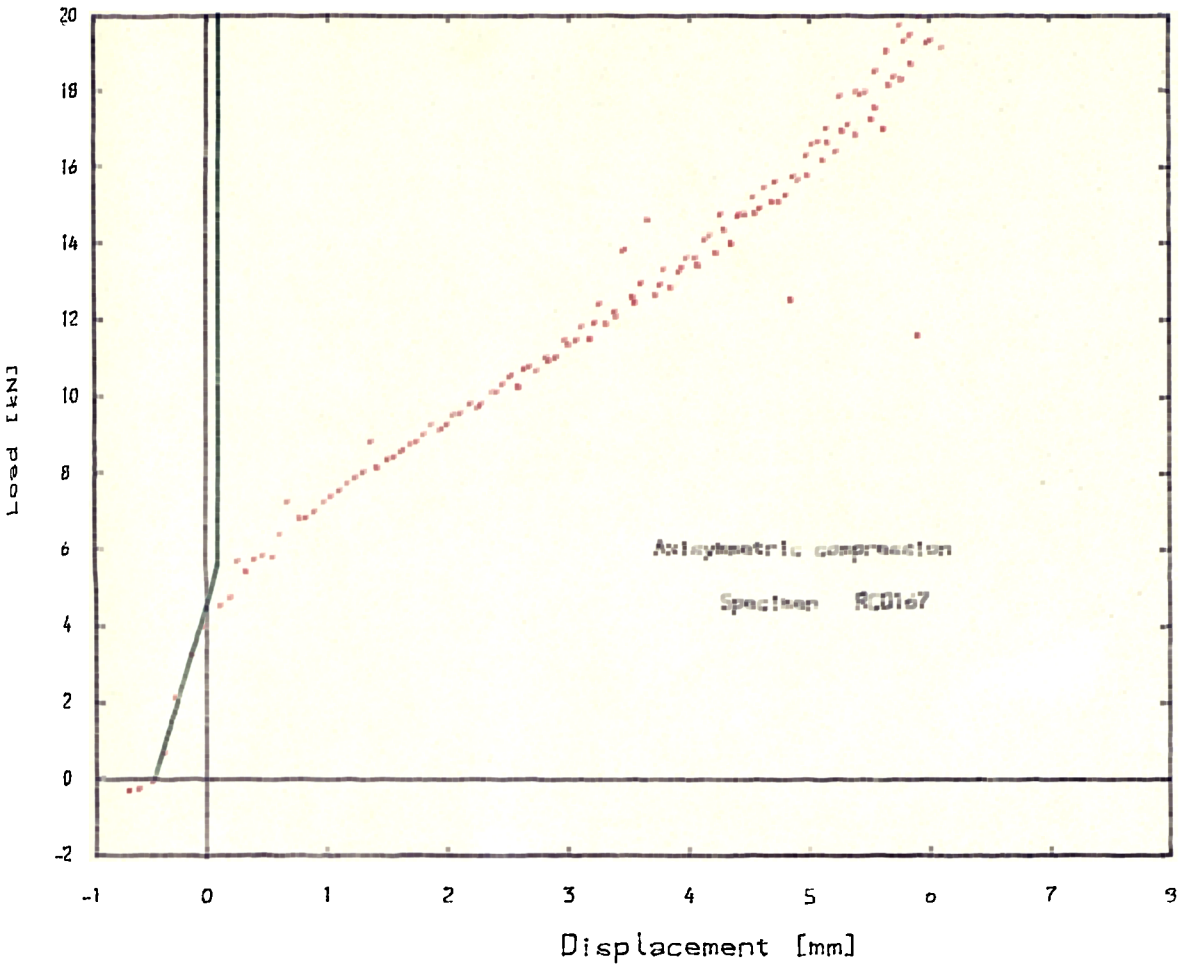
Load [kN]
Axisymmetric compression
Specimen RC01e7
Displacement [mm]

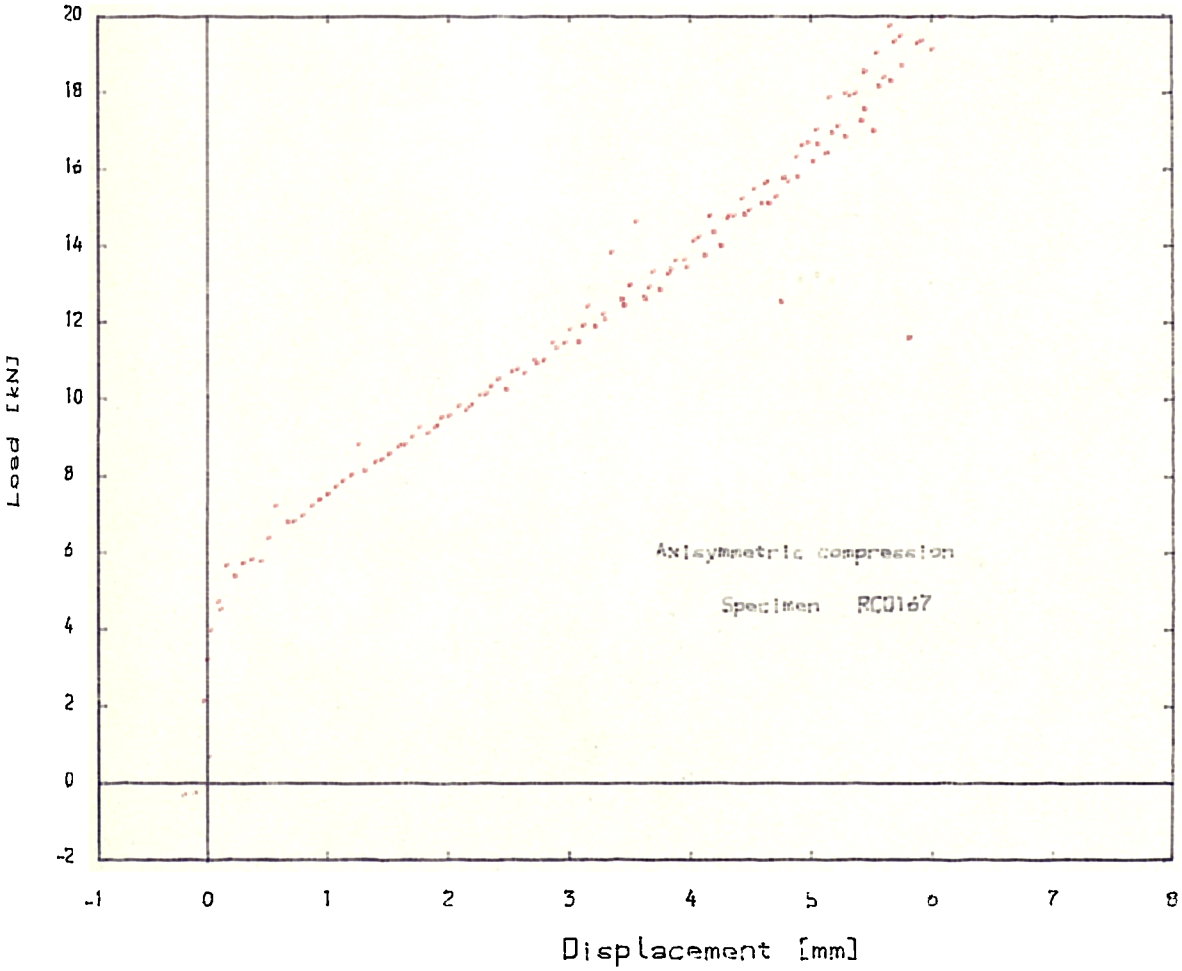
Load [kN]
Axisymmetric compression
Specimen RC01e7
Displacement [mm]

Figure 39.- Load-displacement curves for AISI 316 stainless steel tested under plane strain compression. a.) Before origin correction. b.) After origin correction.

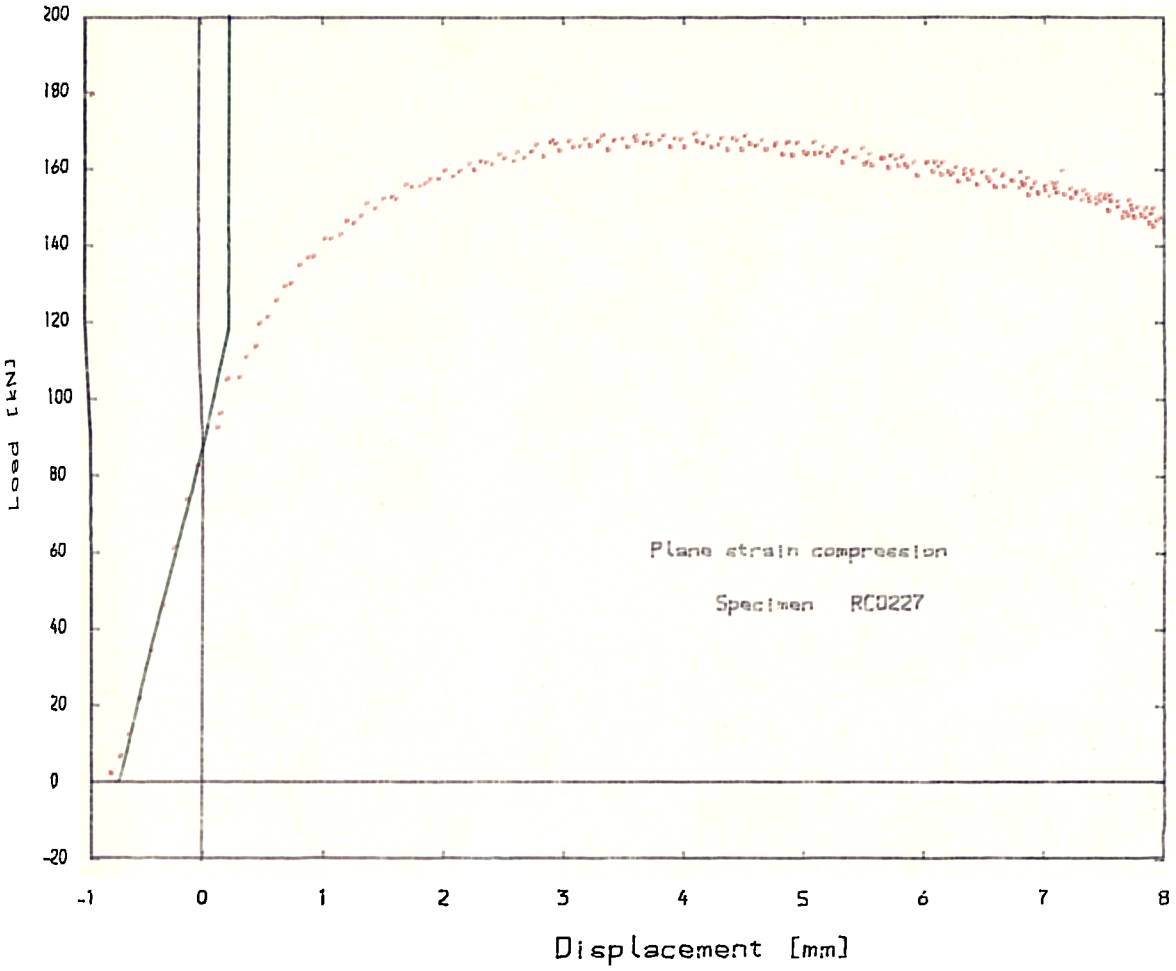
Load [kN]
200
180
160
140
120
100
80
60
40
20
0
-20
-1
0
1
2
3
4
5
6
7
8
Displacement [mm]
Plane strain compression
Specimen RC0227

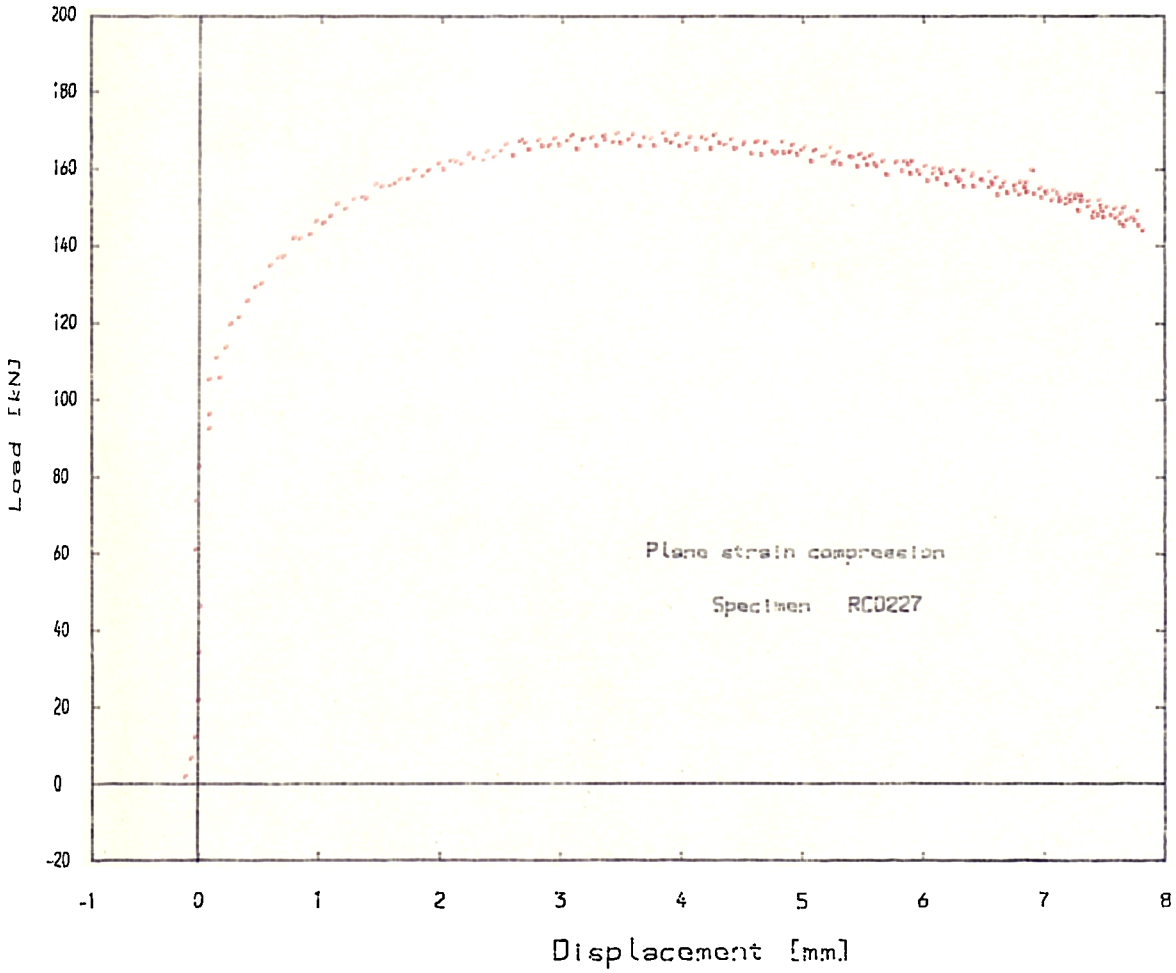
Load [kN]
200
180
160
140
120
100
80
60
40
20
0
-20
-1
0
1
2
3
4
5
6
7
8
Displacement [mm]
Plane strain compression
Specimen RC0227

Figure 40.- Experimental determination of the spread coefficient for the AISI 316 stainless steel tested under plane strain compression.

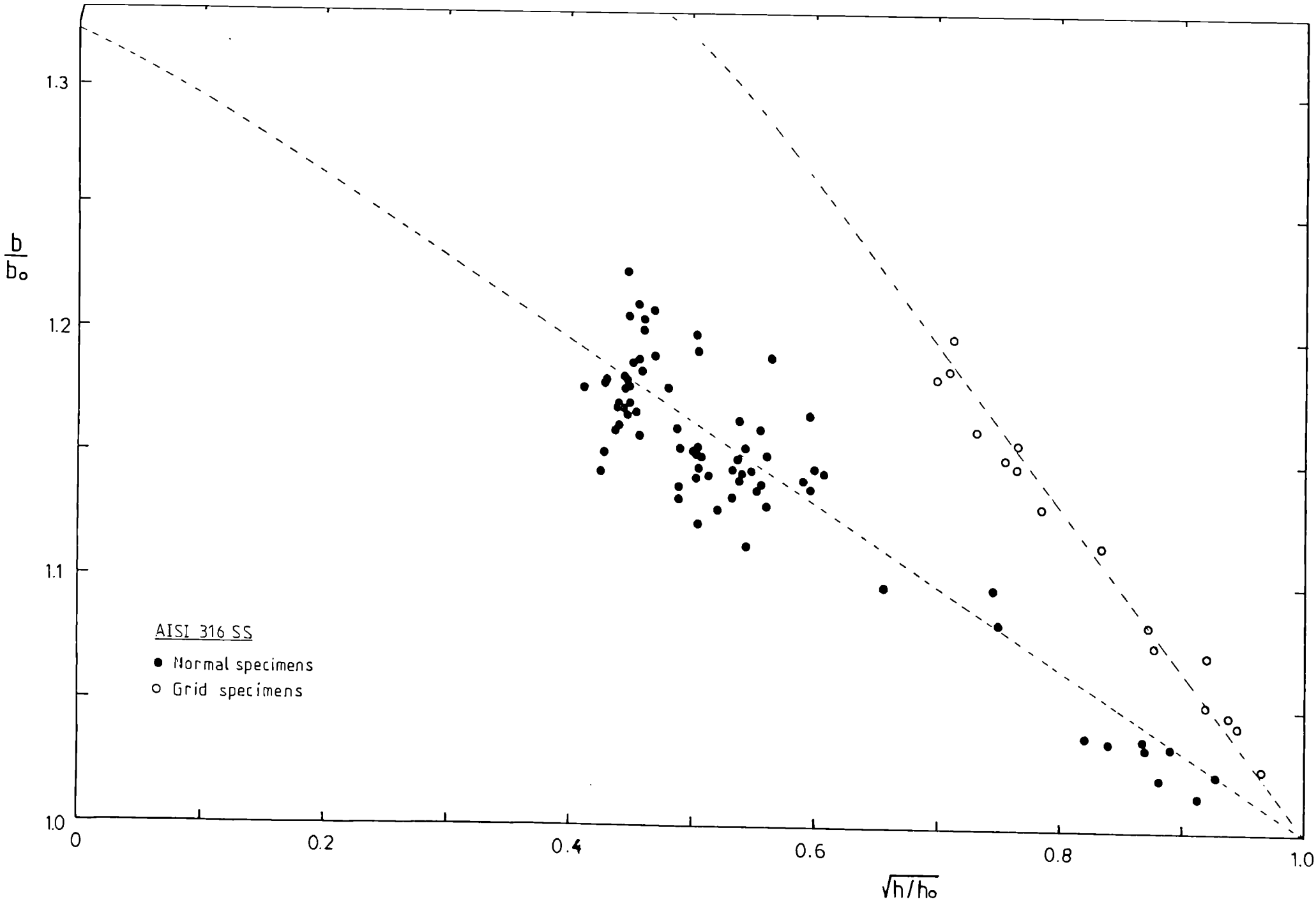
1.3
1.2
1.1
1.0
b/b₀
0
0.2
0.4
0.6
0.8
1.0
√h/h₀
AISI 316 SS
Normal specimens
Grid specimens

Figure 41.- Schematic diagram of the gridded specimens, the testing direction is the same as the specimens marked as normal in the figure 37.

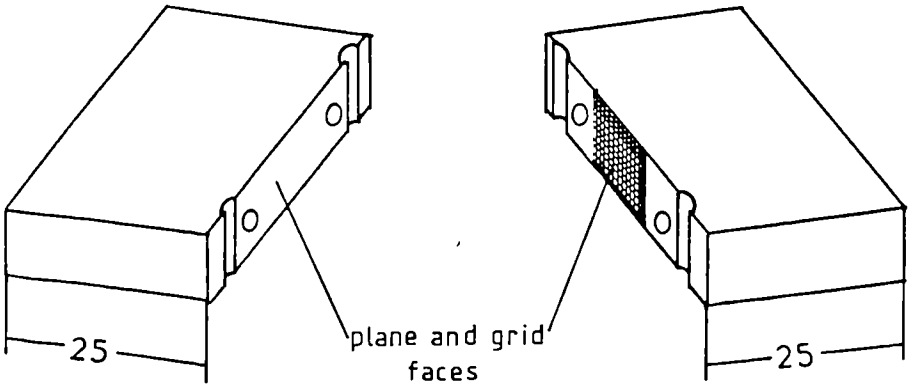
25
plane and grid faces
25

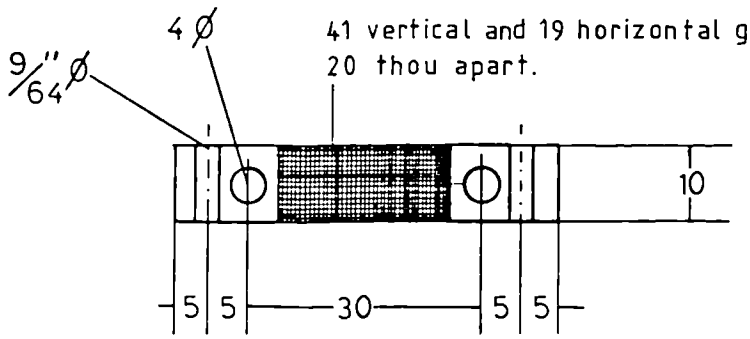
4 Ø
9/64" Ø
41 vertical and 19 horizontal grid lines, 20 thou apart.
10
5
5
30
5
5

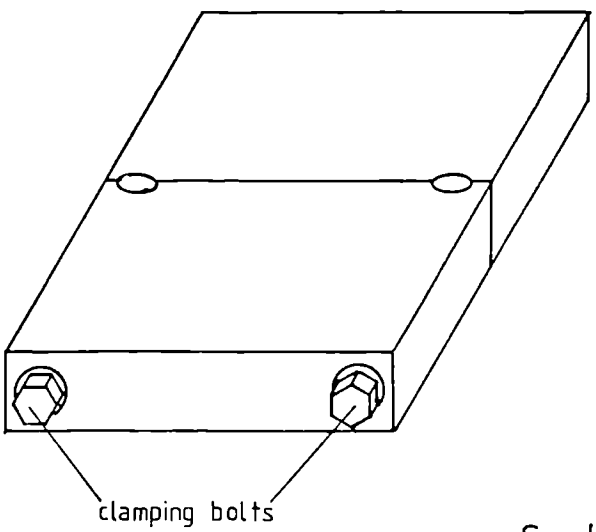
clamping bolts

Scale 1:1

Figure 42.- Schematic diagram of a specimen showing the possible positions of the imbeded thermocouples.

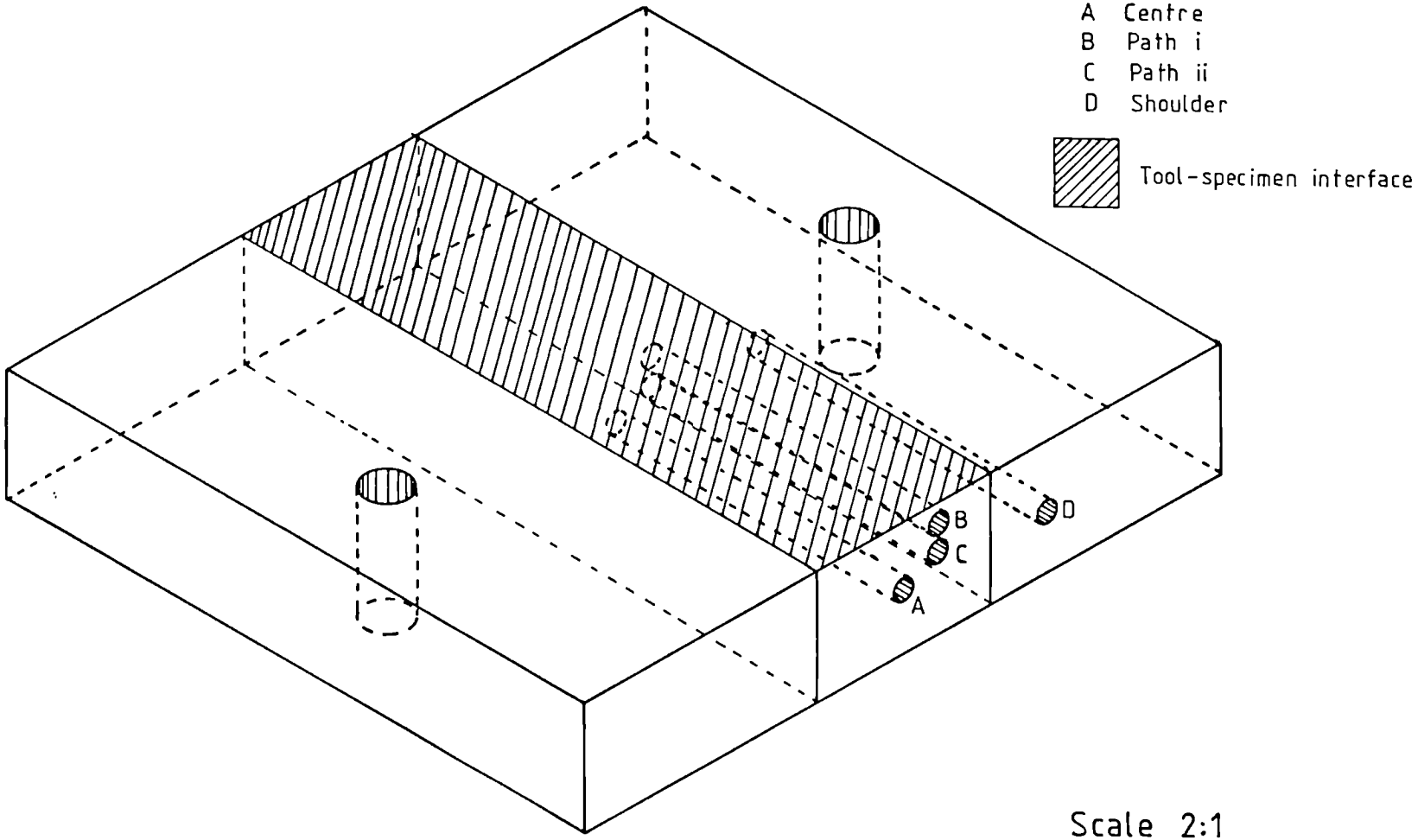
Position of the thermocouples
A Centre
B Path i
C Path ii
D Shoulder
Tool-specimen interface
A
B
C
D
Scale 2:1

Figure 43.- Stress-strain curves for titanium bearing steel tested in axisymmetric compression at 900 C.

a.)

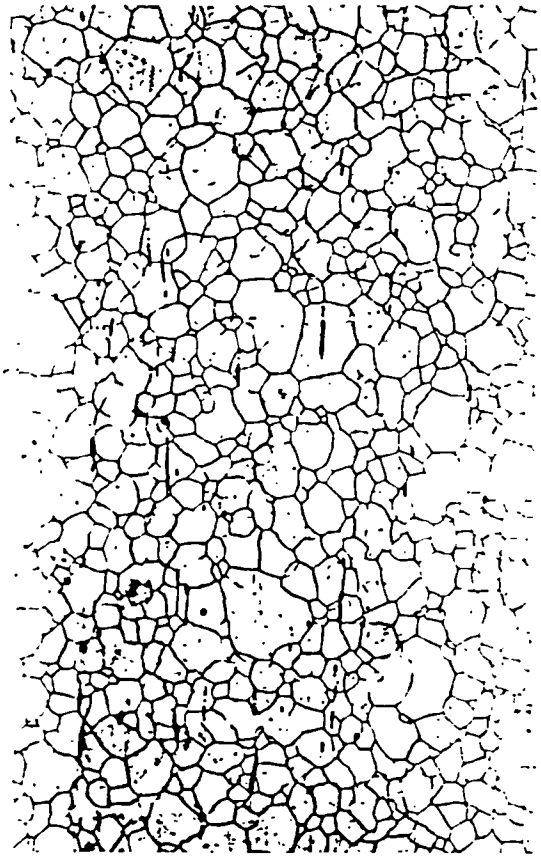

b.)

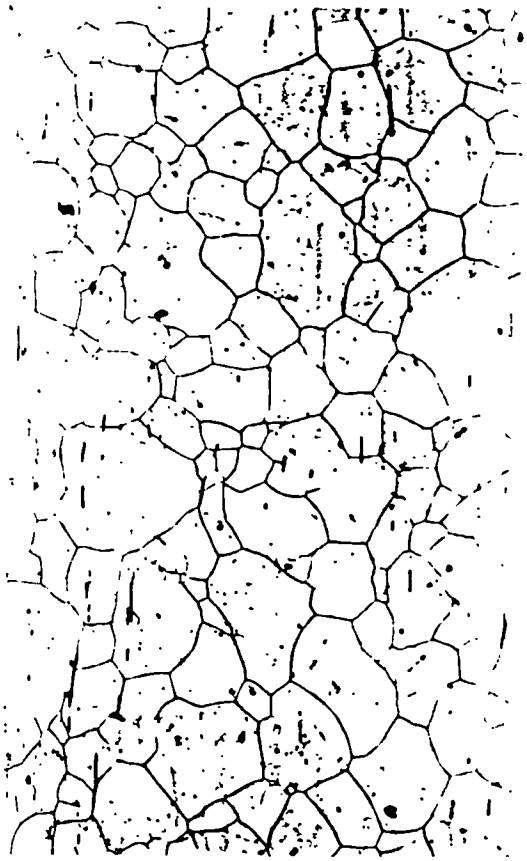

c.)

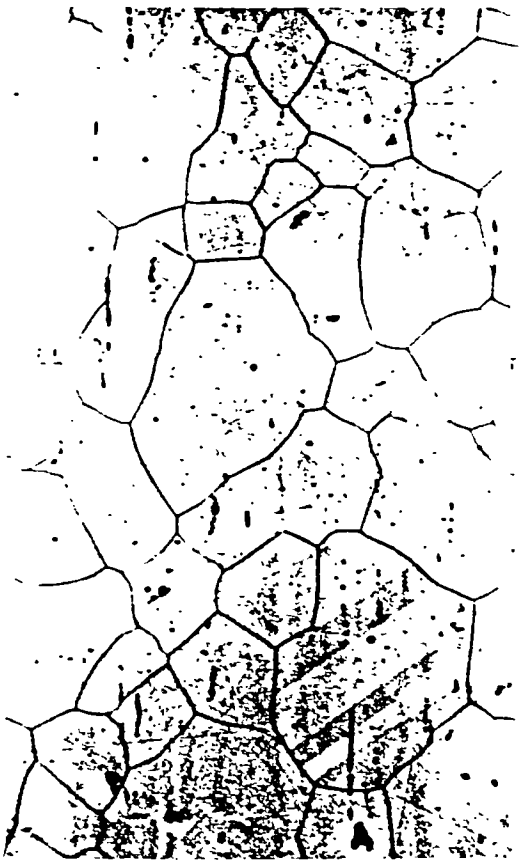

d.)

Figure 48.- Initial grain sizes for specimens from schedules iv, v and torsion, table III.

	Rolling Schedule	Preheating Temperature [C]	Testing Temperature [C]	Grain Size [μm]
a.)	iv	1006	1006	30.9 ± 1.7
b.)	v	1006	1006	31.7 ± 2.0
c.)	torsion	905	905	30.2 ± 1.5
d.)	torsion	1008	1008	42.9 ± 1.9

Electrolytic etching, 100 X.

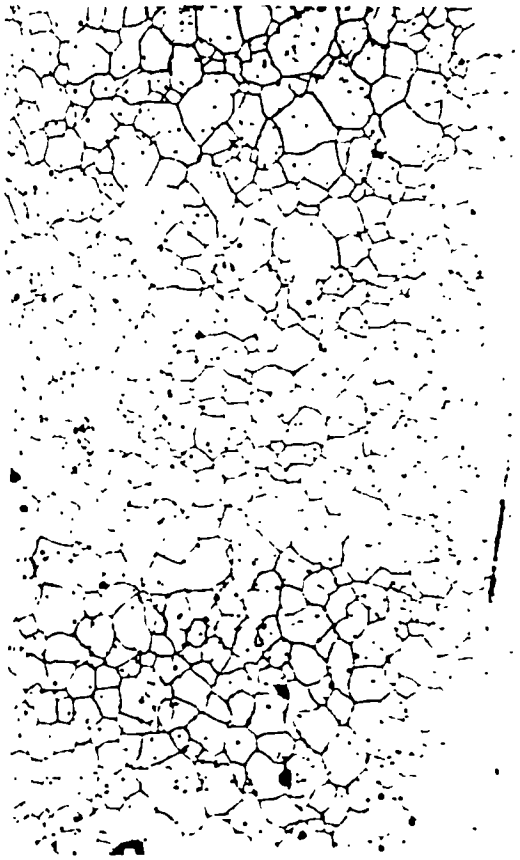

a.)

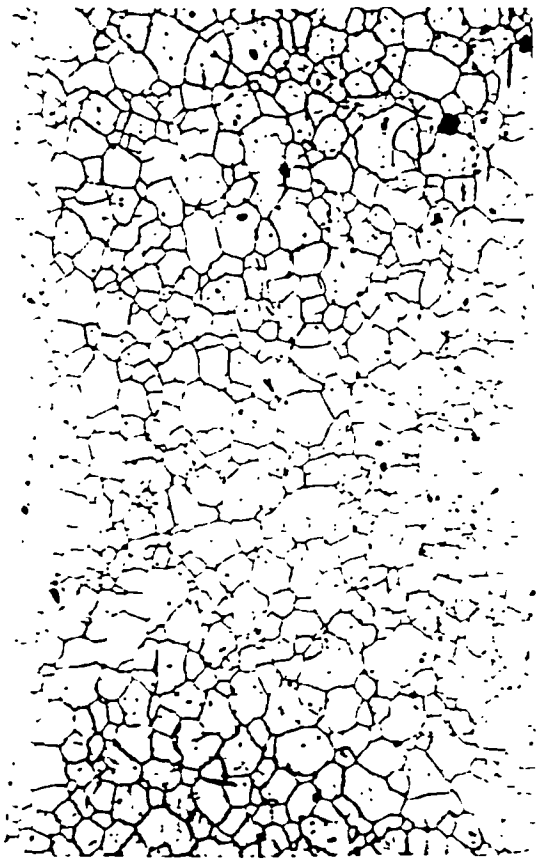

b.)

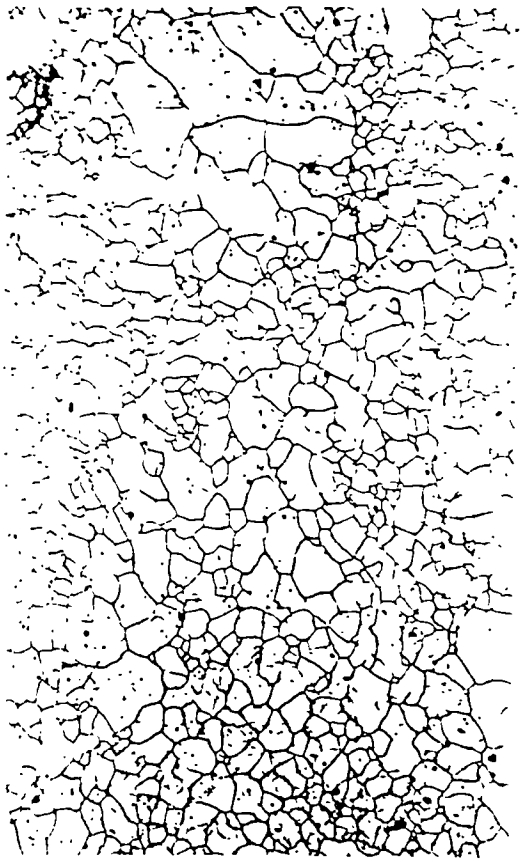

c.)

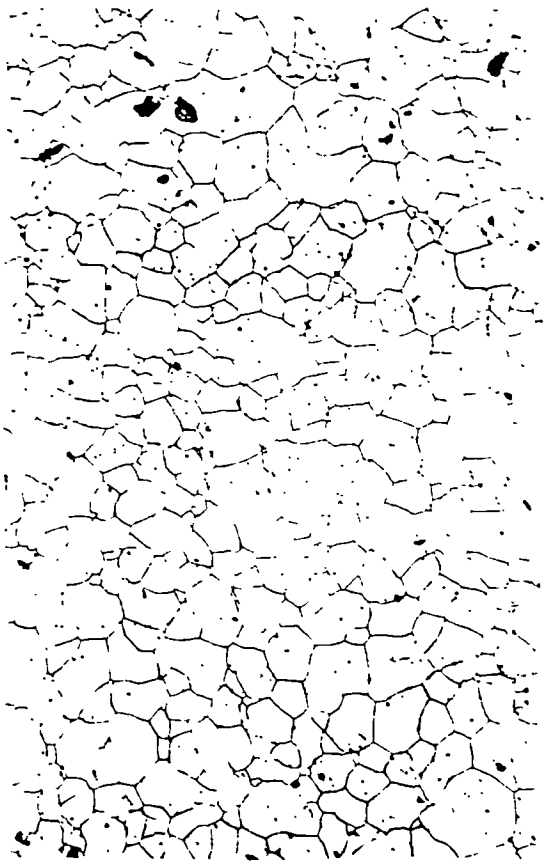

d.)

Figure 49.- Stress-strain curves for AISI type 316 stainless steel in plane strain compression at 910 C, preheating temperature 904 C.

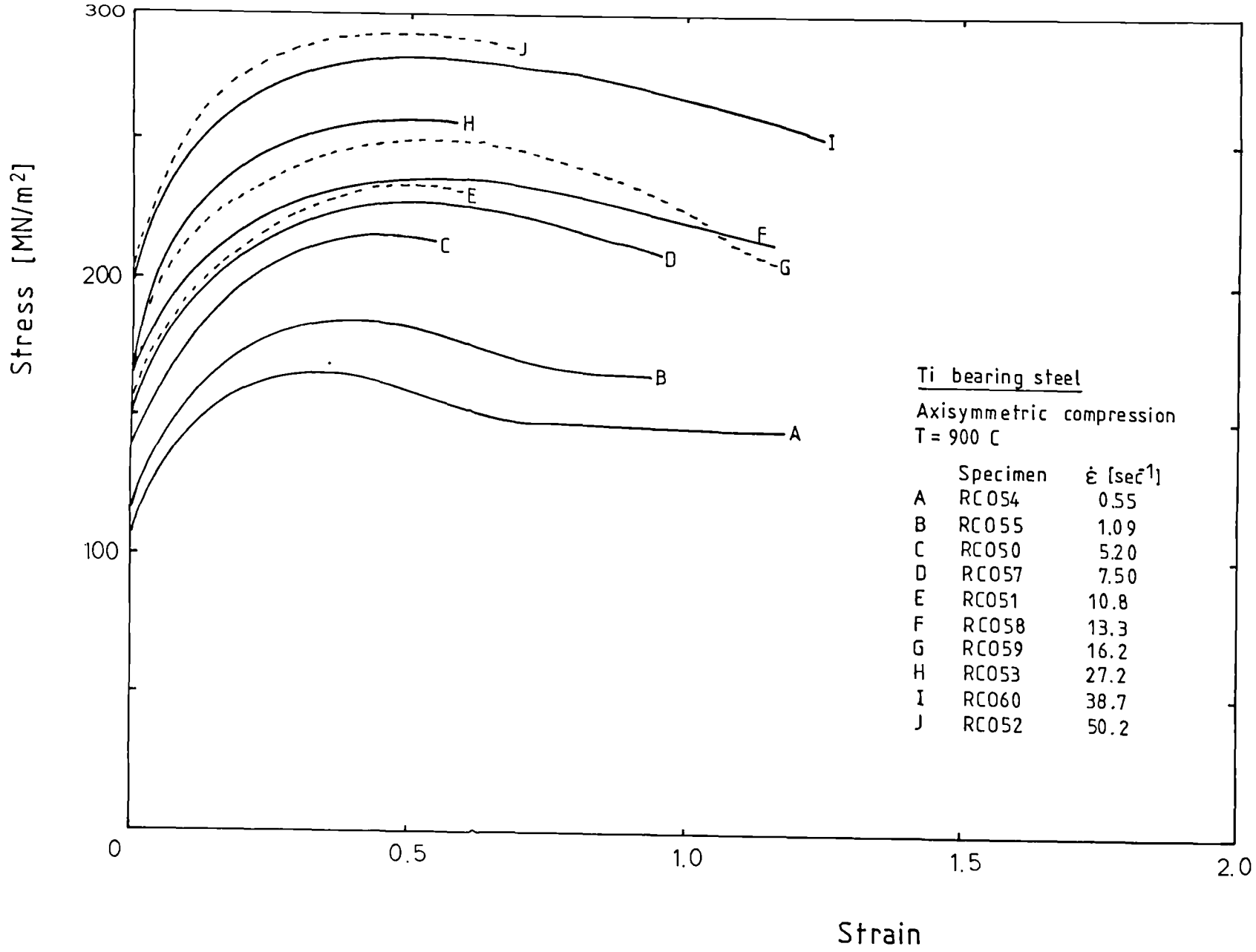
300
200
100
0
0.5
1.0
1.5
2.0
Stress [MN/m²]
Strain
J
H
I
E
F
G
C
D
B
A
Ti bearing steel
Axisymmetric compression
T = 900 C
Specimen ε̇ [sec⁻¹]
A RC054 0.55
B RC055 1.09
C RC050 5.20
D RC057 7.50
E RC051 10.8
F RC058 13.3
G RC059 16.2
H RC053 27.2
I RC060 38.7
J RC052 50.2

Figure 44.- Stress-strain curves for titanium bearing steel tested in axisymmetric and plane strain compression at 1000 C.

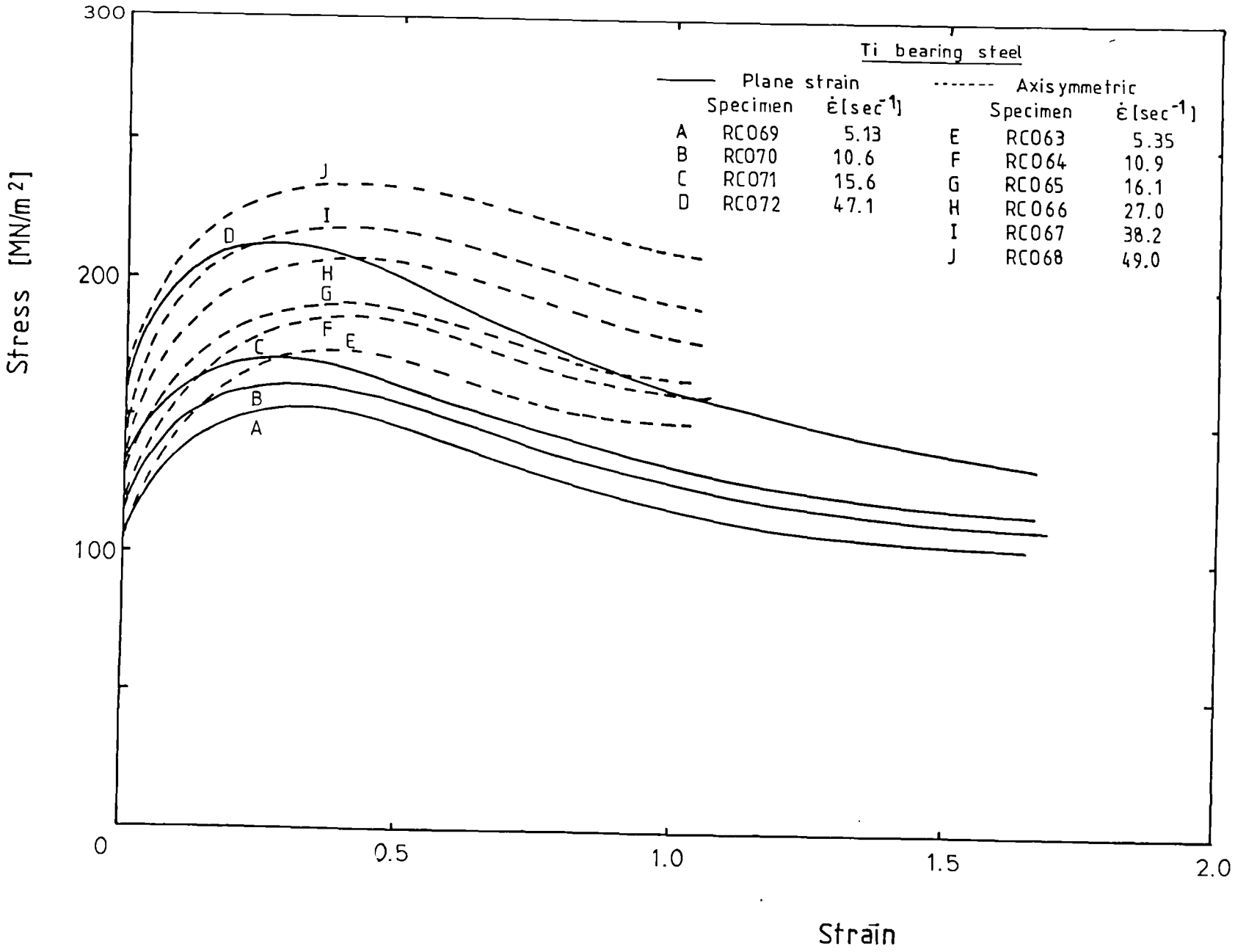
Ti bearing steel
Plane strain
Axisymmetric
Specimen
$\dot{\varepsilon}$ [sec^{-1}]
A RC069 5.13
B RC070 10.6
C RC071 15.6
D RC072 47.1
E RC063 5.35
F RC064 10.9
G RC065 16.1
H RC066 27.0
I RC067 38.2
J RC068 49.0
Stress [MN/m^2]
300
200
100
0
0.5
1.0
1.5
2.0
Strain

Figure 45.- Strain to the peak versus strain rate plot for titanium bearing steel.

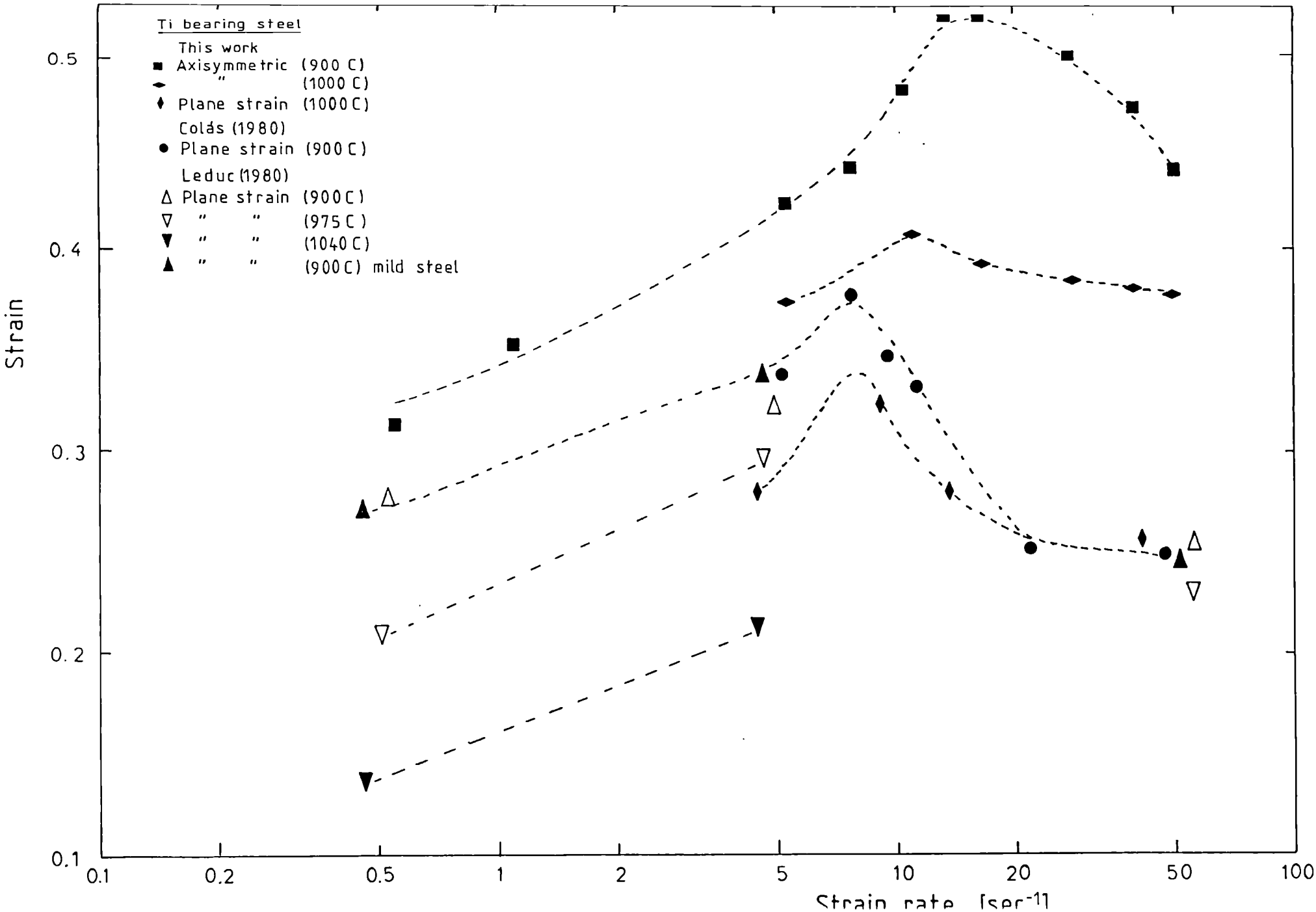
Ti bearing steel
This work
Axisymmetric (900 C)
" (1000 C)
Plane strain (1000 C)
Colás (1980)
Plane strain (900 C)
Leduc (1980)
Plane strain (900 C)
" " (975 C)
" " (1040 C)
" " (900 C) mild steel
Strain
0.5
0.4
0.3
0.2
0.1
0.1
0.2
0.5
1
2
5
10
20
50
100
Strain rate [sec-1]

Figure 46.- Plot of the logarithm of the Zener-Hollomon parameter, Z, versus $\sinh(\alpha\sigma)$.

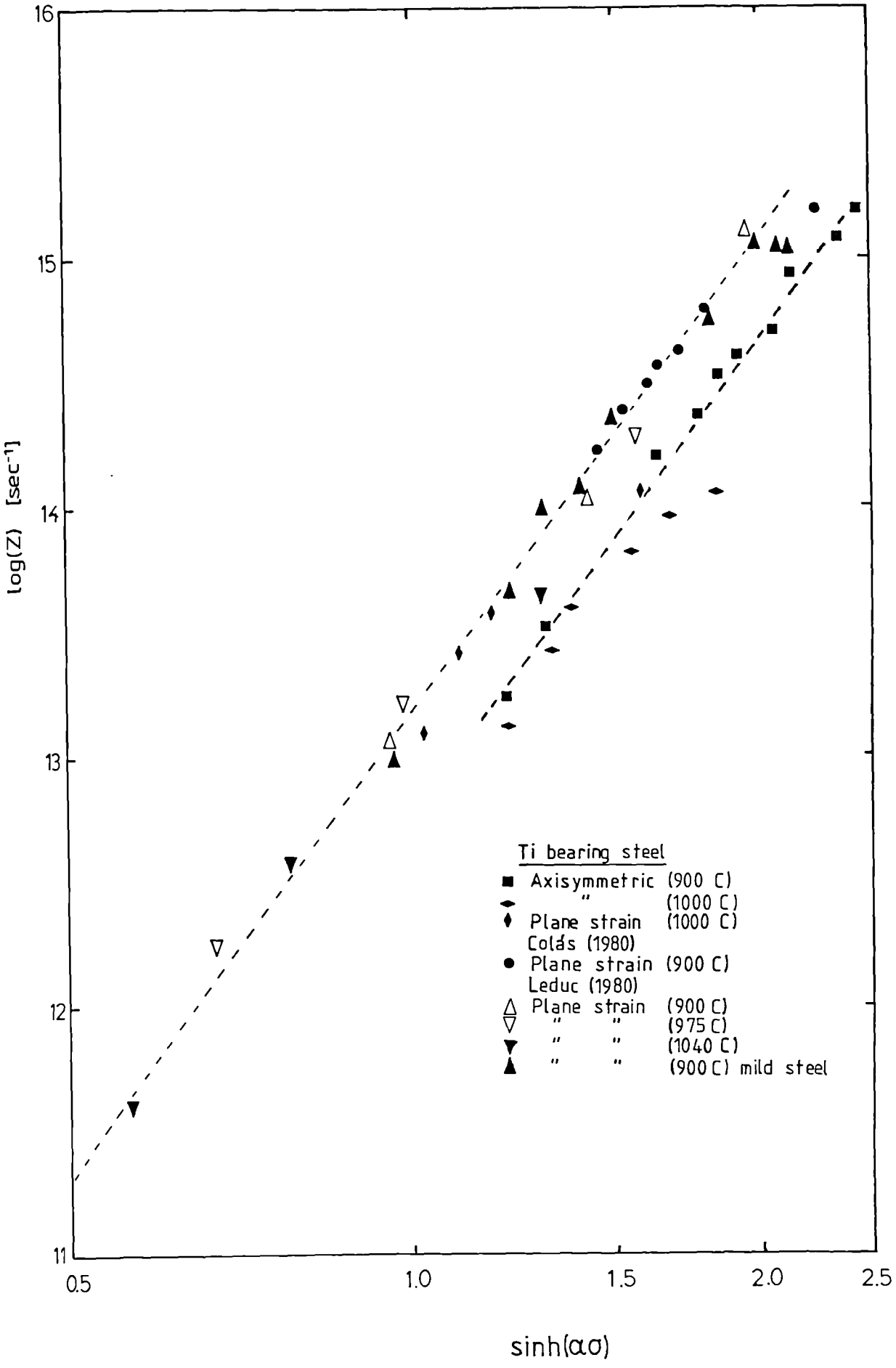
16
15
14
13
12
11
log(Z) [sec⁻¹]
0.5
1.0
1.5
2.0
2.5
sinh(ασ)
Ti bearing steel
Axisymmetric (900 C)
" (1000 C)
Plane strain (1000 C)
Colás (1980)
Plane strain (900 C)
Leduc (1980)
Plane strain (900 C)
" " (975 C)
" " (1040 C)
" " (900 C) mild steel

Figure 47.- Initial grain sizes from specimens obtained from schedule i tested at 910 C, Table III.

	Reheating Temp. [C]	Grain size [μm]
a.)	904	18.9 ± 1.8
b.)	1010	29.6 ± 2.4
c.)	1095	59.3 ± 2.6
d.)	1194	158.4 ± 4.1

Electrolytic etching, 100 X.

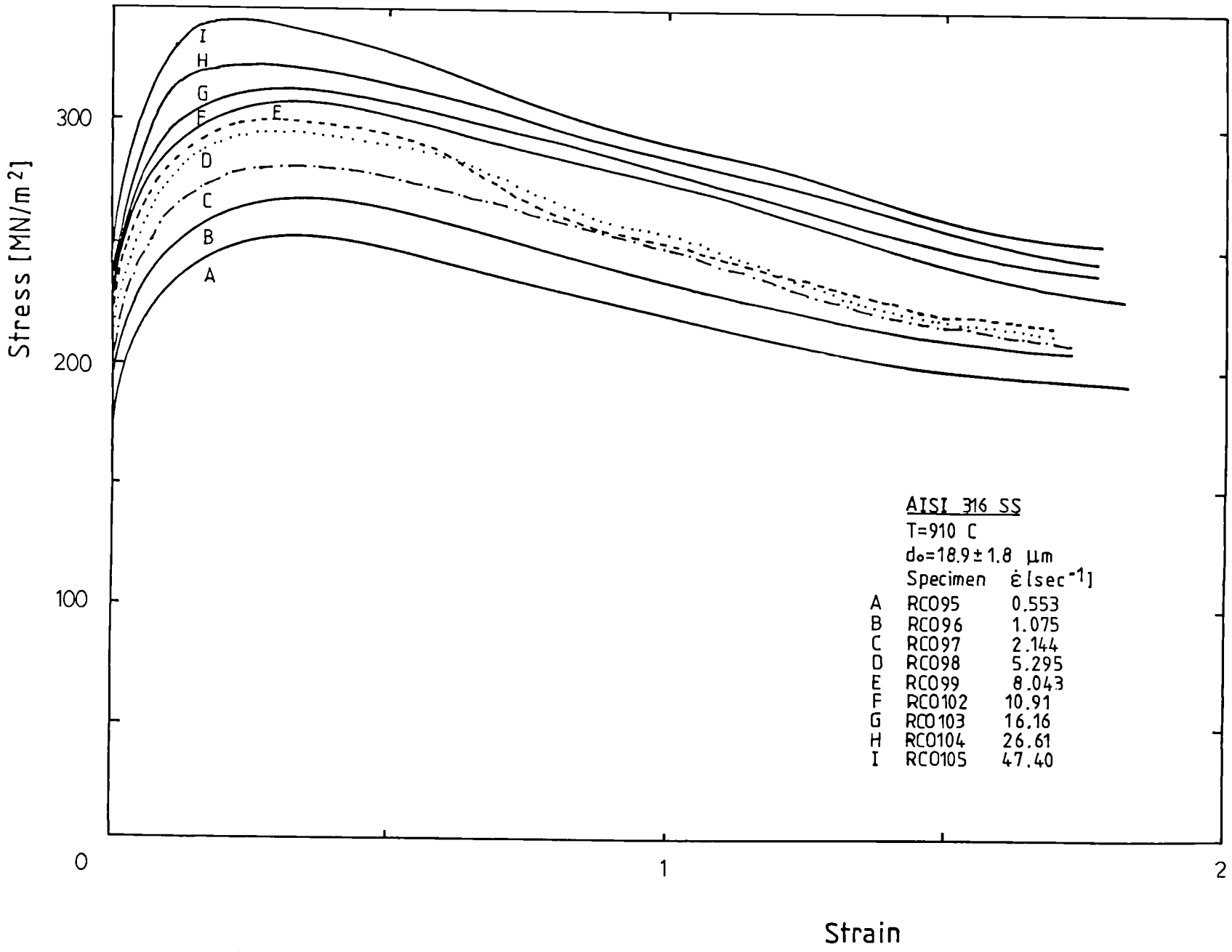
Stress [MN/m²]
300
200
100
0
1
2
Strain
I
H
G
F
E
D
C
B
A
AISI 316 SS
T=910 C
d₀=18.9 ± 1.8 µm
Specimen ε̇ [sec⁻¹]
A RC095 0.553
B RC096 1.075
C RC097 2.144
D RC098 5.295
E RC099 8.043
F RC0102 10.91
G RC0103 16.16
H RC0104 26.61
I RC0105 47.40

Figure 50.- Stress-strain curves for AISI type 316 stainless steel in plane strain compression at 910 C, preheating temperature 1010 C.

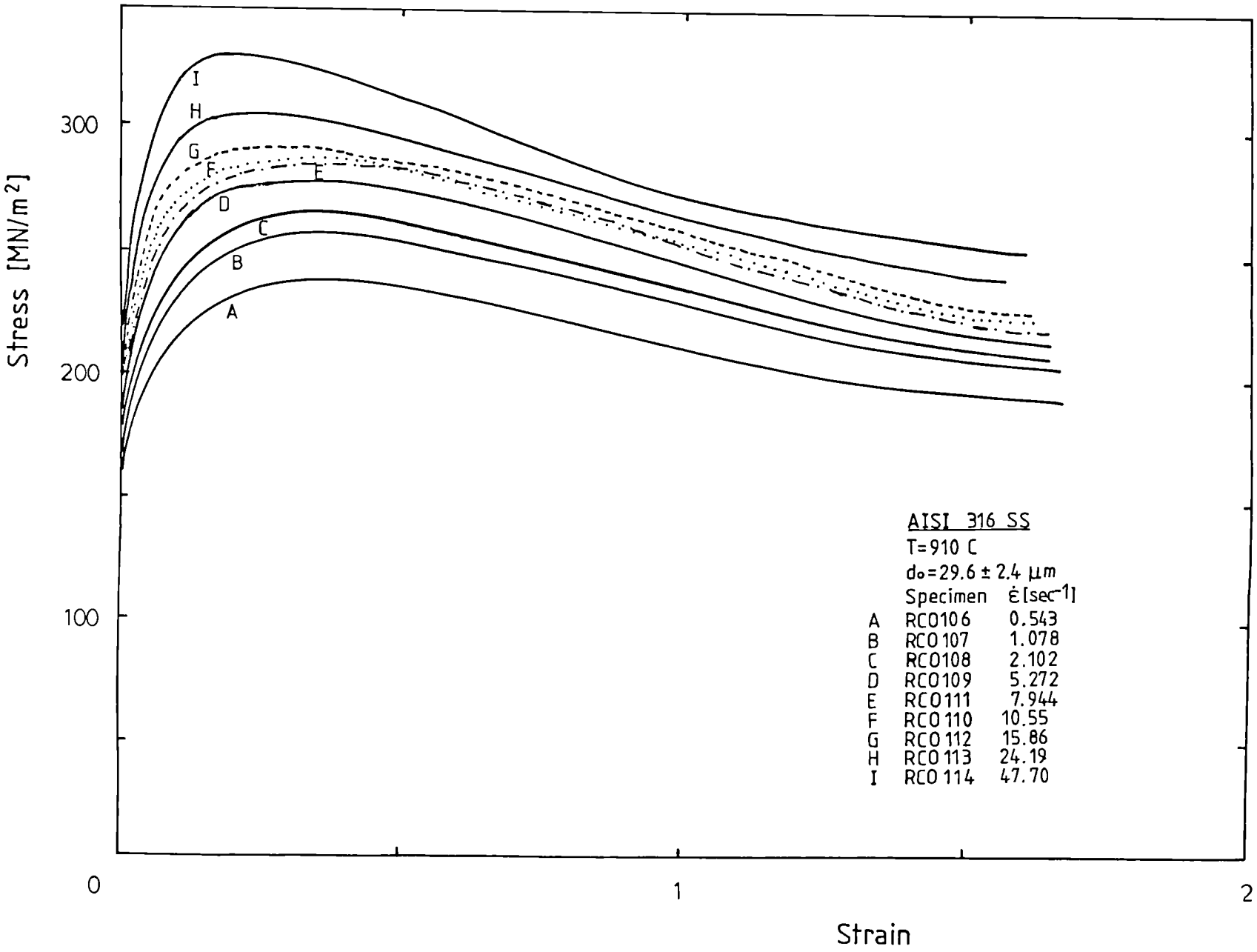
Stress [MN/m²]
300
200
100
0
1
2
Strain
I
H
G
F
E
D
C
B
A
AISI 316 SS
T=910 C
d₀=29.6 ± 2.4 µm
Specimen ε̇[sec⁻¹]
A RCO106 0.543
B RCO107 1.078
C RCO108 2.102
D RCO109 5.272
E RCO111 7.944
F RCO110 10.55
G RCO112 15.86
H RCO113 24.19
I RCO114 47.70

Figure 51.- Stress-strain curves for AISI type 316 stainless steel in plane strain compression at 910 C, preheating temperature 1095 C.

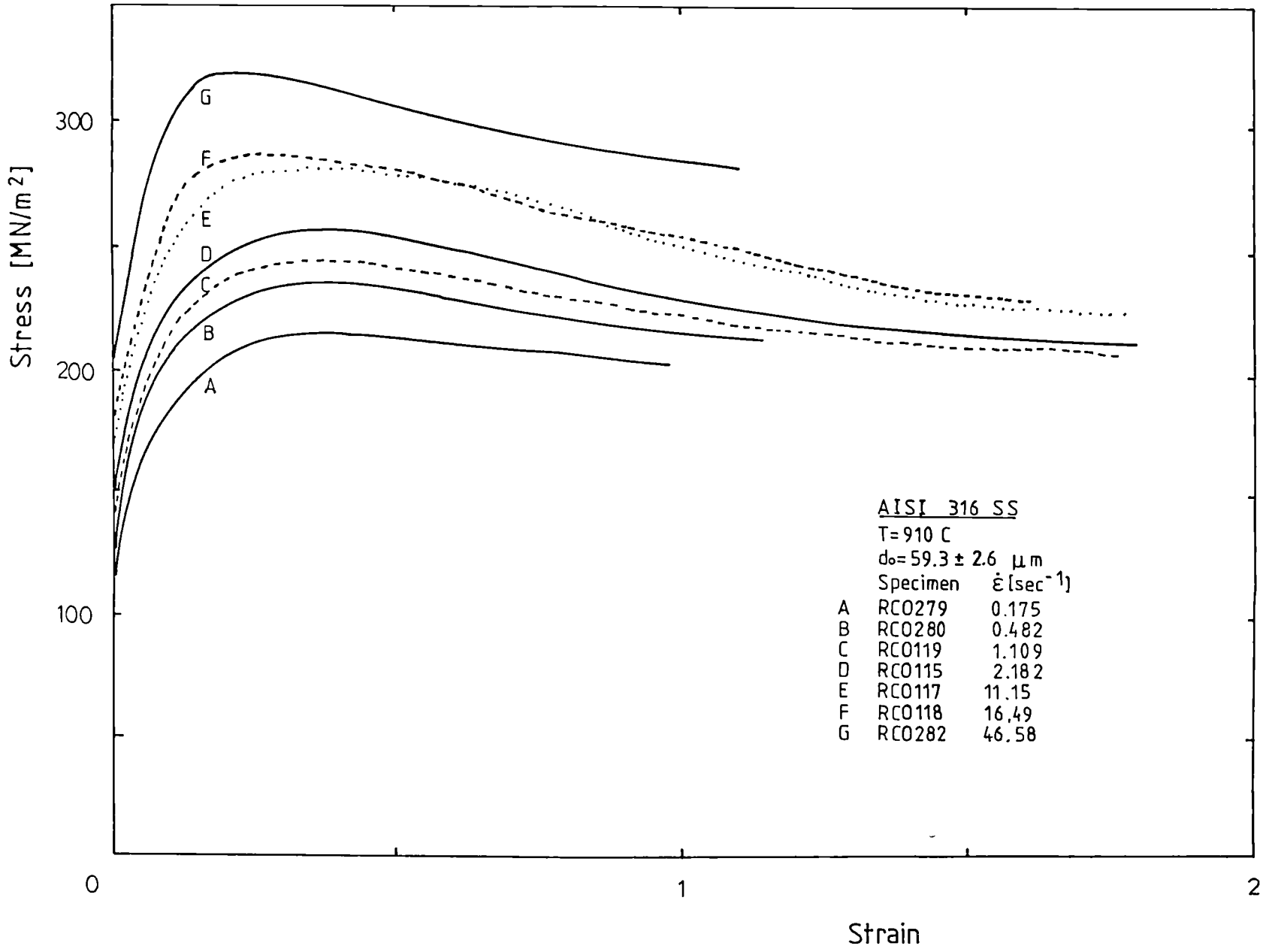
Stress [MN/m²]
300
200
100
0
1
2
Strain
G
F
E
D
C
B
A
AISI 316 SS
T = 910 C
d₀ = 59.3 ± 2.6 µm
Specimen ε̇ [sec⁻¹]
A RC0279 0.175
B RC0280 0.482
C RC0119 1.109
D RC0115 2.182
E RC0117 11.15
F RC0118 16.49
G RC0282 46.58

Figure 52.- Stress-strain curves for AISI type 316 stainless steel in plane strain compression at 910 C, preheating temperature 1194 C.

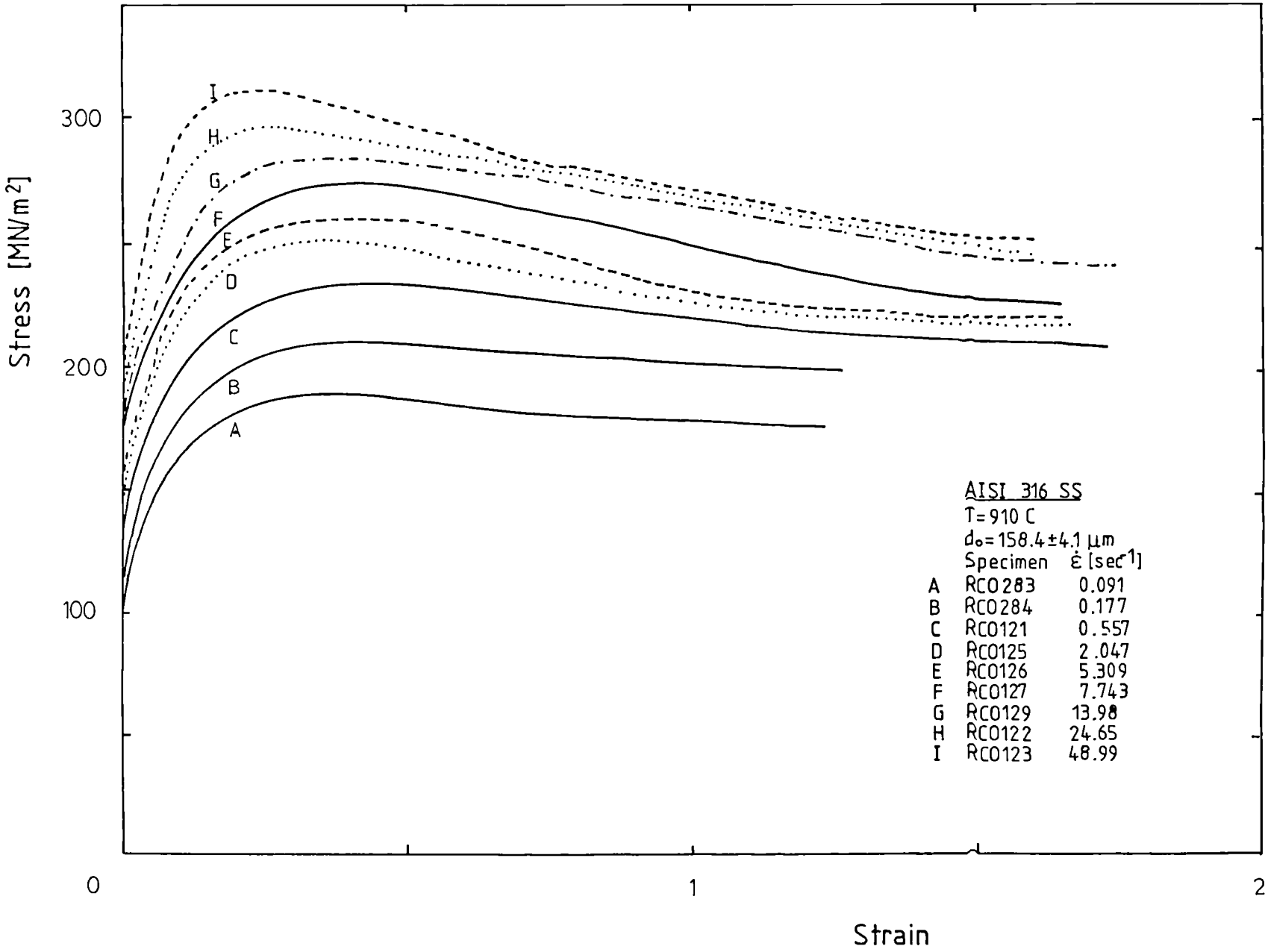
Stress [MN/m²]
300
200
100
0
1
2
Strain
I
H
G
F
E
D
C
B
A
AISI 316 SS
T = 910 C
d_o = 158.4 ± 4.1 µm
Specimen $\dot{\varepsilon}$ [sec⁻¹]
A RC0283 0.091
B RC0284 0.177
C RC0121 0.557
D RC0125 2.047
E RC0126 5.309
F RC0127 7.743
G RC0129 13.98
H RC0122 24.65
I RC0123 48.99

Figure 53.- Stress-strain curves for AISI type 316 stainless steel in plane strain compression at 1006 C, h/w = 0.40.

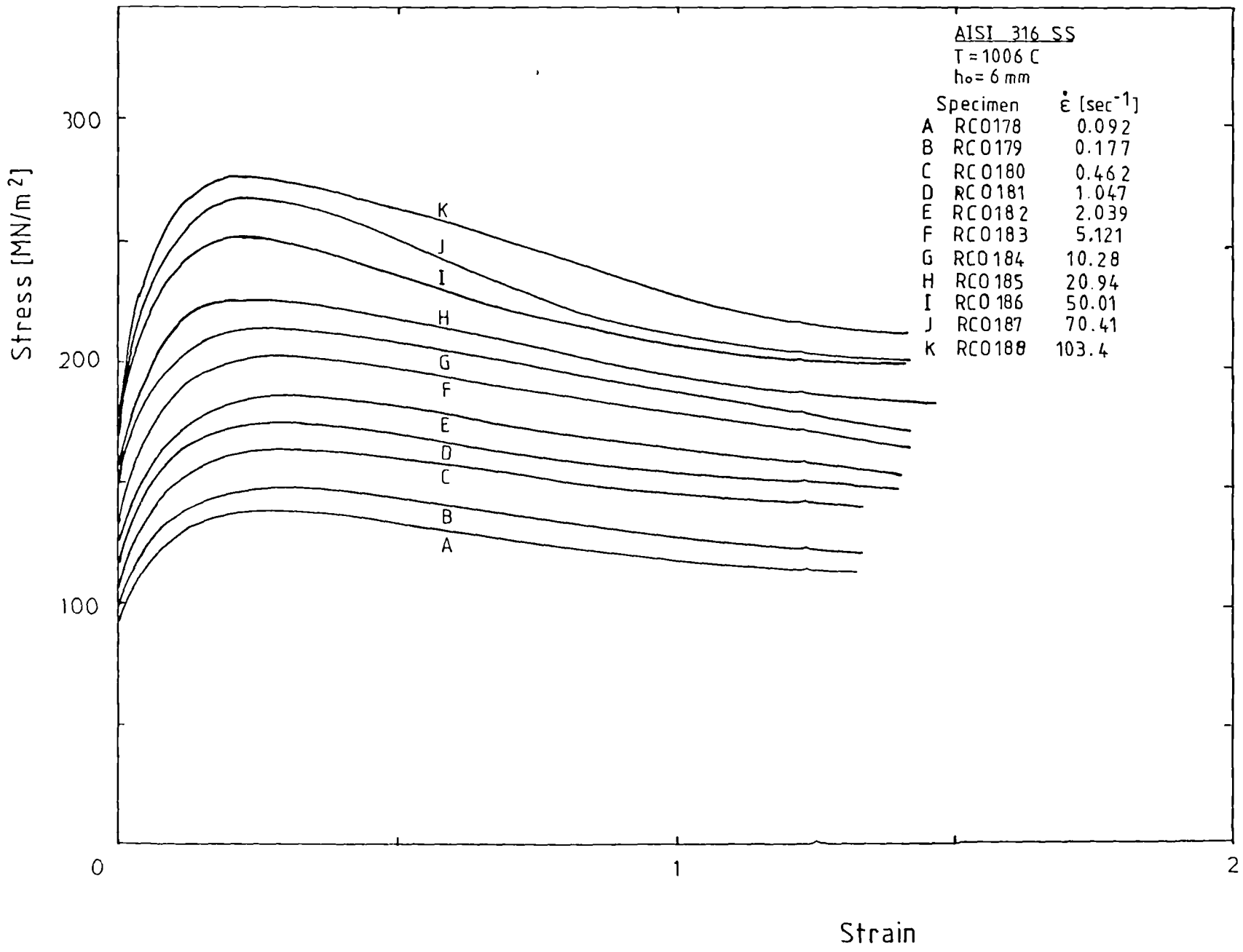
AISI 316 SS
T = 1006 C
h₀ = 6 mm
Specimen ε̇ [sec⁻¹]
A RC0178 0.092
B RC0179 0.177
C RC0180 0.462
D RC0181 1.047
E RC0182 2.039
F RC0183 5.121
G RC0184 10.28
H RC0185 20.94
I RC0186 50.01
J RC0187 70.41
K RC0188 103.4
Stress [MN/m²]
300
200
100
0
1
2
Strain

Figure 54.- Stress-strain curves for AISI type 316 stainless steel in plane strain compression at 1006 C, h/w = 0.53.

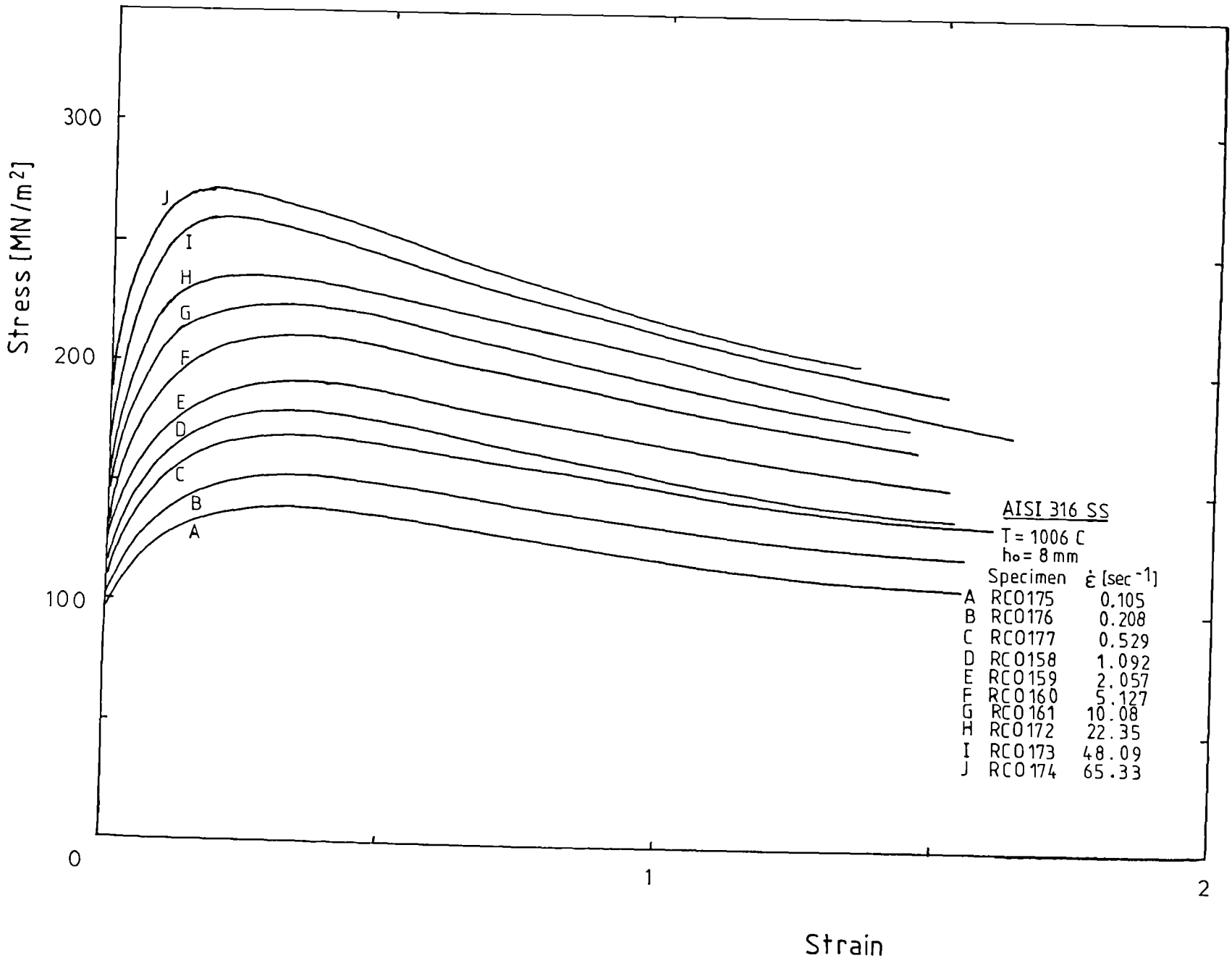
Stress [MN/m²]
300
200
100
0
1
2
Strain
J
I
H
G
F
E
D
C
B
A
AISI 316 SS
T = 1006 C
h₀ = 8 mm
Specimen ε̇ [sec⁻¹]
A RCO175 0.105
B RCO176 0.208
C RCO177 0.529
D RCO158 1.092
E RCO159 2.057
F RCO160 5.127
G RCO161 10.08
H RCO172 22.35
I RCO173 48.09
J RCO174 65.33

Figure 55.- Stress-strain curves for AISI type 316 stainless steel in plane strain compression at 1006 C, h/w = 0.73.

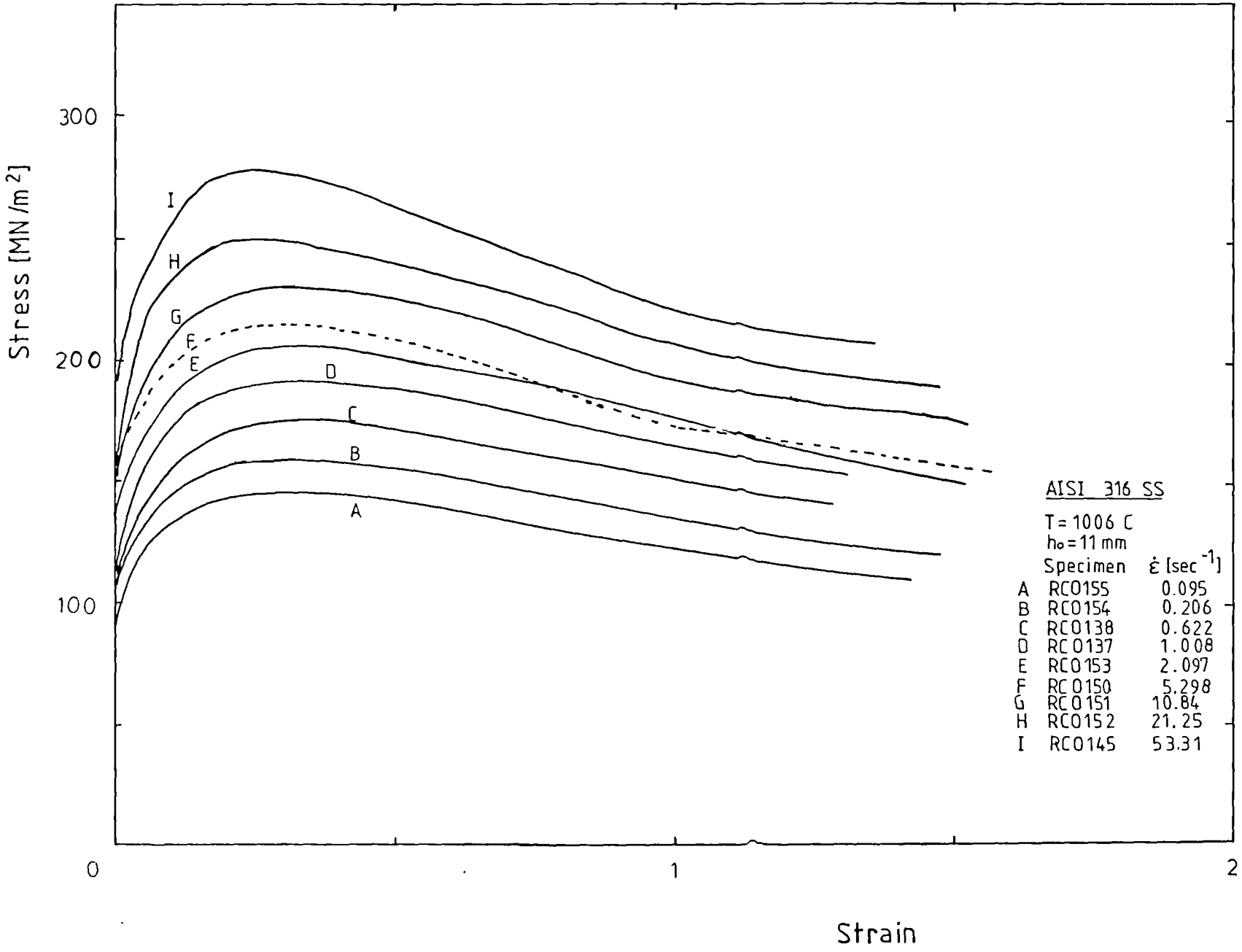
Stress [MN/m²]
300
200
100
0
1
2
Strain
I
H
G
F
E
D
C
B
A
AISI 316 SS
T = 1006 C
h₀ = 11 mm
Specimen
ε̇ [sec⁻¹]
A RC0155 0.095
B RC0154 0.206
C RC0138 0.622
D RC0137 1.008
E RC0153 2.097
F RC0150 5.298
G RC0151 10.84
H RC0152 21.25
I RC0145 53.31

Figure 56.- Stress-strain curves for AISI type 316 stainless steel in plane strain compression at 1006 C, transverse specimens, h/w = 0.73.

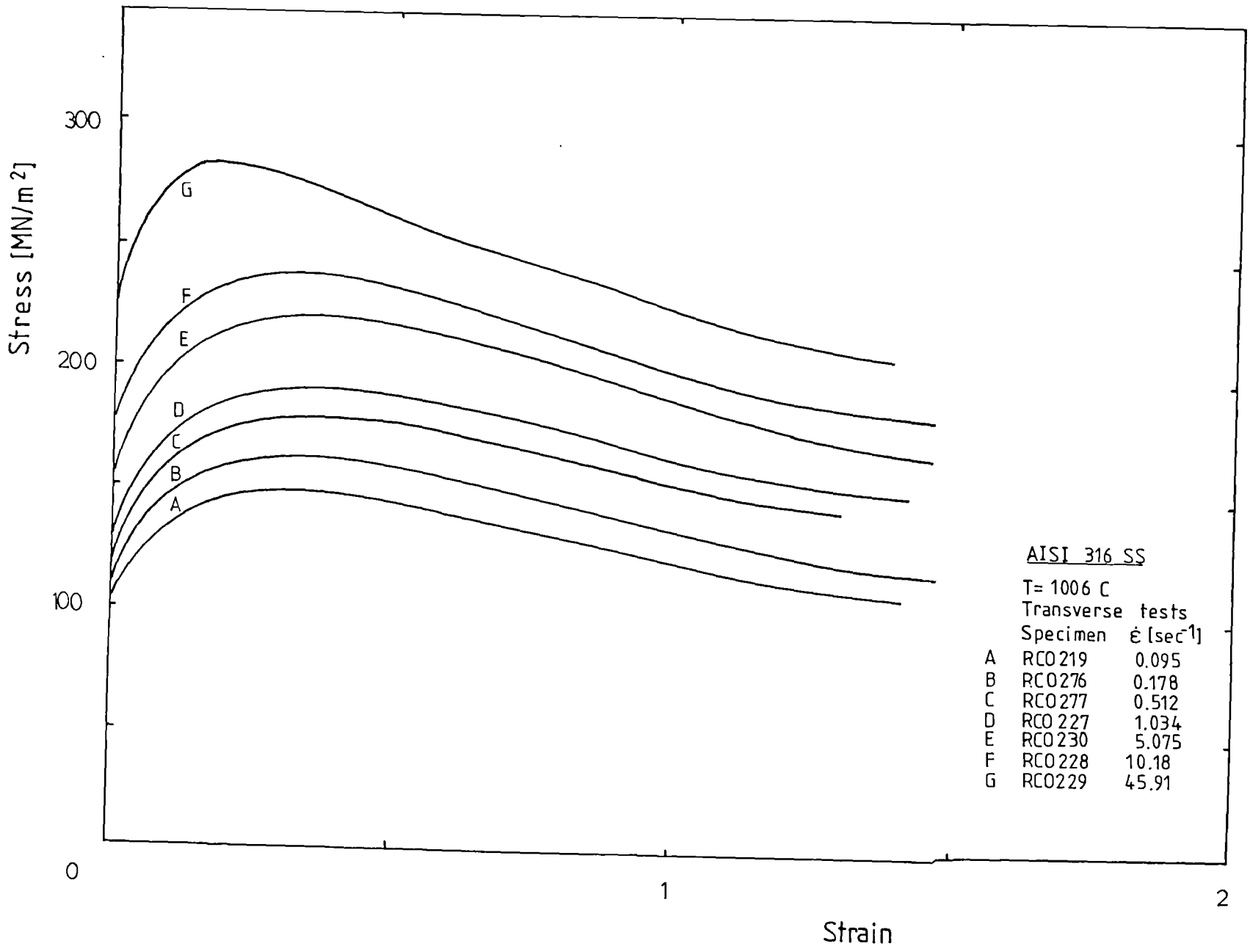
Stress [MN/m²]
300
200
100
0
1
2
Strain
G
F
E
D
C
B
A
AISI 316 SS
T= 1006 C
Transverse tests
Specimen ε̇ [sec⁻¹]
A RCO 219 0.095
B RCO 276 0.178
C RCO 277 0.512
D RCO 227 1.034
E RCO 230 5.075
F RCO 228 10.18
G RCO 229 45.91

Figure 57.- Stress-strain curves for AISI type 316 stainless steel in axisymmetric compression at 1006 C, through the thickness direction. The broken curves correspond to the specimens machined to obtain a width over diameter ratio equal to 1.

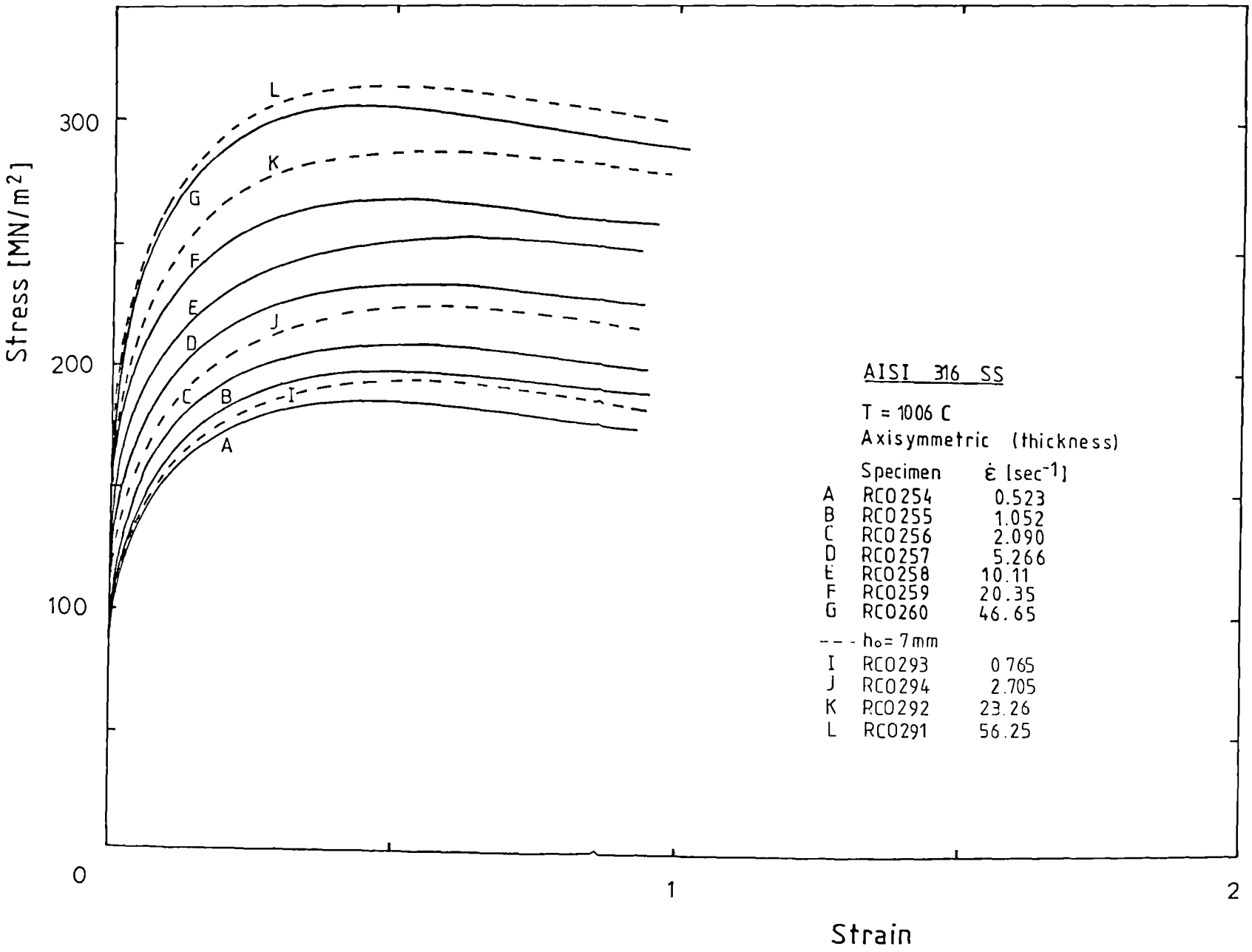
Stress [MN/m²]
300
200
100
0
1
2
Strain
L
K
G
F
E
D
J
C
B
I
A
AISI 316 SS
T = 1006 C
Axisymmetric (thickness)
Specimen
ε̇ [sec⁻¹]
A RC0254 0.523
B RC0255 1.052
C RC0256 2.090
D RC0257 5.266
E RC0258 10.11
F RC0259 20.35
G RC0260 46.65
--- h₀ = 7 mm
I RC0293 0.765
J RC0294 2.705
K RC0292 23.26
L RC0291 56.25

Figure 58.- Stress-strain curves for AISI type 316 stainless steel in axisymmetric compression at 1006 C, through the width direction.

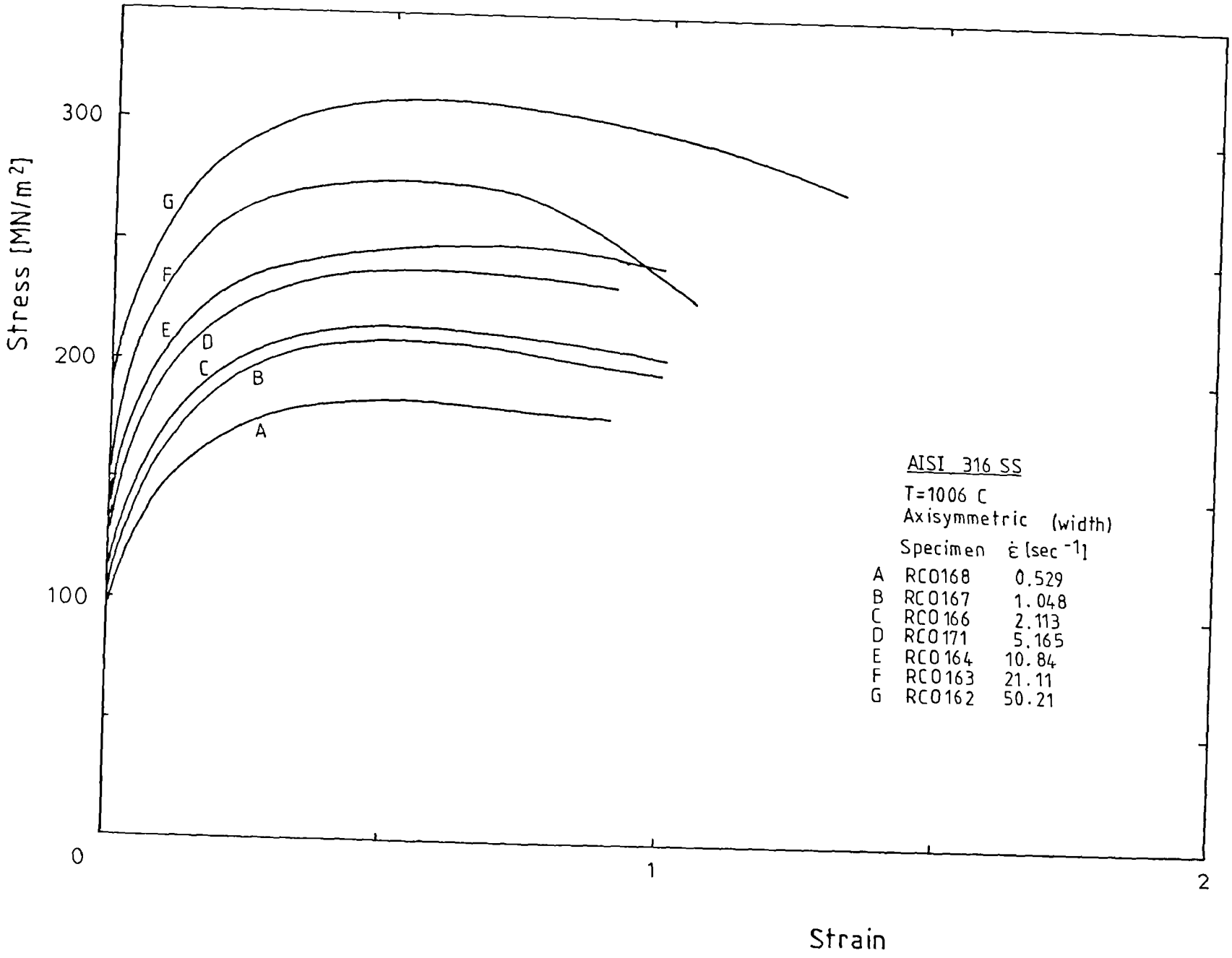
Stress [MN/m²]
300
200
100
0
1
2
Strain
G
F
E
D
C
B
A
AISI 316 SS
T=1006 C
Axisymmetric (width)
Specimen ε̇ [sec⁻¹]
A RC0168 0.529
B RC0167 1.048
C RC0166 2.113
D RC0171 5.165
E RC0164 10.84
F RC0163 21.11
G RC0162 50.21

Figure 59.- Stress-strain curves for AISI type 316 stainless steel in axisymmetric compression at 1006 C, through the length direction.

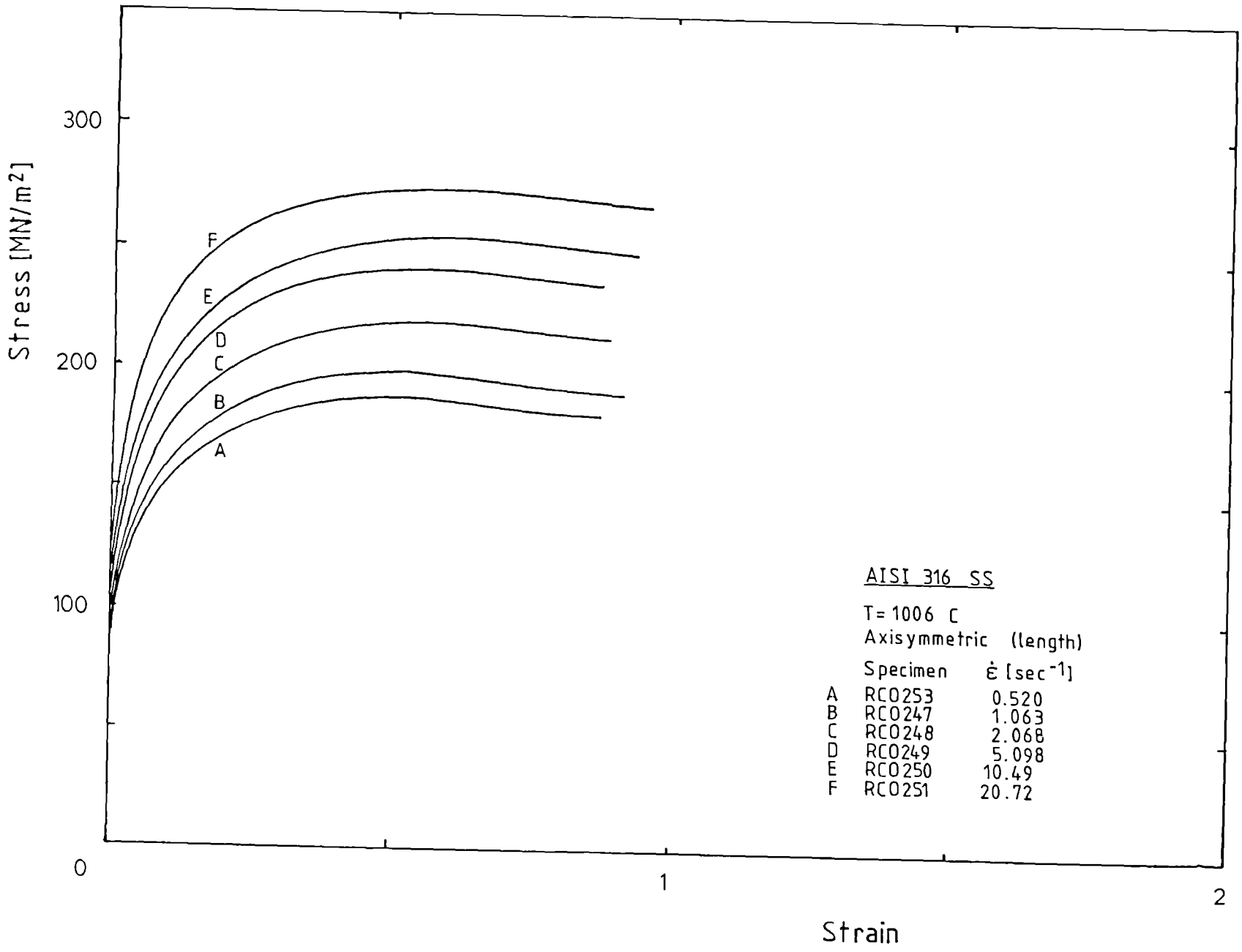
Stress [MN/m²]
300
200
100
0
1
2
Strain
F
E
D
C
B
A
AISI 316 SS
T= 1006 C
Axisymmetric (length)
Specimen ε̇ [sec⁻¹]
A RC0253 0.520
B RC0247 1.063
C RC0248 2.068
D RC0249 5.098
E RC0250 10.49
F RC0251 20.72

Figure 60.- Stress-strain curves for AISI type 316 stainless steel in torsion at 905 C.

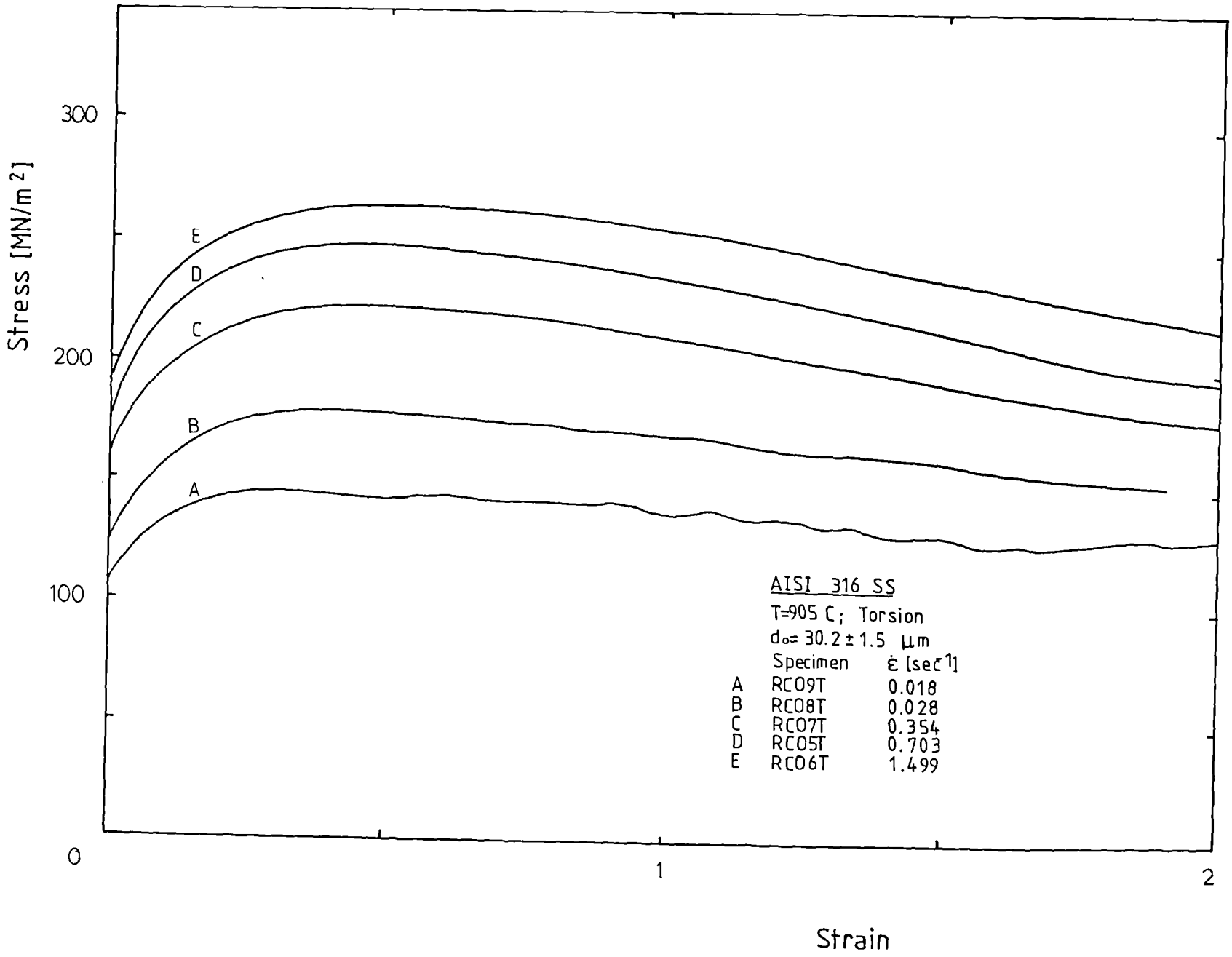
Stress [MN/m²]
300
200
100
0
1
2
Strain
E
D
C
B
A
AISI 316 SS
T=905 C; Torsion
d₀= 30.2 ± 1.5 μm
Specimen
ε̇ [sec⁻¹]
A RC09T 0.018
B RC08T 0.028
C RC07T 0.354
D RC05T 0.703
E RC06T 1.499

Figure 61.- Stress-strain curves for AISI type 316 stainless steel in torsion at 1008 C.

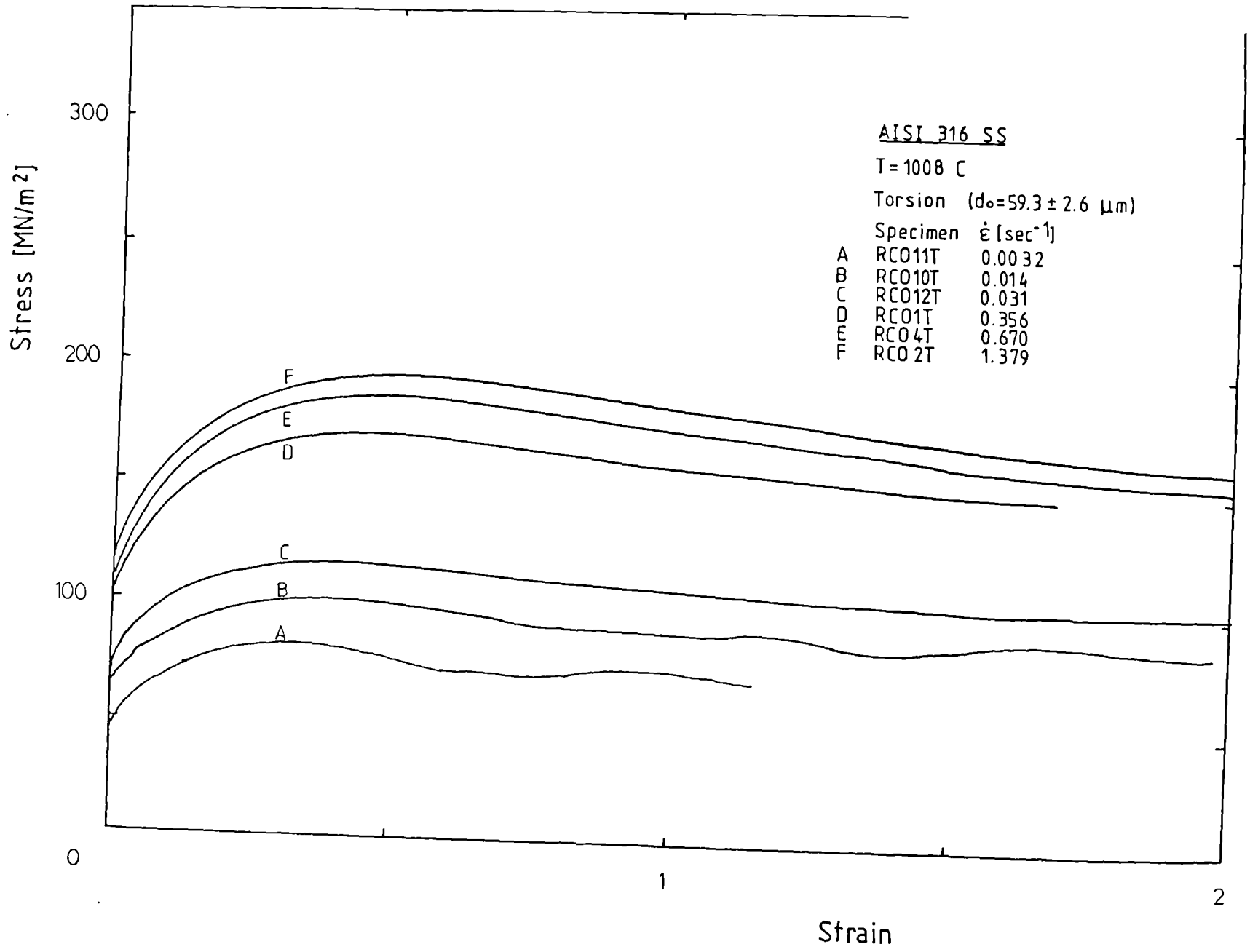
AISI 316 SS
T = 1008 C
Torsion (do = 59.3 ± 2.6 μm)
Specimen ε̇ [sec⁻¹]
A RCO11T 0.0032
B RCO10T 0.014
C RCO12T 0.031
D RCO1T 0.356
E RCO4T 0.670
F RCO2T 1.379
Stress [MN/m²]
300
200
100
0
1
2
Strain
A
B
C
D
E
F

Figure 62.- Strain to the peak versus strain rate plot for specimens tested at around 900 C.

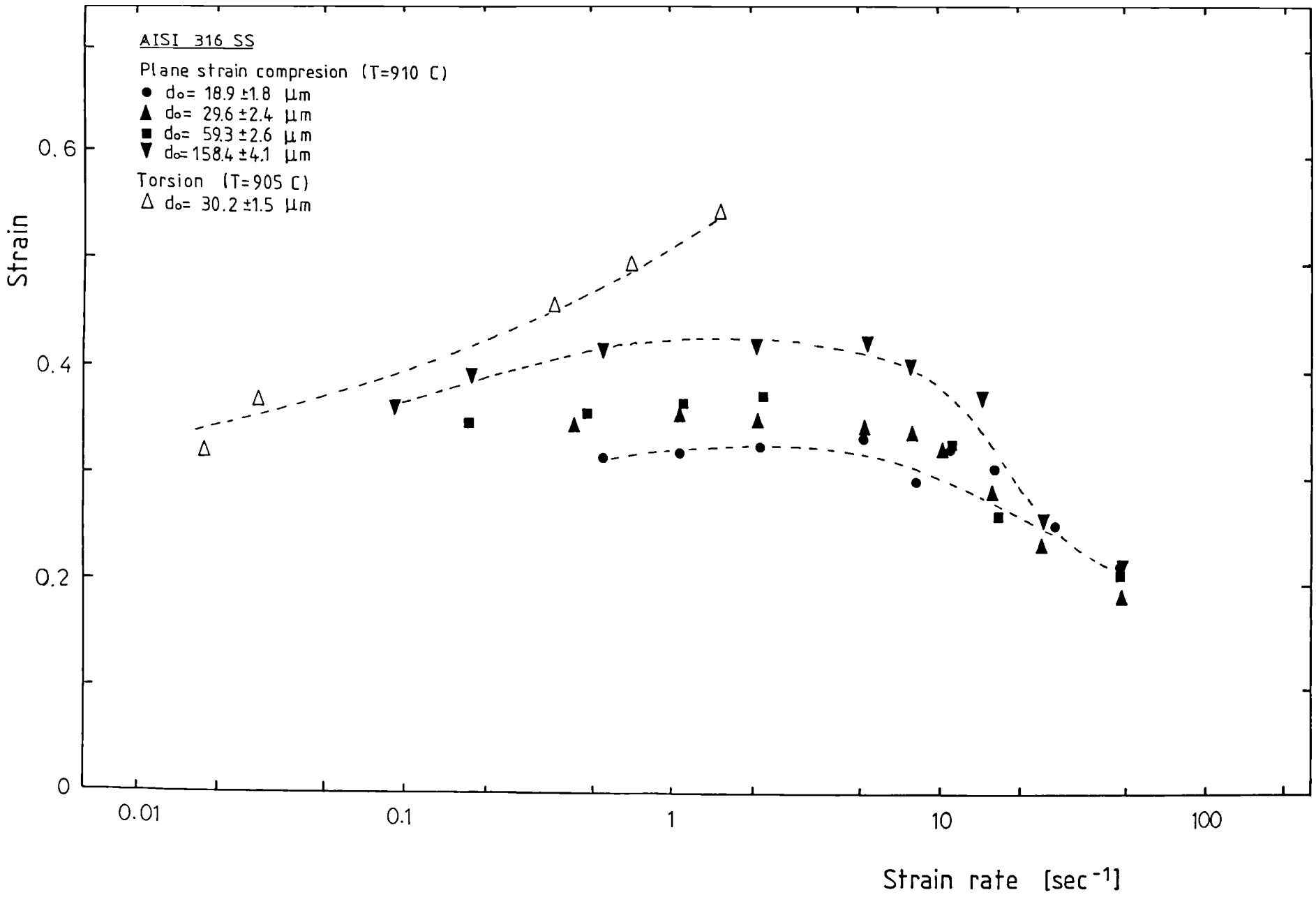
AISI 316 SS
Plane strain compresion (T=910 C)
● do= 18.9 ±1.8 µm
▲ do= 29.6 ±2.4 µm
■ do= 59.3 ±2.6 µm
▼ do= 158.4 ±4.1 µm
Torsion (T=905 C)
△ do= 30.2 ±1.5 µm
Strain
0.6
0.4
0.2
0
0.01
0.1
1
10
100
Strain rate [sec⁻¹]

Figure 63.- Strain to the peak versus strain rate plot for specimens tested at around 1000 c.

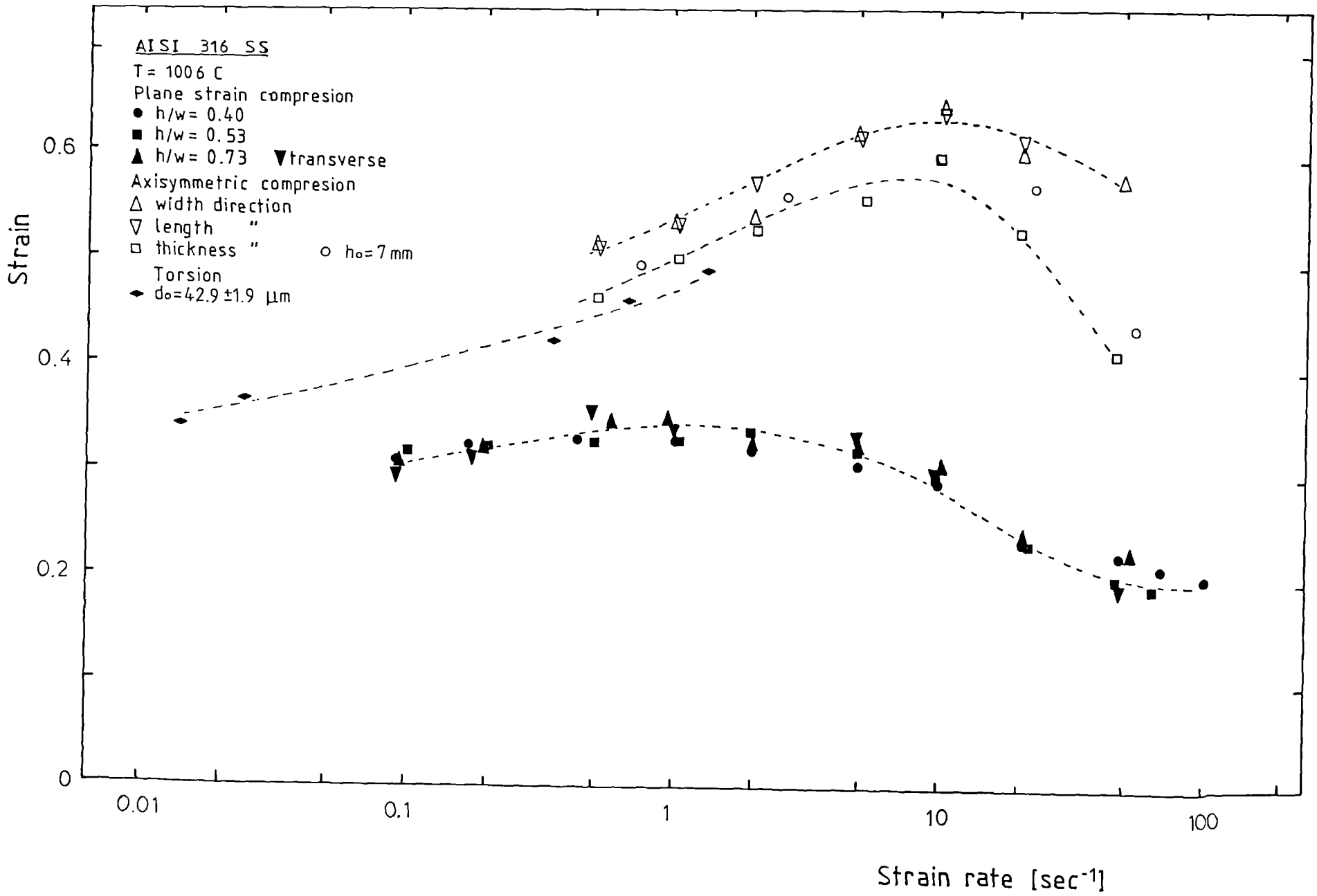
AISI 316 SS
T = 1006 C
Plane strain compresion
● h/w = 0.40
■ h/w = 0.53
▲ h/w = 0.73 ▼transverse
Axisymmetric compresion
△ width direction
▽ length "
□ thickness " ○ h₀ = 7 mm
Torsion
◆ d₀ = 42.9 ±1.9 µm
Strain
0.6
0.4
0.2
0
0.01
0.1
1
10
100
Strain rate [sec⁻¹]

Figure 64.- Plot of values of the stress at 0.15 strain versus strain rate for specimens tested at around 900 C.

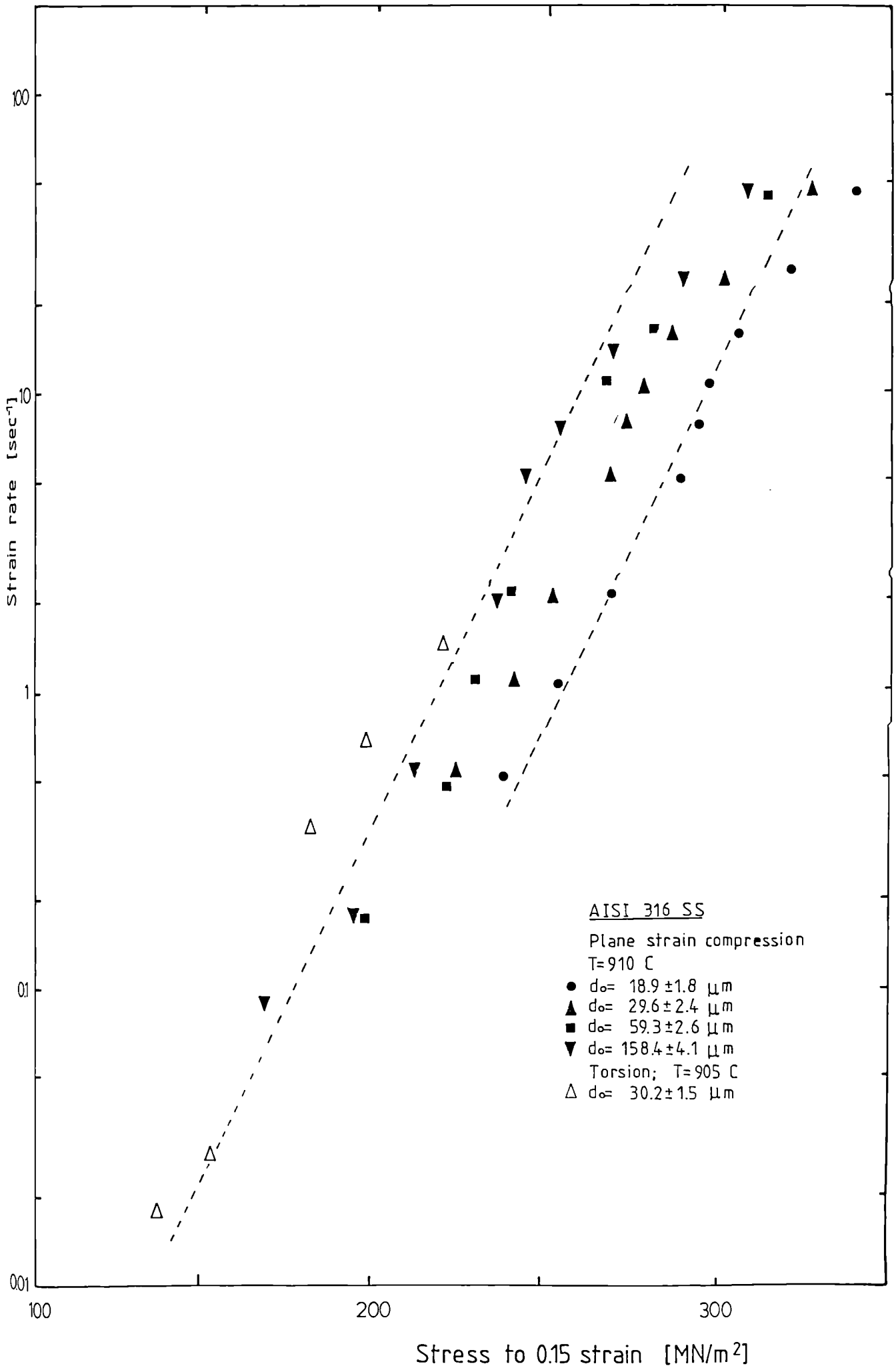
100
10
1
0.1
0.01
Strain rate [sec⁻¹]
100
200
300
Stress to 0.15 strain [MN/m²]
AISI 316 SS
Plane strain compression
T=910 C
● d₀= 18.9 ±1.8 µm
▲ d₀= 29.6 ± 2.4 µm
■ d₀= 59.3 ± 2.6 µm
▼ d₀= 158.4 ± 4.1 µm
Torsion; T=905 C
Δ d₀= 30.2 ± 1.5 µm

Figure 65.- Plot of values of the stress at 0.15 strain versus strain rate for specimens tested at around 1000 C.

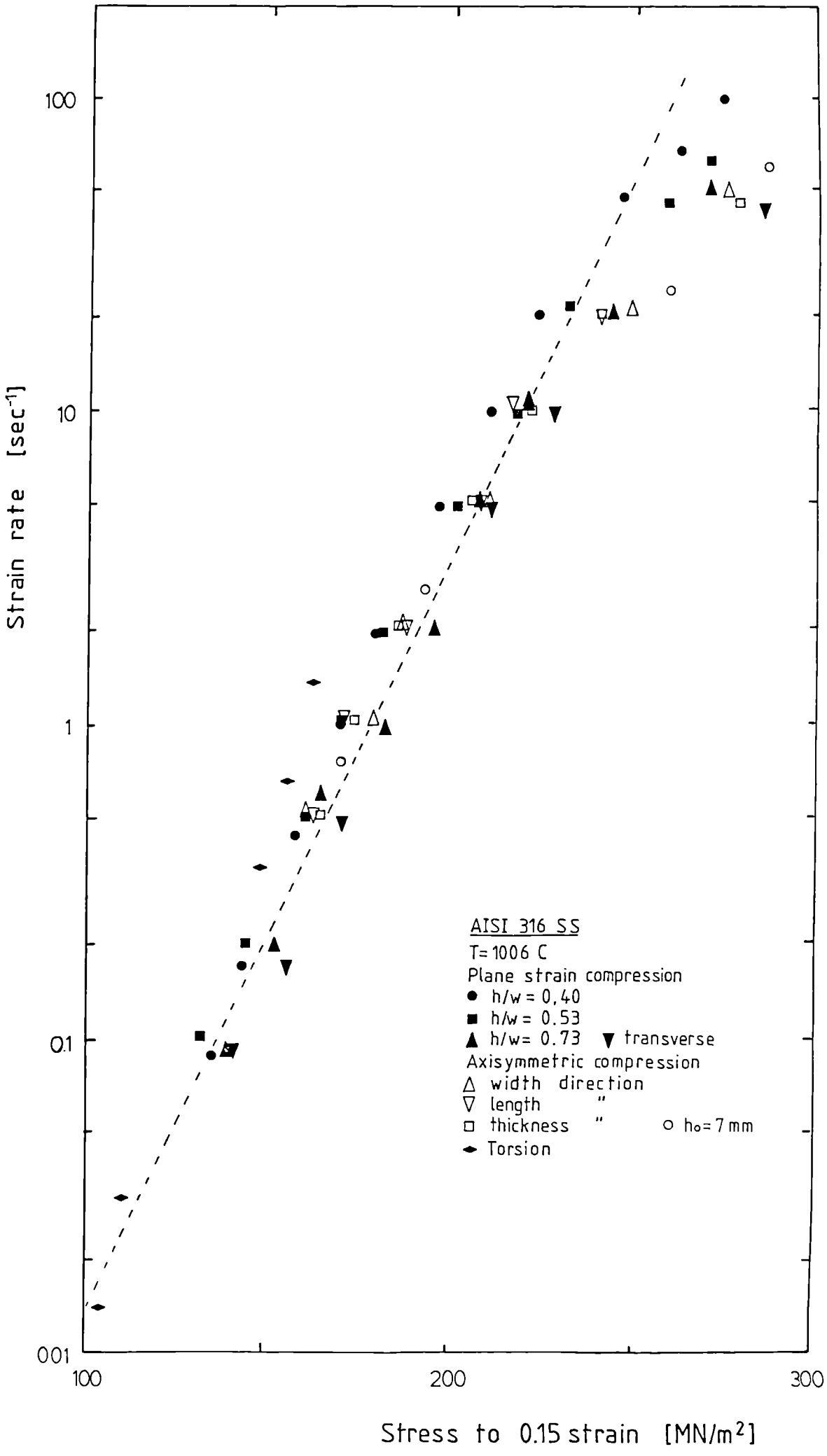
100
10
1
0.1
0.01
100
200
300
Strain rate [sec⁻¹]
Stress to 0.15 strain [MN/m²]
AISI 316 SS
T= 1006 C
Plane strain compression
● h/w = 0,40
■ h/w = 0.53
▲ h/w= 0.73 ▼ transverse
Axisymmetric compression
△ width direction
▽ length "
□ thickness "
○ h₀= 7 mm
◆ Torsion

Figure 66.- Plot of logarithm of the Zener-Hollomon parameter versus logarithm of stress at 0.15 of strain for AISI type 316 stainless steel.

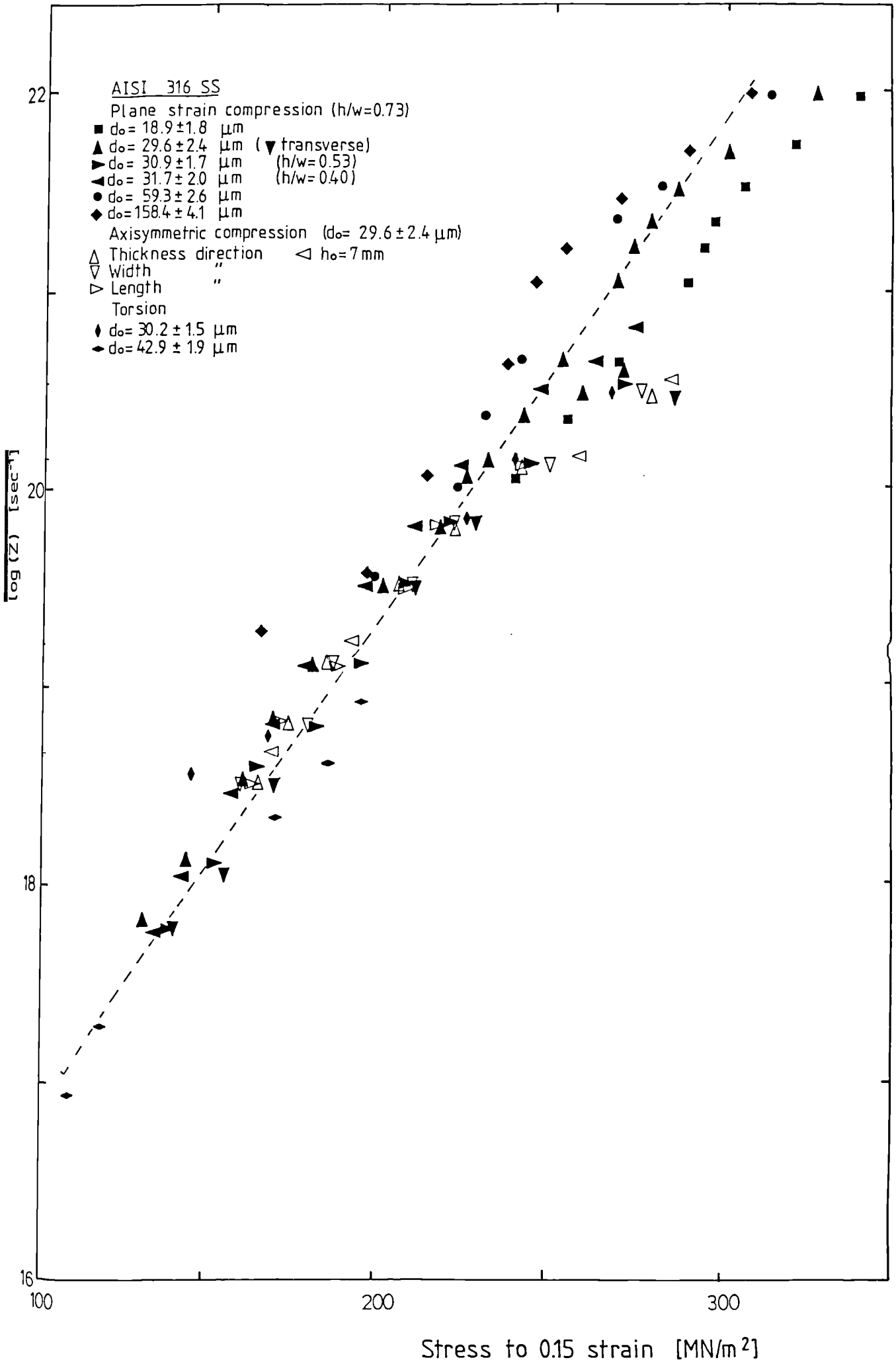
AISI 316 SS
Plane strain compression (h/w=0.73)
■ do= 18.9±1.8 µm
▲ do= 29.6±2.4 µm (▼ transverse)
► do= 30.9±1.7 µm (h/w=0.53)
◄ do= 31.7±2.0 µm (h/w=0.40)
● do= 59.3±2.6 µm
◆ do=158.4±4.1 µm
Axisymmetric compression (do= 29.6±2.4 µm)
△ Thickness direction ◁ ho=7mm
▽ Width "
▷ Length "
Torsion
♦ do= 30.2±1.5 µm
◆ do=42.9±1.9 µm
log (Z) [sec⁻¹]
22
20
18
16
100
200
300
Stress to 0.15 strain [MN/m²]

Figure 67.- Plot of values of peak stress versus strain rate for specimens tested at around 900 C.

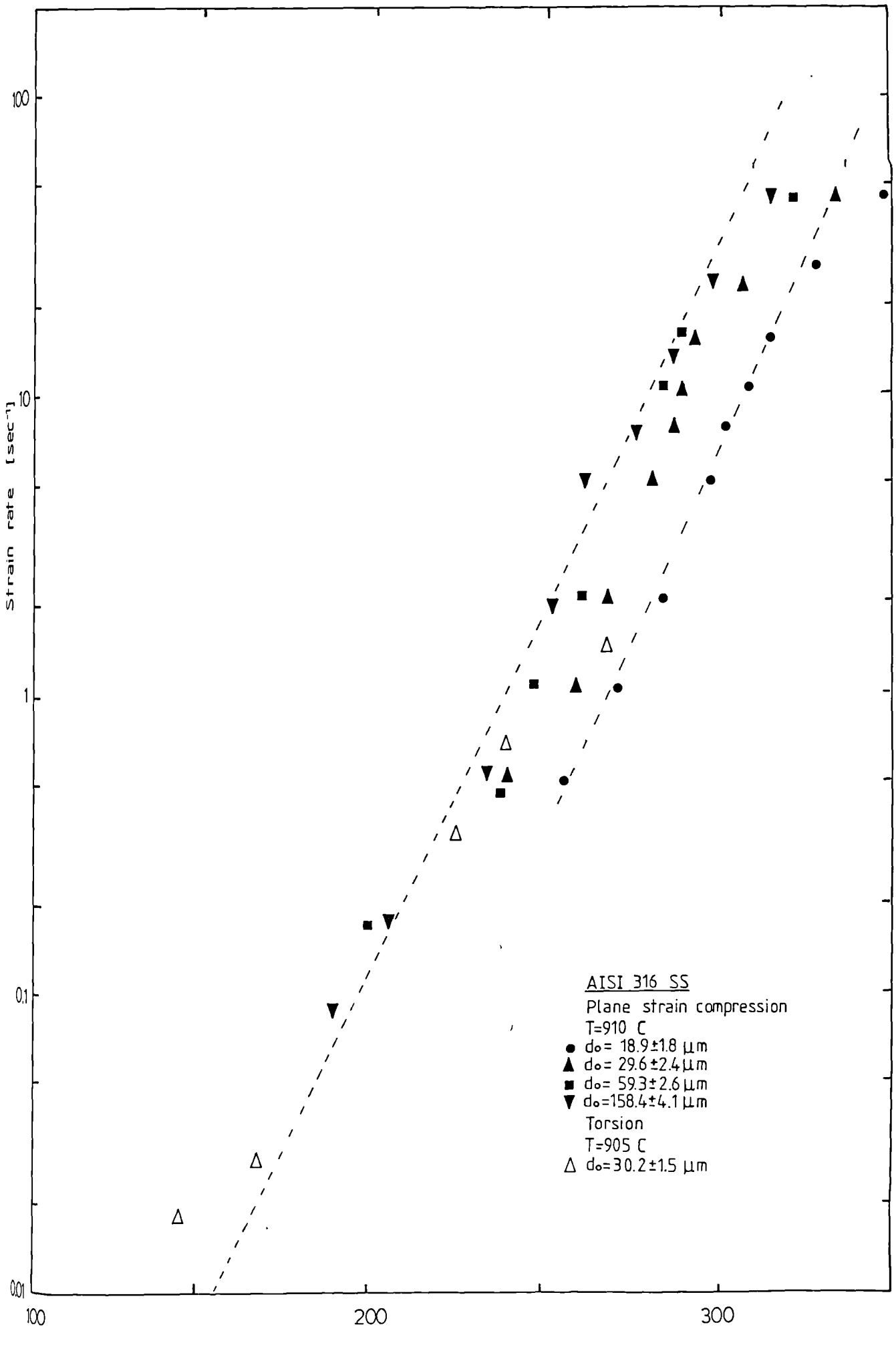
100
10
1
0.1
0.01
Strain rate [sec⁻¹]
100
200
300
Peak stress [MN/m²]
AISI 316 SS
Plane strain compression
T=910 C
● do= 18.9±1.8 µm
▲ do= 29.6±2.4 µm
■ do= 59.3±2.6 µm
▼ do=158.4±4.1 µm
Torsion
T=905 C
Δ do=30.2±1.5 µm

Figure 68.- Plot of values of peak stress versus strain rate for specimens tested at around 1000 C.

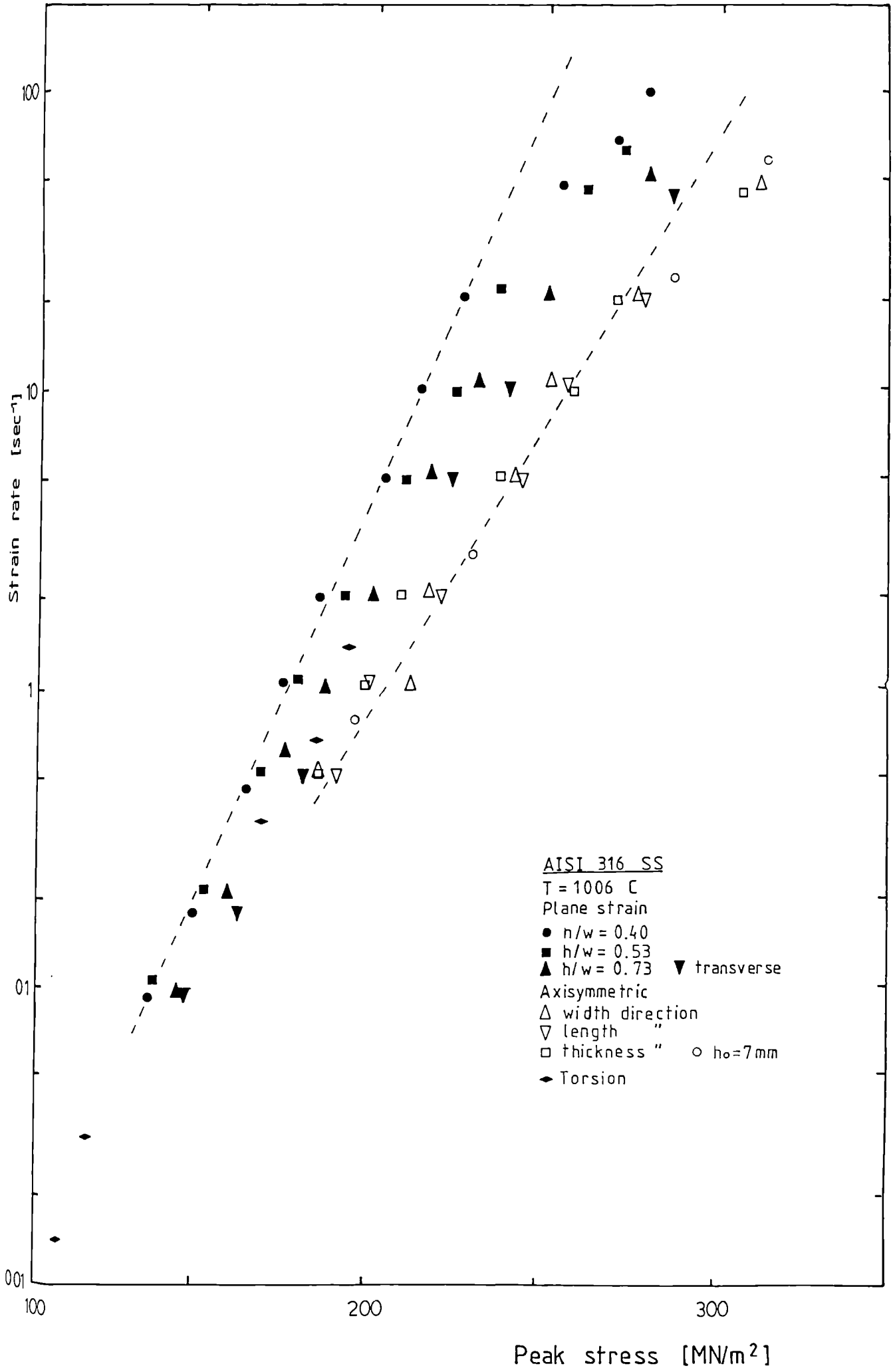
Strain rate [sec⁻¹]
100
10
1
01
001
100
200
300
Peak stress [MN/m²]
AISI 316 SS
T = 1006 C
Plane strain
● h/w = 0.40
■ h/w = 0.53
▲ h/w = 0.73
▼ transverse
Axisymmetric
△ width direction
▽ length "
□ thickness "
○ h₀=7mm
Torsion

Figure 69.- Plot of logarithm of the Zener-Hollomon parameter versus logarithm of peak stress for AISI type 316 stainless steel.

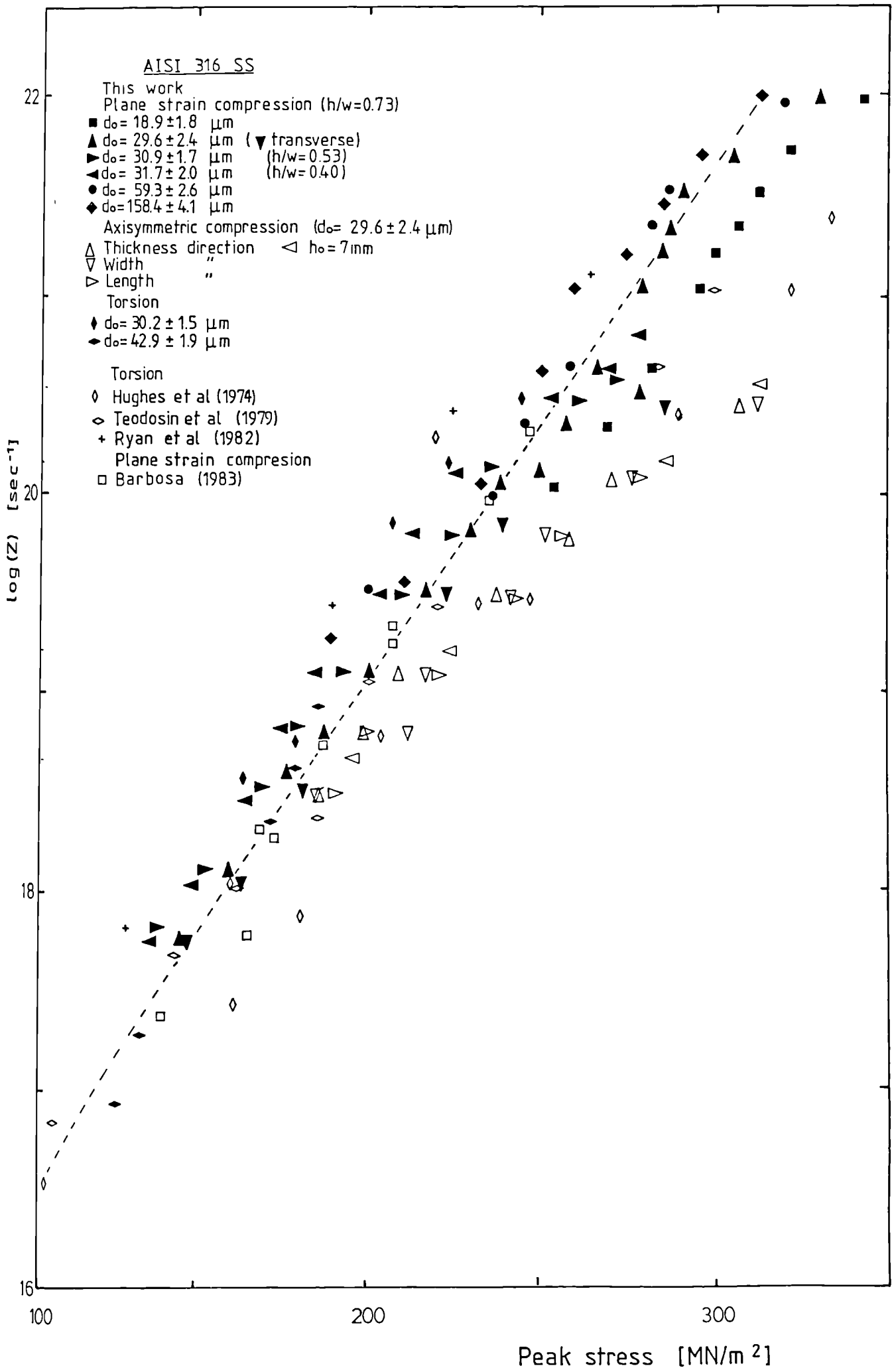
AISI 316 SS
This work
Plane strain compression (h/w=0.73)
■ do= 18.9±1.8 μm
▲ do= 29.6±2.4 μm (▼ transverse)
► do= 30.9±1.7 μm (h/w=0.53)
◄ do= 31.7±2.0 μm (h/w=0.40)
● do= 59.3±2.6 μm
◆ do=158.4±4.1 μm
Axisymmetric compression (do= 29.6±2.4 μm)
△ Thickness direction ◁ ho=7mm
▽ Width "
▷ Length "
Torsion
♦ do= 30.2±1.5 μm
⬬ do=42.9±1.9 μm
Torsion
◊ Hughes et al (1974)
◇ Teodosin et al (1979)
+ Ryan et al (1982)
Plane strain compresion
□ Barbosa (1983)
log (Z) [sec⁻¹]
22
20
18
16
100
200
300
Peak stress [MN/m²]

Figure 70.- Plot of logarithm of the Zener-Hollomon parameter versus logarithm of steady stress for AISI type 316 stainless steel.

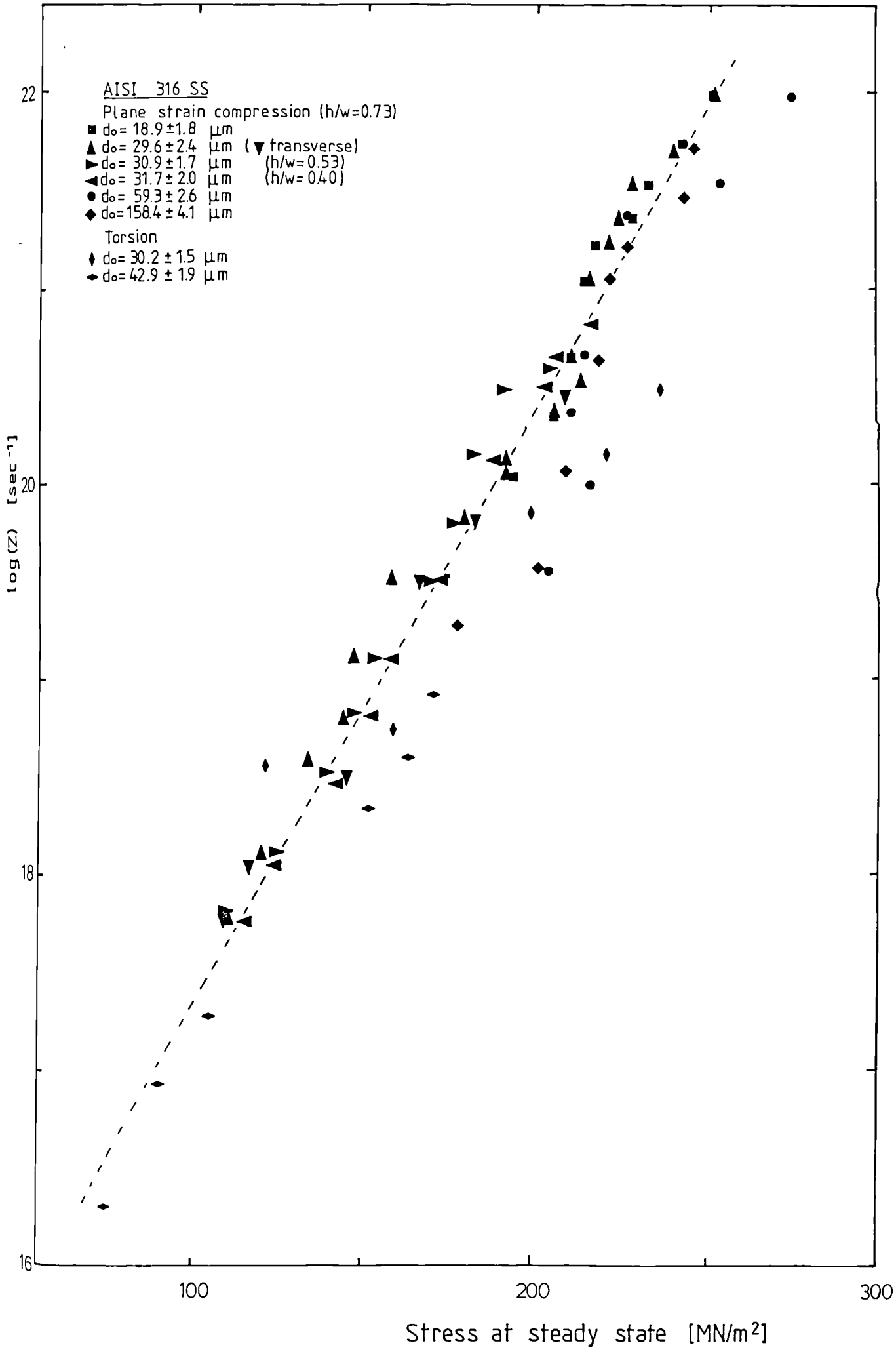
AISI 316 SS
Plane strain compression (h/w=0.73)
■ do= 18.9 ±1.8 µm
▲ do= 29.6 ±2.4 µm (▼ transverse)
► do= 30.9 ±1.7 µm (h/w=0.53)
◄ do= 31.7 ± 2.0 µm (h/w=0.40)
● do= 59.3 ± 2.6 µm
◆ do=158.4 ± 4.1 µm
Torsion
♦ do= 30.2 ± 1.5 µm
⬬ do= 42.9 ± 1.9 µm
log (Z) [sec⁻¹]
22
20
18
16
100
200
300
Stress at steady state [MN/m²]

Figure 71.- Plot of stress to 0.15 strain versus initial grain size for plane strain compression tests at 910 C.

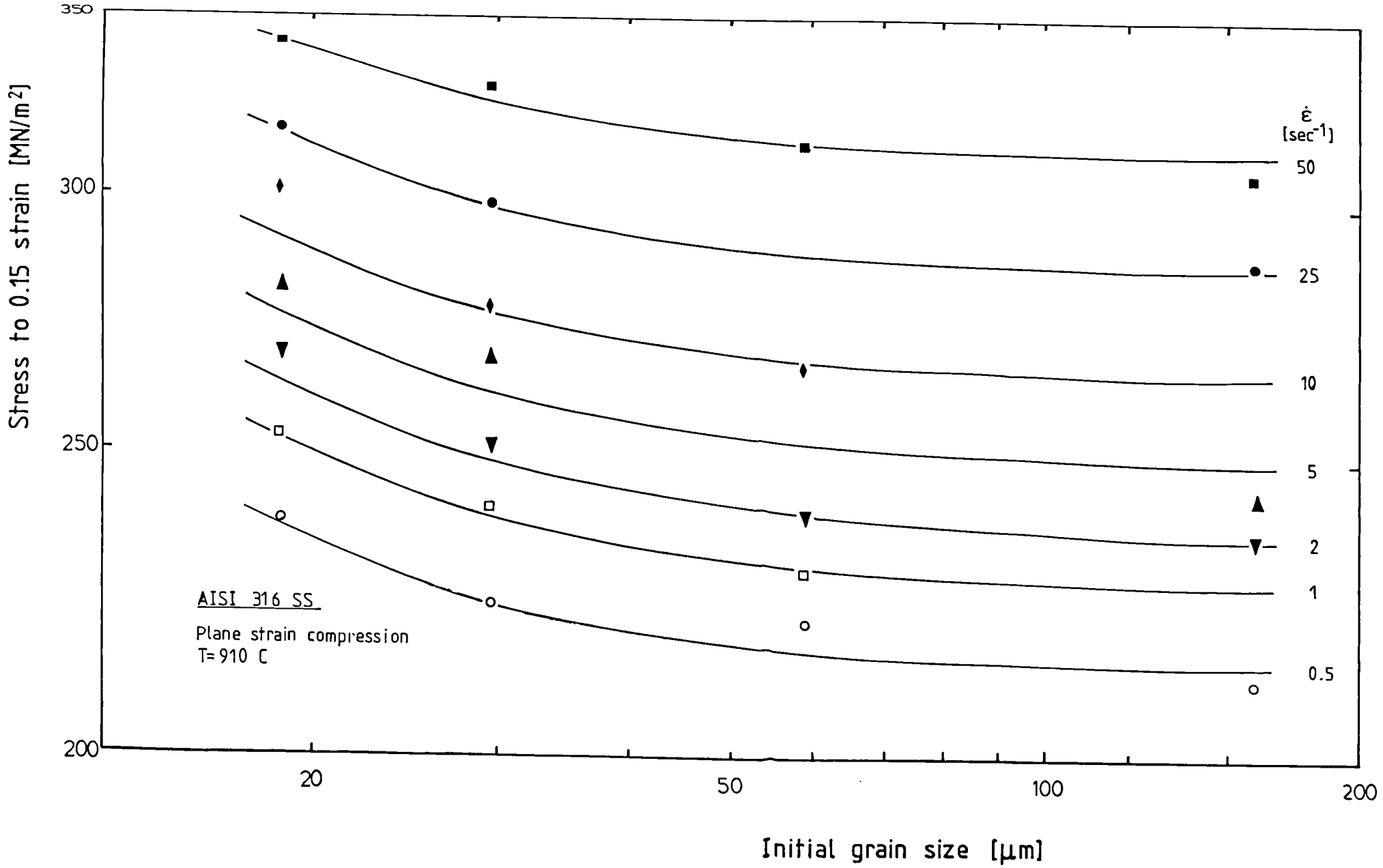
Stress to 0.15 strain [MN/m²]
350
300
250
200
20
50
100
200
Initial grain size [μm]
ε̇ [sec⁻¹]
50
25
10
5
2
1
0.5
AISI 316 SS
Plane strain compression
T=910 C

Figure 72.- Plot of peak stress versus initial grain size for plane strain compression tests at 910 C.

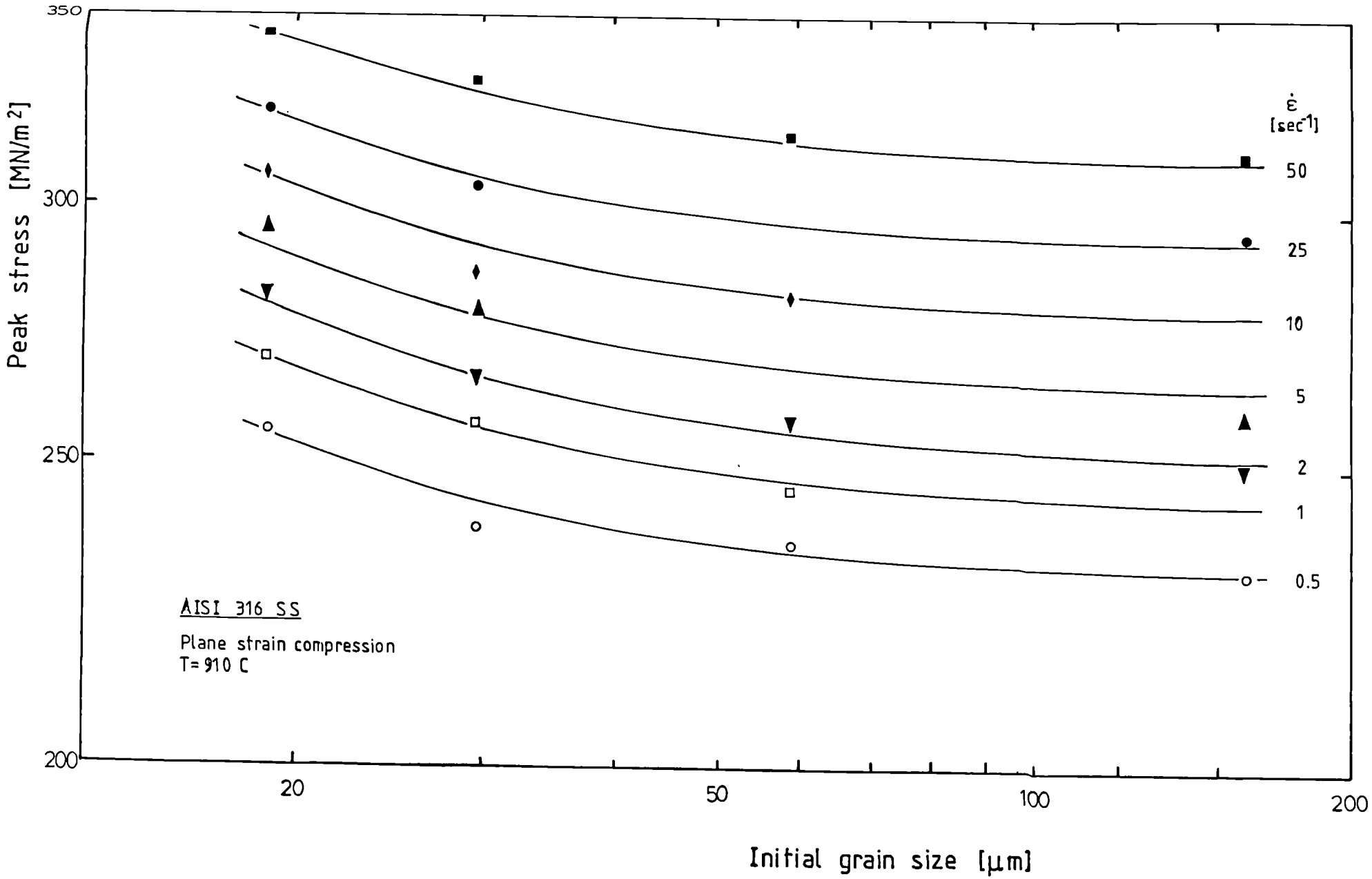
350
300
250
200
Peak stress [MN/m²]
20
50
100
200
Initial grain size [μm]
ε̇ [sec⁻¹]
50
25
10
5
2
1
0.5
AISI 316 SS
Plane strain compression
T= 910 C

Figure 73.- *Double deformation tests at strain rate of 0.5 sec^{-1}.*

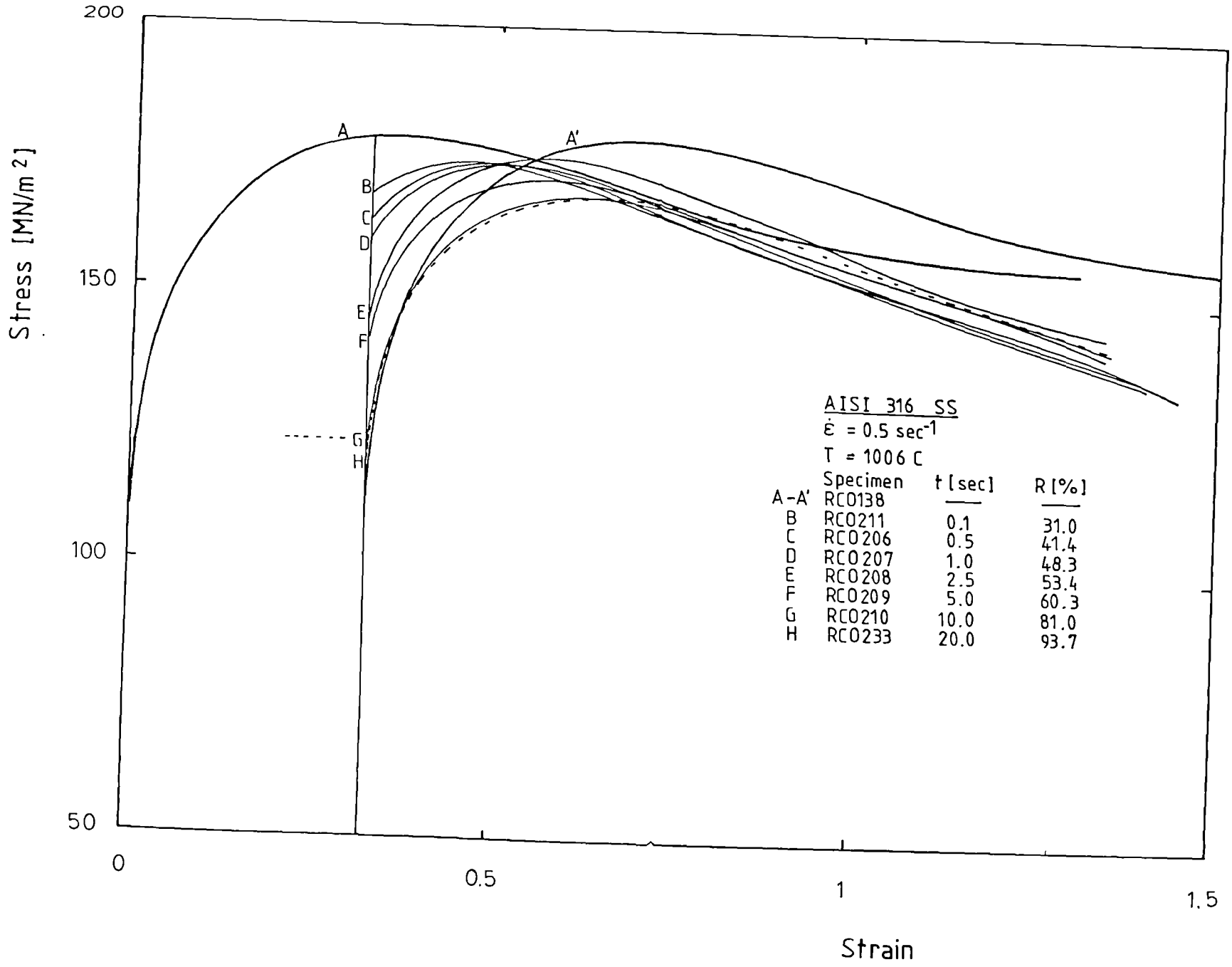
200
150
100
50
0
0.5
1
1.5
Stress [MN/m²]
Strain
A
A'
B
C
D
E
F
G
H
AISI 316 SS
ε̇ = 0.5 sec⁻¹
T = 1006 C
Specimen t [sec] R [%]
A-A' RC0138
B RC0211 0.1 31.0
C RC0206 0.5 41.4
D RC0207 1.0 48.3
E RC0208 2.5 53.4
F RC0209 5.0 60.3
G RC0210 10.0 81.0
H RC0233 20.0 93.7

Figure 74.- Double deformation tests at strain rate of 5 sec^{-1}.

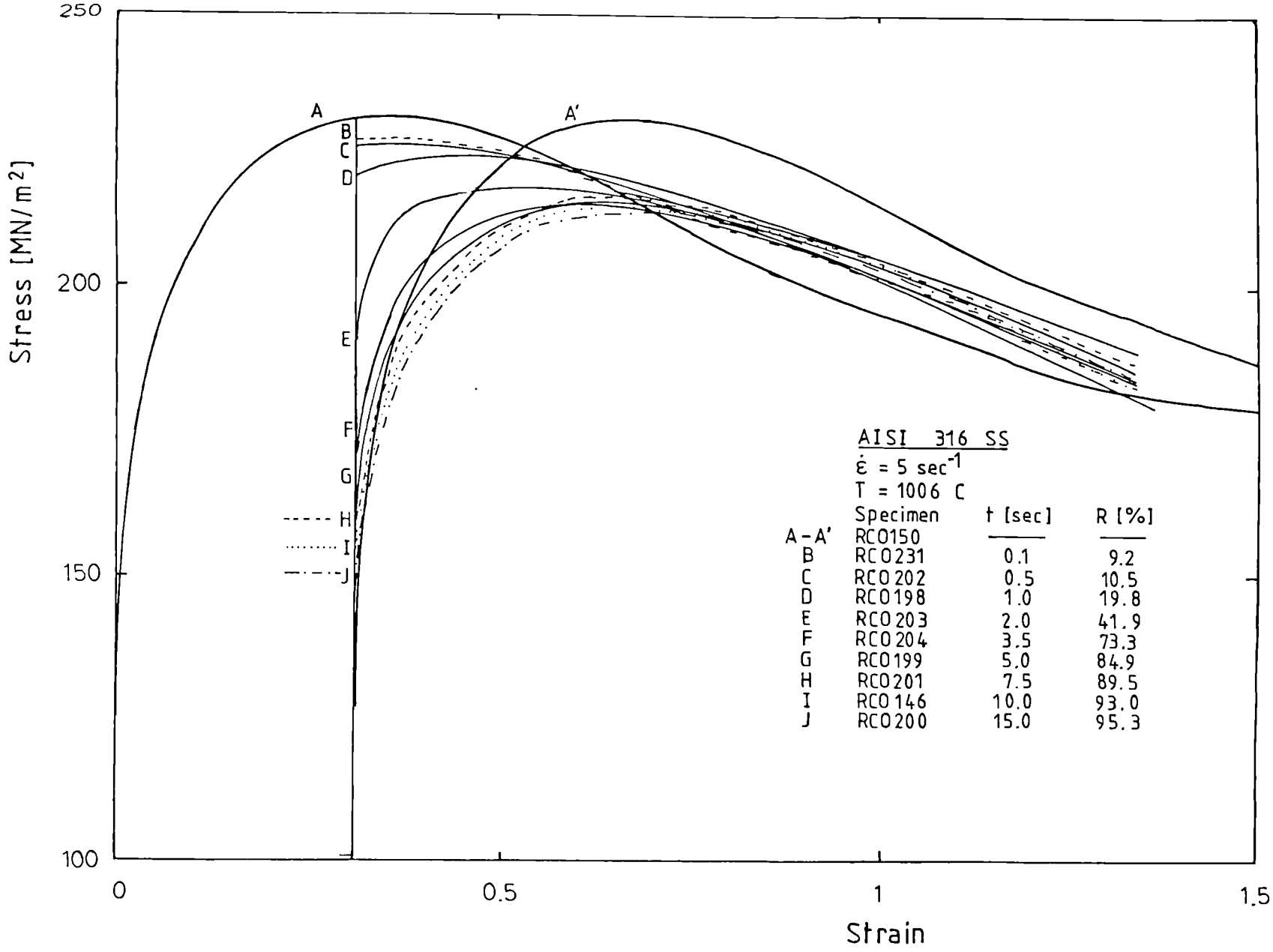
250
200
150
100
Stress [MN/m²]
0
0.5
1
1.5
Strain
A
A'
B
C
D
E
F
G
H
I
J
AISI 316 SS
ε̇ = 5 sec⁻¹
T = 1006 C
Specimen
t [sec]
R [%]
A-A' RC0150
B RC0231 0.1 9.2
C RC0202 0.5 10.5
D RC0198 1.0 19.8
E RC0203 2.0 41.9
F RC0204 3.5 73.3
G RC0199 5.0 84.9
H RC0201 7.5 89.5
I RC0146 10.0 93.0
J RC0200 15.0 95.3

Figure 75.- Restoration curves for the tests shown in figures 73 and 74.

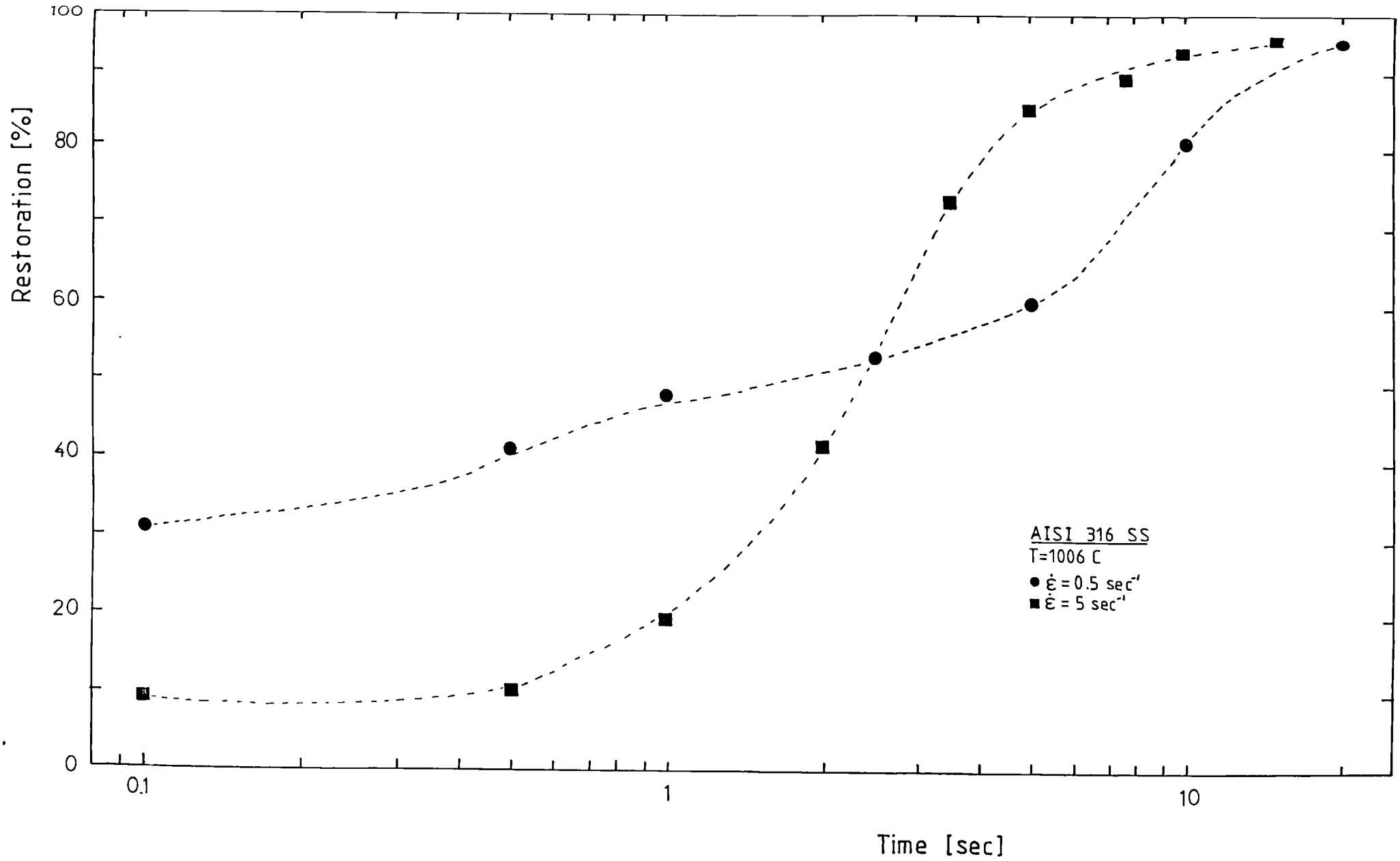
100
80
60
40
20
0
Restoration [%]
0.1
1
10
Time [sec]
AISI 316 SS
T=1006 C
● $\dot{\varepsilon}$ = 0.5 sec^{-1}
■ $\dot{\varepsilon}$ = 5 sec^{-1}

Figure 76.- Stress-strain curves of the interrupted tests used to measured the strain distribution analysis and its correspondence with the microstructure. a.) T = 910 C. b.) T = 1006 C.

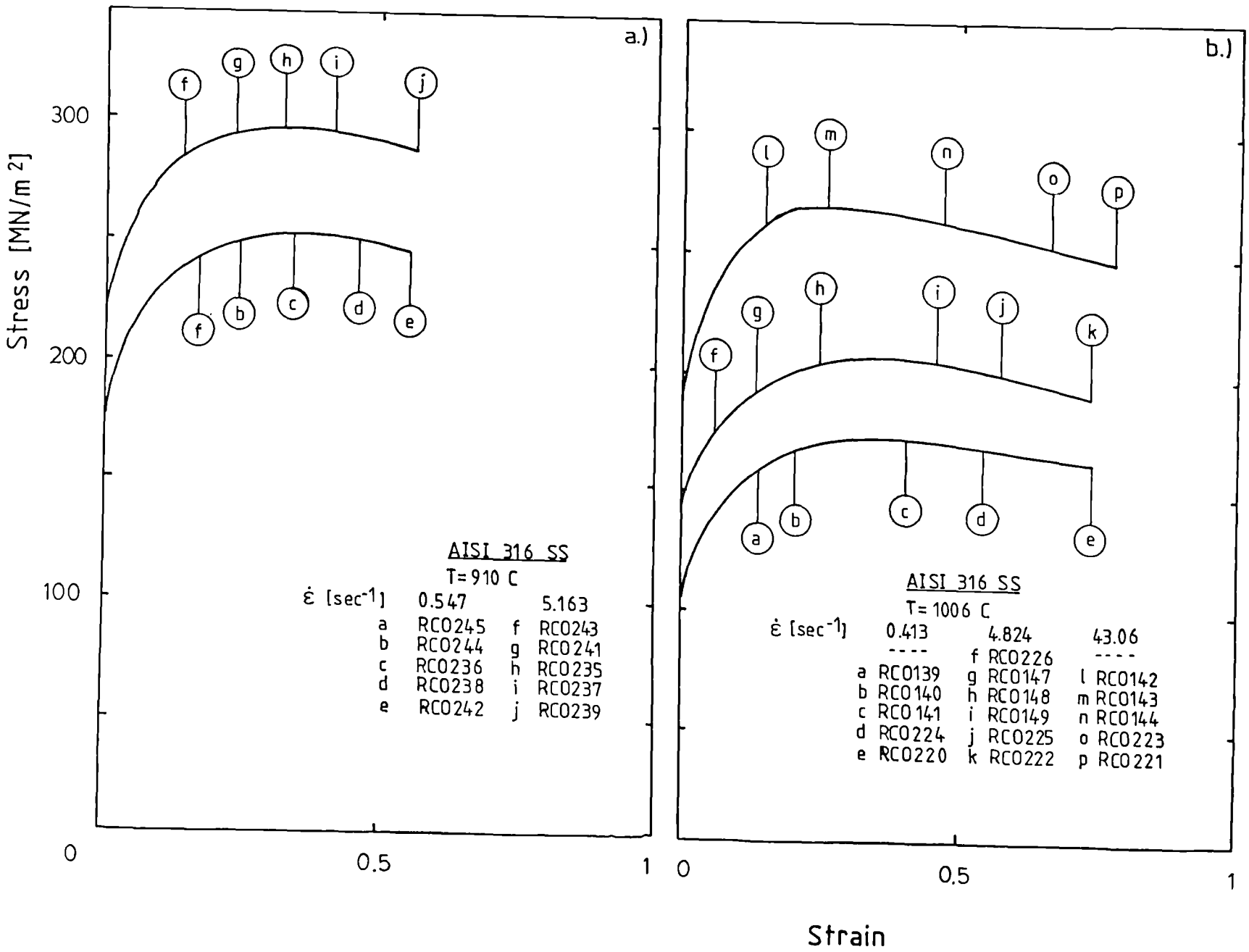
a.)
b.)
Stress [MN/m 2]
300
200
100
0
0.5
1
Strain
AISI 316 SS
T= 910 C
ε̇ [sec-1] 0.547 5.163
a RC0245 f RC0243
b RC0244 g RC0241
c RC0236 h RC0235
d RC0238 i RC0237
e RC0242 j RC0239
AISI 316 SS
T= 1006 C
ε̇ [sec-1] 0.413 4.824 43.06
---- ---- ----
f RC0226
a RC0139 g RC0147 l RC0142
b RC0140 h RC0148 m RC0143
c RC0141 i RC0149 n RC0144
d RC0224 j RC0225 o RC0223
e RC0220 k RC0222 p RC0221

Figure 77.- Photographs of grids after deformation, 5 X.

Specimen	Nominal strain	Strain rate [sec^{-1}]
RC0226	0.058	4.824
RC0139	0.137	0.413
RC0147	0.131	4.824
RC0142	0.147	43.06

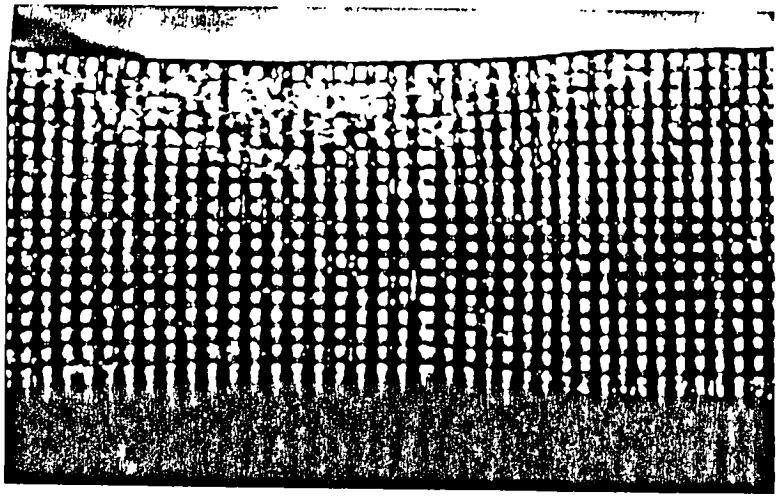

RC0226

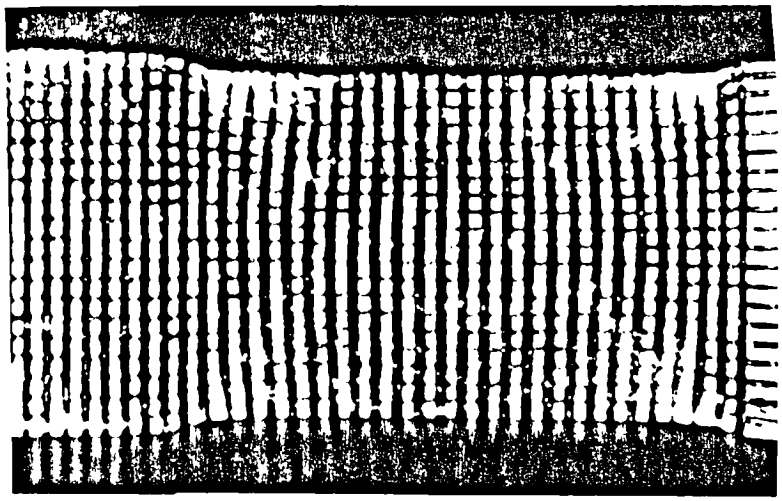

RC0139

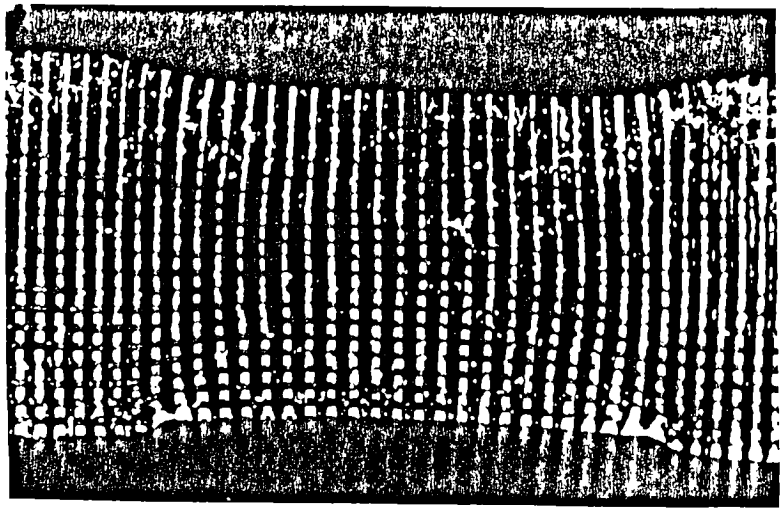

RC0147

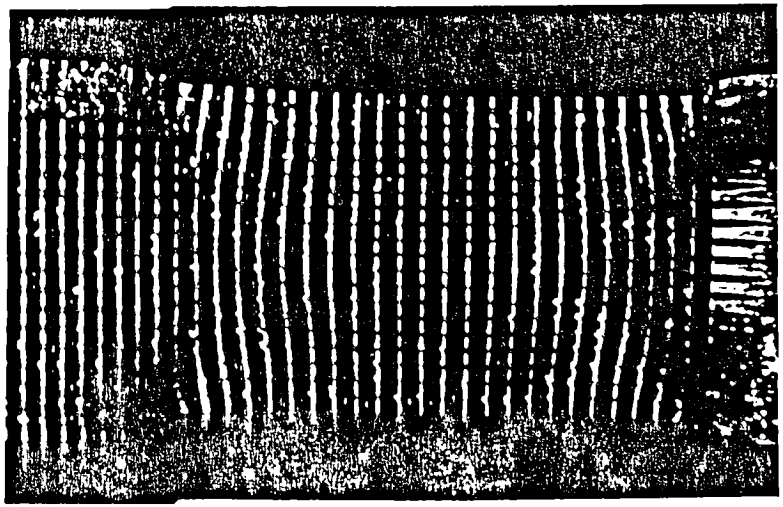

RC0142

Figure 78.- Photographs of grids after deformation, 5 X.

Specimen	Nominal strain	Strain rate [sec^{-1}]
RC0140	0.202	0.413
RC0148	0.243	4.824
RC0143	0.268	43.06

RC0140

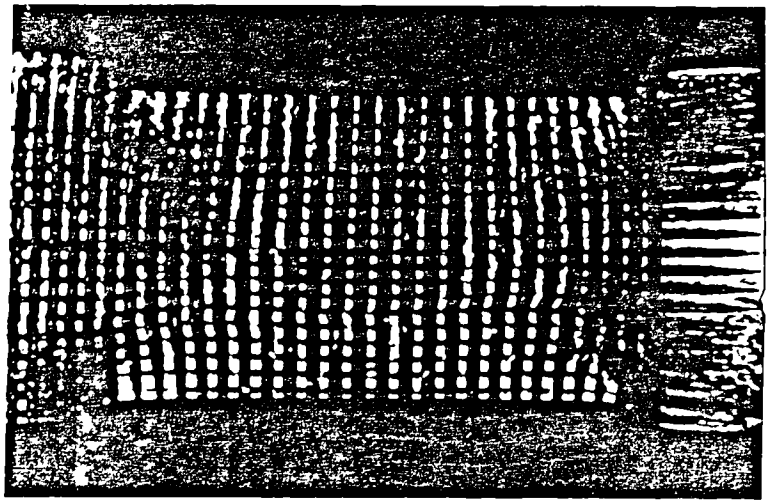

RC0148

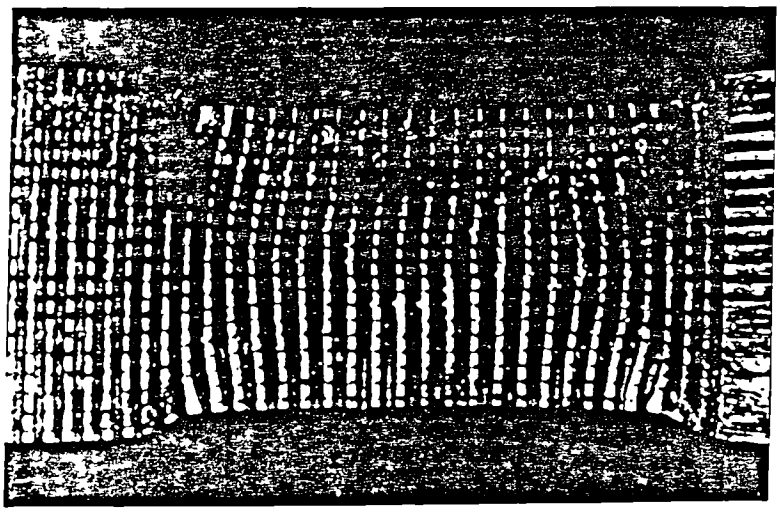

RC0143

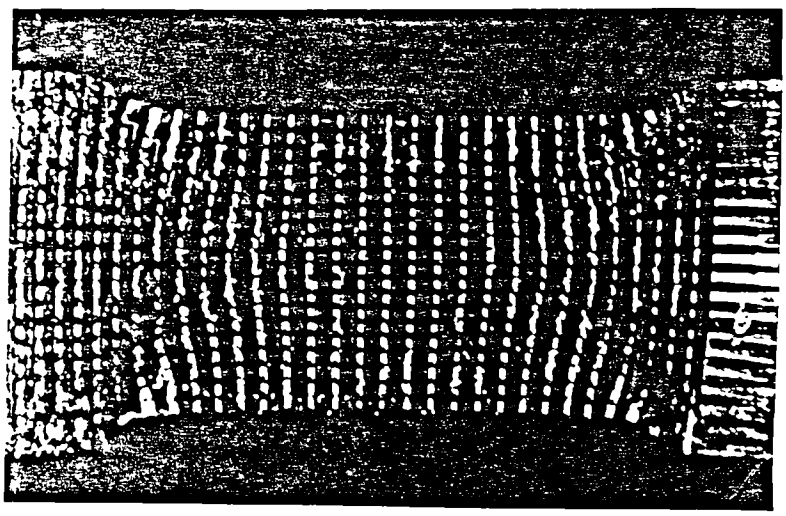

Figure 79.- Photographs of grids after deformation, 5 X.

Specimen	Nominal strain	Strain rate [sec^{-1}]
RC0141	0.401	0.413
RC0149	0.458	4.824
RC0144	0.470	43.06

RC0141

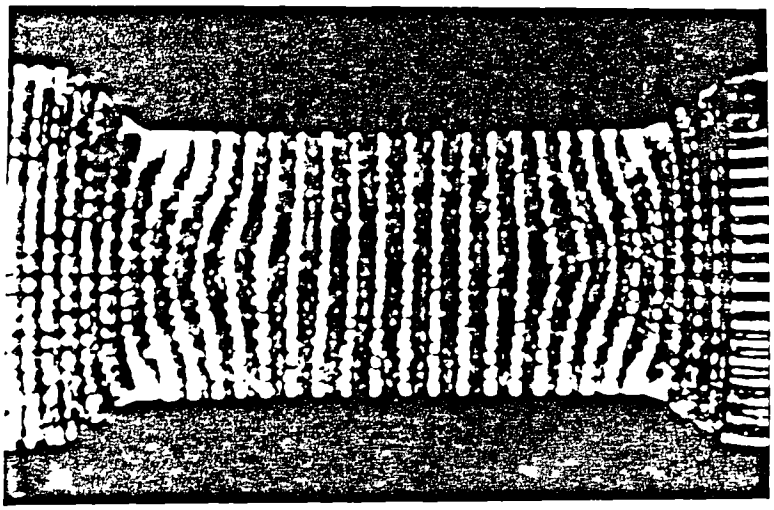

RC0149

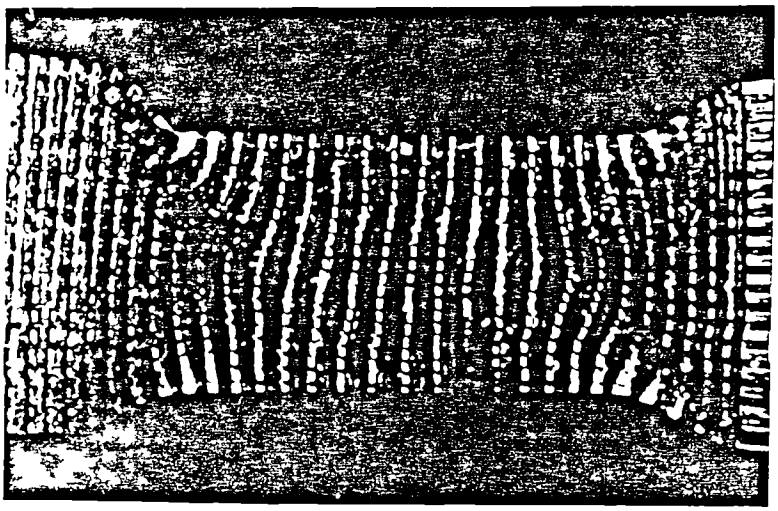

RC0144

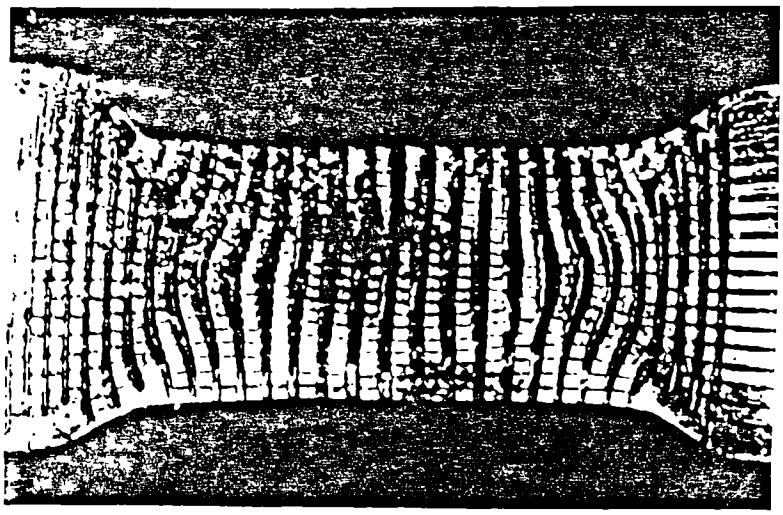

Figure 80.- Photographs of grids after deformation, 5 X.

Specimen	Nominal strain	Strain rate [sec^{-1}]
RC0224	0.538	0.413
RC0225	*0.573*	*4.824*
RC0223	0.662	43.06

RC0224

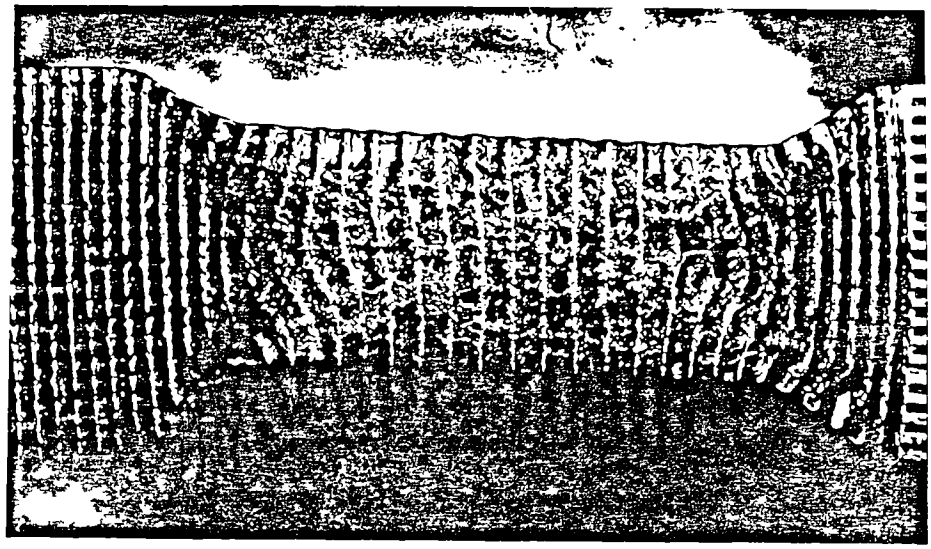

RC0225

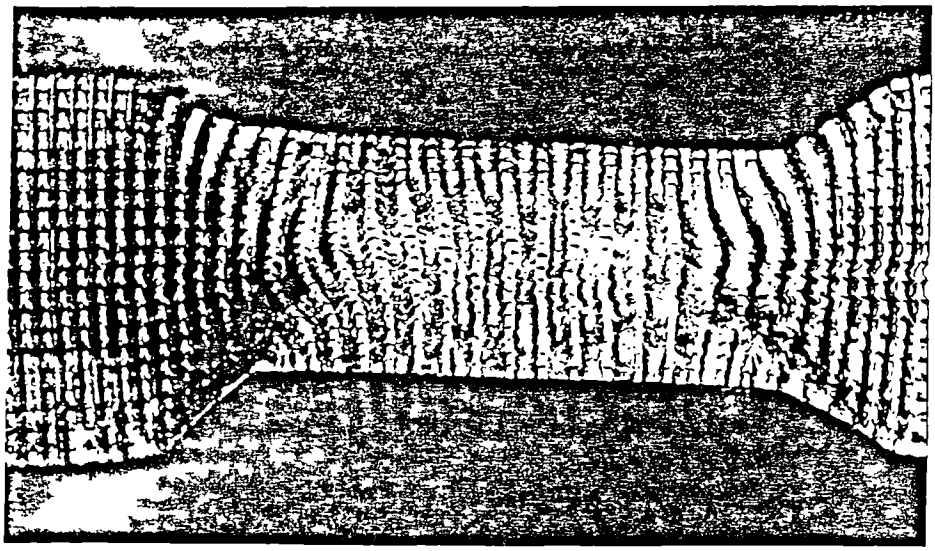

RC0223

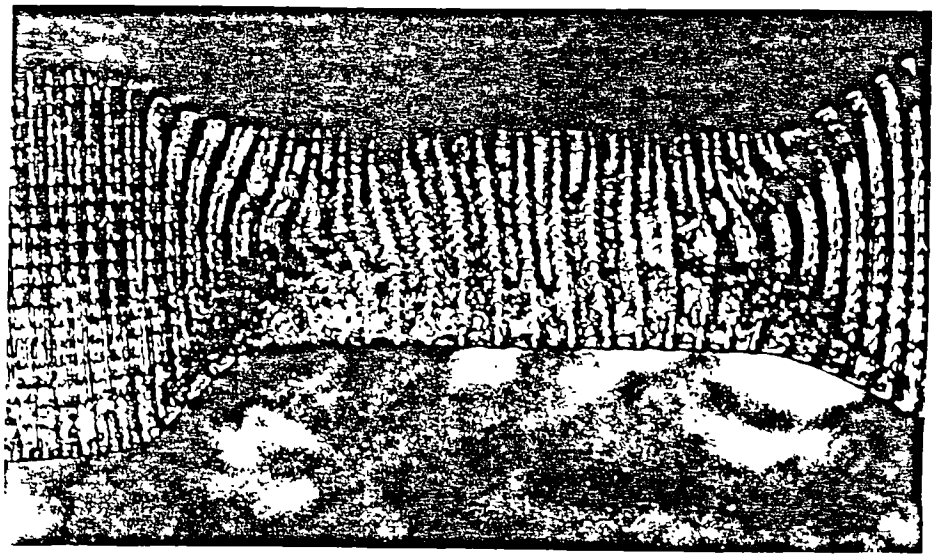

Figure 81.- Photographs of grids after deformation, 5 X.

Specimen	Nominal strain	Strain rate [sec^{-1}]
RC0220	0.735	0.413
RC0222	0.734	4.824
RC0221	0.779	43.06

RC0220

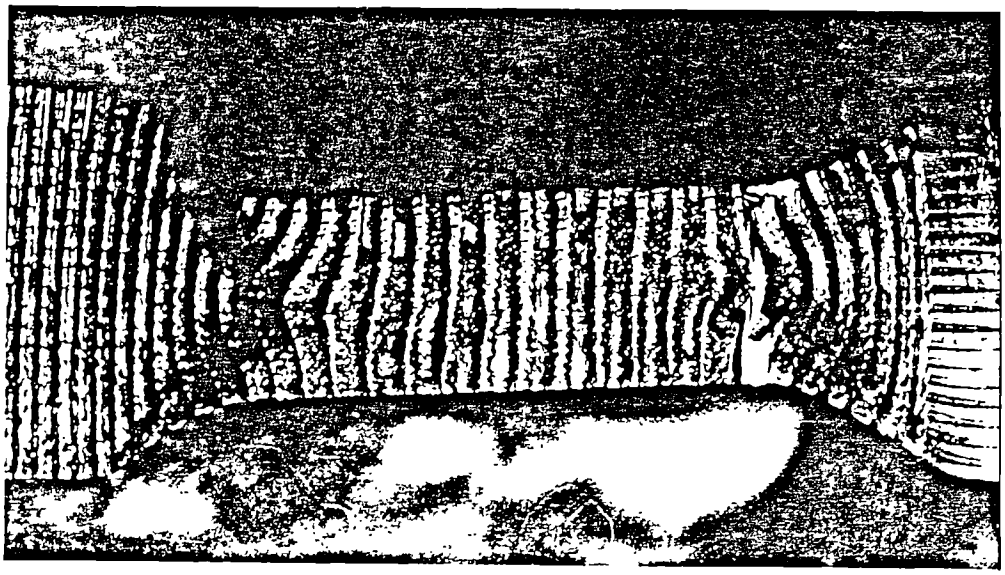

RC0222

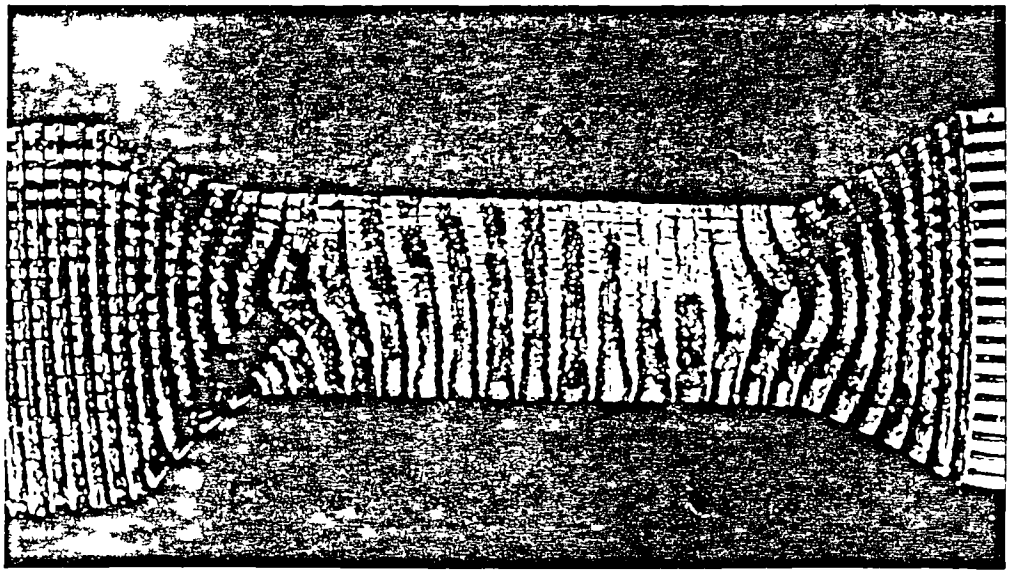

RC0221

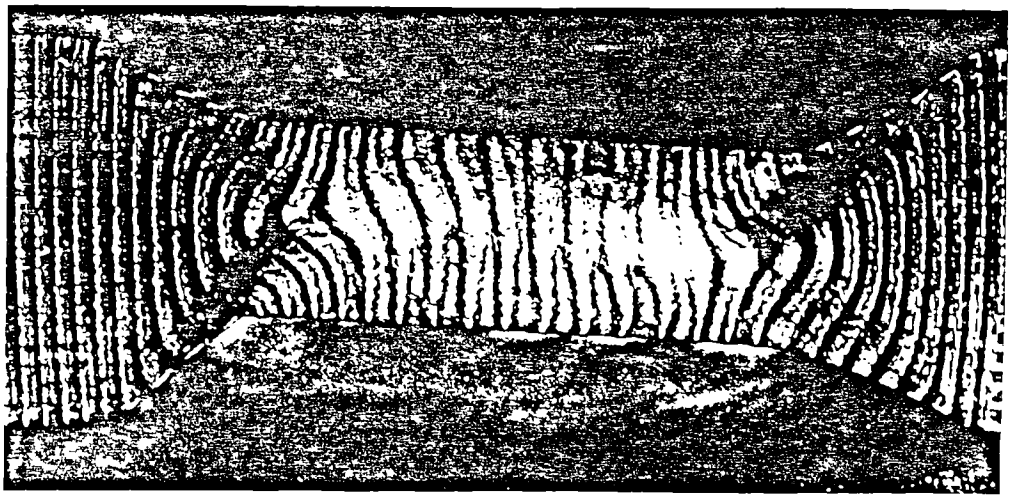

Figure 82.- Deformation paths of the nodes obtained from gridded specimens tested at 0.413 sec^{-1}. Only alternate columns and rows are marked.

AISI 316 SS

$\dot{\epsilon} = 0.413\ sec^{-1}$

A Undeformed
B RC0139
C RC0140
D RC0141
E RC0224
F RC0220

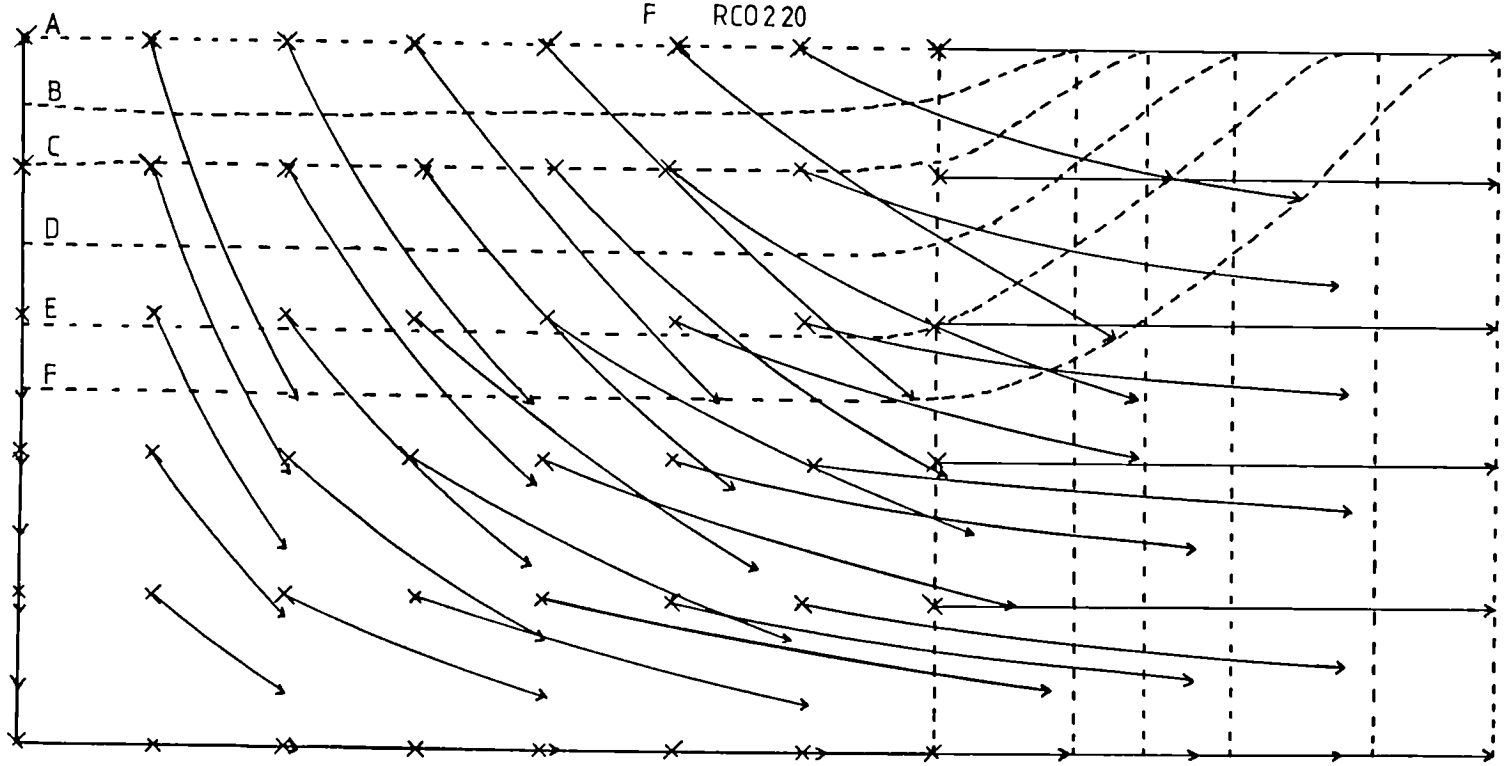

Figure 83.- Deformation paths of the nodes obtained from gridded specimens tested at 4.824 sec^{-1}. Only alternate columns and rows are marked.

AISI 316 SS

$\dot{\varepsilon} = 4.824\ sec^{-1}$

A Undeformed
B RC0147
C RC0148
D RC0149
E RC0225
F RC0222

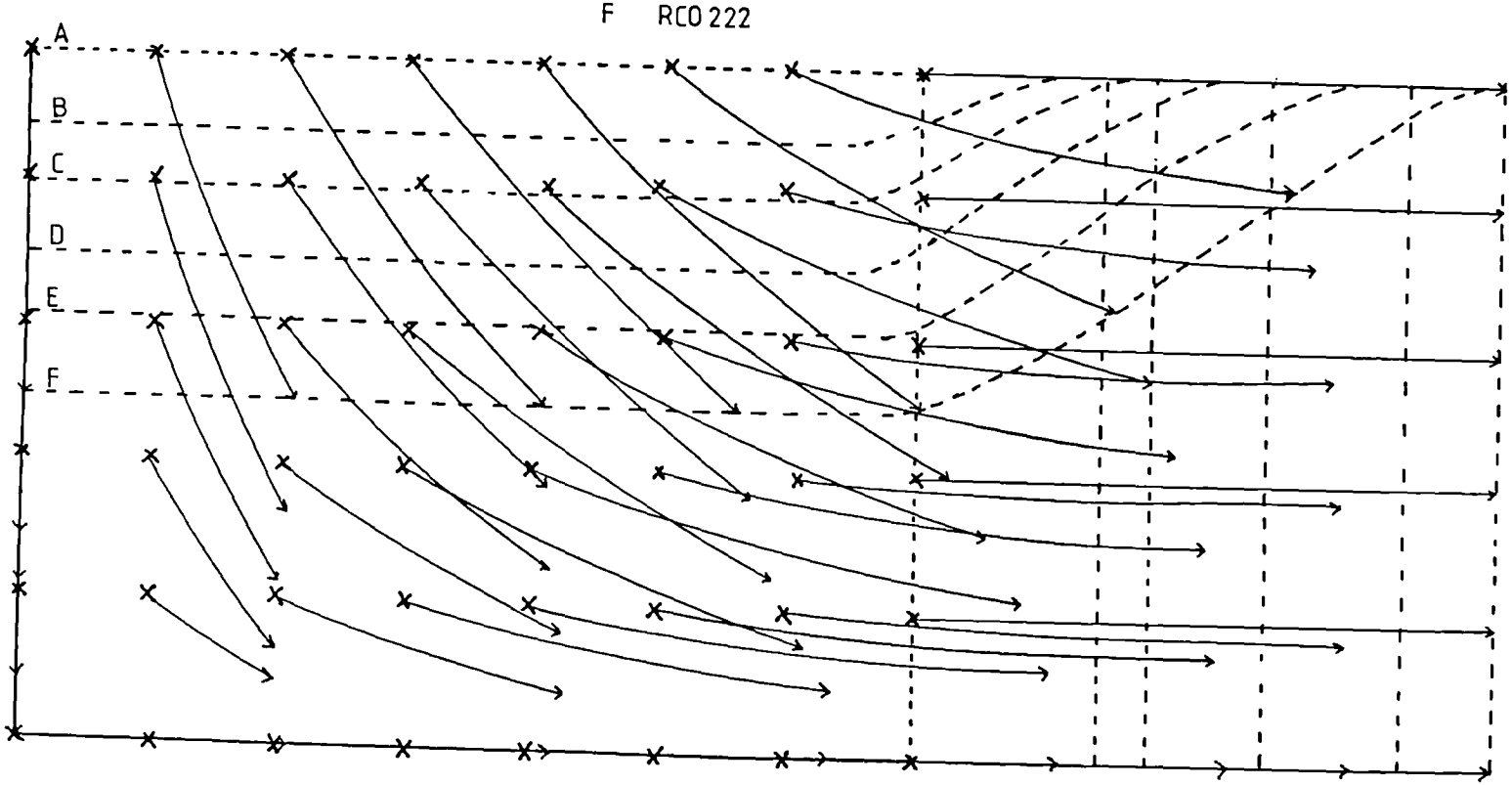

Figure 84.- Deformation paths of the nodes obtained from gridded specimens tested at 43.06 sec^{-1}. Only alternate columns and rows are marked.

AISI 316 SS

$\dot{\epsilon} = 43.06\ sec^{-1}$

A Undeformed
B RC0142
C RC0143
D RC0144
E RC0223
F RC0221

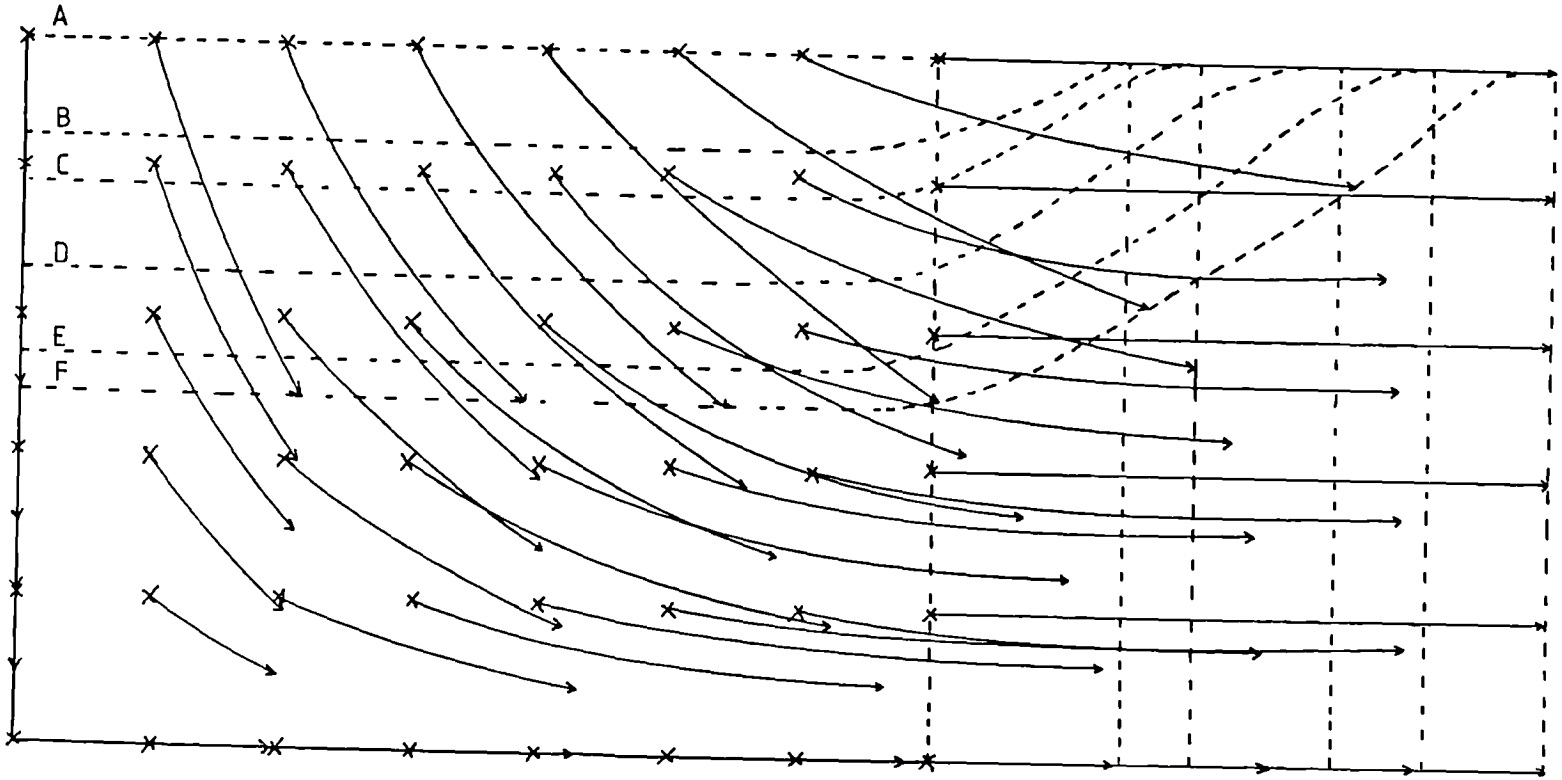

Figure 85.- Strain distribution map of specimens deformed at 0.413 sec^{-1}.

Test	Nominal strain
RC0139	0.137
RC0140	0.202
RC0141	0.401

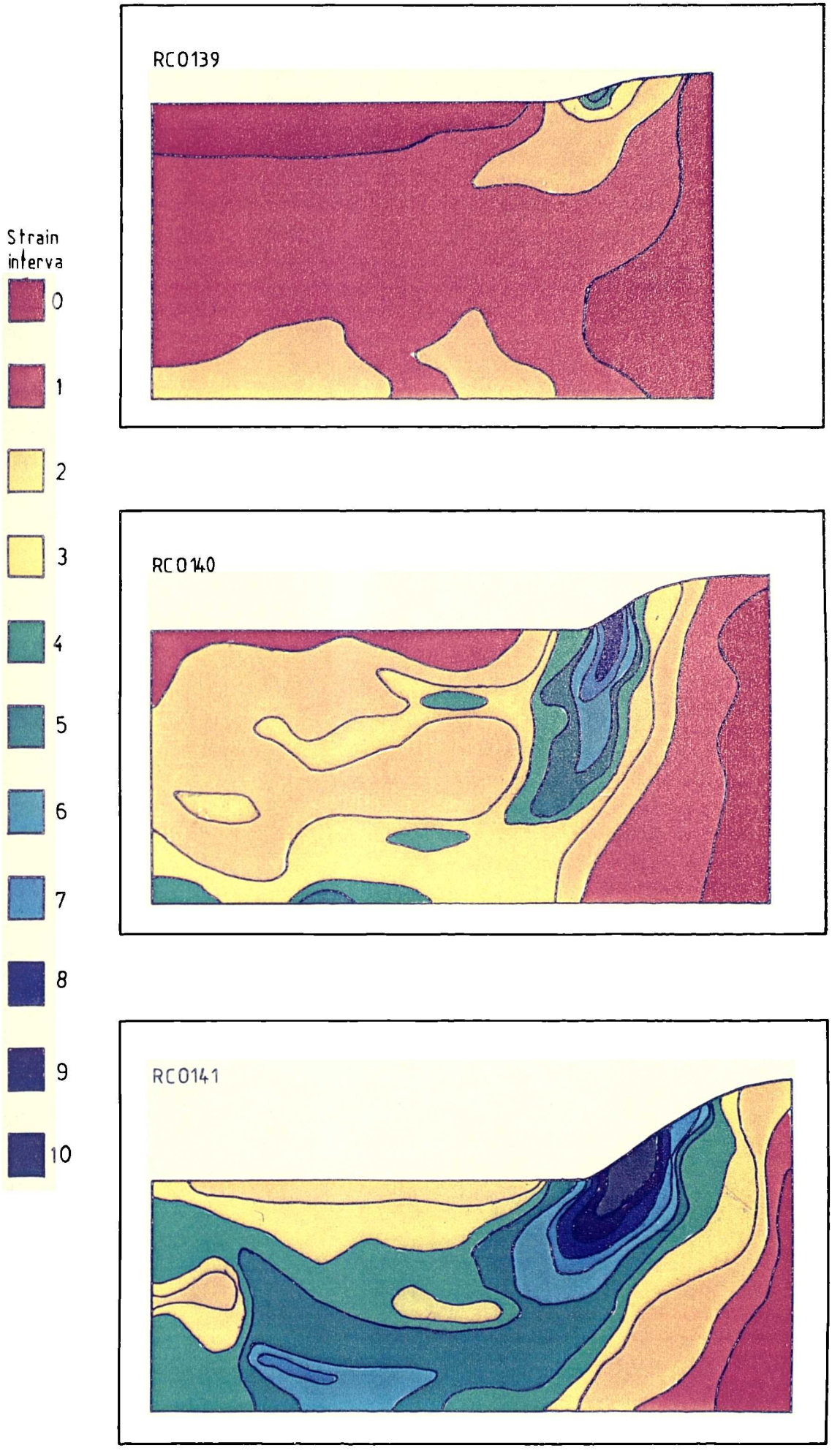
Strain
interva
0
1
2
3
4
5
6
7
8
9
10
RC0139
RC0140
RC0141

Figure 86.- Strain distribution map of specimens deformed at 0.413 sec^{-1}.

Test	Nominal strain
RC0220	0.538
RC0224	0.735

RC0224

RC0220

Strain intervals

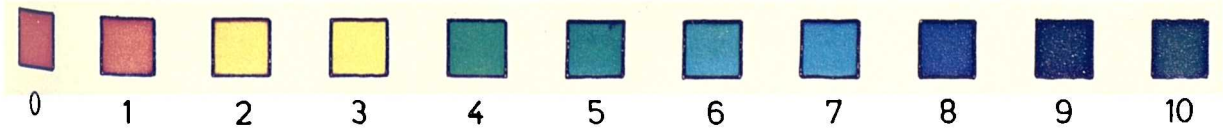

Figure 87.- Strain distribution map of specimen RC0226 deformed at 4.824 sec^{-1}, nominal strain 0.058.

RC0226

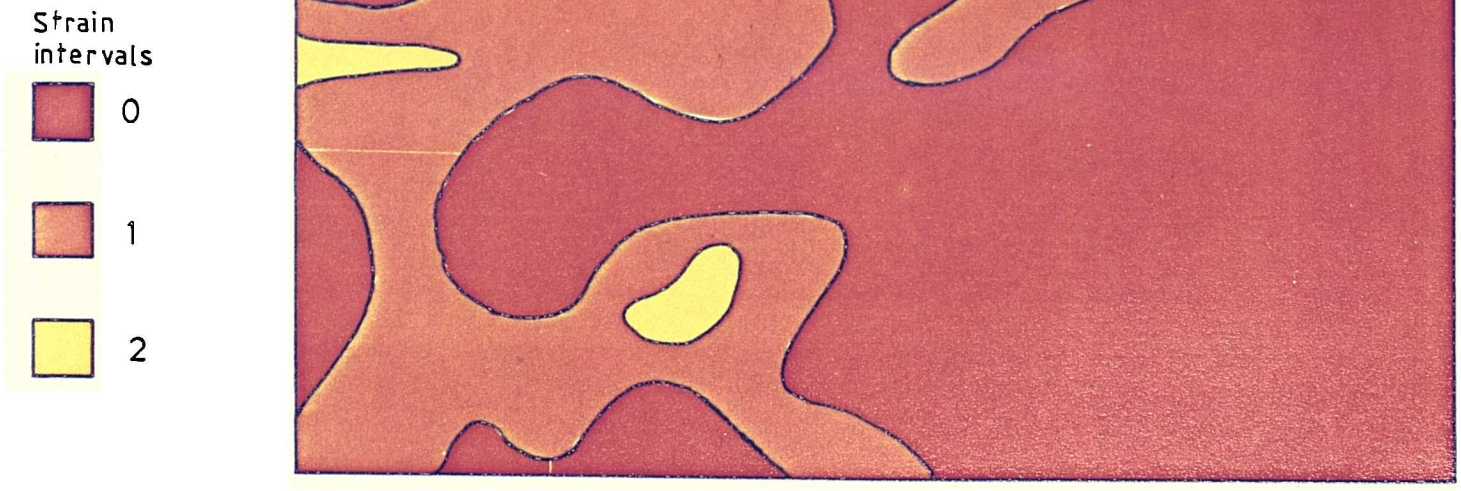

Figure 88.- Strain distribution map of specimens deformed at 4.824 sec^{-1}.

Test	Nominal strain
RC0147	0.131
RC0148	0.243
RC0149	0.458

Str·
inte als

0
1
2
3
4
5
6
7
8
9
10

RC0147

RC0148

RC0149

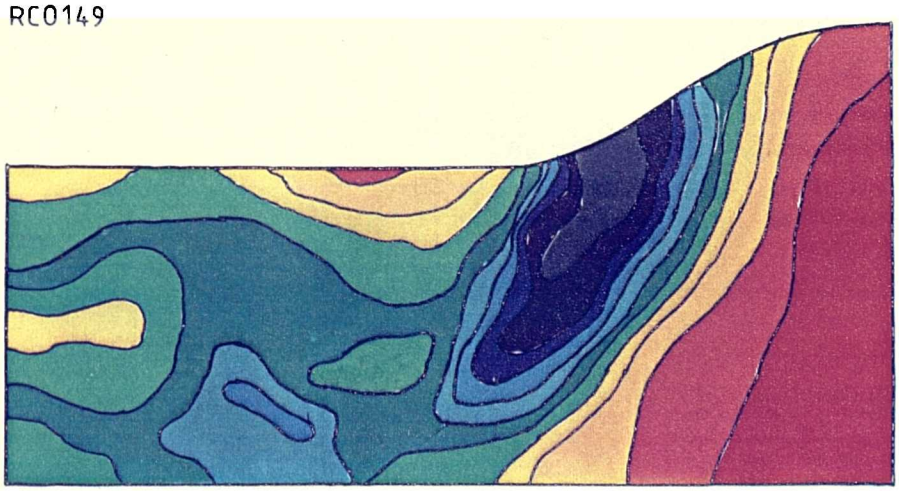

Figure 89.- Strain distribution map of specimens deformed at 4.824 sec^{-1}.

Test	Nominal strain
RC0225	0.573
RC0222	0.734

RC0225

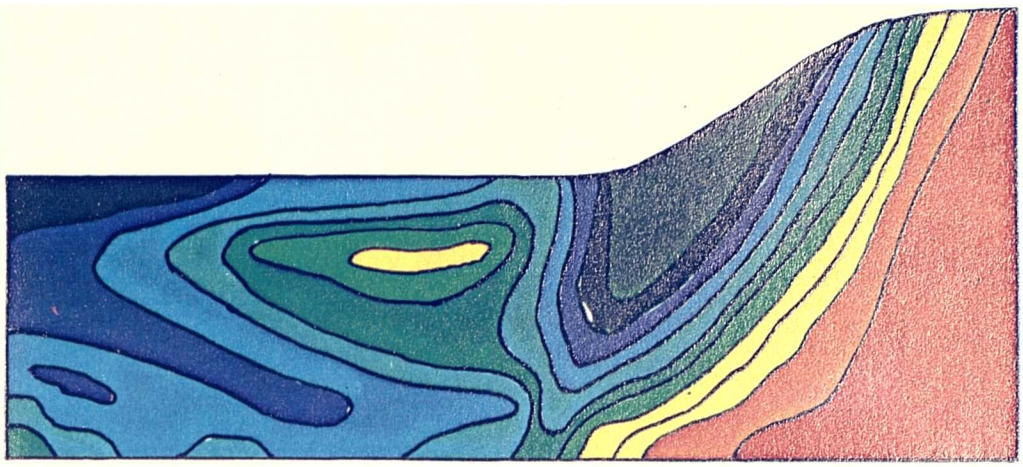

RC0222

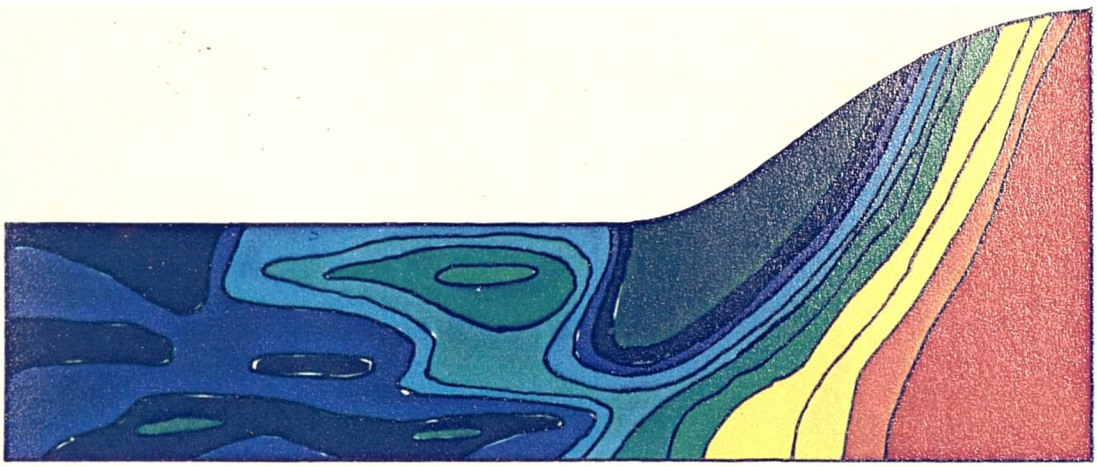

Strain intervals

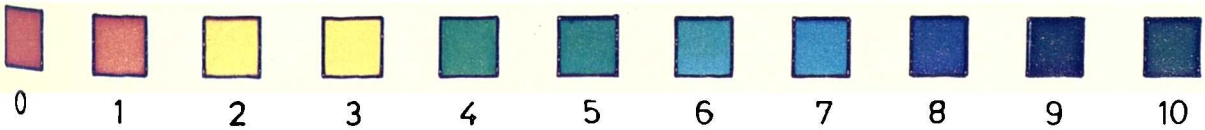

0 1 2 3 4 5 6 7 8 9 10

Figure 90.- Strain distribution map of specimens deformed at 43.06 sec^{-1}.

Test	Nominal strain
RC0142	0.147
RC0143	0.268
RC0144	0.470

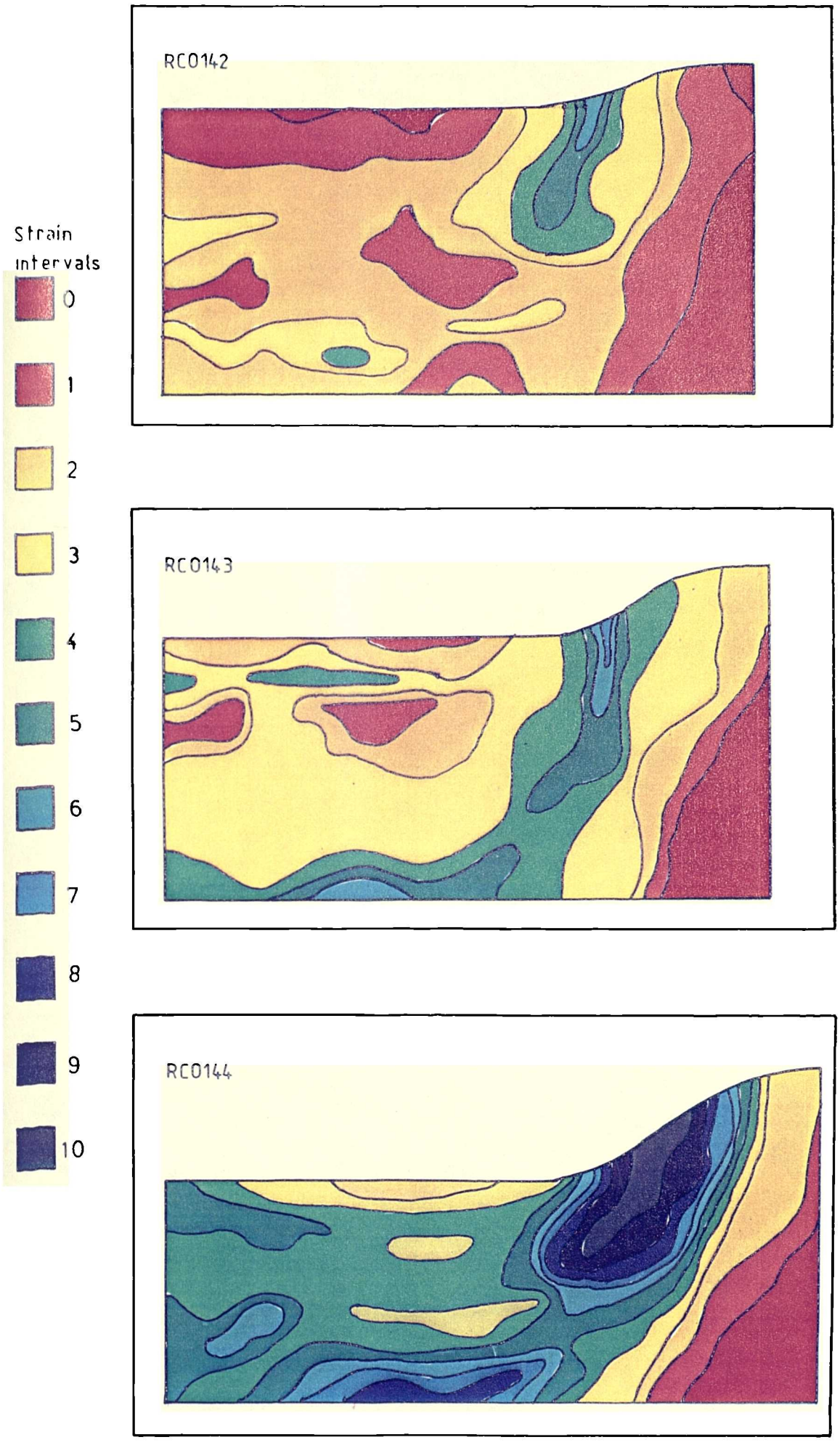
Strain intervals
0
1
2
3
4
5
6
7
8
9
10
RC0142
RC0143
RC0144

Figure 91.- Strain distribution map of specimens deformed at 43.06 sec^{-1}.

Test	Nominal strain
RC0223	0.662
RC0221	0.779

RCO223

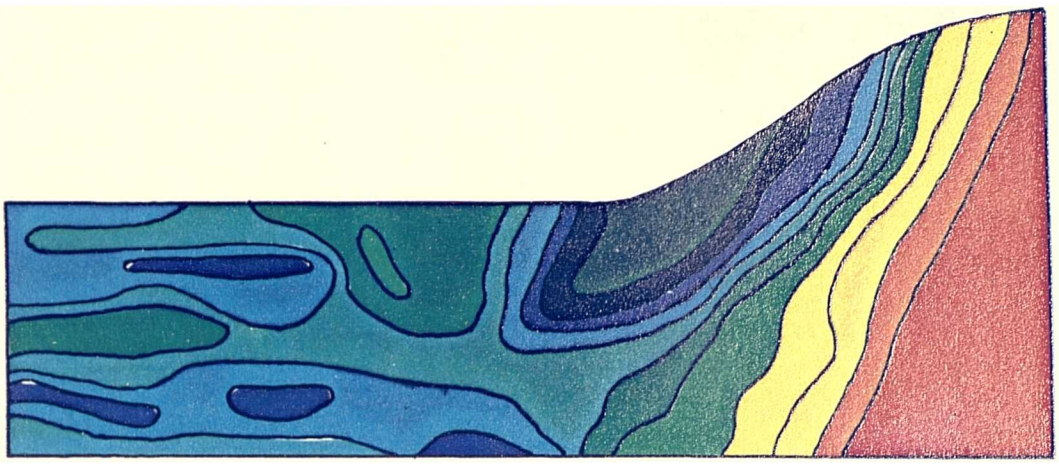

RCO221

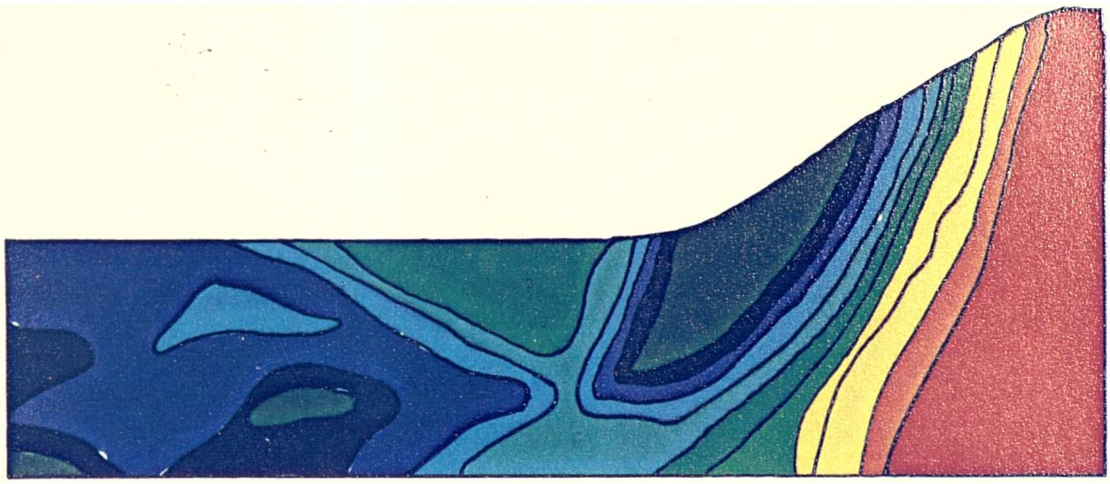

Strain intervals

Figure 92.- Histograms for the specimens deformed at 0.413 sec^{-1}. The strain intervals corresponds to the ones in the previous figures. The normalized intervals are the result of dividing the value of strain in each element by the nominal strain.

	Test
A	RC0139
B	RC0140
C	RC0141
D	RC0224
E	RC0220

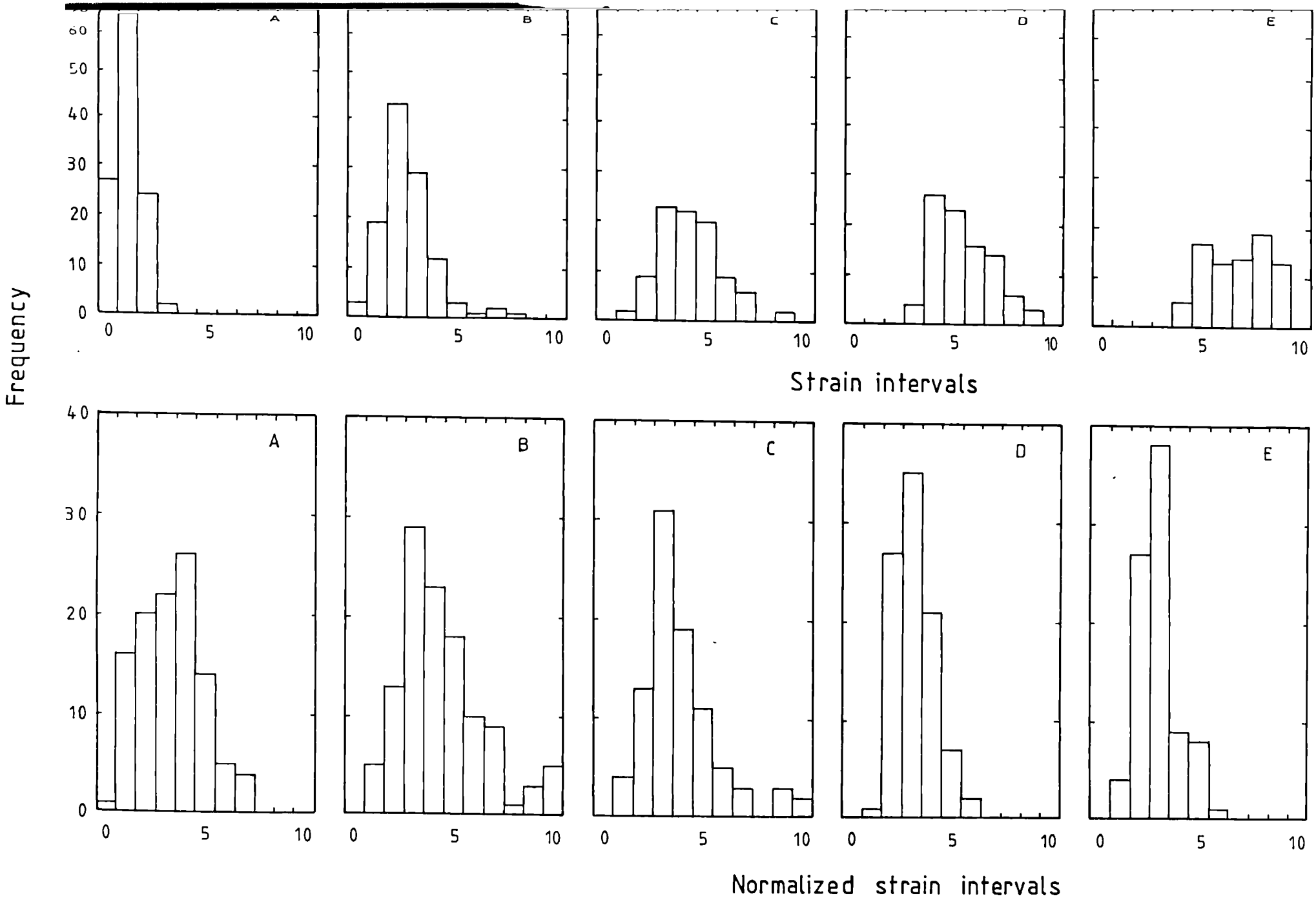
Frequency
A
B
C
D
E
0
10
20
30
40
50
60
0
5
10
Strain intervals
Normalized strain intervals

Figure 93.- Histograms for the specimens deformed at 4.824 sec^{-1}. The strain intervals corresponds to the ones in the previous figures. The normalized intervals are the result of dividing the value of strain in each element by the nominal strain.

	Test
F	RC0147
G	RC0148
H	RC0149
I	RC0225
J	RC0222

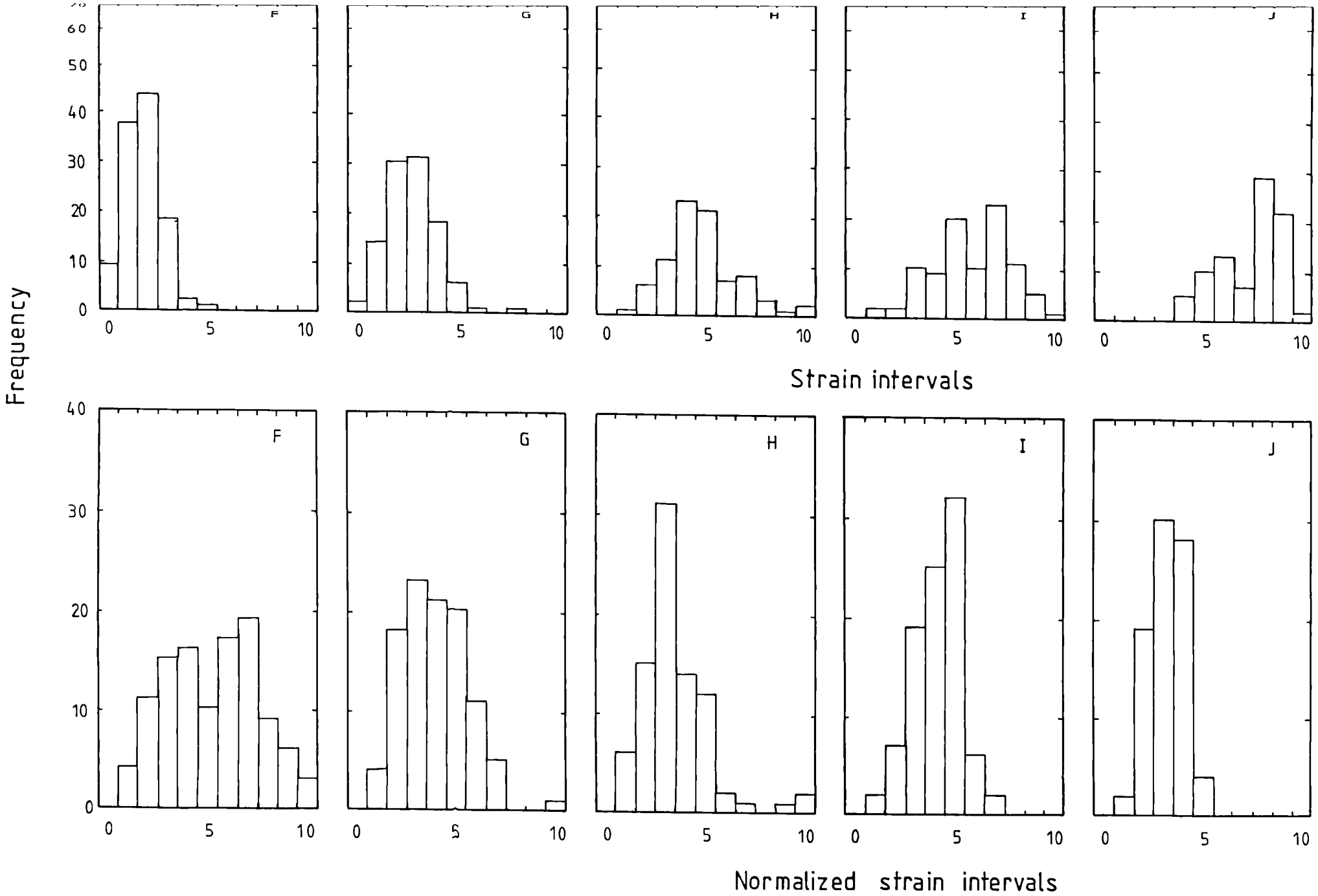
Frequency
F
G
H
I
J
0
5
10
20
30
40
50
60
Strain intervals
Normalized strain intervals

Figure 94.- Histograms for the specimens deformed at 43.06 sec^{-1}. The strain intervals corresponds to the ones in the previous figures. The normalized intervals are the result of dividing the value of strain in each element by the nominal strain.

	Test
K	RC0142
L	RC0143
M	RC0144
N	RC0223
O	RC0221

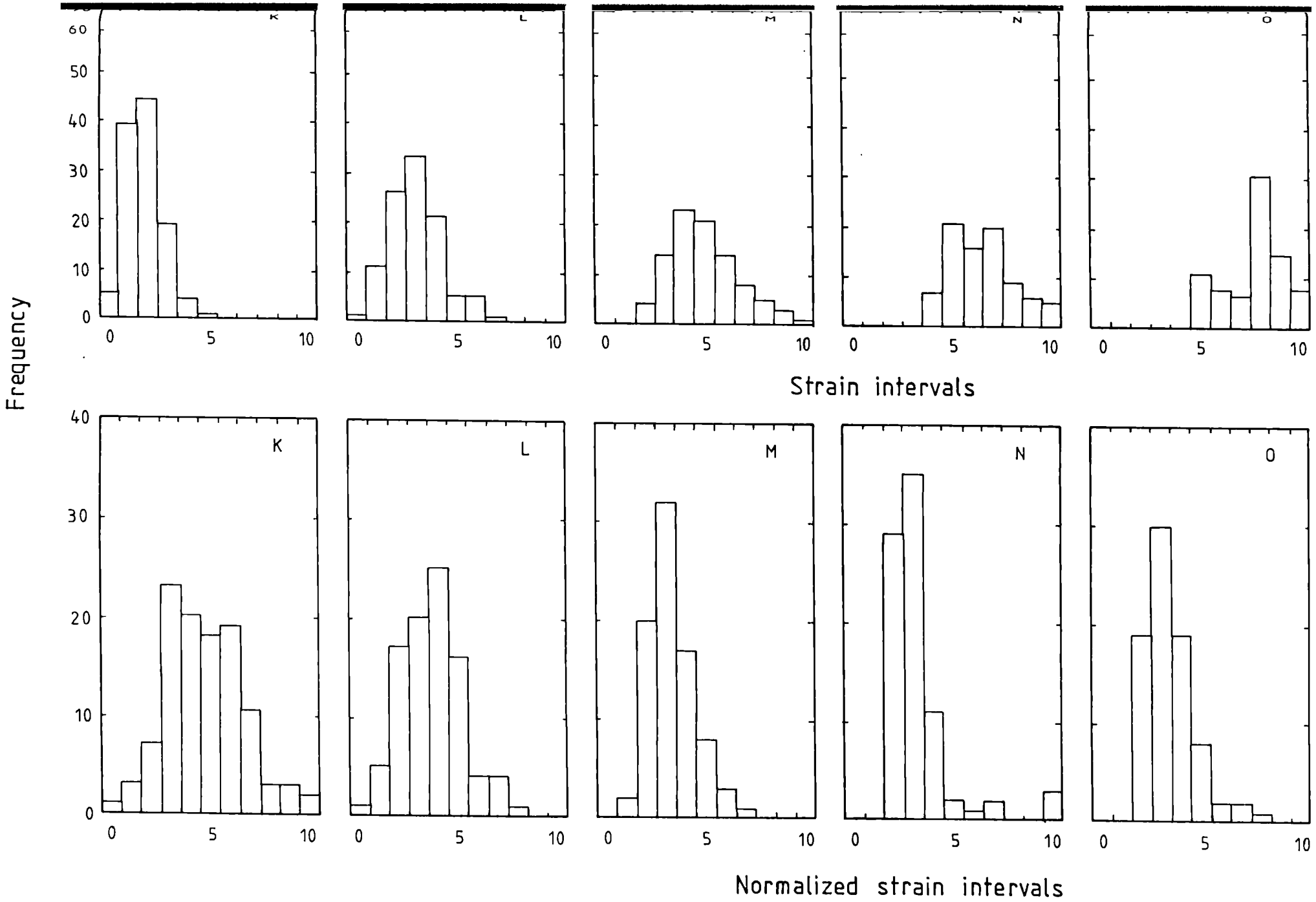
Frequency
K
L
M
N
O
Strain intervals
Normalized strain intervals

Figure 95.- Plot of the calculated average strain (corrected to allow deviation from the plane strain deformation mode) versus the nominal strain for the gridded specimens.

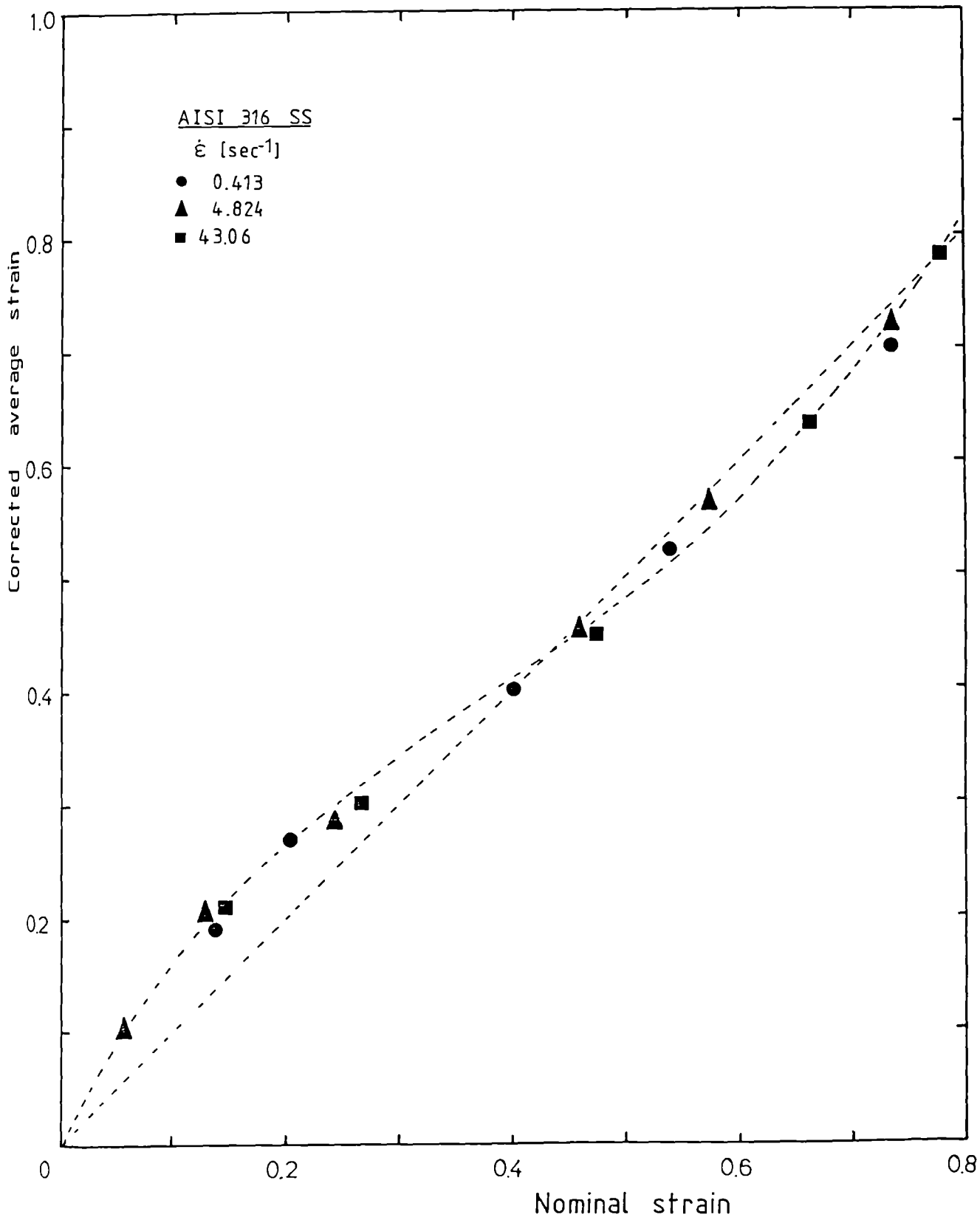
AISI 316 SS
$\dot{\varepsilon}$ [sec^{-1}]
0.413
4.824
43.06
Corrected average strain
Nominal strain
0
0.2
0.4
0.6
0.8
1.0

Figure 96.- Plot of the calculated strain average over the slip line field versus the average strain in the whole specimen area under the tools for the gridded specimens.

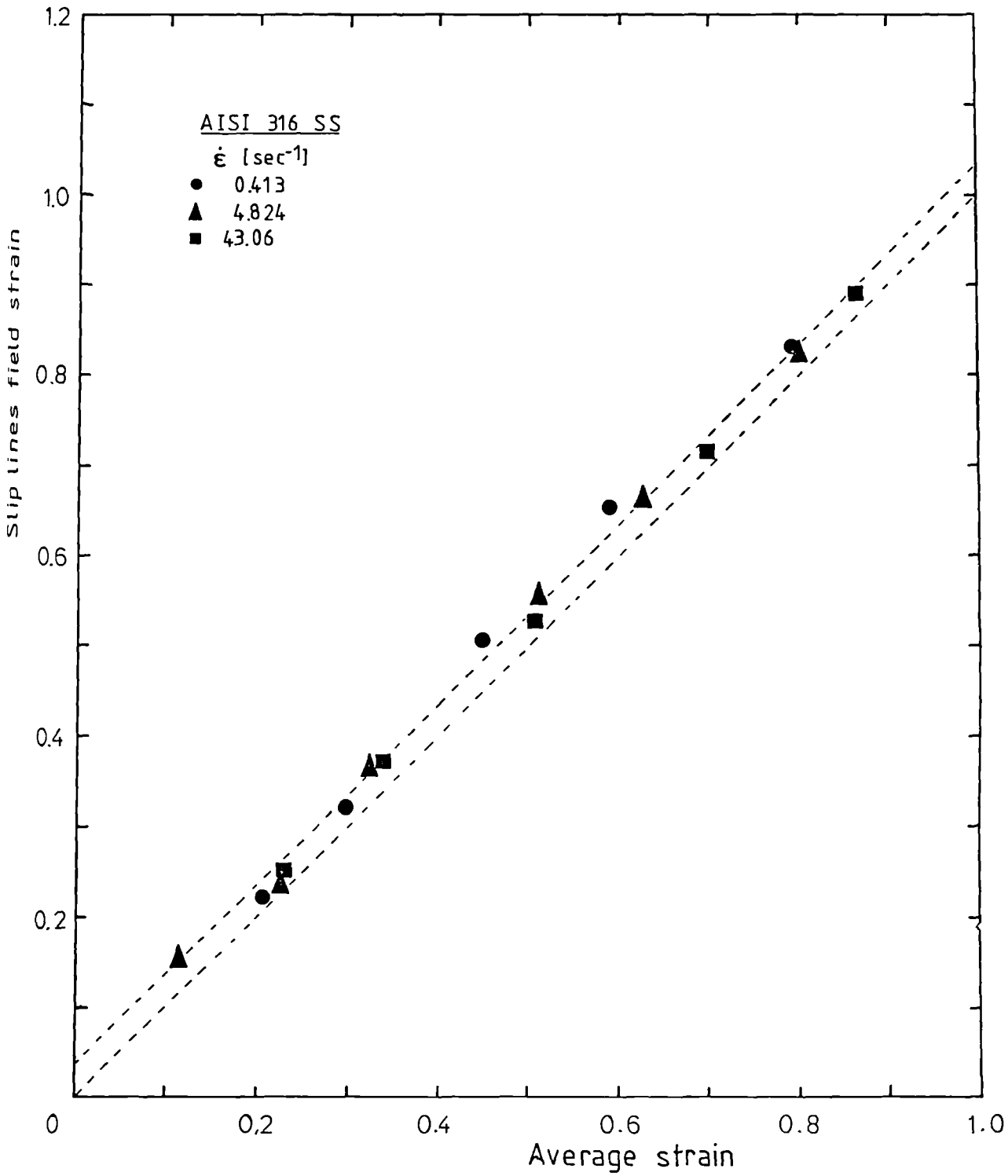
AISI 316 SS
$\dot{\epsilon}$ [sec^{-1}]
0.413
4.824
43.06
Slip lines field strain
Average strain
0
0,2
0.4
0.6
0.8
1.0
1.2

Figure 97.- Plot of the corrected average strain in the 10% of the deforming area with the highest and lowest strains against nominal strain.

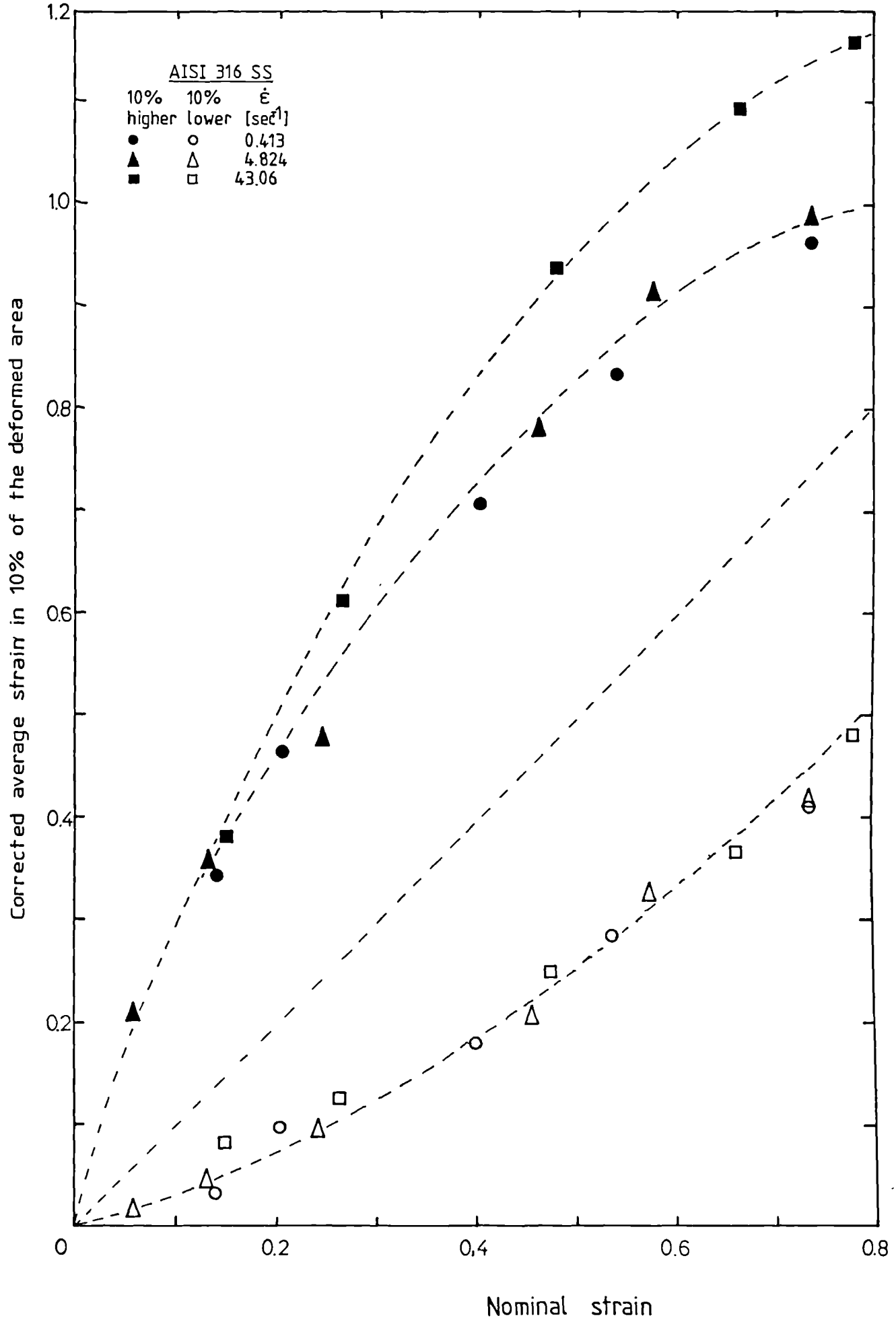
AISI 316 SS
10% higher
10% lower
ε̇ [sec⁻¹]
0.413
4.824
43.06
Corrected average strain in 10% of the deformed area
Nominal strain
0
0.2
0.4
0.6
0.8
1.0
1.2

Figure 98.- Micrographs from the centre of specimens deformed at 0.547 sec^{-1} at 910 C. 500 X.

Specimen	Nominal strain
RC0245	0.162
RC0244	0.240
RC0236	0.334
RC0238	0.451
RC0242	0.547

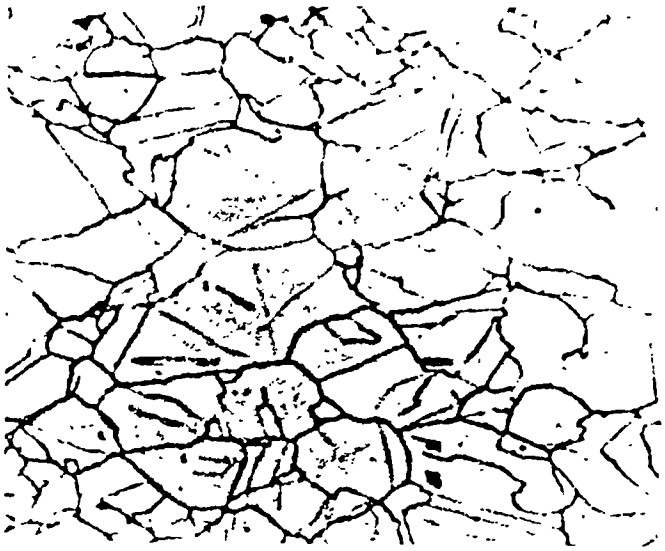

RC0245

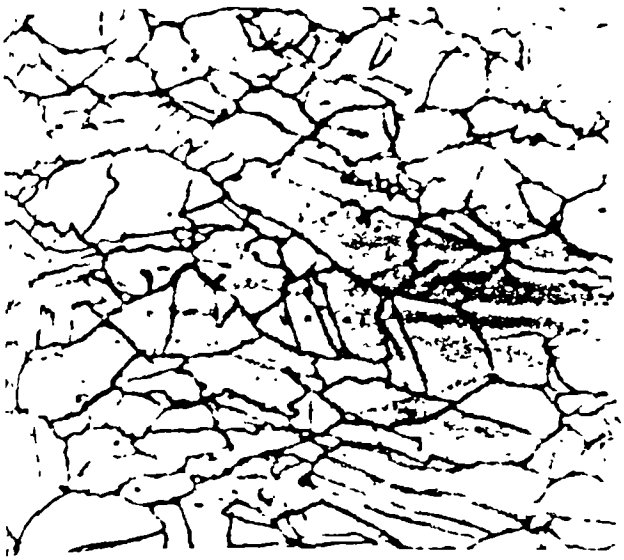

RC0244

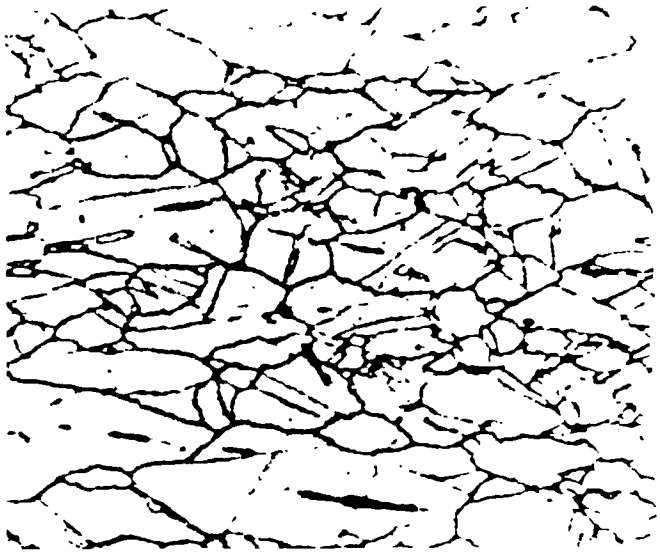

RC0236

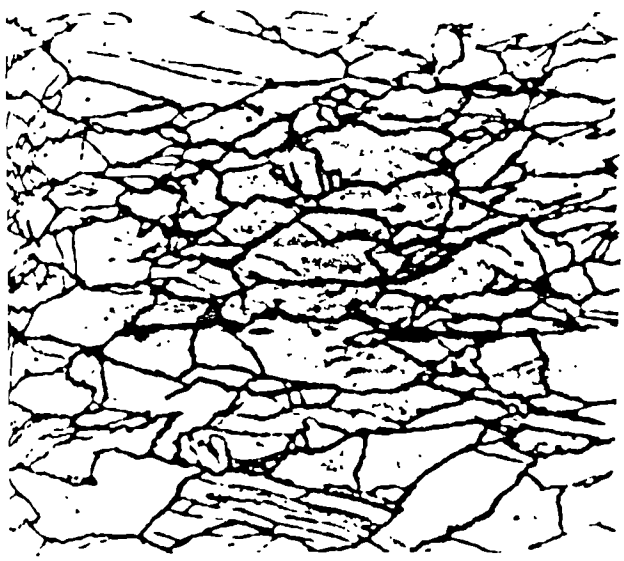

RC0238

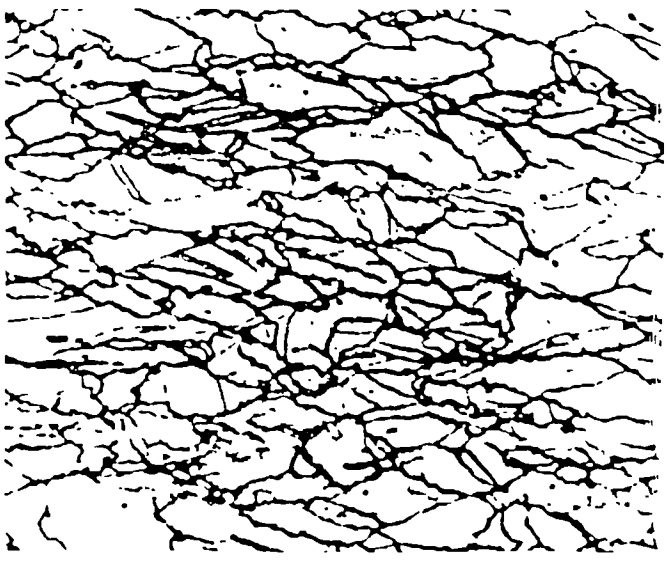

RC0242

Figure 99.- Micrographs from the centre of specimens deformed at 5.163 sec^{-1} at 910 C. 500 X.

Specimen	Nominal strain
RC0243	0.134
RC0241	0.232
RC0235	0.319
RC0237	0.419
RC0239	0.561

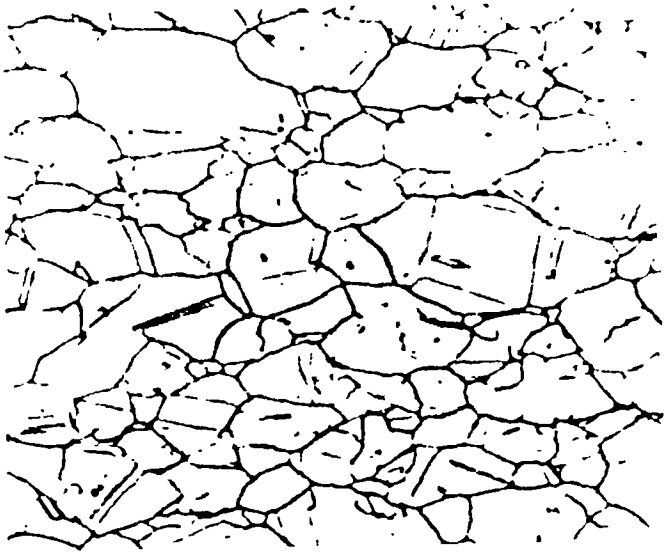

RC0243

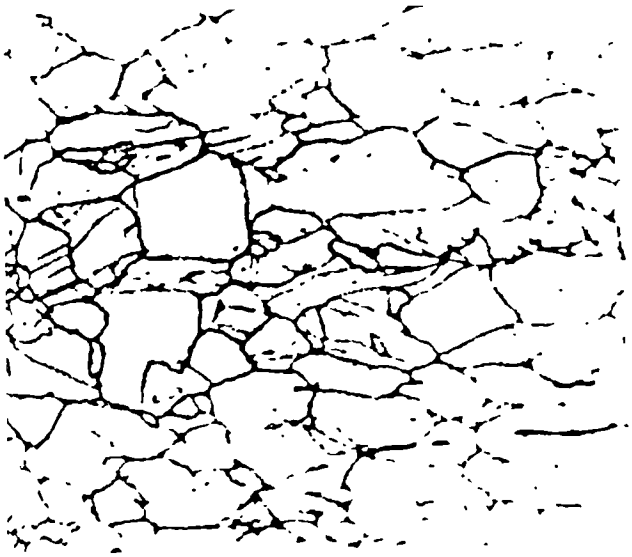

RC0241

RC0235

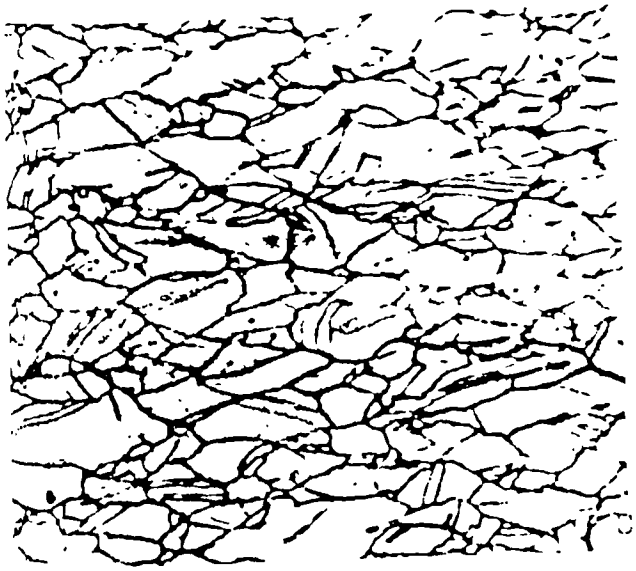

RC0237

RC0239

Figure 100.- Micrographs from the centre of specimens deformed at 0.413 sec^{-1} at 1006 C. 500 X.

Specimen	Nominal strain
RC0139	0.137
RC0140	0.202
RC0141	0.401
RC0224	0.538
RC0220	0.735

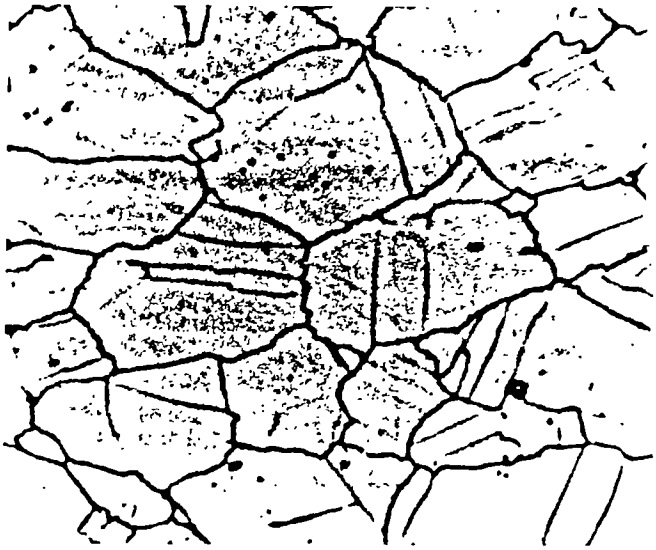

RC0139

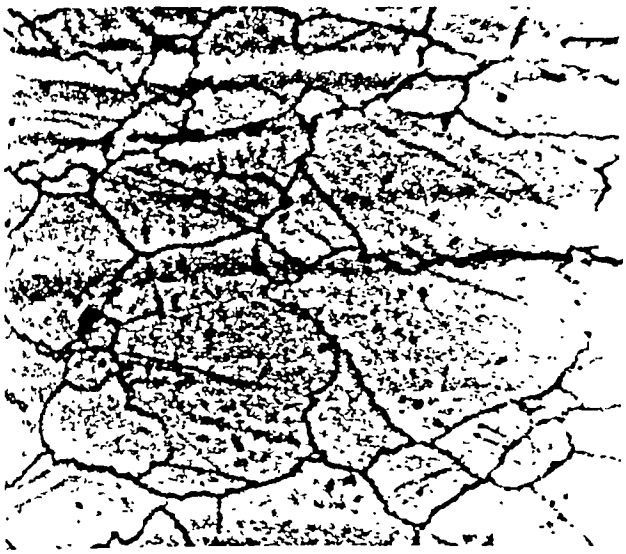

RC0140

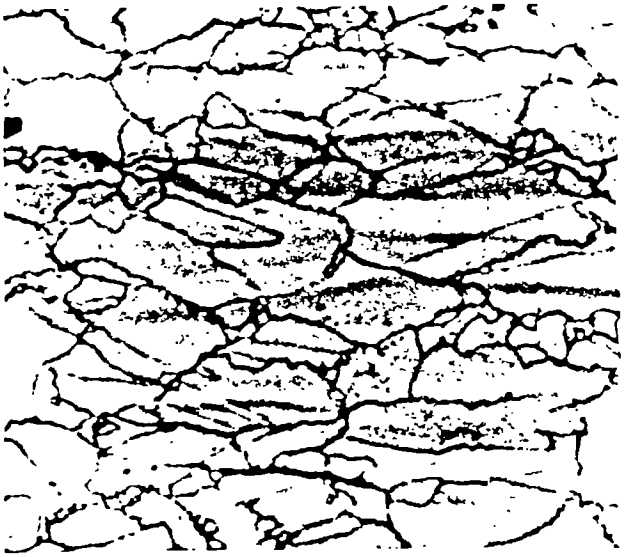

RC0141

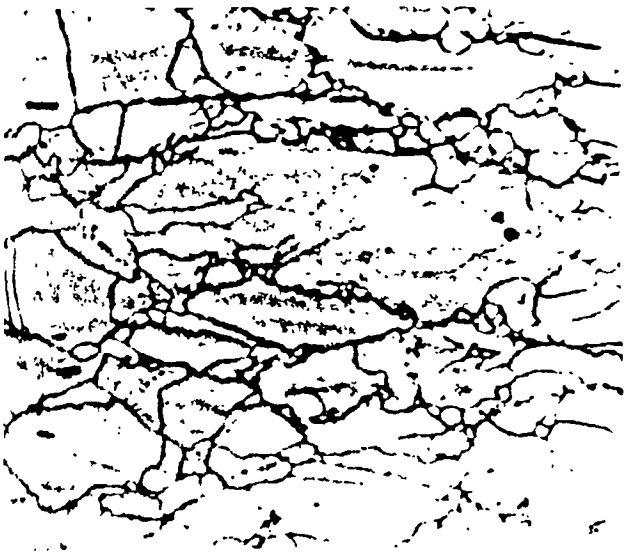

RC0224

RC0220

Figure 101.- Micrographs from the centre of specimens deformed at 4.824 sec^{-1} at 1006 C. 500 X.

Specimen	Nominal strain
RC0226	0.058
RC0147	0.131
RC0148	0.243
RC0149	0.458
RC0225	0.573
RC0222	0.734

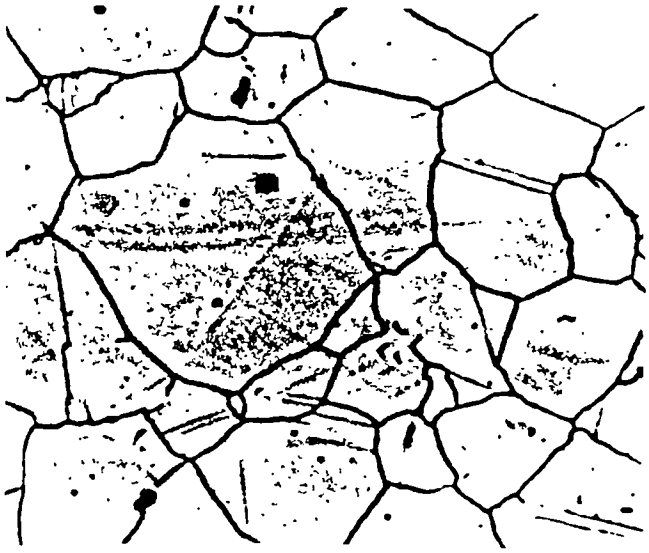

RC0226

RC0147

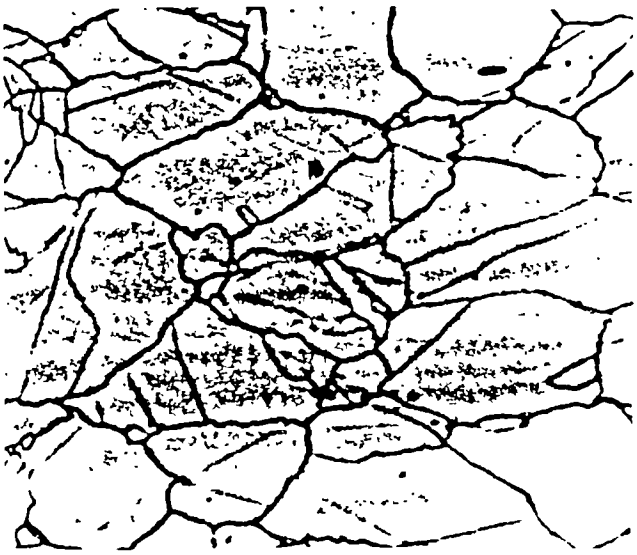

RC0148

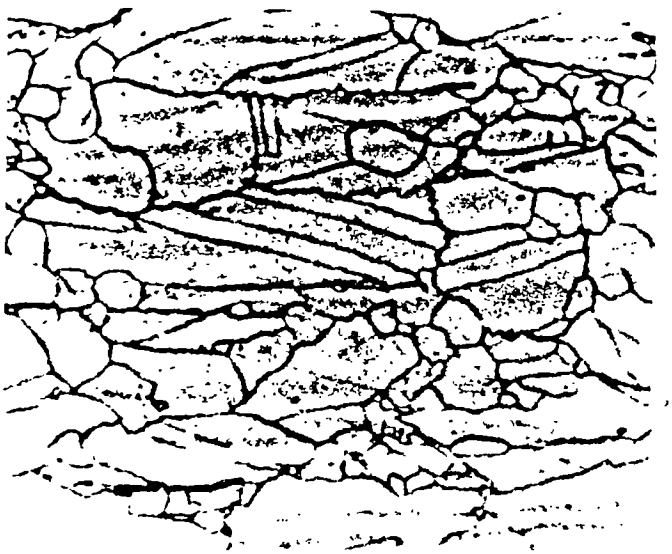

RC0149

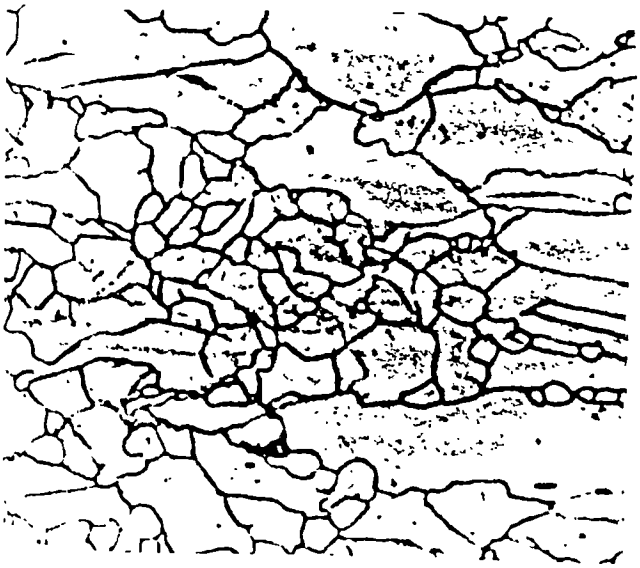

RC0225

RC0222

Figure 102.- Micrographs from the centre of specimens deformed at 43.06 sec^{-1} at 1006 C. 500 X.

Specimen	Nominal strain
RC0142	0.147
RC0143	0.268
RC0144	0.470
RC0223	0.662
RC0221	0.779

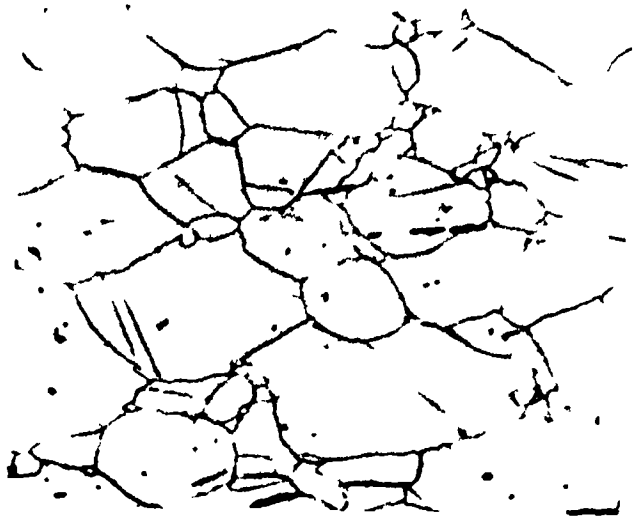

RC0142

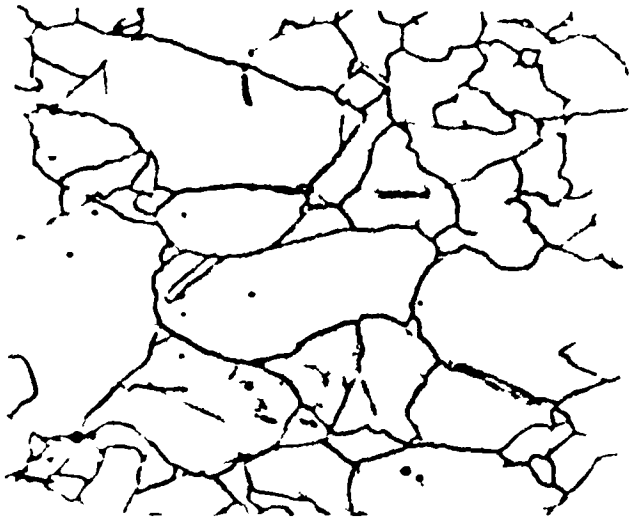

RC0143

RC0144

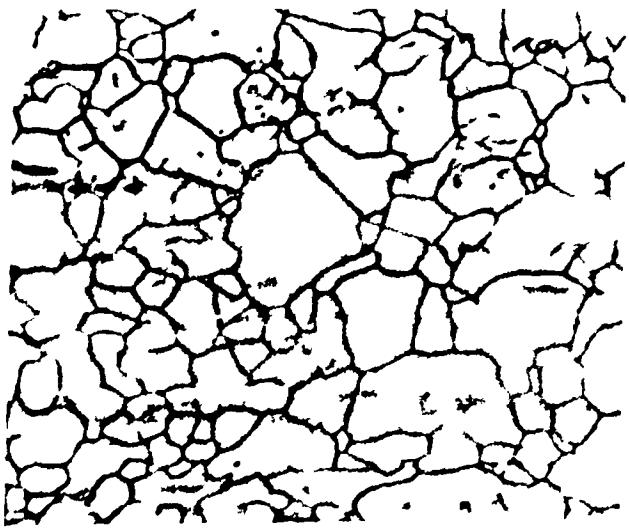

RC0223

RC0221

Figure 103.- Evolution of the grain size during deformation at 910 C.

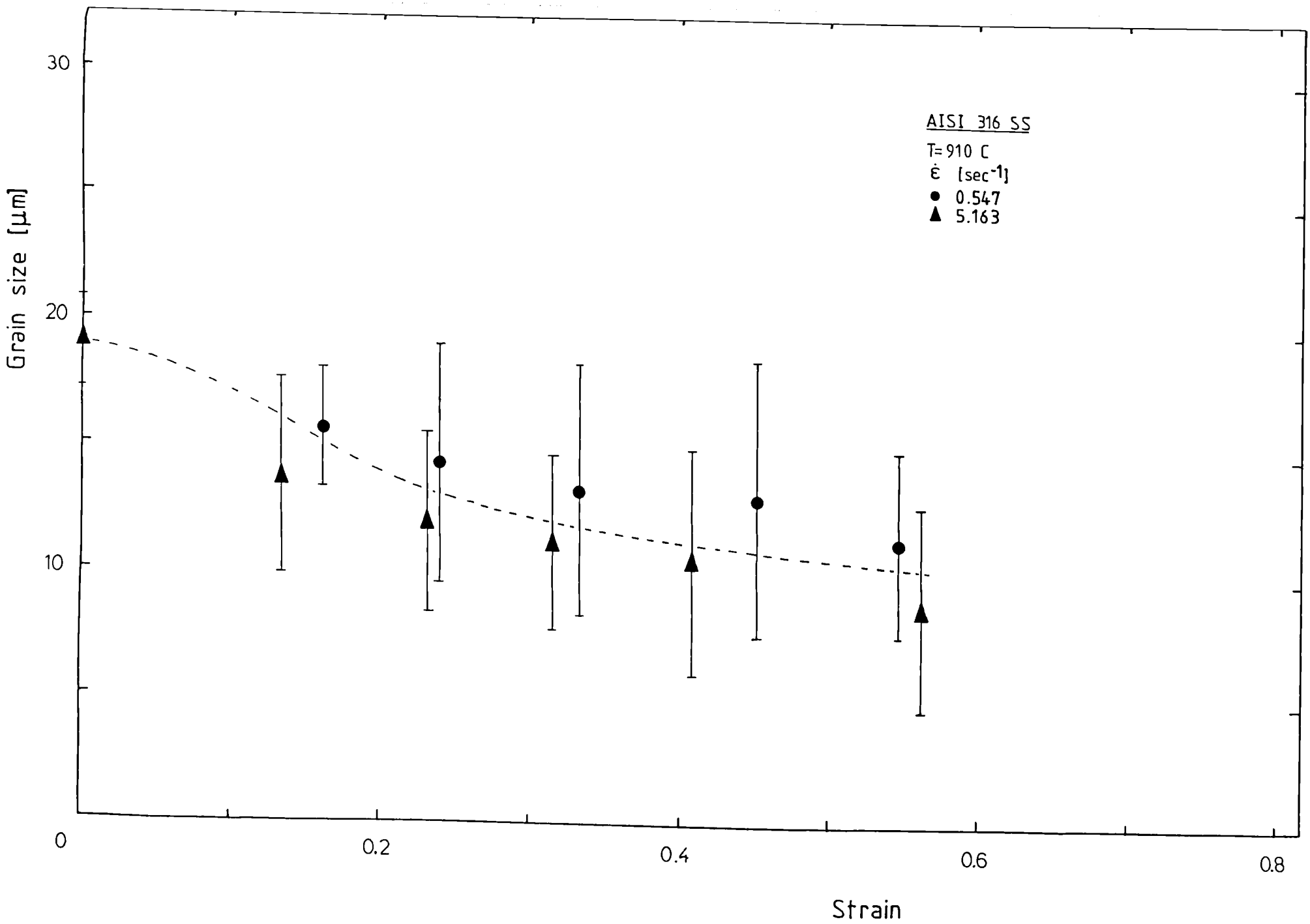
AISI 316 SS
T= 910 C
ε̇ [sec⁻¹]
0.547
5.163
Grain size [μm]
30
20
10
0
0.2
0.4
0.6
0.8
Strain

Figure 104.- Evolution of the grain size during deformation at 1006 C.

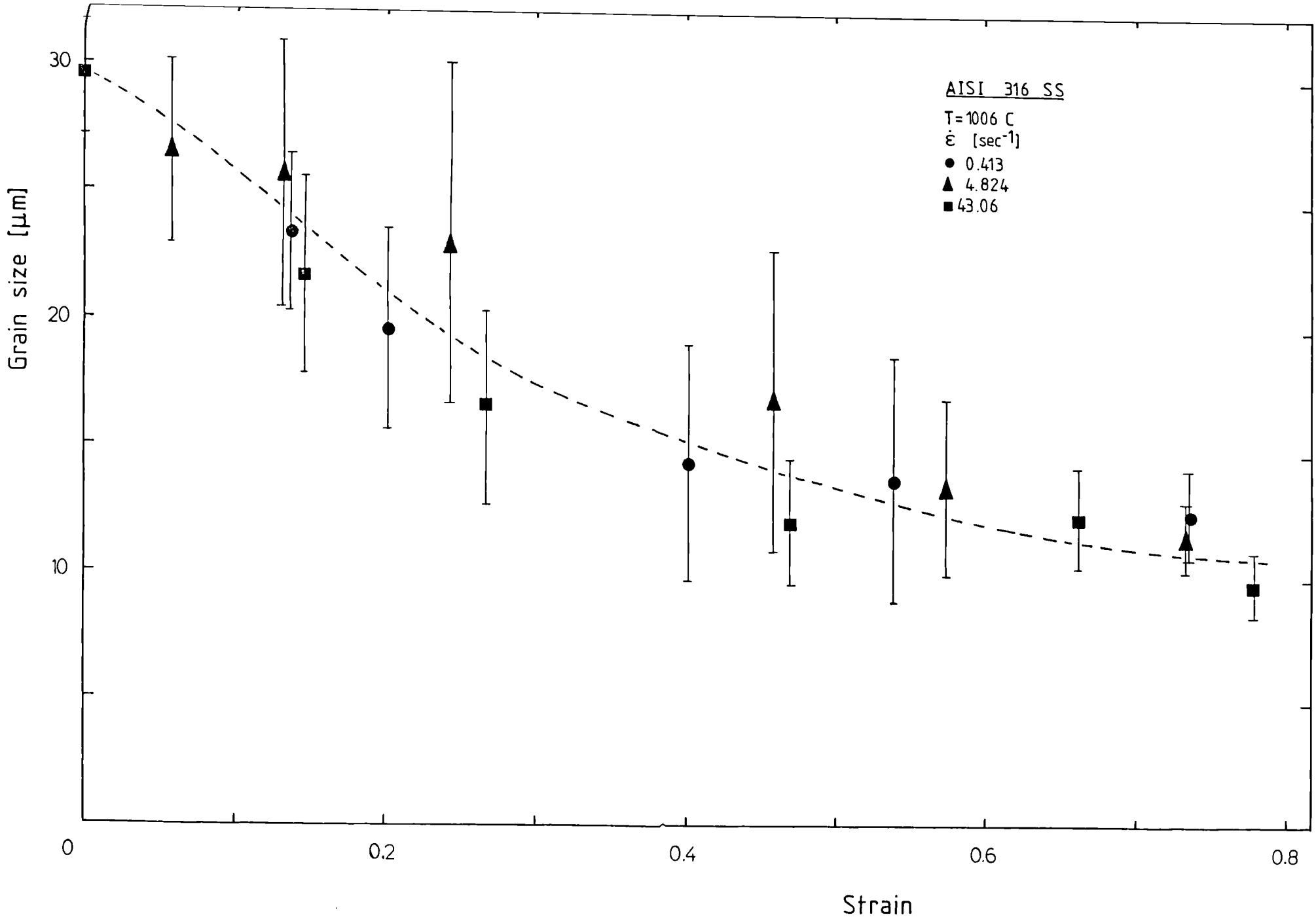
AISI 316 SS
T=1006 C
ε̇ [sec⁻¹]
0.413
4.824
43.06
Grain size [μm]
30
20
10
0
0.2
0.4
0.6
0.8
Strain

Figure 105.- Variation of the grain size against the modified time parameter for the specimens tested at 910 C.

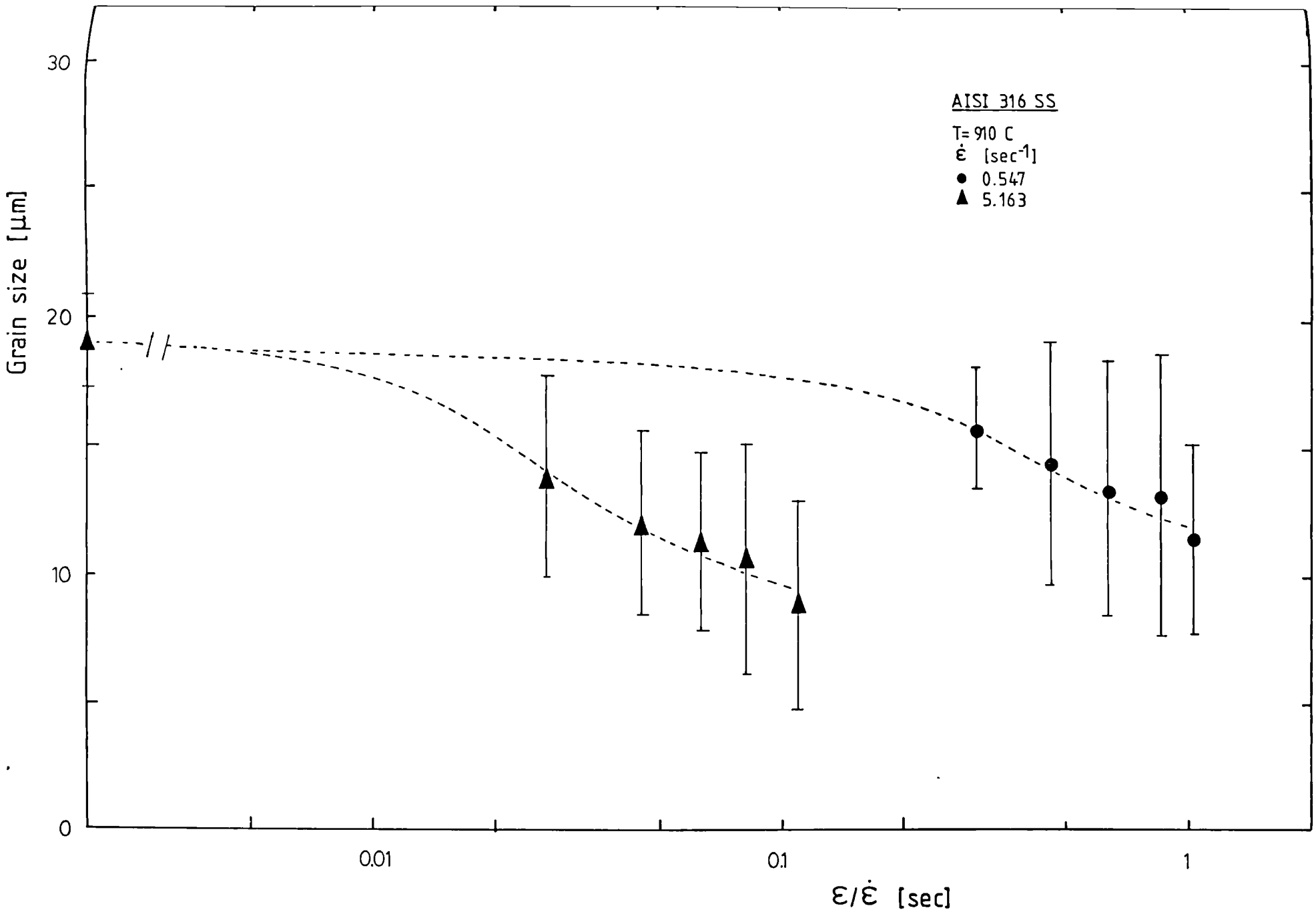
AISI 316 SS
T= 910 C
ε̇ [sec⁻¹]
0.547
5.163
Grain size [μm]
30
20
10
0
0.01
0.1
1
ε/ε̇ [sec]

Figure 106.- Variation of the grain size against the modified time parameter for the specimens tested at 1006 C.

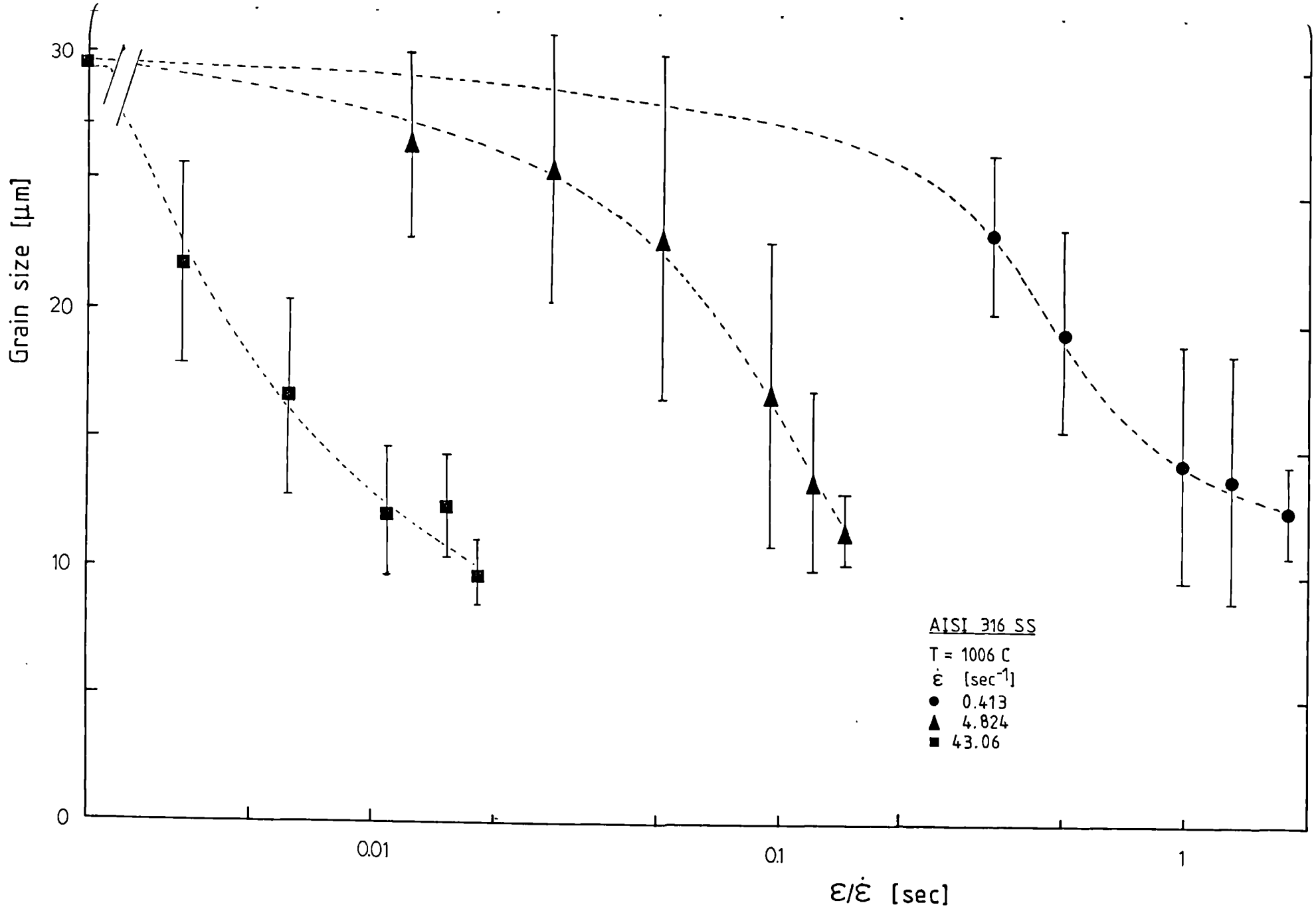
Grain size [μm]
30
20
10
0
0.01
0.1
1
ε/ε̇ [sec]
AISI 316 SS
T = 1006 C
ε̇ [sec⁻¹]
0.413
4.824
43.06

Figure 107.- Dynamic recrystallisation kinetics for the specimens tested at 910 C.

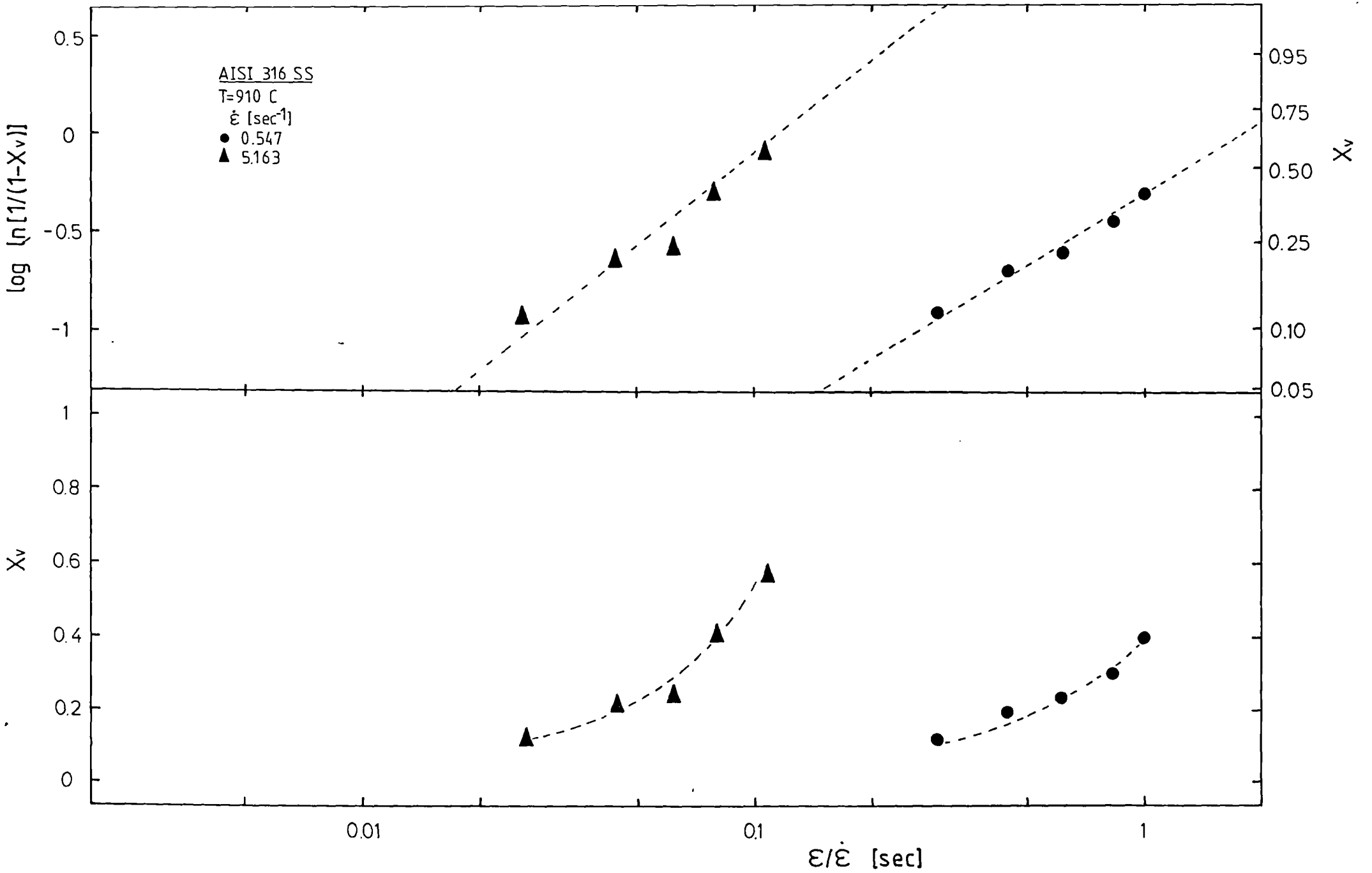
AISI 316 SS
T=910 C
ε̇ [sec⁻¹]
● 0.547
▲ 5.163
log [n[1/(1-Xv)]]
Xv
Xv
ε/ε̇ [sec]
0.5
0
-0.5
-1
0.95
0.75
0.50
0.25
0.10
0.05
1
0.8
0.6
0.4
0.2
0
0.01
0.1
1

Figure 108.- Dynamic recrystallisation kinetics for the specimens tested at 1006 C.

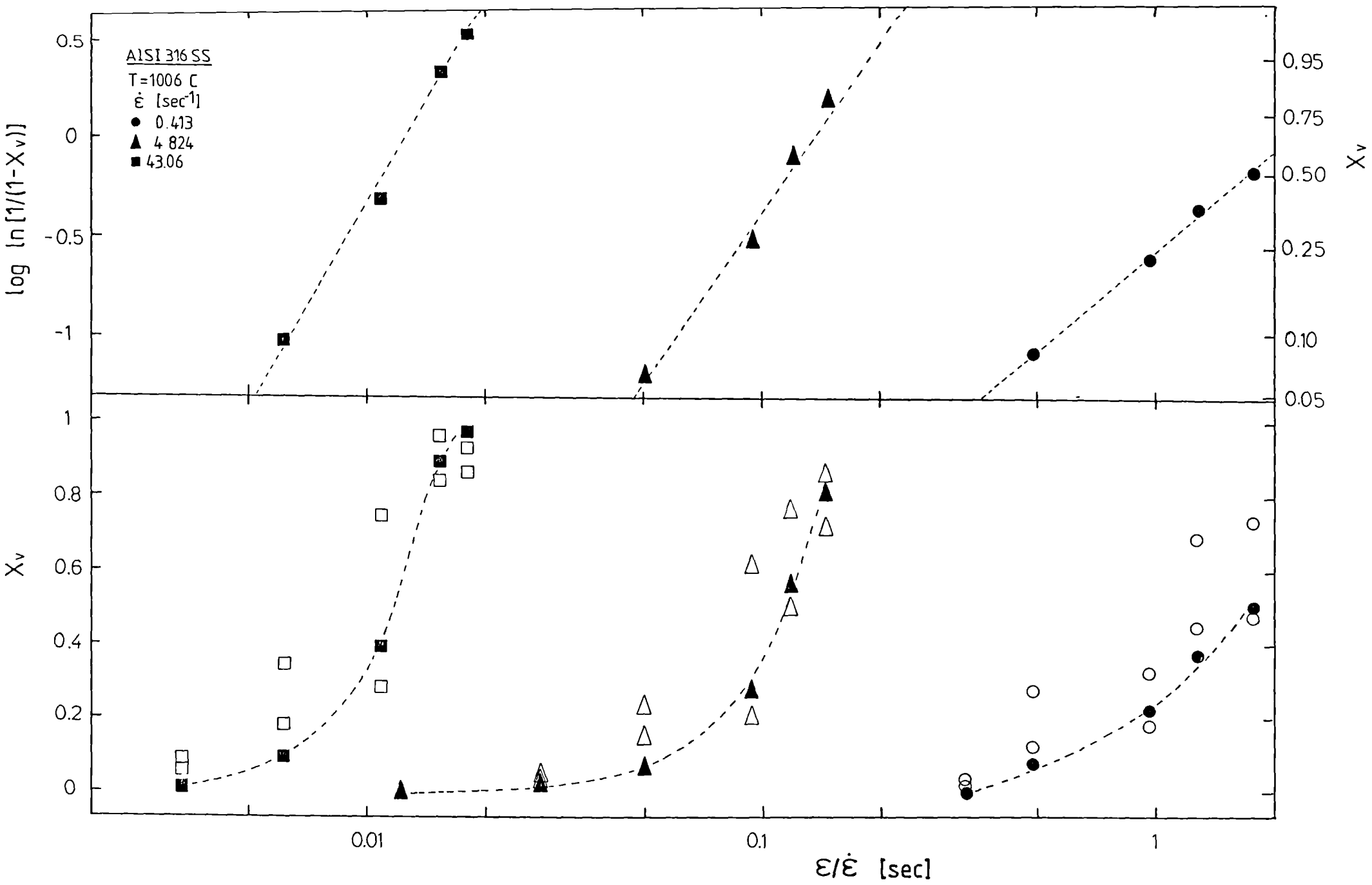
AISI 316 SS
T=1006 C
$\dot{\varepsilon}$ [sec^{-1}]
0.413
4.824
43.06
log [ln [1/(1-Xv)]]
Xv
$\varepsilon/\dot{\varepsilon}$ [sec]
0.5
0
-0.5
-1
0.95
0.75
0.50
0.25
0.10
0.05
1
0.8
0.6
0.4
0.2
0
0.01
0.1
1

Figure 109.- Representation of the recrystallisation kinetics against strain for recrystallised fractions measured over the surface of the specimen, full points, and along lines of constant strain, empty points, for the material deformed at 1006 C.

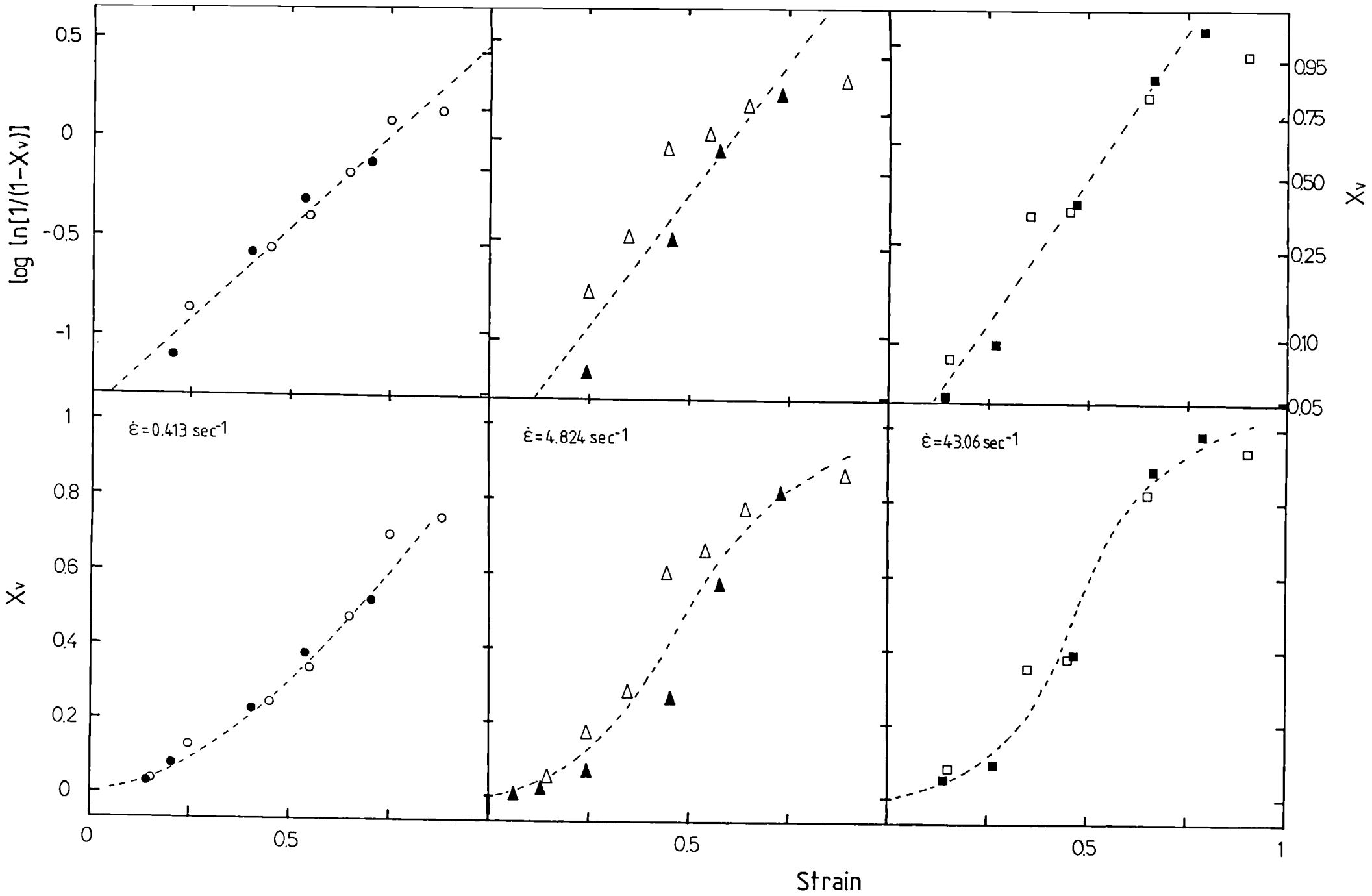
log ln[1/(1-Xv)]
Xv
Strain
ε̇ = 0.413 sec-1
ε̇ = 4.824 sec-1
ε̇ = 43.06 sec-1
0.5
0
-0.5
-1
1
0.8
0.6
0.4
0.2
0
0.5
0.5
0.5
1
0.95
0.75
0.50
0.25
0.10
0.05

Figure 110.- Representation of the recrystallised fraction against the ratio of the nominal strain over the strain to the peak.

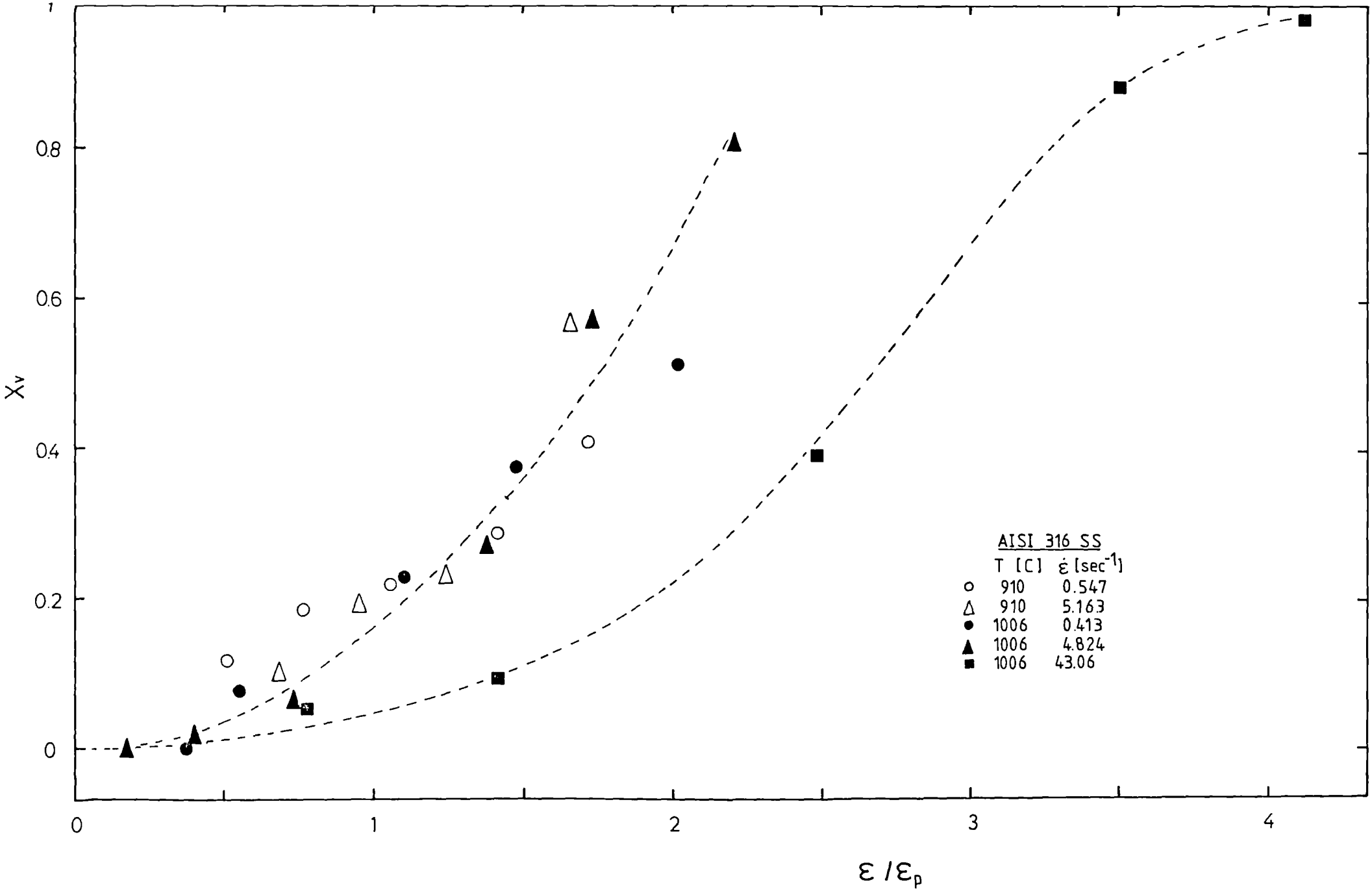
1
0.8
0.6
0.4
0.2
0
X_v
0
1
2
3
4
$\varepsilon / \varepsilon_p$
AISI 316 SS
T [C] $\dot{\varepsilon}$ [sec^{-1}]
910 0.547
910 5.163
1006 0.413
1006 4.824
1006 43.06

Figure 111.- Stress-strain curves for 5 mm thick titanium bearing steel deformed with inserted thermocouples.

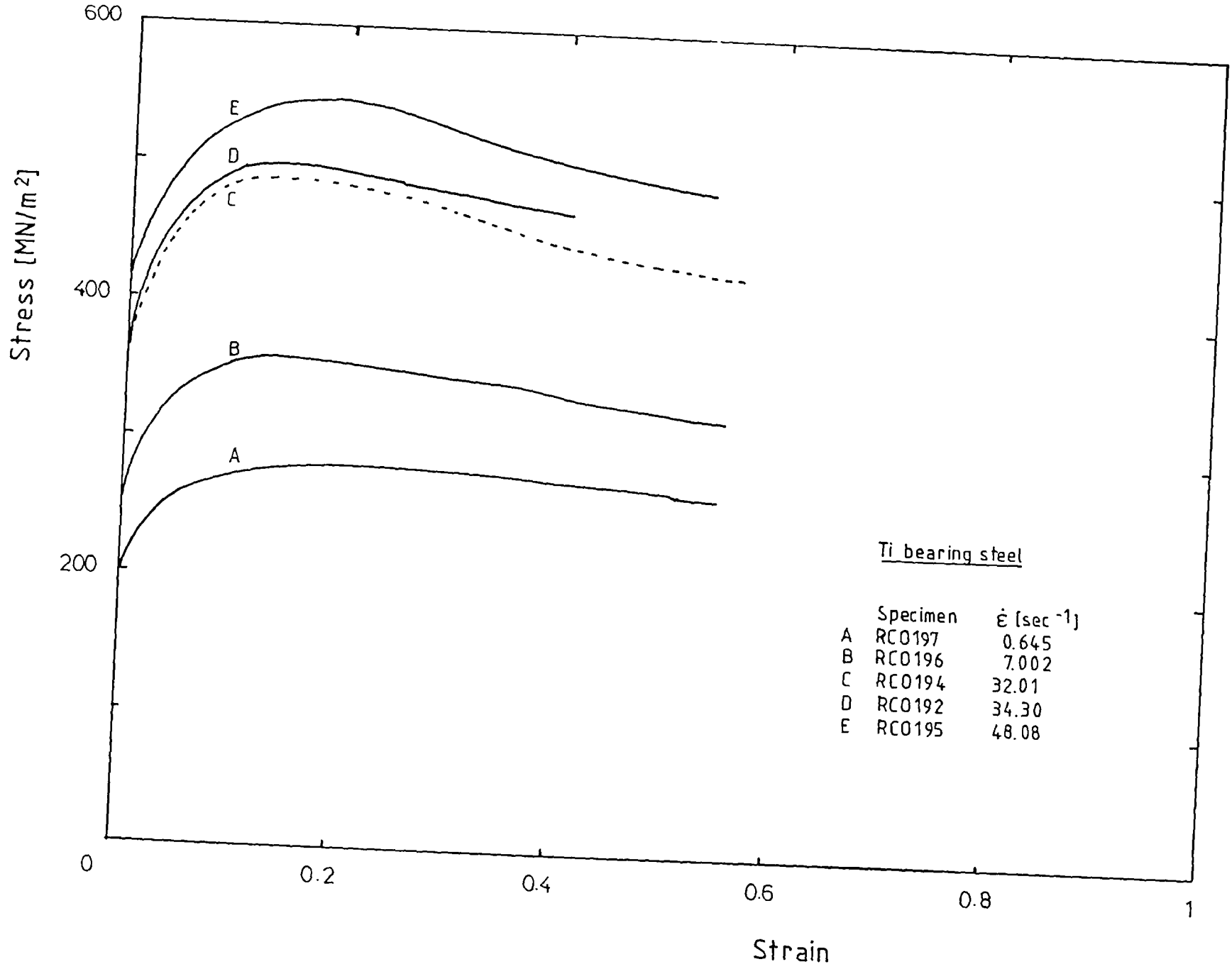
600
400
200
0
Stress [MN/m²]
E
D
C
B
A
0.2
0.4
0.6
0.8
1
Strain
Ti bearing steel
Specimen
ε̇ [sec⁻¹]
A RC0197 0.645
B RC0196 7.002
C RC0194 32.01
D RC0192 34.30
E RC0195 48.08

Figure 112.- Temperature-strain curves for the 5 mm thick titanium specimens.

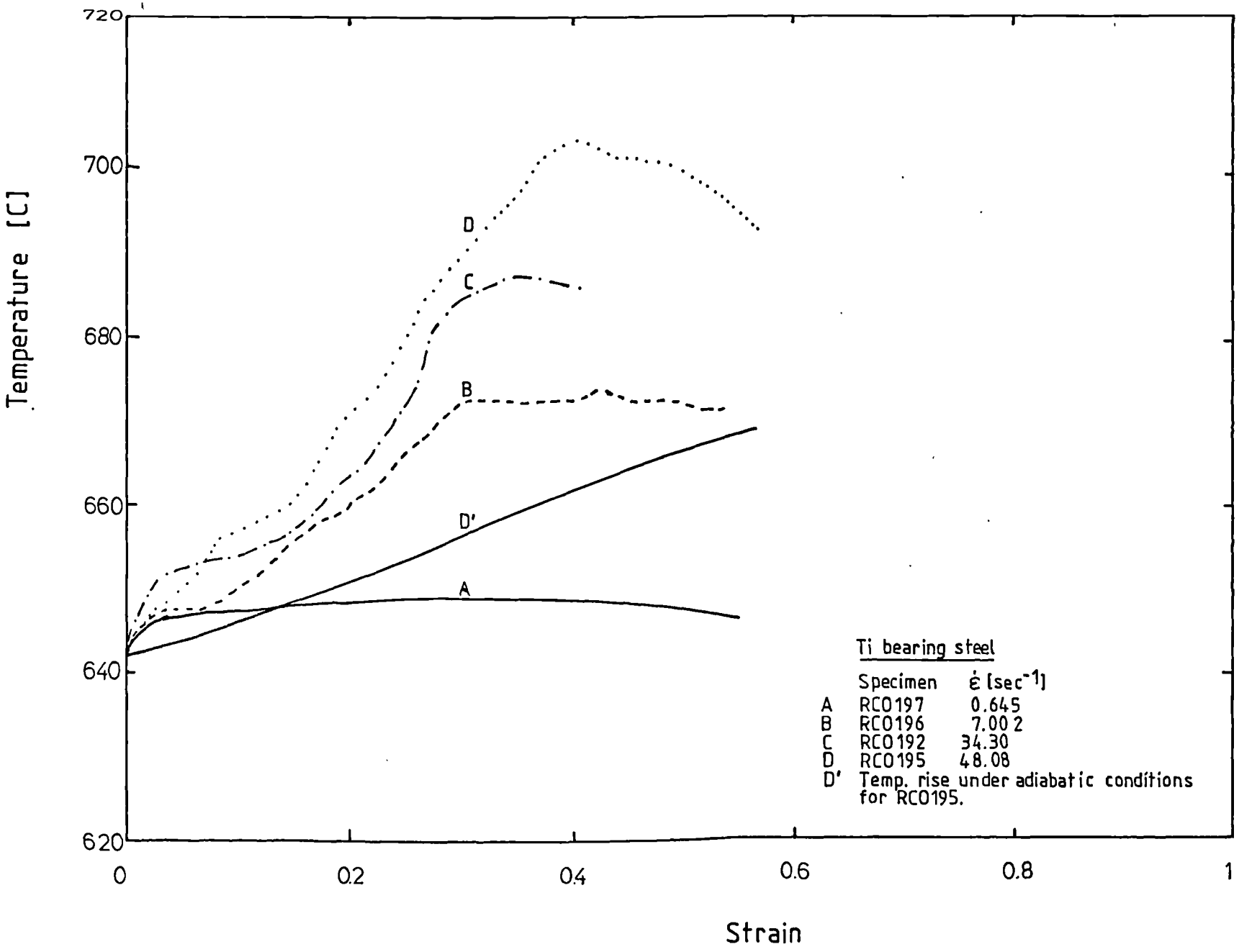
720
700
680
660
640
620
Temperature [C]
0
0.2
0.4
0.6
0.8
1
Strain
D
C
B
D'
A
Ti bearing steel
Specimen ε̇ [sec⁻¹]
A RC0197 0.645
B RC0196 7.002
C RC0192 34.30
D RC0195 48.08
D' Temp. rise under adiabatic conditions for RC0195.

Figure 113.- Stress-strain curves for the AISI type 316 stainless steel deformed with thermocouples in the centre. Specimen RC0275 was 6 mm thick, RC0274 was 8 mm. Specimen RC0272 was deformed with one thermocouple in the centre and one in the shoulder.

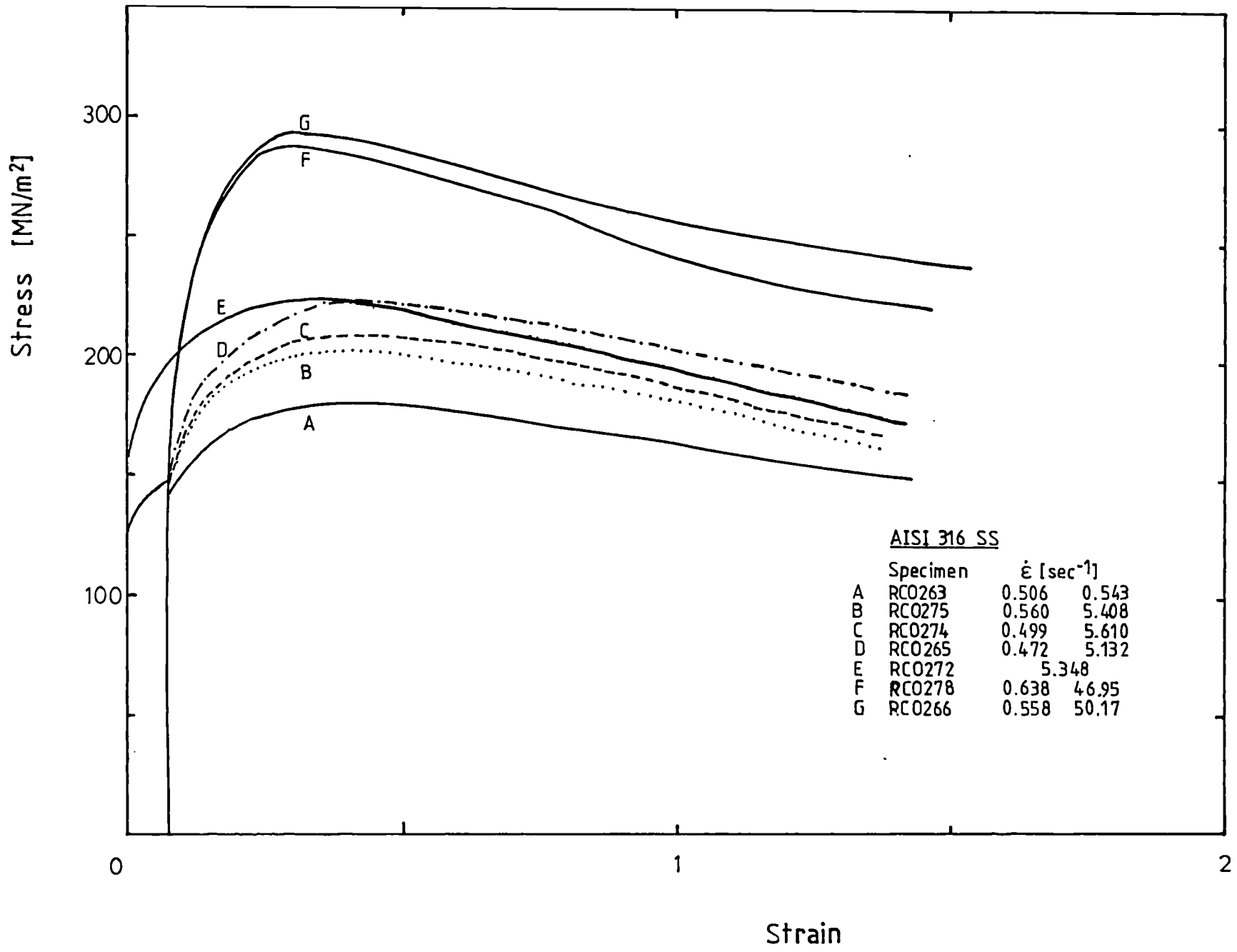
Stress [MN/m²]
300
200
100
0
1
2
Strain
G
F
E
C
D
B
A
AISI 316 SS
Specimen
ε̇ [sec⁻¹]
A RC0263 0.506 0.543
B RC0275 0.560 5.408
C RC0274 0.499 5.610
D RC0265 0.472 5.132
E RC0272 5.348
F RC0278 0.638 46.95
G RC0266 0.558 50.17

Figure 114.- Temperature-strain curves for stainless steel specimens tested at 0.5 and 50 sec^{-1}. The temperature output was via the servo-hydraulic machine.

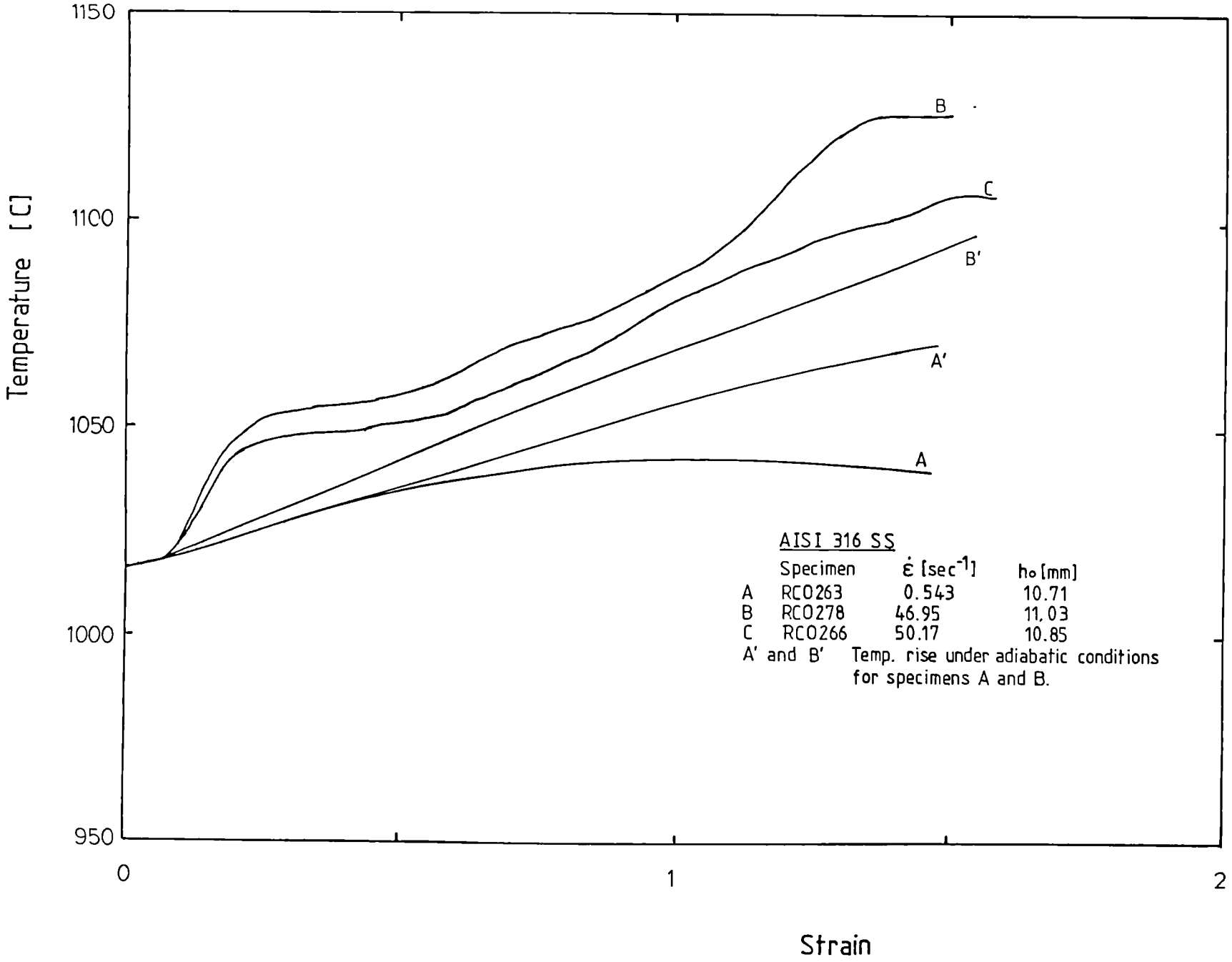
1150
1100
1050
1000
950
Temperature [C]
0
1
2
Strain
B
C
B'
A'
A
AISI 316 SS
Specimen
ε̇ [sec⁻¹]
h₀ [mm]
A RC0263 0.543 10.71
B RC0278 46.95 11.03
C RC0266 50.17 10.85
A' and B' Temp. rise under adiabatic conditions for specimens A and B.

Figure 115.- Temperature-strain curves for stainless steel specimens tested at 5 sec^{1}. The temperature output was via the servo-hydraulic machine.

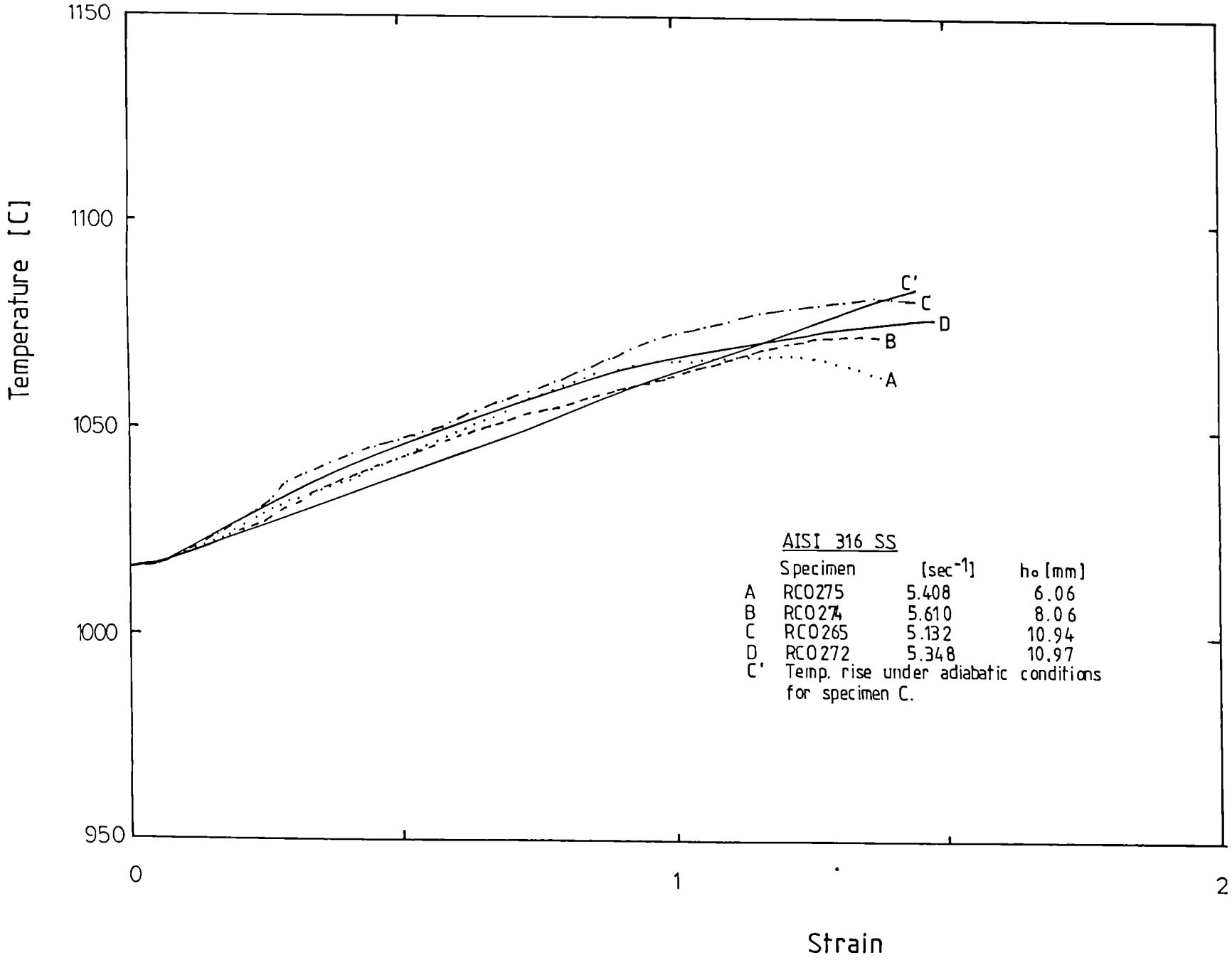
1150
1100
1050
1000
950
Temperature [C]
0
1
2
Strain
C'
C
D
B
A
AISI 316 SS
Specimen [sec⁻¹] h₀ [mm]
A RC0275 5.408 6.06
B RC0274 5.610 8.06
C RC0265 5.132 10.94
D RC0272 5.348 10.97
C' Temp. rise under adiabatic conditions for specimen C.

Figure 116.- Temperature-strain curves for stainless steel specimens. The temperature output was via the ultraviolet recorder in order to follow the whole temperature evolution.

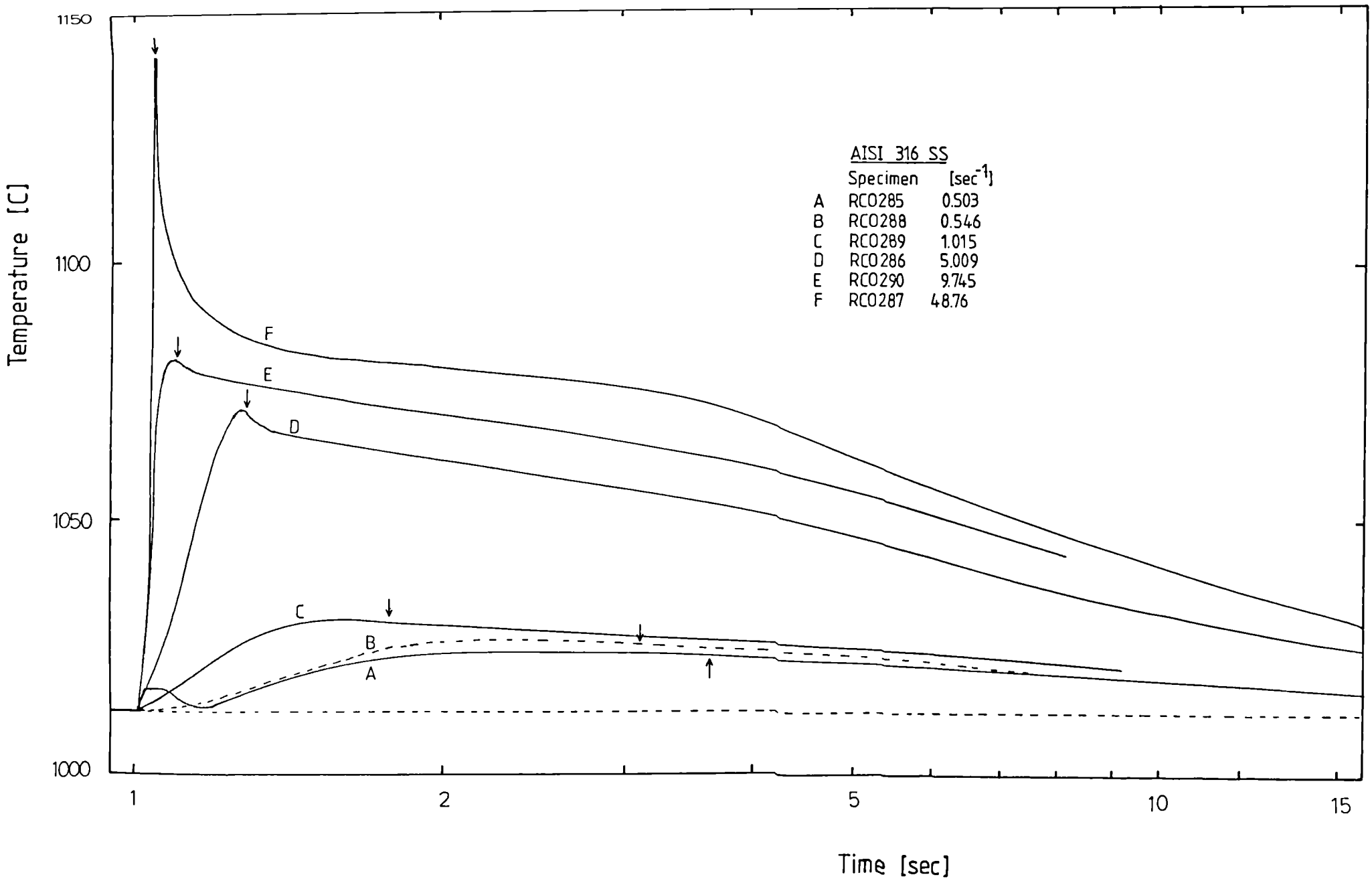
AISI 316 SS
Specimen [sec^{-1}]
A RC0285 0.503
B RC0288 0.546
C RC0289 1.015
D RC0286 5.009
E RC0290 9.745
F RC0287 48.76
Temperature [C]
1150
1100
1050
1000
1
2
5
10
15
Time [sec]

Figure 117.- Increase of temperature versus strain rate plot for the stainless steel specimens in figures 114 to 116.

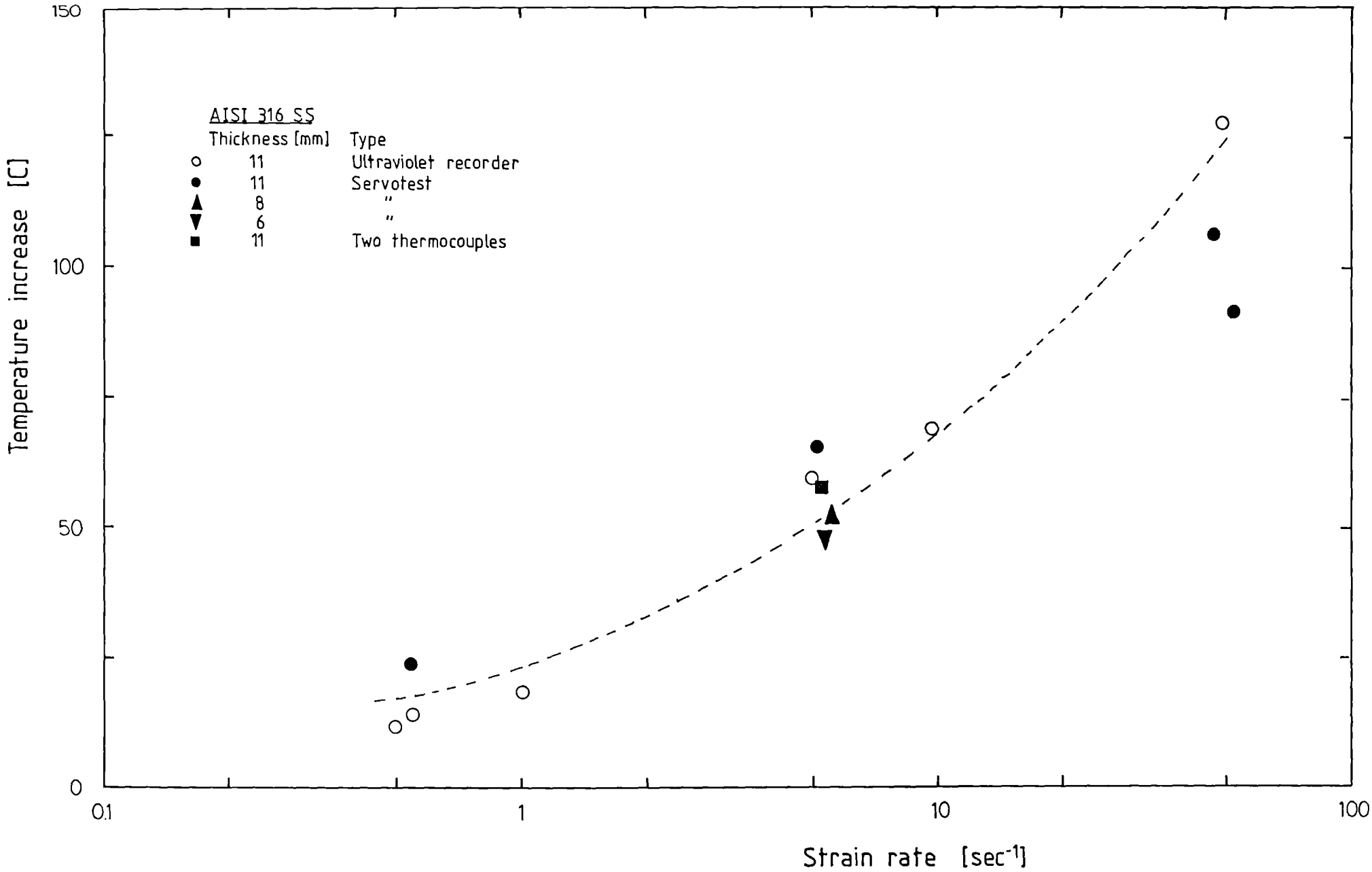
AISI 316 SS
Thickness [mm] Type
11 Ultraviolet recorder
11 Servotest
8 "
6 "
11 Two thermocouples
Temperature increase [C]
150
100
50
0
0.1
1
10
100
Strain rate [sec-1]

Figure 118.- Temperature-strain plot for the specimens deformed at 0.5 sec^{-1} with two thermocouples.

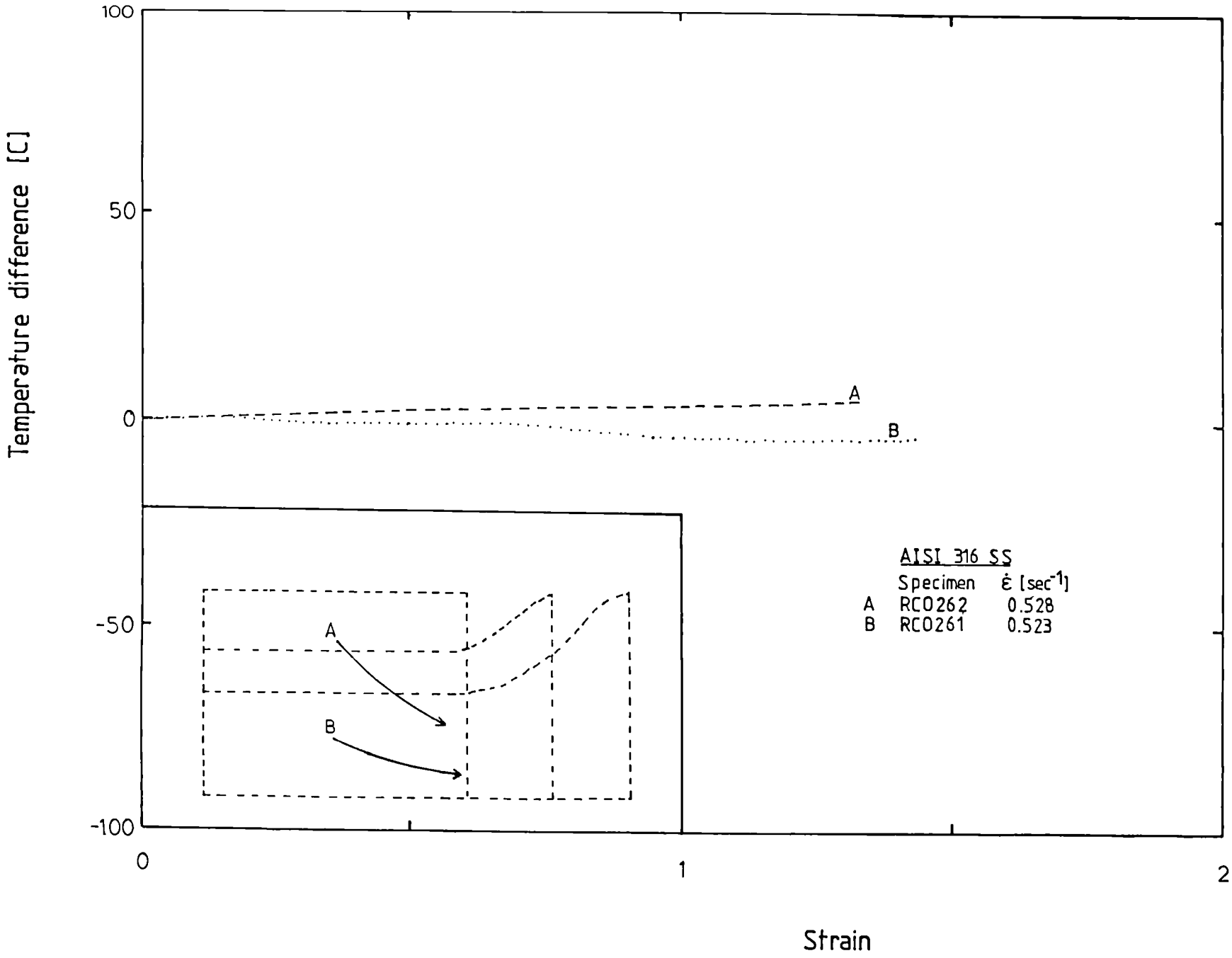
Temperature difference [C]
100
50
0
-50
-100
0
1
2
Strain
A
B
AISI 316 SS
Specimen
ε̇ [sec⁻¹]
A RC0262 0.528
B RC0261 0.523

Figure 119.- Temperature-strain plot for the specimens deformed at 5 sec^{-1} with two thermocouples.

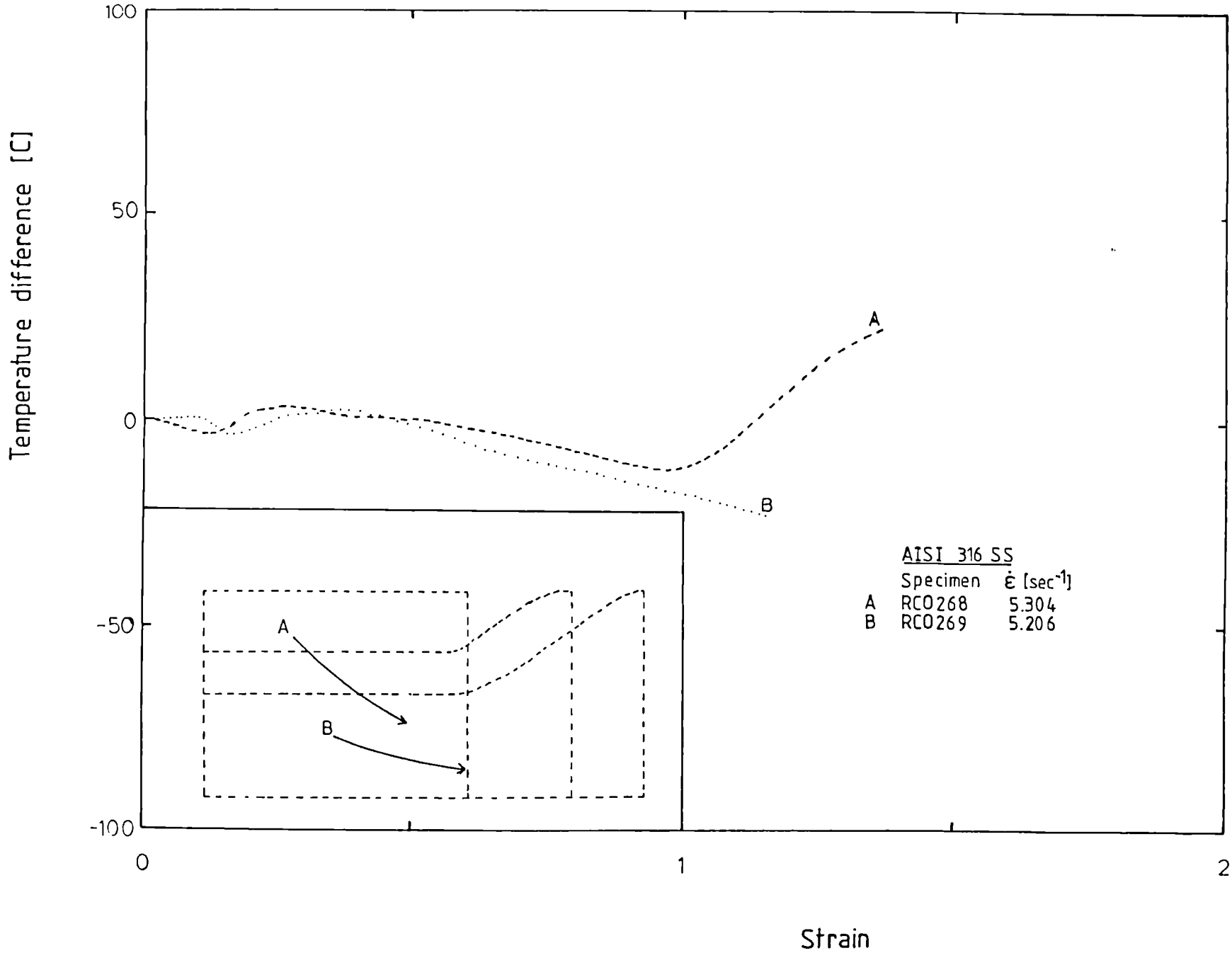
Temperature difference [C]
100
50
0
-50
-100
0
1
2
Strain
A
B
AISI 316 SS
Specimen ε̇ [sec⁻¹]
A RC0268 5.304
B RC0269 5.206

Figure 120.- Temperature-strain plot for the specimens deformed at 50 sec^{-1} with two thermocouples.

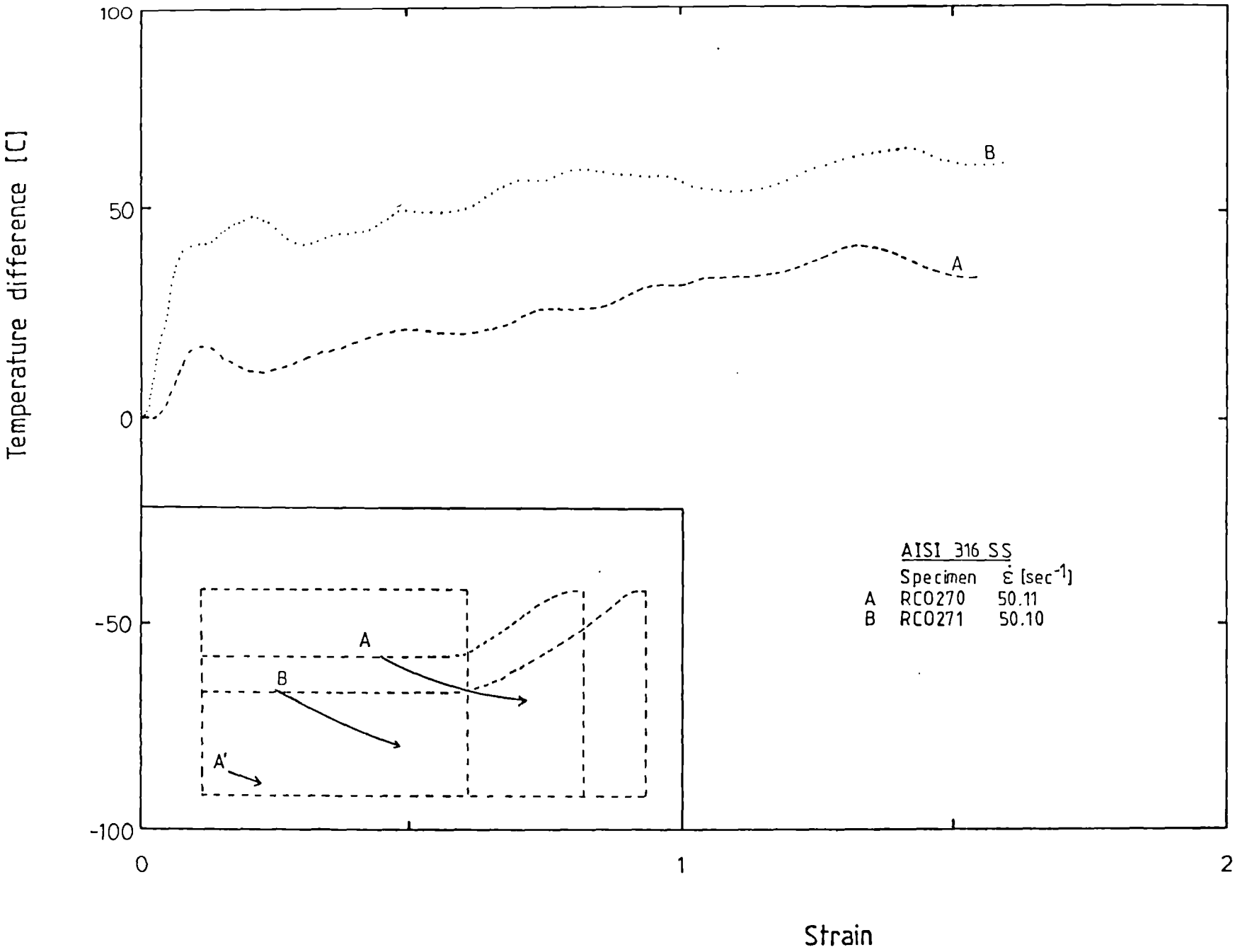
Temperature difference [C]
100
50
0
-50
-100
0
1
2
Strain
B
A
A
B
A'
AISI 316 SS
Specimen
$\dot{\varepsilon}$ [sec^{-1}]
A RC0270 50.11
B RC0271 50.10

Figure 121.- Initial velocity versus stress for the stress-strain data obtained when testing plane strain specimens at 1006 C with different initial thickness.

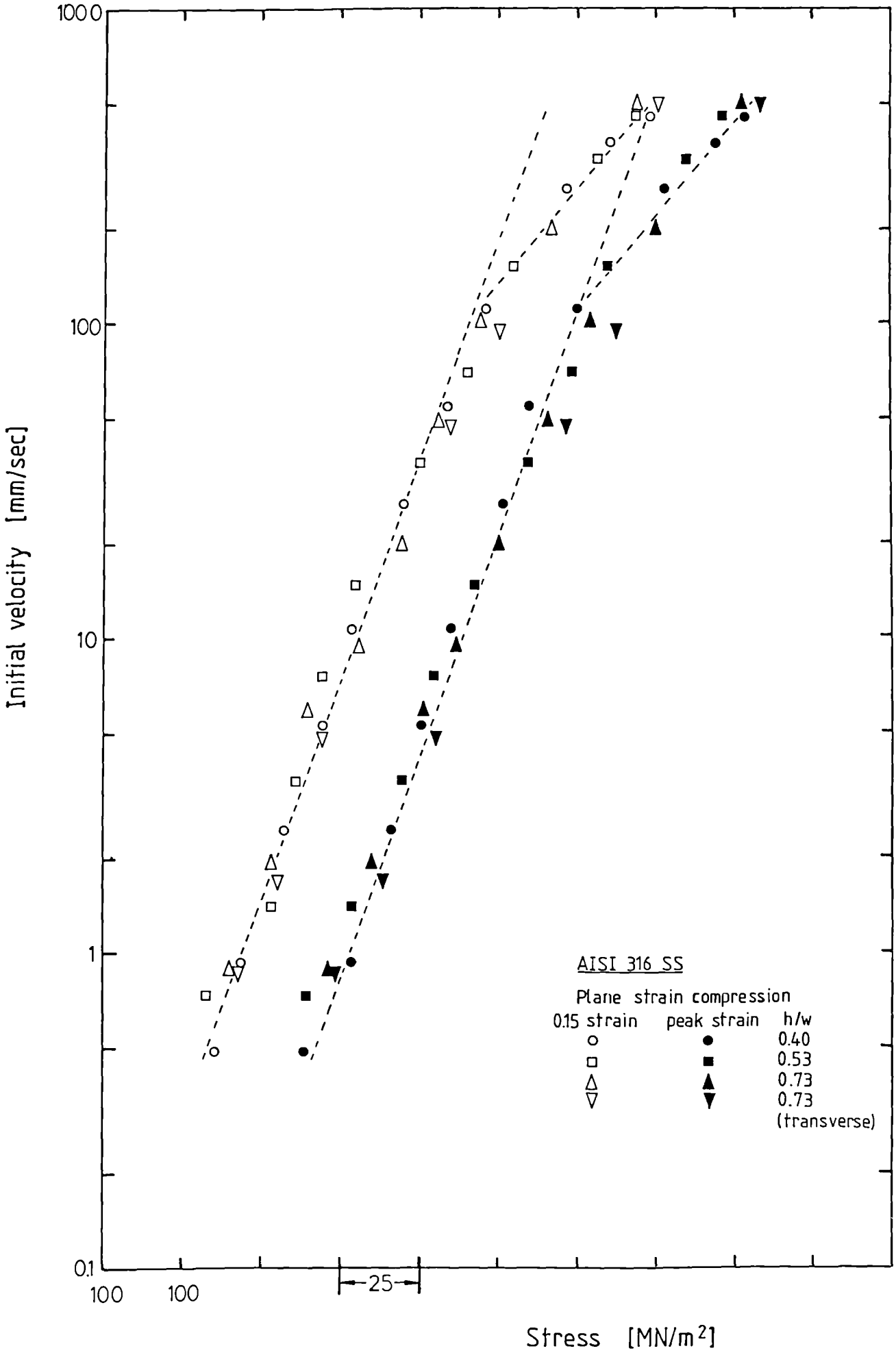
1000
100
10
1
0.1
100
100
25
Initial velocity [mm/sec]
Stress [MN/m²]
AISI 316 SS
Plane strain compression
0.15 strain
peak strain
h/w
0.40
0.53
0.73
0.73
(transverse)

Figure 122.- Traces of the experimental data from figure 63. Different corrections are carried out to compensate for strain heterogeneity.

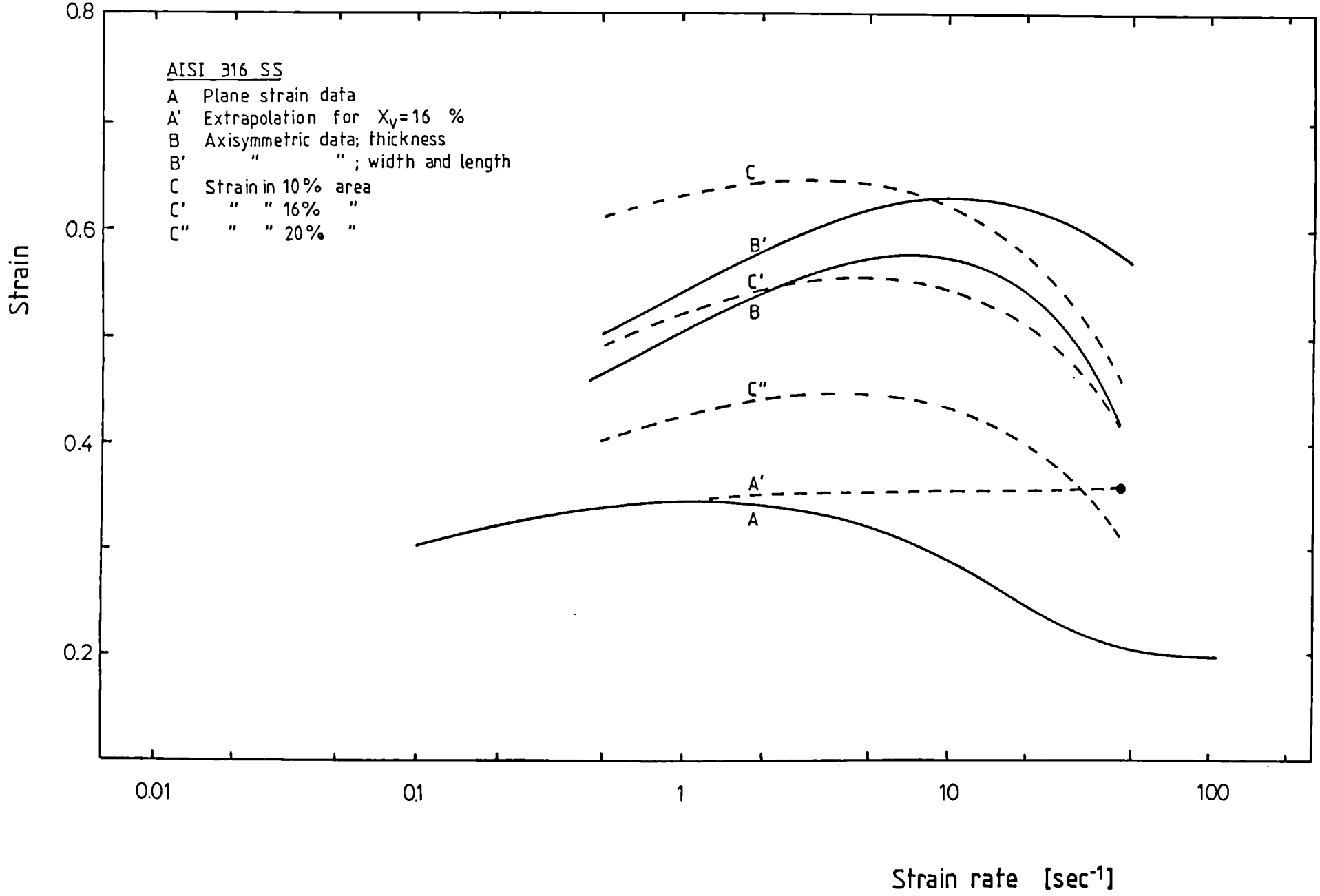
AISI 316 SS
A Plane strain data
A' Extrapolation for X_V=16 %
B Axisymmetric data; thickness
B' " " ; width and length
C Strain in 10% area
C' " " 16% "
C" " " 20% "
C
B'
C'
B
C"
A'
A
0.8
0.6
0.4
0.2
Strain
0.01
0.1
1
10
100
Strain rate [sec^{-1}]

Figure 123.- Stress-strain curves obtained from specimens deformed at around 1000 C under different testing conditions.

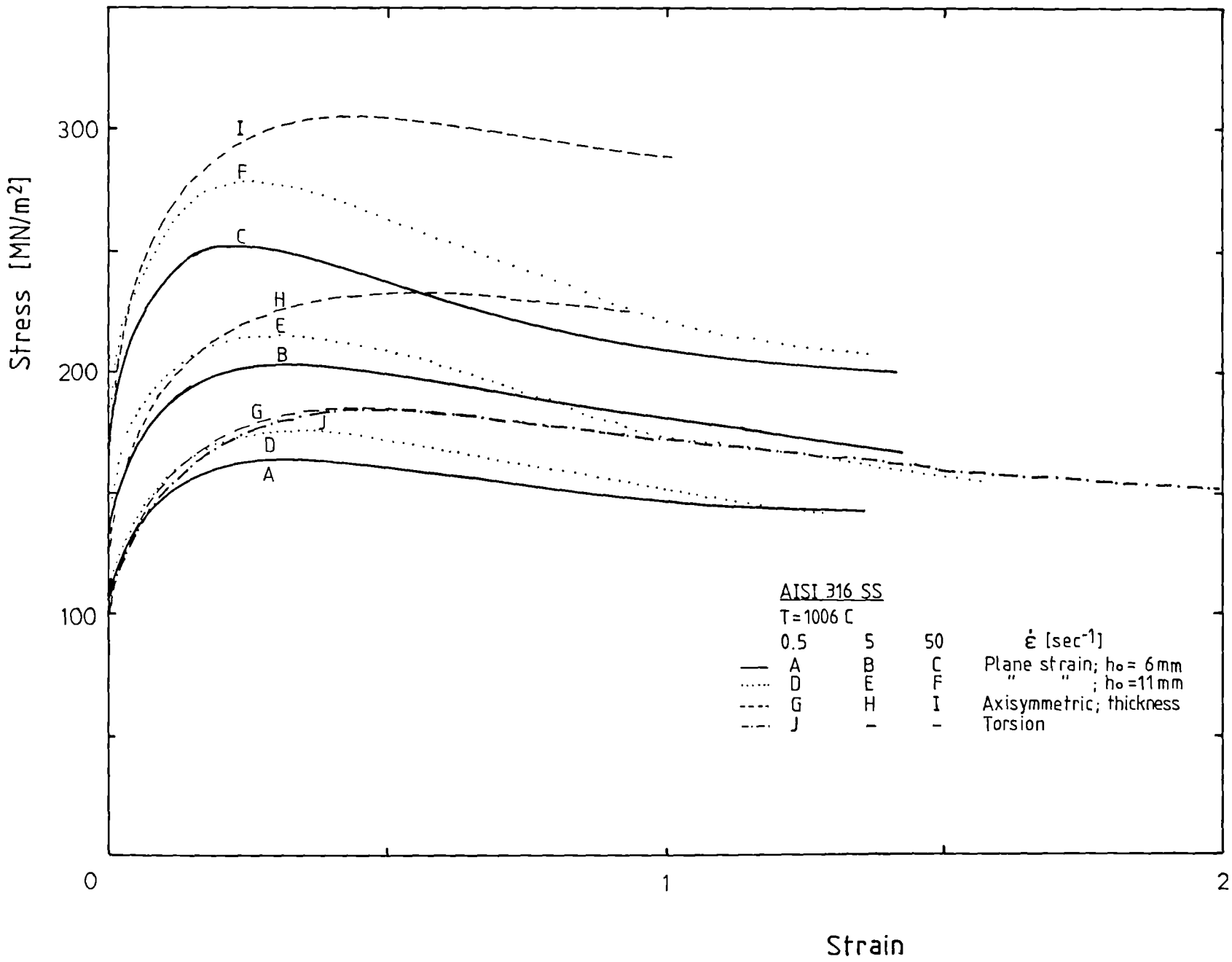
Stress [MN/m²]
300
200
100
0
1
2
Strain
I
F
C
H
E
B
G
J
D
A
AISI 316 SS
T = 1006 C
0.5 5 50 ε̇ [sec⁻¹]
A B C Plane strain; h₀ = 6 mm
D E F " " ; h₀ = 11 mm
G H I Axisymmetric; thickness
J – – Torsion

Figure 124.- Alpha-strain curves for the plane strain specimens, 6 mm thick, from figure 123. Key as in that figure.

Figure 125.- Alpha-strain curves for the plane strain specimens, 11 mm thick, from figure 123. Key as in that figure.

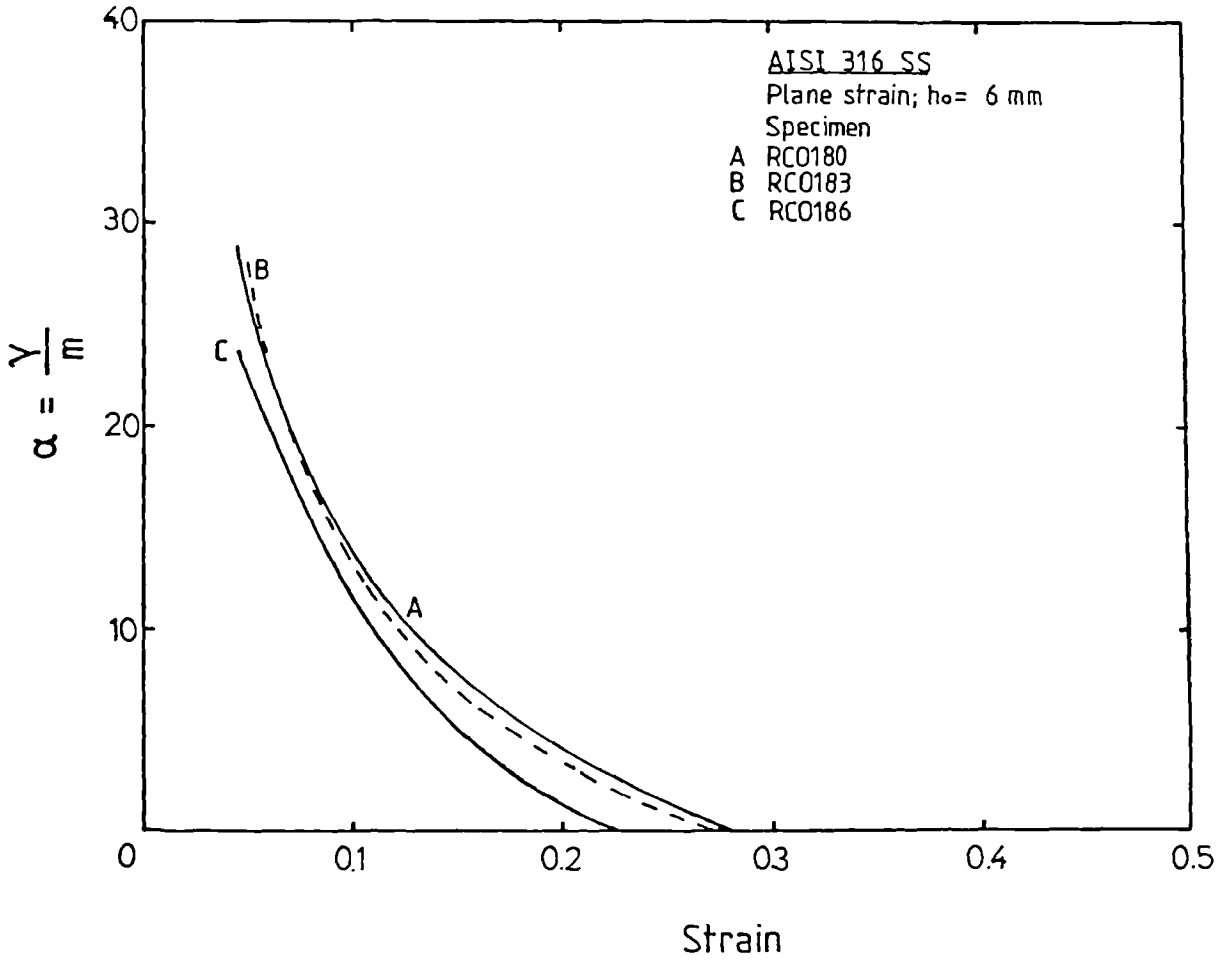
AISI 316 SS
Plane strain; ho= 6 mm
Specimen
A RC0180
B RC0183
C RC0186
α = γ/m
Strain
0
0.1
0.2
0.3
0.4
0.5
10
20
30
40
A
B
C

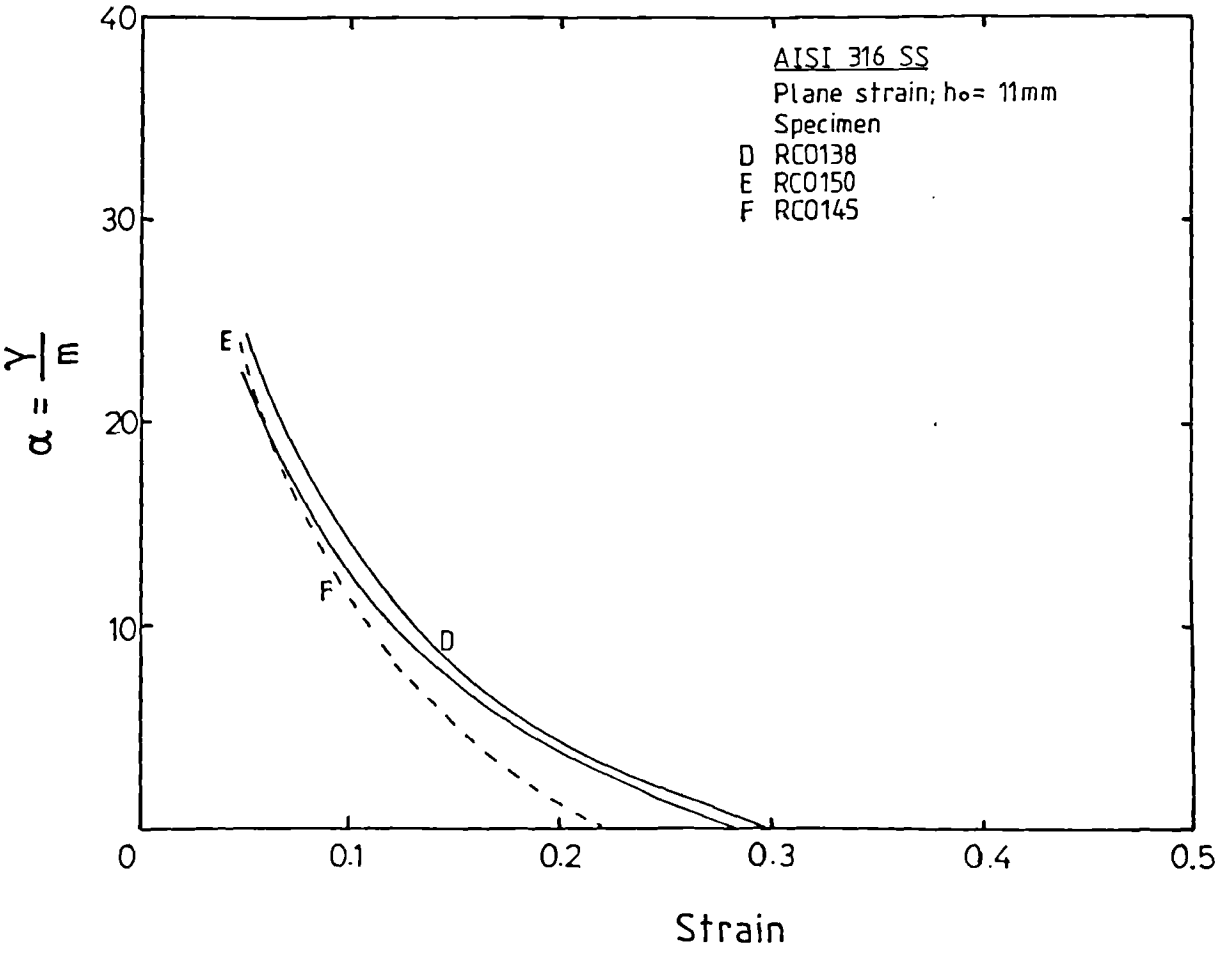
AISI 316 SS
Plane strain; ho= 11mm
Specimen
D RC0138
E RC0150
F RC0145
α = γ/m
Strain
0
0.1
0.2
0.3
0.4
0.5
10
20
30
40
D
E
F

Figure 126.- Alpha-strain curves for the axisymmetric specimens from figure 123. Key as in that figure.

Figure 127.- Alpha-strain curves for the torsion specimens from figure 123. Key as in that figure.

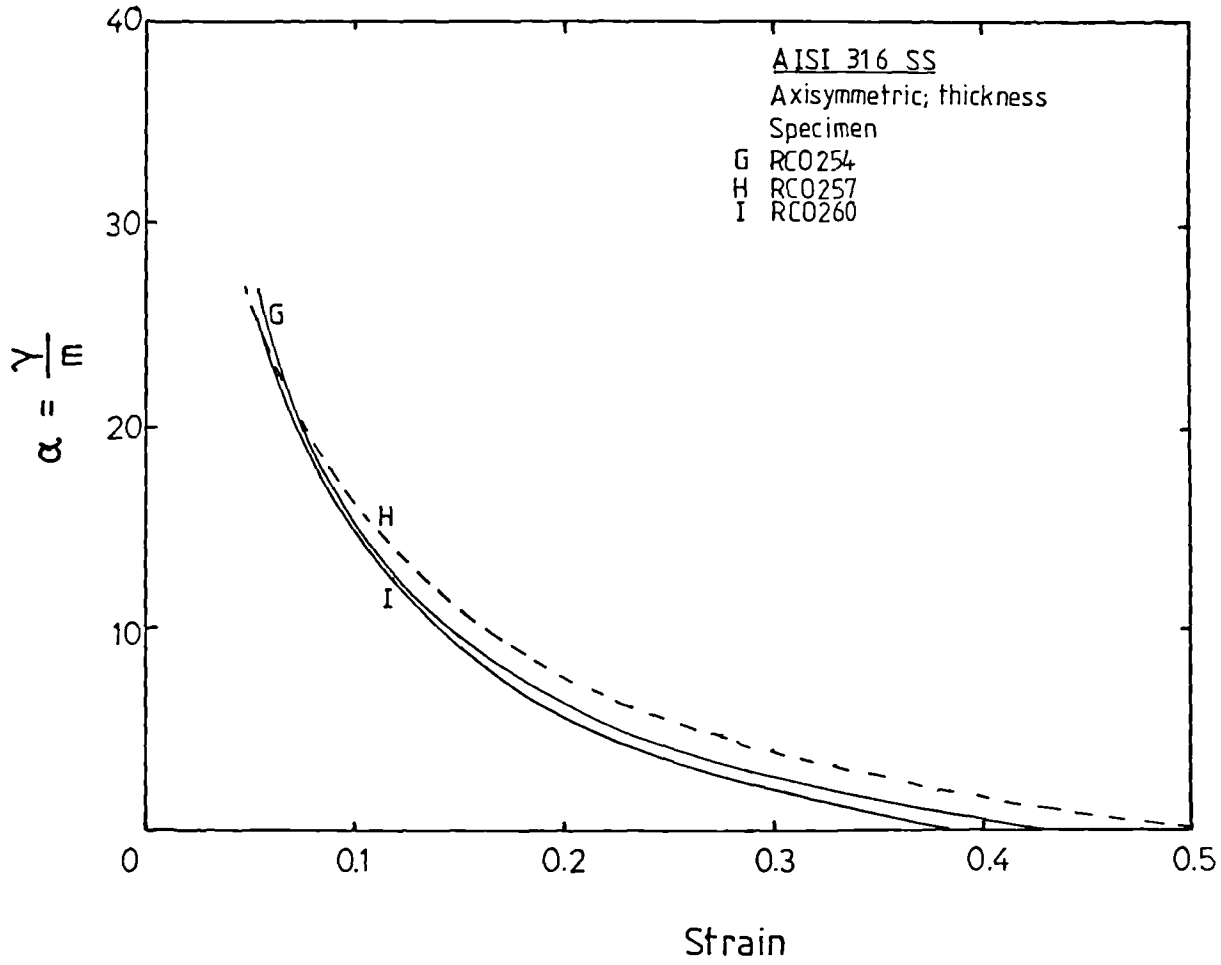
AISI 316 SS
Axisymmetric; thickness
Specimen
G RC0254
H RC0257
I RC0260
G
H
I
40
30
20
10
0
0.1
0.2
0.3
0.4
0.5
α = γ/ε
Strain

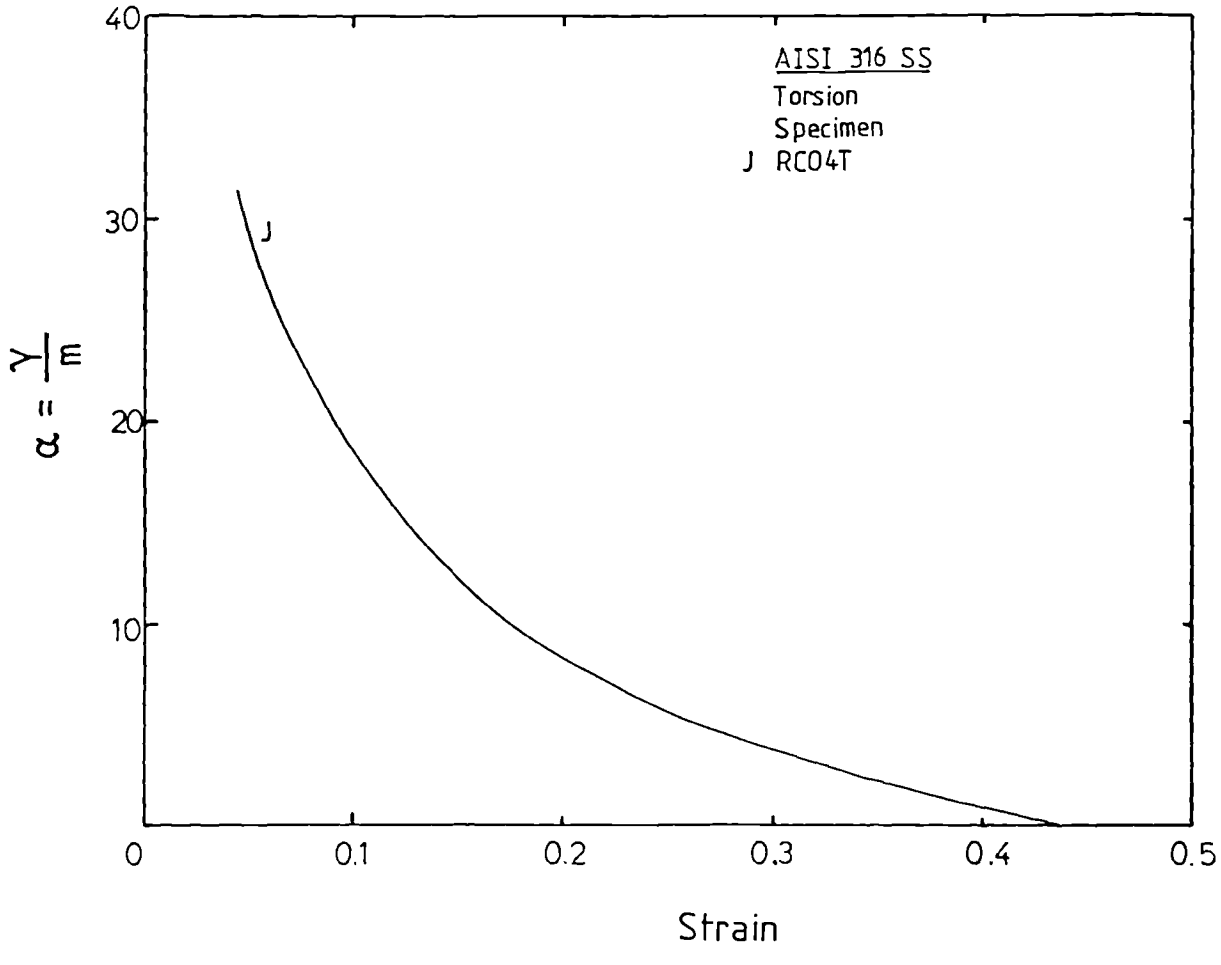
AISI 316 SS
Torsion
Specimen
J RC04T
J
40
30
20
10
0
0.1
0.2
0.3
0.4
0.5
α = γ/ε
Strain

Figure 128.- Plot of the strain measured when $\alpha = 5$ against strain rate for the curves in figures 124 to 127.

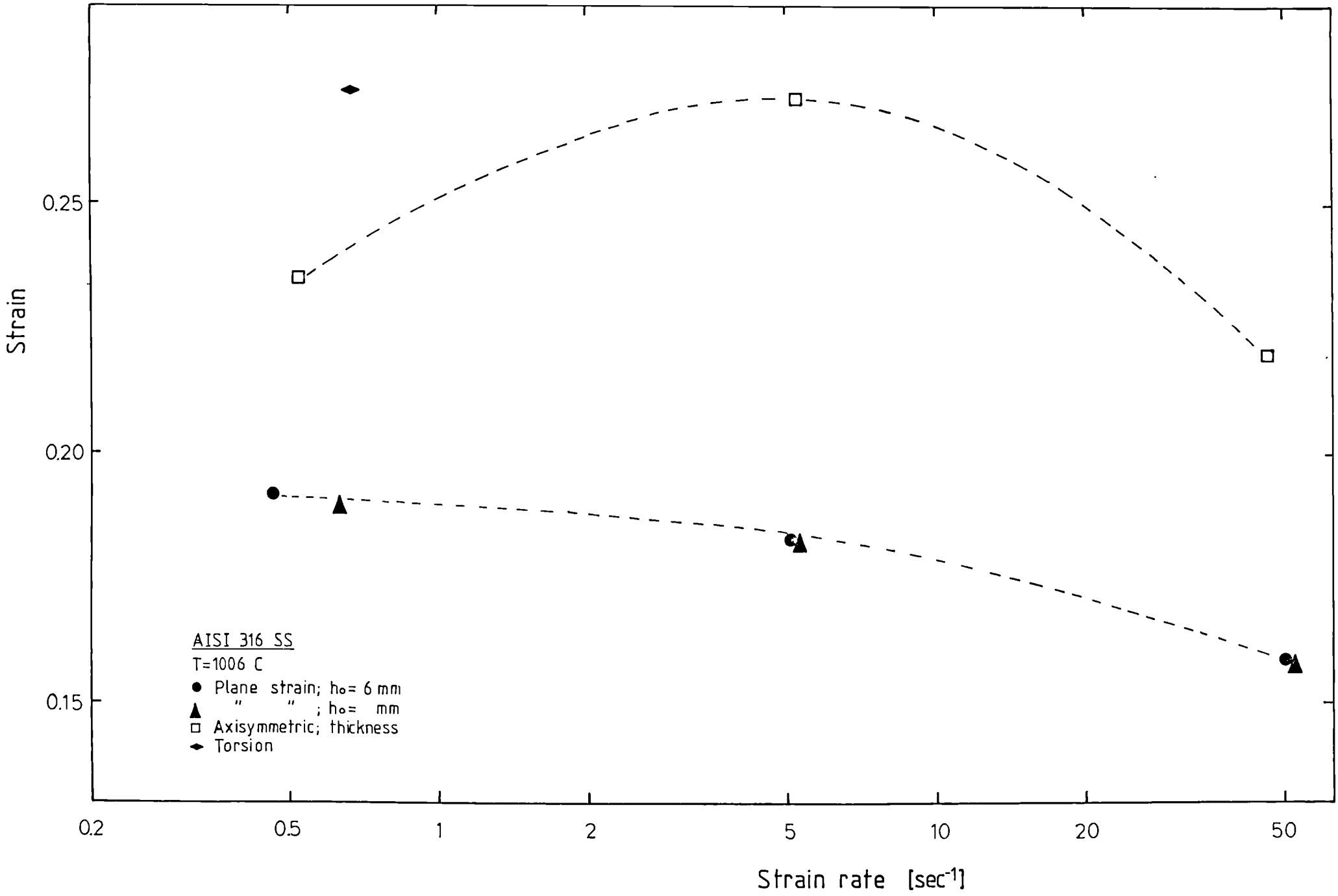
Strain
0.25
0.20
0.15
AISI 316 SS
T=1006 C
● Plane strain; h₀= 6 mm
▲ " " ; h₀= mm
□ Axisymmetric; thickness
◆ Torsion
0.2
0.5
1
2
5
10
20
50
Strain rate [sec⁻¹]

Figure 129.- Load-displacement curves for the axisymmetric specimens shown in figure 123. Key as in that figure.

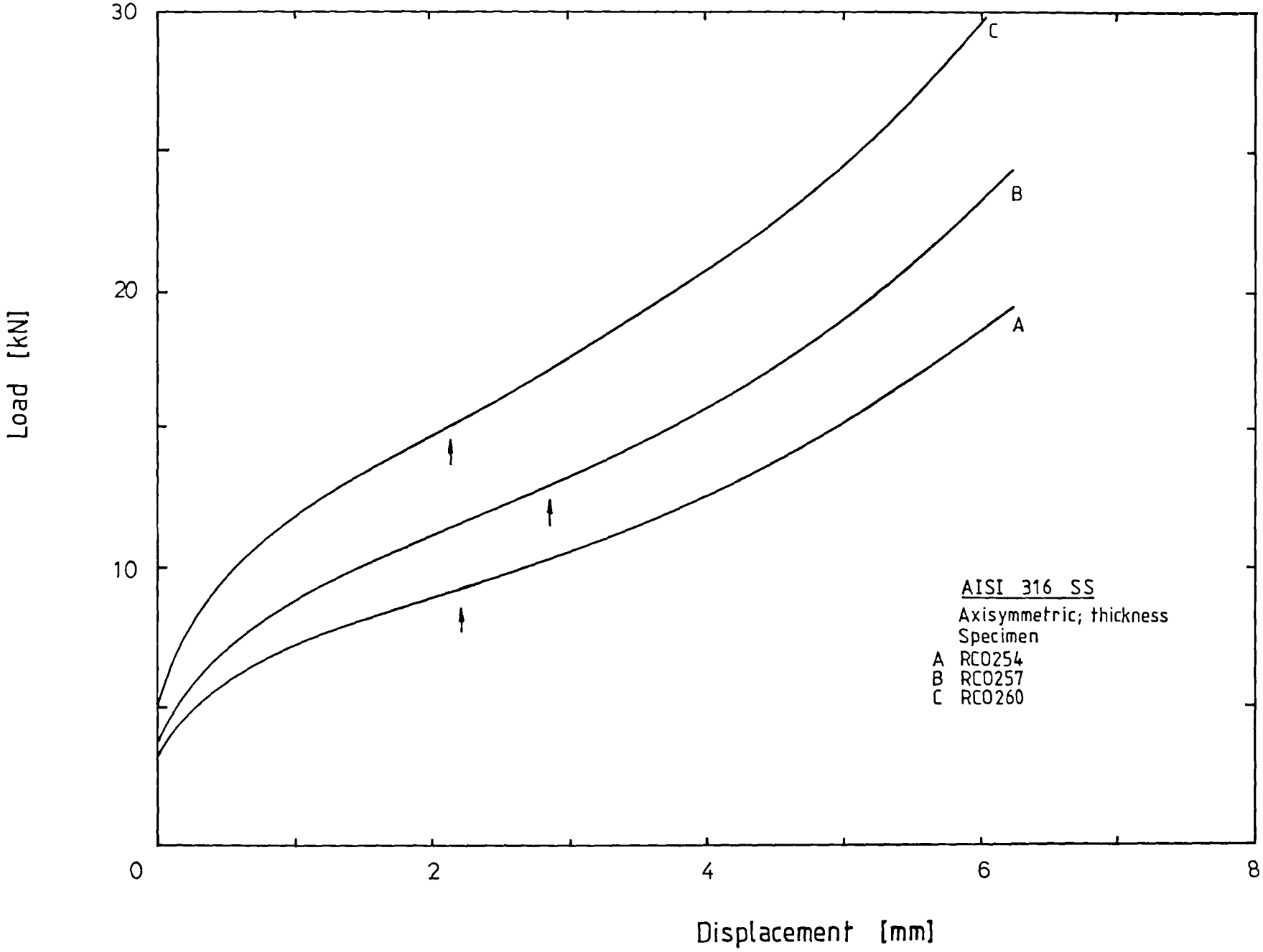
30
20
10
0
2
4
6
8
Load [kN]
Displacement [mm]
C
B
A
AISI 316 SS
Axisymmetric; thickness
Specimen
A RCO254
B RCO257
C RCO260

Figure 130.- Influence of the stress level and of the temperature increase rate in an hypothetical work hardening and recovery only material. a.) Stress-strain curves. b.) Temperature-strain curves.

A Hypothetical material.

B Low stress; full adiabatic conditions.

B' Low stress; half of the adiabatic rise in temperature.

C High stress; full adiabatic conditions.

C' High stress; half of the adiabatic rise in temperature.

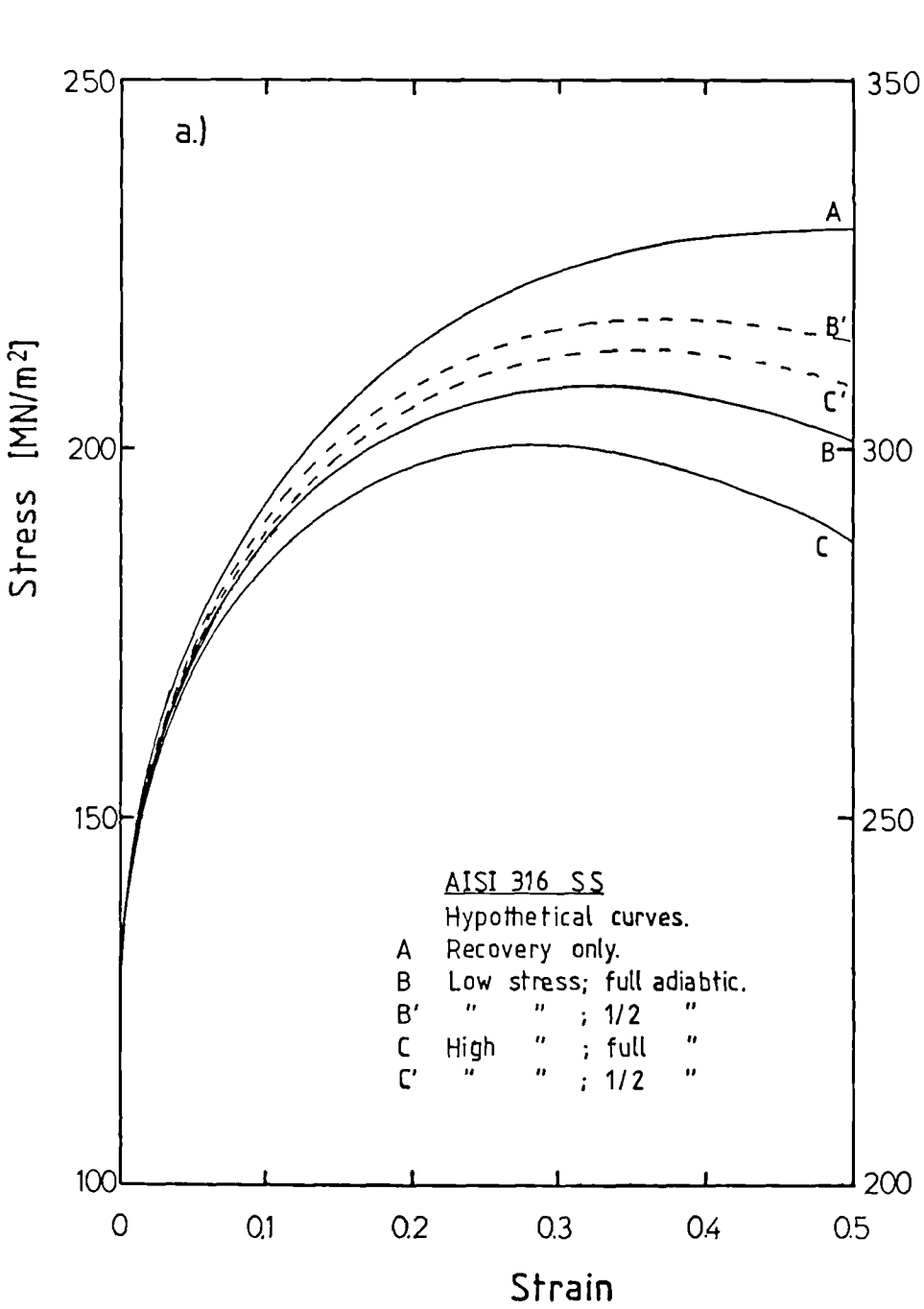
a.)
Stress [MN/m²]
Strain
250
200
150
100
350
300
250
200
0
0.1
0.2
0.3
0.4
0.5
A
B'
C'
B
C
AISI 316 SS
Hypothetical curves.
A Recovery only.
B Low stress; full adiabtic.
B' " " ; 1/2 "
C High " ; full "
C' " " ; 1/2 "

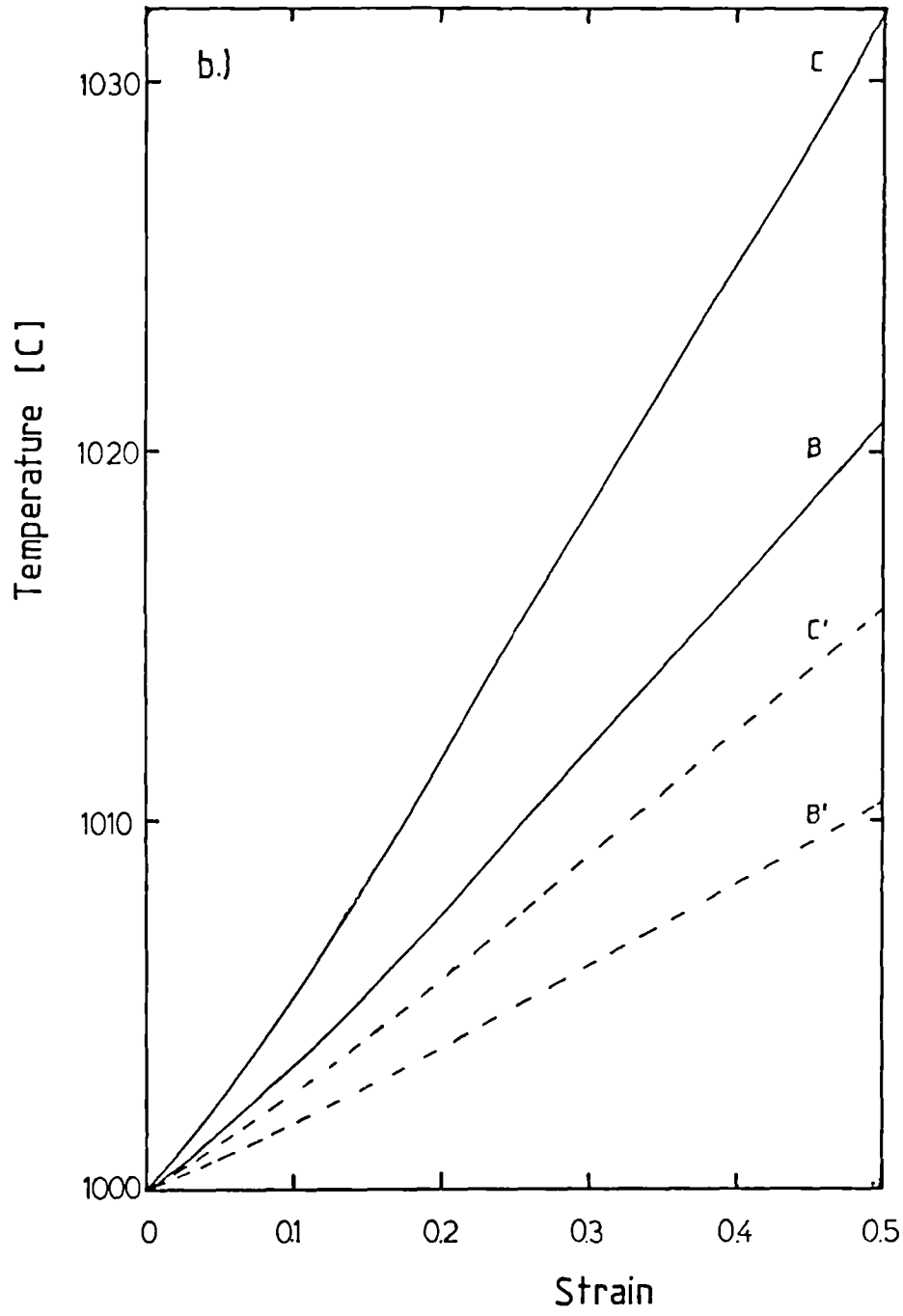
b.)
Temperature [C]
Strain
1030
1020
1010
1000
0
0.1
0.2
0.3
0.4
0.5
C
B
C'
B'

Figure 131.- Approximated positions of the inserted thermocouples. The points marked A, A' and B correspond to those in figures 118 to 120.

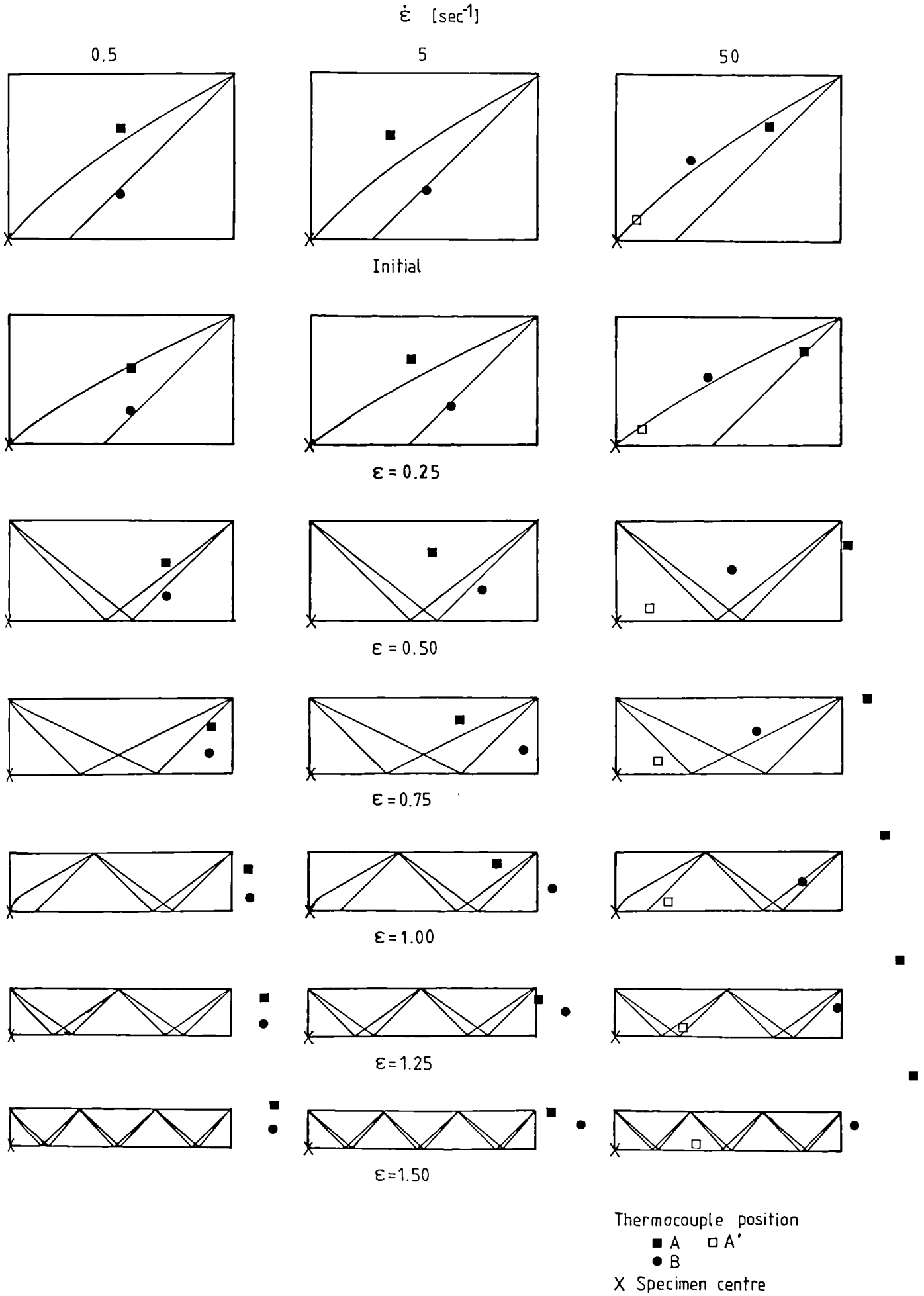
$\dot{\varepsilon}$ [sec^{-1}]
0.5
5
50
Initial
ε = 0.25
ε = 0.50
ε = 0.75
ε = 1.00
ε = 1.25
ε = 1.50
Thermocouple position
A
A'
B
X Specimen centre

Figure 132.- Strain in the slip line field, as measured from the gridded specimens, plotted against the polynomial

$$\varepsilon_s = 0.0095 + 2.16\varepsilon_n - 3.64\varepsilon_n^2 + 2.98\varepsilon_n^3$$

is fitted though the data.

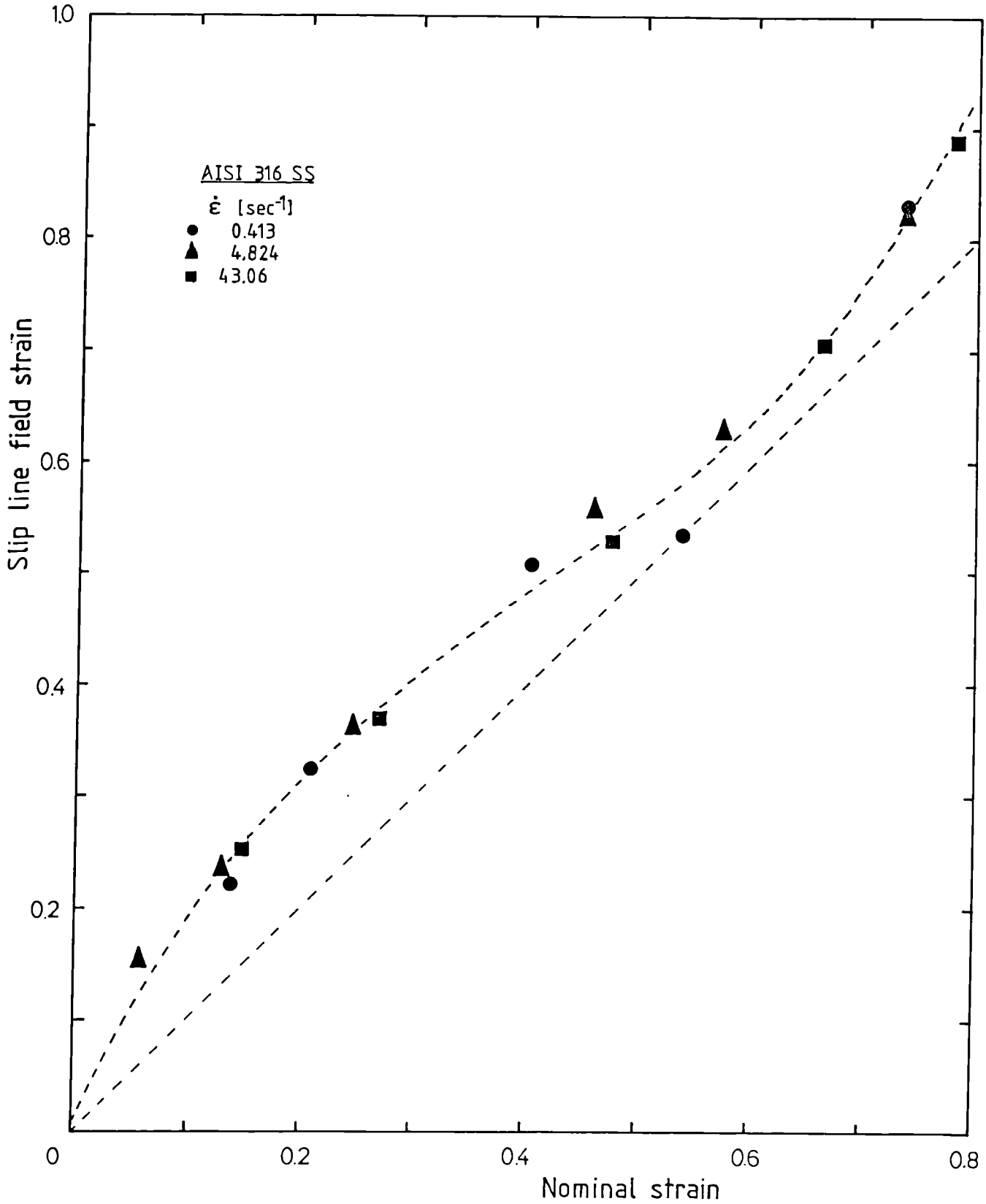
AISI 316 SS
$\dot{\varepsilon}$ [sec^{-1}]
0.413
4.824
43.06
Slip line field strain
Nominal strain
0
0.2
0.4
0.6
0.8
1.0

Figure 133.- Comparison of the stress-strain curves obtained under axisymmetric and plane strain compression. The corrections allowed for the axisymmetric test are shown.

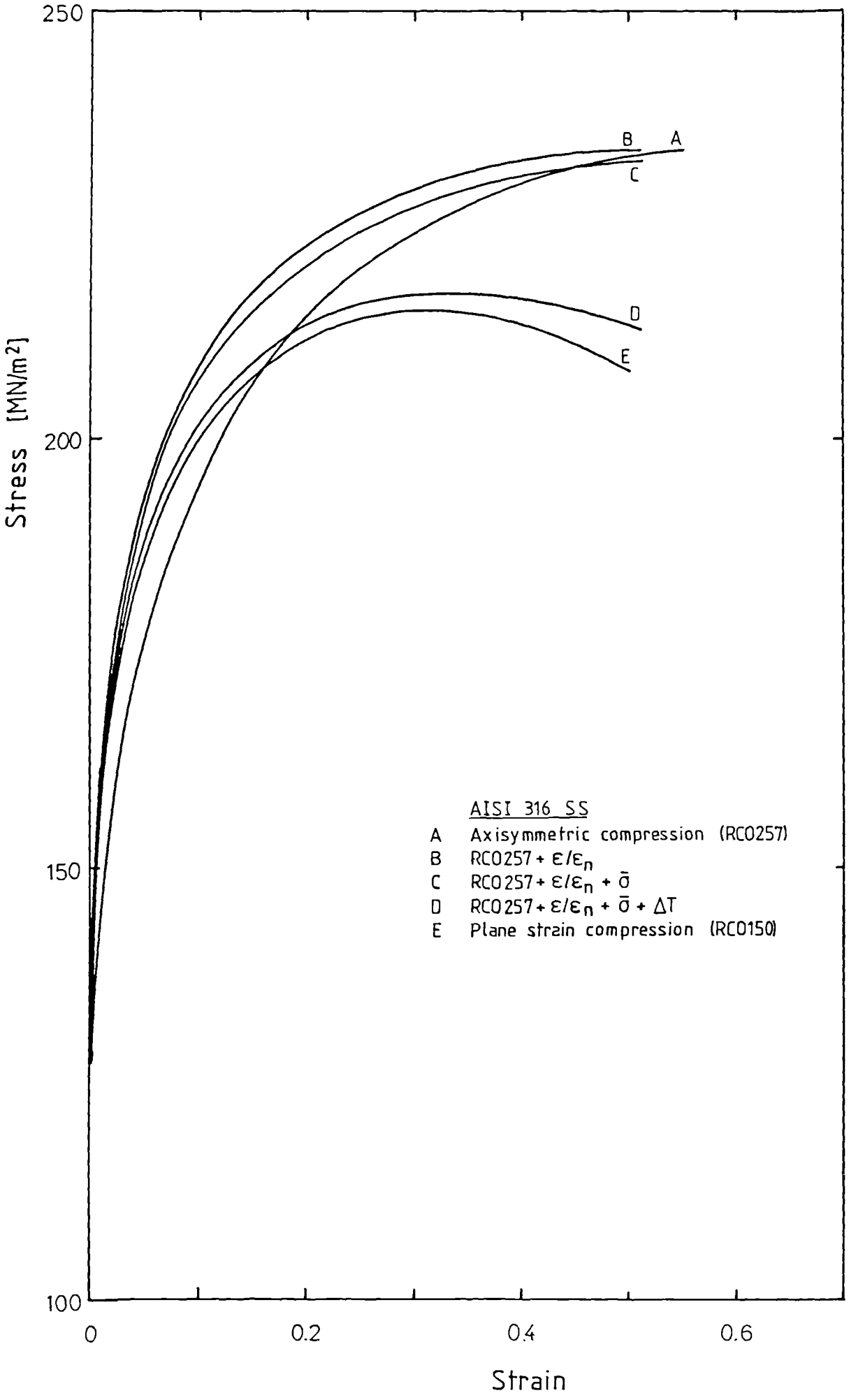
250
200
150
100
0
0.2
0.4
0.6
Stress [MN/m²]
Strain
B
A
C
D
E
AISI 316 SS
A Axisymmetric compression (RC0257)
B RC0257 + ε/εn
C RC0257 + ε/εn + σ̄
D RC0257 + ε/εn + σ̄ + ΔT
E Plane strain compression (RC0150)

Figure 134.- Schematic variation of the local shear strain rate against a.) constant tool width over specimen height, b.) strain.

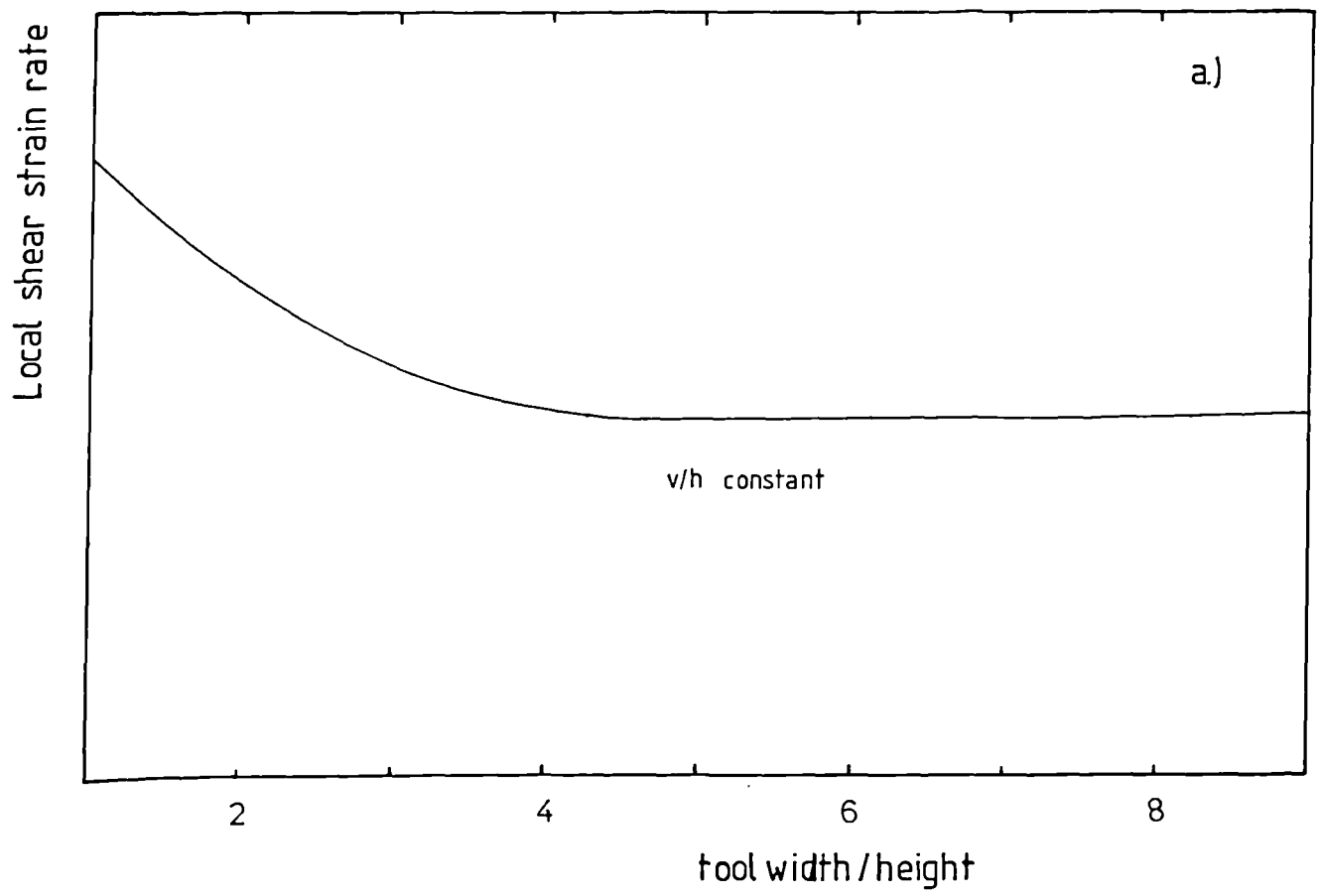
a.)
Local shear strain rate
v/h constant
2
4
6
8
tool width / height

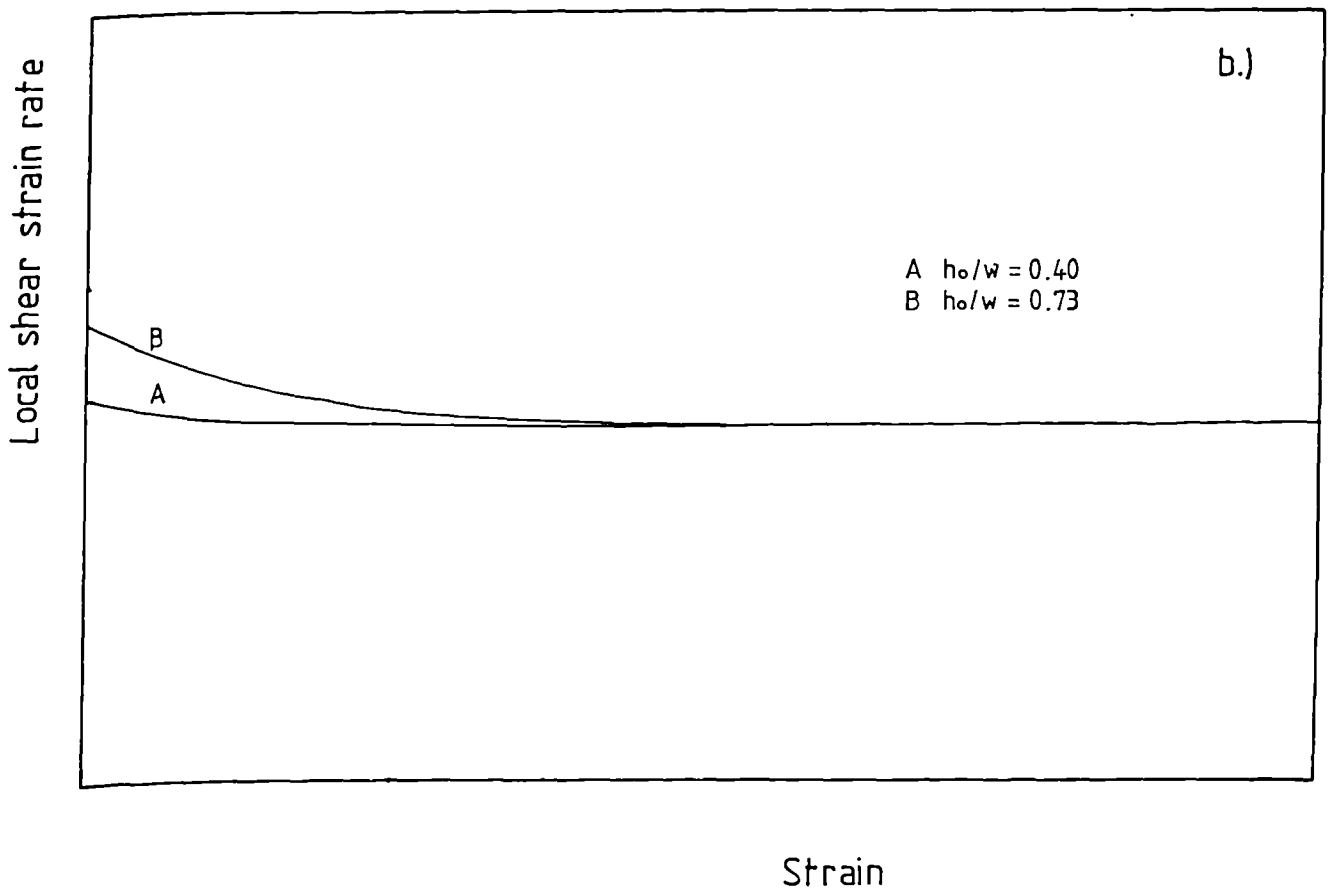
b.)
Local shear strain rate
A ho/w = 0.40
B ho/w = 0.73
B
A
Strain

Figure 135.- Comparison of stress-strain curves obtained in plane strain compression with specimens with different original geometry.

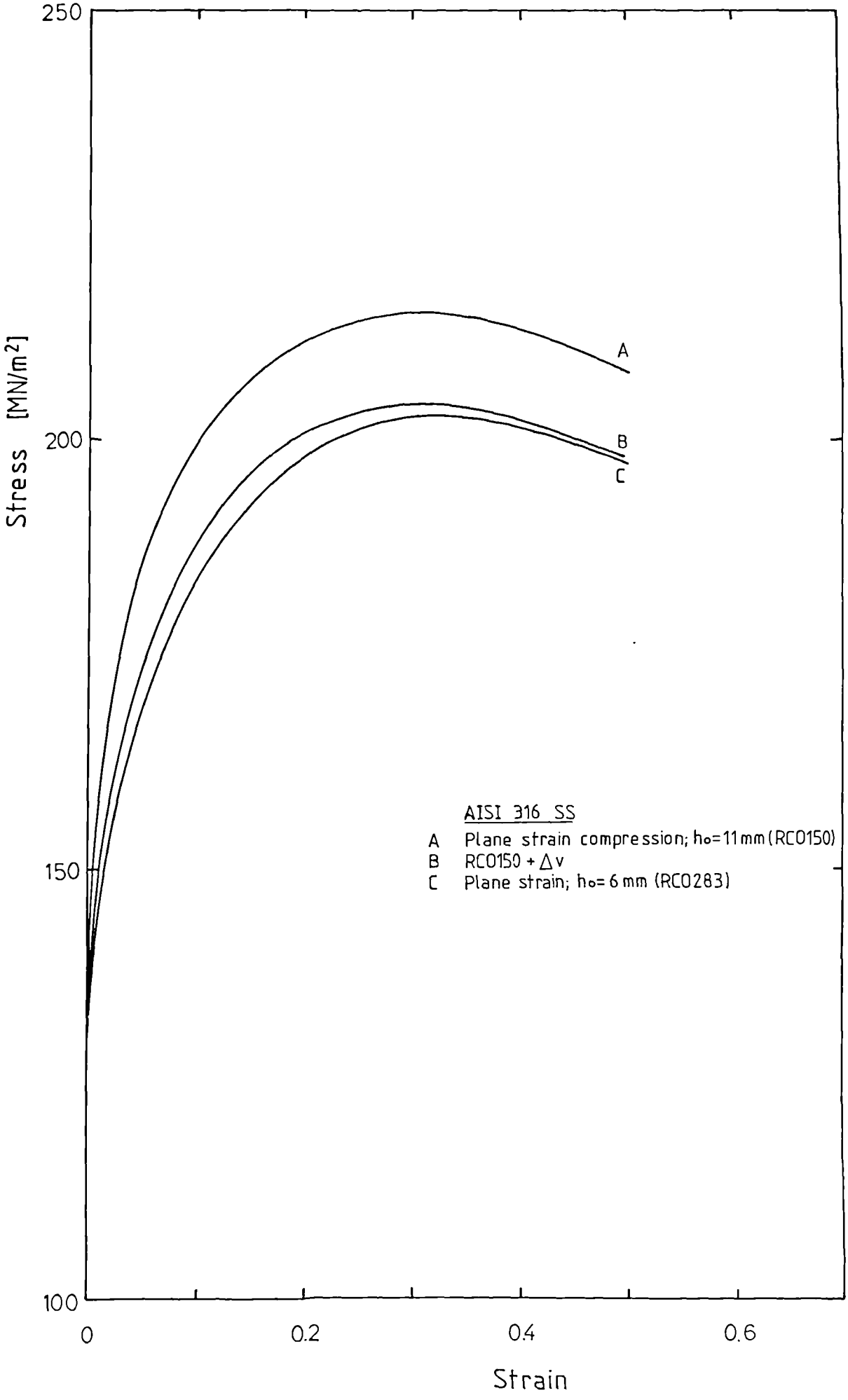
250
200
150
100
Stress [MN/m²]
0
0.2
0.4
0.6
Strain
A
B
C
AISI 316 SS
A Plane strain compression; h₀=11 mm (RC0150)
B RC0150 + Δv
C Plane strain; h₀= 6 mm (RC0283)